

FACULTY OF MEDICINE AND HEALTH SCIENCES

Department of Radiology and Nuclear Medicine

**Functional changes in the visually stimulated cortex of
patients with migraine without aura: an interictal fMRI study**

Functionele veranderingen in de visueel gestimuleerde cortex van
patiënten met migraine zonder aura: een interictale fMRI studie

Benedicte Descamps

2012

Promotors:

Prof. Dr. Eric Achten

Prof. Dr. Koen Paemeleire

Thesis submitted in fulfillment of the requirements for the degree of
Doctor in Medical Sciences

This work was supported by the Agency for Innovation through Science and Technology, Flanders (IWT-Vlaanderen, SB-51437, SB-53437) and performed at GifMI (Ghent Institute for Functional and Metabolic Imaging).



Ghent University, Faculty of Medicine and Health Sciences

Department of Radiology and Nuclear Medicine

De Pintelaan 185

9000 Ghent

BELGIUM

“Tout vient à point à qui peut attendre”

(François Rabelais, 1534)

Members of the supervisory committee:

- prof. dr. Eric Achten, promotor
- prof. dr. Karel Deblaere
- prof. dr. Luc Leybaert
- prof. dr. Koen Paemeleire, promotor

Members of the examination committee:

- prof. dr. Carlos De Wagter (chairman)
- prof. dr. Paul Boon – UGent
- prof. dr. Robrecht Raedt – UGent
- prof. dr. Jean Schoenen – ULG
- prof. dr. Stefan Sunaert – KUL
- prof. dr. ir. Stefaan Vandenberghe – UGent

**Functional changes in the visually stimulated cortex
of patients with migraine without aura: an interictal fMRI study**

Table of contents

Abbreviations and symbols	9
Samenvatting.....	13
Summary	17
Résumé.....	19
Part 1 – Introduction	23
Chapter 1: Migraine	25
1. Epidemiology and criteria for migraine diagnosis.....	25
2. Medical treatment	27
3. Pathophysiology.....	28
3.1. <i>Migraine is a chronic disorder with episodic manifestations.....</i>	<i>28</i>
3.2. <i>Anatomical and functional organisation of the normal brain</i>	<i>29</i>
3.3. <i>Genetics</i>	<i>33</i>
3.4. <i>The interictal phase</i>	<i>34</i>
3.5. <i>The ictal phase.....</i>	<i>37</i>
Chapter 2: Imaging in migraine	43
1. Structural imaging in migraine.....	43
2. Functional imaging in migraine.....	45

2.1. Positron Emission Tomography (PET) and Single-Photon Emission Computed Tomography (SPECT)	45
2.2. Functional Magnetic Resonance Imaging (fMRI)	46
2.3. Transcranial Doppler (TCD) and near-infrared spectroscopy (NIRS).....	48
Chapter 3: functional Magnetic Resonance Imaging (fMRI)	51
1. From NMR to fMRI: principles	51
1.1. Nuclear Magnetic Resonance (NMR).....	51
1.2. Magnetic Resonance Imaging	53
2. The BOLD signal	59
3. Haemodynamic refractory effects and their nonlinearities.....	65
3.1. Effect of stimulus duration	65
3.2. Effect of limited interstimulus intervals.....	66
Part 2 – Research work	73
Chapter 4: Aims of the research	75
Chapter 5: Results	77
1. Quantifying haemodynamic refractory BOLD effects in normal subjects at the single-subject level using an inverse logit fitting procedure	79
2. Absence of haemodynamic refractory effects in patients with migraine without aura – an interictal fMRI study	89
3. Combining haemodynamic and metabolic patient data reveals the presence of subgroups	103
Chapter 6: General discussion	105
1. Discussion and future perspectives	105

2. Conclusion.....	113
References	115
Appendices	133
A. International Classification of Headache Disorders, 2 nd Edition (ICHD-II), according to the International Headache Society.....	133
B. ¹ H-MRS of brain metabolites in migraine without aura: absolute quantification using the phantom replacement technique	141
C. ³¹ P-MRS demonstrates a reduction in absolute concentrations of high-energy phosphates in the occipital lobe of migraine without aura patients.....	159
Acknowledgements.....	173
Curriculum Vitae	177

Abbreviations and symbols

BOLD	blood-oxygenation-level-dependent
CBF	cerebral blood flow
CBV	cerebral blood volume
CGRP	calcitonin gene-related peptide
CMRO ₂	cerebral metabolic rate of oxygen
2D	two dimensional
3D	three dimensional
EP	evoked potential
EPI	echo planar imaging
¹⁸ F-FDG	¹⁸ F-fluorodeoxyglucose, ¹⁸ F labelled deoxyglucose
FFA	fusiform face area
FHM	familial hemiplegic migraine
FLAIR	FLuid Attenuated Inversion Recovery
fMRI	functional Magnetic Resonance Imaging
GE	gradient echo
GTN	glyceryl trinitrate
G _x	frequency-encoding gradient along X-axis
G _y	phase-encoding gradient along Y-axis
G _z	slice-selection gradient along Z-axis
HREs	haemodynamic refractory effects
HRF	haemodynamic response function
ICHD-II	International Classification of Headache Disorders, 2nd edition
IHS	the International Headache Society
IL	inverse logit

ABBREVIATIONS

ISI	interstimulus interval
LFP	local field potentials
min	minute
mm	millimeter
MOH	medication-overuse headache
MwA	migraine with aura
MwoA	migraine without aura
MR(I)	Magnetic Resonance (Imaging)
MRS	Magnetic Resonance Spectroscopy
M_{XY}	transversal magnetization
M_z	longitudinal magnetization
NIRS	near-infrared spectroscopy
NMR	Nuclear Magnetic Resonance
NSAIDs	nonsteroidal anti-inflammatory drugs
NVU	neurovascular unit
NO	nitric oxide
PAG	periaqueductal gray matter
PET	positron emission tomography
ppm	parts per million
REF	reference condition (in our experiments)
RF	radiofrequency
ROI	region of interest
1S, 2S, 6S	three experimental conditions with 1, 2 and 6 seconds ISI, respectively
SD	standard deviation
SE	standard error of the mean
SNP	single nucleotide polymorphism
SNR	signal-to-noise ratio
SPECT	single-photon emission computed tomography

SPM	Statistical Parametric Mapping
TCA	tricarboxylic acid
TCC	trigeminocervical complex
TE	echo time
TR	repetition time
TTH	tension-type headache
TVS	trigeminovascular system
V ₁	first (ophthalmic) division of fifth cranial (trigeminal) nerve
V1	primary visual cortex
VBM	voxel-based morphometry
VEP	visual evoked potential

Samenvatting

Migraine is een primaire hoofdpijnaandoening met een eenjaarsprevalentie van minstens 11%. Het is de meest voorkomende neurologische aandoening en heeft een enorme economische en sociale impact. De Wereld Gezondheidsorganisatie erkent dat migraine een ernstige, invaliderende aandoening is, die de levenskwaliteit van de patiënt negatief beïnvloedt, ook al zijn de symptomen niet permanent aanwezig. De interictale periode, wanneer de patiënt hoofdpijn-vrij is, wordt afgewisseld met episodische hoofdpijnaanvallen, de ictale fase genoemd. Een hoofdpijnaanval duurt 4 tot 72 uur wanneer die niet of niet succesvol behandeld wordt, en gaat gepaard met geassocieerde symptomen, waarvan fotofobie, fonofobie en nausea de bekendste zijn.

Migraine wordt verder onderverdeeld in verschillende subtypes, waarvan migraine zonder aura (MwoA) en migraine met aura (MwA) de meest voorkomende zijn. Hoewel er wereldwijd veel onderzoek gebeurt naar migraine, zowel naar de hoofdpijn en de aura als naar de interictale aandoening, is de neurobiologie ervan nog steeds niet volledig begrepen.

Deze thesis had tot doel om interictale functionele veranderingen in de hersenen van patiënten met MwoA te identificeren, gebruik makend van functionele magnetische resonantie beeldvorming (fMRI).

In hoofdstuk 1 vatten we de huidige kennis over de fysiopathologie van migraine samen. Wat gebeurt er tijdens een aanval? Waarom ervaren patiënten hoofdpijn, hoewel het hersenweefsel zelf gevoelloos is? Waarom ontwikkelen patiënten opeens een migraine-aanval in tegenstelling tot mensen zonder migraine? Welke zijn de interictale afwijkingen in de hersenen van migrainepatiënten? Wat is de rol van het genoom?

De bevindingen van studies met structurele en functionele hersenbeeldvorming bij migrainepatiënten worden besproken in hoofdstuk 2. Een MRI scan is de beste modaliteit om hersenen te evalueren door het excellent contrast in zachte weefsels. Structurele beeldvorming draagt echter niet bij aan de migraine diagnose, noch is beeldvorming expliciet vermeld in de huidige diagnostische criteria. Nochtans kan conventionele structurele MR beeldvorming noodzakelijk zijn om onderliggende pathologieën, zoals een

hersentumor of hydrocefalie, uit te sluiten. Functionele informatie wordt verkregen met positron emissie tomografie (PET) scans, nabij-infrarood spectroscopie of fMRI. We stellen vast dat de interictale haemodynamische respons functie bij migrainepatiënten tot op heden nog niet bestudeerd werd.

In hoofdstuk 3 wijden we uit over de principes van MRI en fMRI. We beschrijven de eigenschappen van het BOLD-signaal, dat gewoonlijk gebruikt wordt bij fMRI en afhankelijk is van de oxygenatiegraad van het bloed, en we onderzoeken de niet-lineariteiten van de haemodynamische respons functie, ook wel de haemodynamische refractaire effecten genoemd.

De onderzoeksdoelstellingen worden opgesomd in hoofdstuk 4.

In hoofdstuk 5 beschrijven we de resultaten van ons onderzoekswerk. Eerst gaan we dieper in op de methodologie om haemodynamische signalen op het individuele niveau te meten en te kwantificeren, om nuttige informatie over refractaire effecten bij dat individu te bekomen. Data-acquisitie, -extractie, -fitting en -kwantificatie worden in detail beschreven. We gebruiken een fitting algoritme met inverse logit functies, zodat informatie optimaal uit één dataset kan gehaald worden zonder dat de data in een gestandaardiseerd model geduwd worden.

In het tweede deel van dit hoofdstuk wordt de methode toegepast op patiënten-data. Er zijn daarvoor 21 patiënten met MwoA gescand. De patiëntenselectie was gebaseerd op strenge criteria om een homogene groep te bekomen. De patiënten-data worden vergeleken met referentiegegevens. Onze bevindingen suggereren dat de haemodynamische refractaire effecten niet voorkomen bij patiënten, wat mogelijks verband houdt met het ontbreken van habituatie bij metingen van geëvokeerde potentialen.

Tenslotte onderzoeken we of het combineren van haemodynamische en metabole gegevens, die in dezelfde patiënten op dezelfde dag verzameld worden, bijkomende informatie oplevert. We gaan na of zo'n gecombineerde dataset bruikbaar is om met voldoende hoge sensitiviteit en specificiteit te kunnen bepalen of het gescande subject een migrainepatiënt is of niet. We tonen aan dat onze homogene patiëntengroep kan onderverdeeld worden in verschillende subgroepen.

We besluiten dat we een methode ontwikkeld hebben om haemodynamische refractaire effecten op het individueel niveau op te sporen en te kwantificeren. Het toepassen van deze methode bij patiënten met MwoA toont aan dat een subgroep van deze patiënten geen haemodynamische refractaire effecten vertonen, terwijl een tweede subgroep metabole problemen heeft. We eindigen hoofdstuk 6 met enkele suggesties voor toekomstig onderzoek.

Summary

Migraine is a primary headache disorder with a one-year prevalence of at least 11%. It is the most prevalent of all neurological disorders and has an enormous economic and social impact. The World Health Organisation recognizes that migraine is a severe and disabling condition, affecting the patients' quality of life, although the symptoms are not permanently present. The interictal period, in which the patient is pain-free, is interspersed with episodic headache attacks, called the ictal period. The headache attacks last 4 to 72 hours when untreated or unsuccessfully treated, and are accompanied by associated symptoms, of which photophobia, phonophobia and nausea are best known. Migraine is further subdivided into several subtypes of which migraine without aura (MwoA) and migraine with aura (MwA) are the most common. Although there is a lot of migraine research going on worldwide, on the headache and the aura as well as on the interictal disorder, its neurobiology is still incompletely understood.

The aim of this thesis was to identify interictal functional changes in the brain of patients with MwoA, using functional magnetic resonance imaging (fMRI).

In Chapter 1, we summarize the current knowledge about migraine pathophysiology. What happens during an attack? Why do patients experience a headache while the brain tissue itself is insensate? Why do patients suddenly develop an attack while people without migraine don't? What are the interictal brain anomalies in migraineurs? What is the role of the genome?

The findings from both structural and functional neuroimaging studies in migraineurs are discussed in Chapter 2. An MRI scan is the best modality to evaluate the brain due to its excellent soft tissue contrast. Structural imaging does not contribute to the diagnosis of migraine, nor is imaging explicitly mentioned in the current diagnostic criteria. However, conventional structural MRI may be necessary to exclude underlying pathologies, such as brain tumor or hydrocephalus. Functional information is obtained with positron emission tomography (PET) scans, near-infrared spectroscopy or fMRI. We find that, to date, the interictal haemodynamic response function has not been studied with fMRI in patients with MwoA.

In Chapter 3, we elaborate on the principles of MRI and fMRI. We describe the characteristics of the blood-oxygenation-level-dependent (BOLD) signal, which is commonly used in fMRI, and we investigate the nonlinearities of the haemodynamic response function, also called haemodynamic refractory effects (HREs).

The research objectives are listed in Chapter 4.

In Chapter 5, we describe the results of the research work. First, we elaborate on the methodology to measure and quantify haemodynamic signals at the single-subject level for obtaining useful information on refractory effects from that particular subject. Data acquisition, extraction, fitting and quantification are described in detail. We use a fitting algorithm with inverse logit functions, to optimize information extraction from one data set, without forcing the data into any standardized model.

In the second part of this chapter, the method is applied on real patient data. Therefore, we acquired data in 21 patients with MwoA. Patient selection has occurred on the basis of stringent exclusion criteria to create a homogeneous patient group. The patient data are compared with reference data. Our findings suggest that patients lack HREs, possibly related to their lack of habituation in evoked potential measurements.

Finally, we investigate whether the combination of haemodynamic and metabolic data, obtained in the same patients during the same day, offers additional information. We consider the usefulness of such a data set to determine – with high sensitivity and specificity – whether the scanned subject is a migraineur or not. We show that our homogeneous patient group can be subdivided into several subgroups.

In conclusion, we established a methodology to detect and quantify HREs at the single-subject level. Application of this method to patients with MwoA reveals that a subgroup of these patients lack HREs, while a second subgroup has metabolic problems. We end Chapter 6 with some suggestions for future research.

Résumé

La migraine est une céphalée primaire qui a une prévalence d'au moins 11% par an. Elle est la plus prévalente de toutes les affectations neurologiques et elle a un énorme impact économique et social. L'Organisation Mondiale de la Santé (OMS) reconnaît que la migraine est une condition grave qui mène à des conditions de vie invalidantes et qui affecte la qualité de vie du patient, bien que les symptômes ne sont pas constamment présents. La période interictale, pendant laquelle le patient n'éprouve pas de douleurs, alterne avec des crises de mal de tête épisodiques, la période ictale. Les crises de mal de tête durent de 4h à 72h si elles ne sont pas traitées ou traitées sans succès, et s'accompagnent de symptômes associés, parmi lesquels la photophobie, la phonophobie et la nausée sont les symptômes les plus connus. La migraine est subdivisée en plusieurs sous-types parmi lesquels la migraine sans aura (MwoA) et la migraine avec aura (MwA) sont les plus courants. Bien qu'il y ait beaucoup de recherche scientifique sur la migraine au niveau mondial, tant sur le mal de tête et l'aura comme sur l'affectation interictale, la neurobiologie de la migraine reste partiellement inconnue.

Le but de cette thèse était l'identification des changements interictaux fonctionnels dans le cerveau des patients qui souffrent de MwoA, tout en employant l'imagerie par résonance magnétique fonctionnelle (IRMf).

Dans le premier chapitre nous résumons les connaissances actuelles sur la physiopathologie de la migraine. Qu'est-ce qui se passe lors d'une crise? Pourquoi les patients éprouvent-ils un mal de tête tandis que le cerveau lui-même n'éprouve pas de douleur? Pourquoi les patients développent-ils une crise tandis que les personnes sans migraine n'en développent pas? Quelles sont les anomalies cérébrales interictales dont souffrent les patients de migraine? Quel est le rôle du génome?

Les résultats des études d'imagerie cérébrale structurelle et fonctionnelle chez les patients de migraine sont présentés dans le deuxième chapitre. Le balayage IRM est la meilleure modalité pour évaluer le cerveau en raison de son excellent contraste des tissus doux. L'imagerie structurelle ne contribue pas à la diagnose de migraine et l'imagerie n'est pas non plus mentionnée explicitement parmi les critères diagnostiques actuels. Néanmoins l'IRM structurelle conventionnelle peut être nécessaire afin d'exclure des pathologies sous-

jaçentes, telles que les tumeurs cérébrales, l'hydrocéphalie, etc. Des informations fonctionnelles peuvent être obtenues avec des images TEP, la spectroscopie proche infrarouge ou IRMf. Nous avons constaté que, jusqu'à présent, la fonction de réponse hémodynamique interictale chez les patients n'a pas encore été examinée avec l'IRMf.

Dans le troisième chapitre nous développons les principes de l'IRM et IRMf. Nous décrivons les caractéristiques du contraste BOLD, qui dépend du niveau d'oxygénation du sang et qui est couramment utilisé dans l'IRMf, et nous examinons les non-linéarités de la fonction de réponse hémodynamique qui sont également appelées les effets réfractaires hémodynamiques.

Nous présentons les objectifs de notre recherche dans le quatrième chapitre.

Dans le cinquième chapitre nous décrivons les résultats de la recherche scientifique. D'abord nous développons la méthodologie pour mesurer et quantifier les signaux hémodynamiques au niveau de l'individu afin d'obtenir des informations utiles sur les effets réfractaires de l'individu. Nous décrivons en détail l'acquisition, l'extraction, l'insertion et la quantification des données. Nous utilisons un algorithme d'insertion aux fonctions réciproques logit, afin d'optimiser l'extraction d'informations d'un set de données sans forcer les données dans un modèle standardisé.

Dans la deuxième partie de ce chapitre nous appliquons la méthode sur les données réelles des patients. A cette fin nous avons acquis des données chez 21 patients MwoA. La sélection des patients a été faite à base de critères d'exclusion rigoureux afin de créer un groupe de patients homogène. Les données des patients ont été comparées avec les données de référence. Nos constatations suggèrent que les patients manquent d'effets hémodynamiques réfractaires, ce qui peut être lié à leur manque d'accoutumance en cas de potentiels évoqués.

En dernier lieu nous examinons si la combinaison de données hémodynamiques et métaboliques, obtenues chez les mêmes patients lors de la même journée, donne des informations supplémentaires. Nous vérifions si un tel set de données permet de déterminer – avec haute sensibilité et spécificité – si l'individu passé sous le scanner est un patient de

migraine ou non. Nous démontrons que notre groupe de patients homogène peut être subdivisé en plusieurs sous-groupes.

Nous concluons que nous avons établi une méthodologie pour détecter et quantifier les effets hémodynamiques réfractaires au niveau de l'individu. L'application de cette méthode à des patients MwoA révèle qu'un premier sous-groupe de ces patients manque d'effets hémodynamiques réfractaires tandis qu'un deuxième sous-groupe souffre de problèmes métaboliques. Nous finissons le sixième chapitre avec des suggestions de recherche future.

Part 1 – Introduction

Chapter 1: Migraine

1. Epidemiology and criteria for migraine diagnosis

Migraine is a severe and disabling neurological disorder with a global one-year prevalence of at least 11%. Typically, more women (15-18%) than men (7%) suffer from migraine (1). Migraine is the most prevalent of all neurological disorders and has an enormous economic and social impact. In 2006, a study of the IDEWE (External Service for Prevention and Protection at Work) reported an estimated annual loss of around 1.150.000 working days in Flanders and Brussels due to migraine (2). In the “Global Burden of Disease” analysis, the World Health Organisation recognizes that migraine is a severe and disabling condition, affecting the patients’ quality of life, even though the symptoms are not permanently present. Migraine is the third most prevalent condition worldwide, after iron-deficiency anaemia and mild hearing loss, with an estimated 324 million sufferers (3).

Criteria for migraine are defined in the second edition of the International Classification of Headache Disorders (ICHD-II) (4), which is enclosed in Appendix A. Migraine is a chronic, primary headache disorder with episodic headache attacks, lasting four to seventy-two hours when untreated or unsuccessfully treated. The headache cannot be attributed to another disorder, such as brain tumour or hydrocephaly. In addition to this, at least two of the following headache characteristics must be present:

- unilateral location
- pulsating quality
- moderate to severe pain intensity

- aggravation by routine physical activity (or causing avoidance of this).

The migraine headache is accompanied by at least one of the following symptoms:

- photophobia and phonophobia
- nausea and/or vomiting.

Probably many patients with migraine are not aware of their condition and are undiagnosed or misdiagnosed, because they do not all meet the standard image of the migraine patient with unilateral pulsating headache. The estimated migraine prevalence is only the tip of the migraine iceberg and migraine remains an underdiagnosed condition (5). Migraine is further subdivided into several subtypes of which migraine without aura (MwoA) and migraine with aura (MwA, approximately 20 to 30% of all migraine patients) are the most common. The aura is a collective term for reversible focal neurological symptoms that usually develop gradually over 5 to 20 minutes and last for less than 60 minutes, e.g. positive and/or negative visual or sensory symptoms, speech disturbance, etc. For example, patients often describe a scintillating scotoma, i.e., the combination of a positive and a negative symptom, respectively. A visual migraine is depicted in Figure 1. Cortical spreading depression (CSD), first described in rabbits by Leão in 1944 (6), is thought to be the mechanism underlying migraine aura (7). CSD is preceded by an initial rim of spreading hyperemia, in response to increased neuronal excitation, and then followed by the spreading oligemia accompanying the depression, which is due to a transient failure in the brain ion homeostasis (8). Investigating the aura phenomenon is more straightforward than the headache itself, due to the concrete homologue. The aura and CSD originate in the occipital brain regions and propagate at the same speed (around 2 to 6 mm/min (9)), which is similar to the propagation of the spreading hypoperfusion (2 mm/min (10)). We note that during the aura

only a spreading oligemia is observed. Patients with MwA were also examined with functional magnetic resonance imaging (fMRI) during their aura and blood-oxygenation-level-dependent (BOLD) signal changes were reported that demonstrated several characteristics of CSD (11). Throughout this work, we will focus on patients with MwA, to avoid interference of the aura biology, because we use visual stimuli in our research.

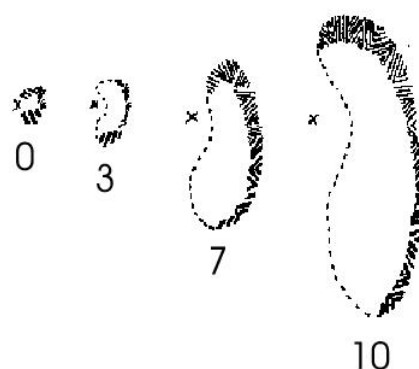


Figure 1 In 1941, neuroscientist Karl S. Lashley illustrated his own visual aura with positive and negative features: a scintillating scotoma. He indicated the time (in minutes) to spread from the macular area to the edge of the visual field (12).

2. Medical treatment

The acute phase of a migraine attack can be blocked by triptans, a class of drugs specifically developed for the treatment of migraine headache. These serotonin-agonists can stop the headache because they occupy 5-HT_{1B} and 5-HT_{1D} receptors in the trigeminovascular system (see paragraph 3.2). However, triptans are expensive and only chosen if non-specific acute migraine treatments such as non steroidal anti-inflammatory drugs (NSAIDs, e.g., ibuprofen, naproxen, diclofenac), acetylsalicylic acid or paracetamol do not block the attack sufficiently. Ergotamines are also a specific acute treatment, but not recommended anymore (13). Antiemetics such as domperidone can reduce the nausea and vomiting.

Patients are often asked to keep a headache diary. This diary provides a lot of information for the neurologist to get insight into the patients' attacks, their frequency, severity, etc. Also, patterns linked to medication-use or -overuse or the menstrual cycle can come up. The management of migraine comprises advice concerning trigger avoidance: appropriate sleep routine, regular meals, regular exercise, smoking cessation, moderate or no alcohol and caffeine consumption, proper stress management.

A prophylactic treatment can be considered for patients with multiple disabling attacks per month. Five categories commonly used in prophylactic treatments are β -blockers (e.g., propranolol, metoprolol), antiepileptic drugs (e.g., topiramate, valproate), antidepressants (e.g., amitriptyline), calcium channel-blockers (e.g., flunarizine), and metabolic enhancers (e.g., riboflavin). The mechanisms of action for most prophylactic drugs is unknown.

These prophylactic treatments can be combined or preceded by relaxation therapy or cognitive-behavioural therapy (14-16).

3. Pathophysiology

3.1. Migraine is a chronic disorder with episodic manifestations

Migraine is a disorder rather than a disease, in which several phases can be distinguished (Figure 2). The interictal period, in which the patient is headache-free and does not experience any of the associated symptoms, is interspersed with episodic manifestations, the ictal period. Reported precipitating factors or triggers that induce an attack are stress and mental tension, lack of sleep, postponing or skipping a meal, consumption of certain beverages (e.g., drinks containing alcohol, caffeine-overuse) or food, changing hormone levels in female patients, weather changes, etc (17-20). The headache attack can be

preceded by premonitory symptoms (e.g. tiredness and yawning, difficulty concentrating, a stiff neck, hyperactivity, etc.) and an aura (21). After the headache is resolved and recovered, the patient may experience postdromal symptoms, resembling the prodromal ones. Not all patients experience all the phases.

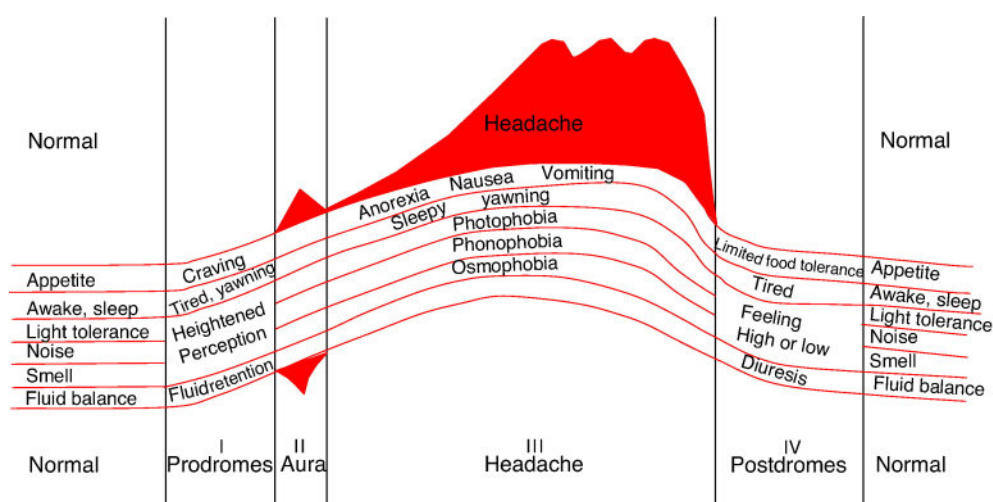


Figure 2 Several subphases can be distinguished within the ictal phase of a migraine attack; note that the associated symptoms are persistently present and (may) worsen during the headache phase ((22), adapted from Blau (23)).

Migraine is a multifactorial disorder, in which multiple neurotransmitters systems, complex genetics, and environmental factors play a role. Numerous migraine studies have been published that reveal ictal and interictal abnormalities. We summarize the most important literature in the next paragraphs.

Although there is a lot of migraine research going on worldwide, on the headache and the aura as well as on the interictal disorder, its neurobiology is still incompletely understood (24).

3.2. Anatomical and functional organisation of the normal brain

Brain tissue itself is insensate, but the meninges and large intracranial blood vessels are innervated by nociceptive neurons of the ophthalmic division of the trigeminal nerve (V_1) and the upper cervical nerves, the latter for the infratentorial dura mater. The

trigeminovascular system (TVS) consists of the pseudo-unipolar V_1 neurons and the intracranial blood vessels they innervate. The neuronal cell bodies are located in the trigeminal ganglion, lying close to the brainstem. Afferents leave the ganglion to enter the brainstem at the level of the pons and continue to the trigeminocervical complex (TCC), a region at the cervicomedullar junction. This TCC comprises the trigeminal nucleus caudalis, which is a subnucleus from the spinal trigeminal nucleus, and the superficial layers of the spinal dorsal horns of C1 and C2 (the uppermost cervical regions of the spinal cord), which are all interconnected (25). The second-order neurons in the TCC have projections to hypothalamus, dorsolateral pontine tegmentum, rostral ventromedial medulla, periaqueductal grey matter (PAG), locus coeruleus, etc, as well as connections with neurons that project to the contralateral thalamus and cortex (Figure 3). Hypothalamus and thalamic nuclei play an important role in the modulation of pain perception (26): the perception of a painful stimulus depends on the situation and can be modulated by diencephalic and brain stem nuclei. Finally, inhibitory interneurons are found in the thalamocortical loops. They have a regulatory function and should provide a functional balance between somatosensory cortex and thalamus (27).

At the cellular level, the smallest functional unit in the brain is the neurovascular unit (NVU), which consists of a neuron, an astrocyte and a capillary (Figure 4). Astrocytes play an important role in the normal neurophysiology and are therefore not just cells with a supportive function, inferior to the neuron. First, there is their involvement in the *neurometabolic* coupling.

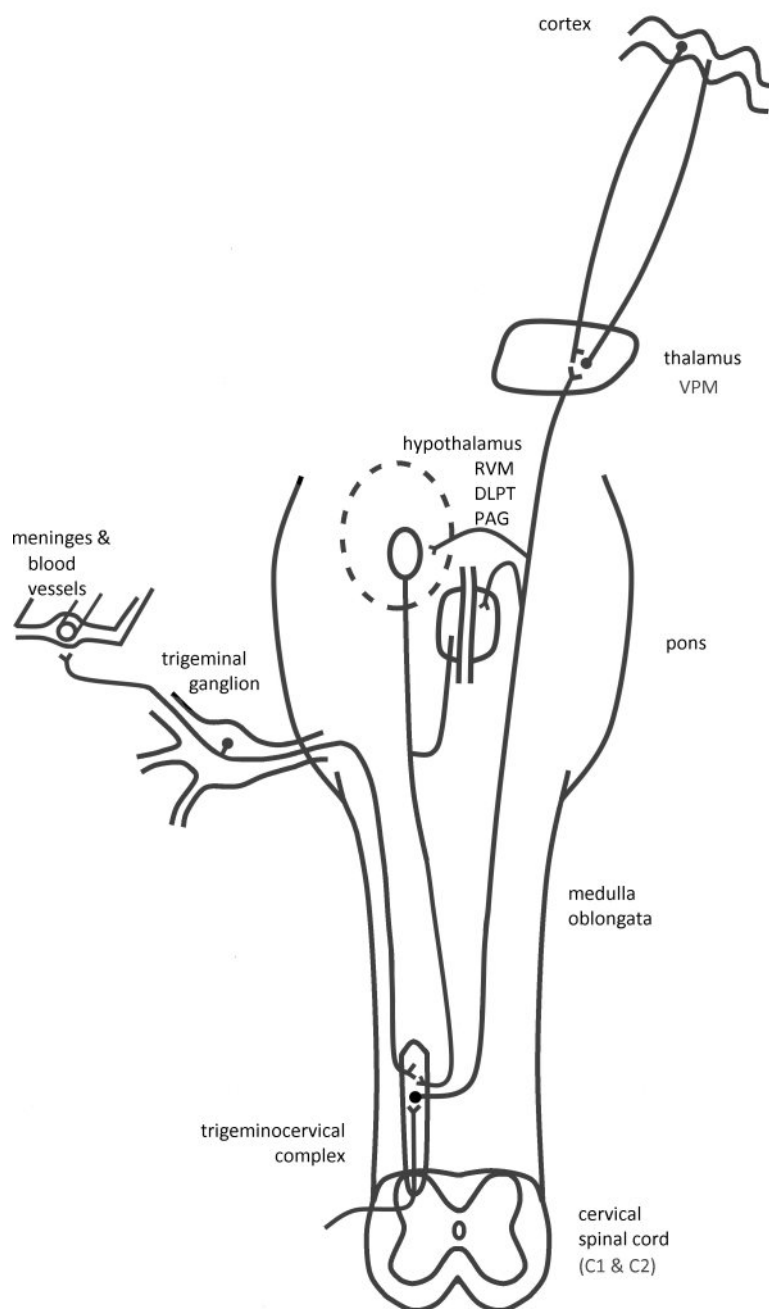


Figure 3 The major connections involved in the trigeminocervical complex. Neurons from the ophthalmic division of the trigeminal nerve innervate the meninges and blood vessels. Their cell bodies are found in the trigeminal ganglion. Afferents leave the ganglion, pass through the pons and end on second-order neurons in the trigeminocervical complex, which comprises the nucleus caudalis - a part of the spinal trigeminal nucleus - and superficial layers of the spinal dorsal horns of C1 and C2. Projections towards and from hypothalamus, rostral ventromedial medulla (RVM), dorsolateral pontine tegmentum (DLPT) and peri-aqueductal grey (PAG) are known, as well as the projections towards the cortex, via the trigeminothalamic (or quintothalamic) tract and a passage in the contralateral thalamus (ventral posteromedial nucleus, VPM).

Neuronal activity is determined by electric and synaptic activity, with action potentials, neurotransmitter release and postsynaptic chemical and electrical responses. Neuronal activation stimulates increased glucose consumption. Neuronal glycolysis is necessary to replenish the high-energy molecule adenosine-tri-phosphate (ATP). Pyruvate is produced as a first intermediate molecule. Neurotransmitter release (e.g., the most abundant one: glutamate) into the synaptic cleft excites the postsynaptic neuron and astrocytes extract these neurotransmitters from the synaptic cleft, together with sodium ions. The astrocytes use sodium-potassium pumps on their membrane to restore the transmembrane ion gradients, at the cost of ATP consumption. Therefore, they also possess glucose transporters for glucose uptake from the blood (28). Astrocytic glycolysis produces lactate, which is subsequently shuttled to the neurons for further processing. This is called the astrocyte-neuron lactate shuttle hypothesis (29, 30). There, lactate is first converted to pyruvate. The mitochondria in the neurons are responsible for the pyruvate processing, which leads to ATP production via the tricarboxylic acid (TCA) cycle and oxidative phosphorylation (31). Astrocytes are also involved in the *neurovascular* coupling: the CBF changes related to neuronal activation are influenced by the astrocytes' release of vasoactive compounds, which influence the smooth muscles surrounding the endothelial cells. Conditions of reduced nitric oxide (NO) – an important molecule in migraine research – cause the astrocytes to convert arachidonic acid into eicosanoids and prostaglandins with a vasodilating effect due to smooth muscle relaxation, while elevated NO levels inhibit their production. Arachidonic acid is then processed in smooth muscle cells and converted into eicosanoids with vasoconstriction effects (32).

Glutamate, adenosine, lactate, K^+ , etc. also possess vasoactive properties, both directly and indirectly, via feedback and feedforward mechanisms (33). A detailed description of their mechanism of action and pathways is beyond the scope of this thesis.

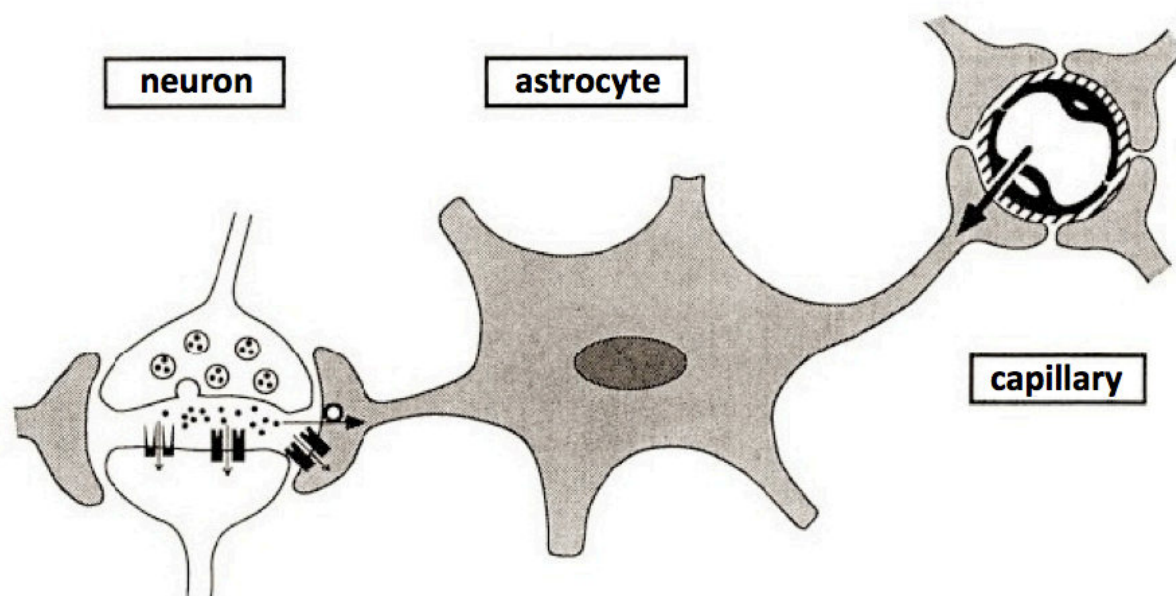


Figure 4 Within the neurovascular unit the astrocyte plays a key role for both clearance of the synaptic cleft after neurotransmitter release and uptake of glucose from capillaries. Adapted from Tsacopoulos et al. (34).

3.3. Genetics

The high prevalence of migraine in certain families suggests that there is a strong hereditary component for migraine in these families. Population-based twin cohort studies confirm this (35-37). In only one subtype of migraine monogenic mutations are linked to the disorder, namely familial hemiplegic migraine (FHM). This rare form of MWA shows an autosomal dominant hereditary pattern. Currently, three gene mutations are identified. The subtypes FHM1, FHM2, and FHM3 are characterized by mutations in *CACNA1A*, encoding the $\alpha 1$ subunit of a neuronal voltage-gated Ca^{2+} -channel (38), *ATP1A2*, encoding the $\alpha 2$ subunit of the Na^+/K^+ -ATPase pump located on astrocytes (39, 40), and *SCN1A*, encoding a neuronal voltage-gated Na^+ -channel (41), respectively. Sometimes, the FHM subtypes are called

channelopathies, because the mechanism can be, at least partly, attributed to defects in these ion channels.

To date, no monogenic forms of migraine could be identified for MwoA, but a variety of gene polymorphisms, most often irreproducible, have been described (42). The contribution of and the interaction between multiple genes is highly likely due to the complexity of migraine pathophysiology. Just recently, three genome-wide association studies (43-45) have reported on genetic susceptibility variants in large migraine populations. Two genetic variants are located within or between genes involved in the homeostasis of the excitatory neurotransmitter glutamate. A third type lies close to a gene coding for a cold and pain sensor, while the role of a fourth variant still remains unclear (46). The presence of particular single nucleotide polymorphisms (SNPs) indicates an increased risk for migraine. However, contrary to migraine-associated gene mutations in FHM, these SNPs are only risk factors and so far, no explicit, direct link to MwoA has been demonstrated (47). Obviously, in the near future, more genetic susceptibility variants either in the nuclear DNA or the mitochondrial DNA, will be discovered that can be linked to migraine pathogenesis.

3.4. The interictal phase

Since migraine is a chronic disorder with episodic manifestations, scientists are looking for interictal, measurable differences between patients with migraine and healthy people, that may (at least partly) explain why migraine patients develop an attack while healthy people remain headache-free when they are exposed to the same triggers and/or conditions.

In the interictal phase, some differences in brain functioning between patients and healthy controls can be demonstrated. In 1995, Schoenen et al. were the first to describe the lack of habituation in patients with migraine, demonstrated with visual evoked potential (VEP)

measurements (48). Habituation is a phenomenon of decreasing response amplitude to repetitive stimulation in healthy controls (49). Migraineurs do not show this phenomenon, on the contrary, even a transient potentiation of their responses has been observed. The lack of habituation in migraine patients of evoked brain potentials (EP) is not exclusively related to VEP measurements, and has been described with other types of stimuli, such as auditory, somatosensory and painful stimuli (reviewed by Coppola et al. (49)), blink reflex (50) and cognitive event-related potentials (51). A hyperventilation study indicated that the lack of habituation in patients with MwoA is worsened through hypocapnia (52).

Competing theories try to explain the lack of electrophysiological habituation. Arguments that the migraine brain is dysexcitable (either hyperexcitable or hypoexcitable), as well as evidence for altered preactivation levels are discussed below.

The migraine brain seems hyperexcitable compared to controls (53-56), leading to potentiation or at least no decreased EP amplitudes. On the other hand, it has been proposed that migraineurs have a malfunction of the intracortical inhibition (57), which would be reflected in the absence of the protective phenomenon habituation. However, both theories have been questioned in many papers. Huang et al. demonstrated some limitations to the hyperexcitability-theory, not fully refuting it (58), while Áfra et al. reported several times on hypoexcitability (59, 60). The same group also argued against reduced intracortical inhibition (61).

This leads to the point of view of the altered preactivation levels in patients. During EP measurements the peak amplitude in the first averaged block is initially lowered compared to controls (62, 63). This indicates that the preactivation levels in migraineurs are decreased, perhaps due to abnormalities in the thalamocortical networks, namely reduced

thalamocortical activation (61, 64) or due to hypoactivation in certain subcortico-cortical serotonergic pathways (65). This hypothesis is supported by the ictal and immediate pre-ictal normalization of EP amplitudes (66).

We want to mention that the interictal lack of habituation in migraineurs is also characterized by a strong familial influence (67), although this finding is based on statistics, not on genetic screening.

Other interictal findings cover haemodynamic abnormalities and NO hypersensitivity, or point towards problems at the level of the energy metabolism.

Interictal transcranial Doppler (TCD) studies reported mostly on increased blood flow mean velocities in cerebral arteries and increased cerebrovascular reactivity to carbon dioxide in migraineurs compared to controls (68-73). Patients are also hypersensitive to NO, e.g. by infusion of glyceryl trinitrate (GTN), a donor of NO (74). Both patients and controls develop a headache immediately after infusion, but patients also develop a delayed headache with migraine characteristics (75, 76).

Several observations in migraine patients are correlated with attack frequency and disorder duration. Although migraine attacks do not cause apparent damage to the brain, some phenomena are more often present or pronounced, (probably) due to repetitive attacks, such as an increased risk for white matter lesions (77), iron accumulations in deep brain nuclei (78, 79) or glucose hypometabolism in selective brain regions involved in the central pain processing (80).

Furthermore, several studies indicate that there might be a problem with the mitochondrial energy metabolism in migraineurs. The group of Montagna did a lot of work on metabolism

in patients with migraine, using muscle biopsy and magnetic resonance spectroscopy (MRS). Besides reports on changes in enzymes involved in the respiratory chain, such as cytochrome c oxidase, mono-amine oxidase and succinate dehydrogenase (81), they also demonstrated low phosphocreatine (PCr) levels and a decreased phosphorylation potential in the interictal migraine brain (82). None of these mitochondrial changes are generalizable to all patients. The hypothesis on metabolism is strengthened by a recent study of our group with ^{31}P -MRS, which demonstrated interictal reductions in adenosine triphosphate (ATP) and – again – PCr concentrations in patients with MwoA compared to controls (83). An attack may originate when triggers provoke an increased demand of the energy metabolism, while the energy reserve is decreased. An imbalance between ATP production and consumption is proposed as a problem in a subgroup of patients. In addition to this, cytosolic free magnesium, which is an essential element in the energy metabolism at the level of ATP synthesis, is found lower in migraineurs, rather as a consequence of the deficient metabolism than as its cause (84).

3.5. The ictal phase

There are three major models explaining the development of a migraine headache: (I) a brainstem dysfunction as the generator of the attacks, (II) CSD, also clinically silent CSD, and (III) a vulnerable cortex due to an increased metabolic strain. The following paragraphs discuss each theory. Figure 5 summarizes the different theories.

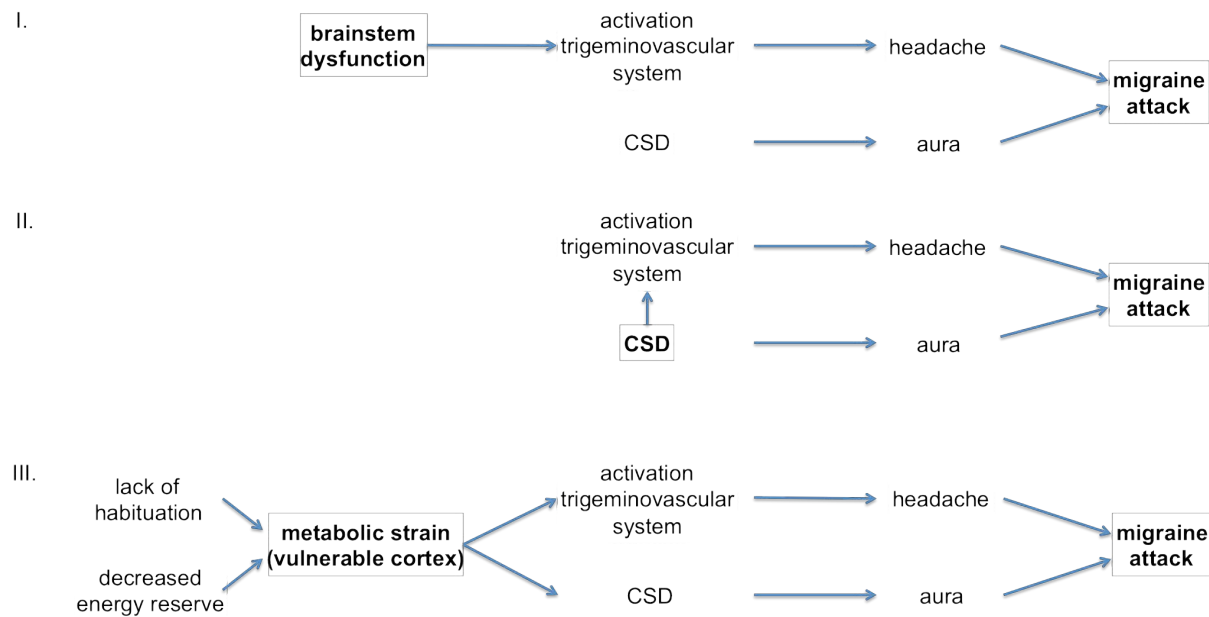


Figure 5 Three models explaining the development of a migraine attack. In each model, the activation of the trigeminovascular system is essential in developing migraine, but the generator is different. In the first model, a brainstem dysfunction activates the TVS (24). CSD is an unrelated, additional event, not integrated in this model. The second theory assigns the key role to CSD (85) with a clinically silent CSD in patients with MwoA. The third model states that a habituation deficit together with a reduced mitochondrial energy reserve contribute to a cortex which is vulnerable to recurrent attacks (86).

I. Brainstem dysfunction

Activation of the TVS plays a key role during a migraine attack (87). Neural events originating in the brainstem give signals to the innervated blood vessels resulting in the release of vasoactive compounds (88, 89). The subsequent vasodilation results in pain perception. Calcitonin gene-related peptide (CGRP) is an example of such a vasoactive substance, which is released upon trigeminal nerve activation. Since CGRP levels are elevated during a migraine attack, CGRP seemed an interesting target for new drugs. CGRP-antagonists are currently being developed for acute migraine treatment (90). NO is another vasoactive substance, which is naturally present throughout the body and produced by NO synthase.

Trigeminal nerve activation causes the synthesis and release of NO in the intracranial blood vessels, which also has a vasodilating effect. In experimental settings, a delayed migraine attack can be induced by oral or intravenous administration of GTN. However, an imaging study could not reveal increases in cerebral or meningeal blood vessel diameter during or between attacks, suggesting that vasodilation is not essentially associated with attacks (91).

In the past, migraine was thought a vascular disorder, solely caused by vasodilation (92), but nowadays, it is commonly accepted that migraine is a complex neurovascular disorder with contributions from both the vascular compartment as well as the neurons and glial tissue. Pain is supposed to be a warning sign that something is wrong, but in patients with migraine the system is activated from time to time without an apparent reason for the alarm system to switch on. Contrary to past assumptions, central structures play a key role in the generation of an attack, rather than peripheral sensory input (93). For example, Welch demonstrated a permanently impaired iron homeostasis in the PAG, suggesting that PAG is a potential generator of migraine attacks by disturbing the normal nociceptive systems (79). This is in line with earlier reports from Weiller et al., showing persistent abnormal activity in brainstem nuclei even after successful acute treatment (94).

II. Cortical Spreading Depression

It was already mentioned that some patients experience an aura (see this chapter's paragraphs 1 and 3.1), which can be defined as sensory or visual perceptions with a gradual character, speech disturbance, etc, often but not exclusively preceding a migraine attack. Electrophysiological as well as perfusion studies revealed an initial, brief phase of increased activity and hyperaemia, followed by a prolonged spreading depression and oligemia (8, 11, 95-97). Several studies hypothesize that this phenomenon occurs in any migraine patient,

albeit often a clinically silent CSD (98-100). Is it possible that the CSD is the initiator of a migraine attack? Two theories argue it is. Since the CSD originates in the occipital cortex, close to the meninges, it is hypothesized that the initial depolarizations stimulate the meninges via their peripheral nociceptors, which in turn activate the TVS. Another point of view is that the CSD eventually reaches the brainstem and causes direct activation of central trigeminovascular neurons (101-104).

III. Vulnerable cortex

In paragraph 3.4, we elaborated both on the lack of habituation in migraineurs and on the decreased mitochondrial energy reserve reflected by altered PCr- and ATP-concentrations. Both phenomena increase the metabolic strain in migraine patients and make the migraine cortex vulnerable to develop attacks (86).

Despite the ictal and interictal findings, a coherent theory to explain the complete migraine neurobiology, culminating into episodic headache attacks, is lacking. Given that several interictal cortical abnormalities are consequently found in many migraine studies, it is obvious that migraine is not only a trigeminovascular problem. Now that the influence of multiple factors and pathways on migraine pathophysiology are discussed, it is reasonable to look at migraine as a “threshold disorder” (Figure 6). Several factors from different perspectives contribute to the vulnerability of a patient. Genetic predisposition through the presence of susceptibility SNPs, or other innate factors such as defects in metabolism, brainstem or thalamocortical circuits, altered haemodynamics, etc. may all influence the migraine threshold. A patient with more predisposing factors will have the lower threshold.

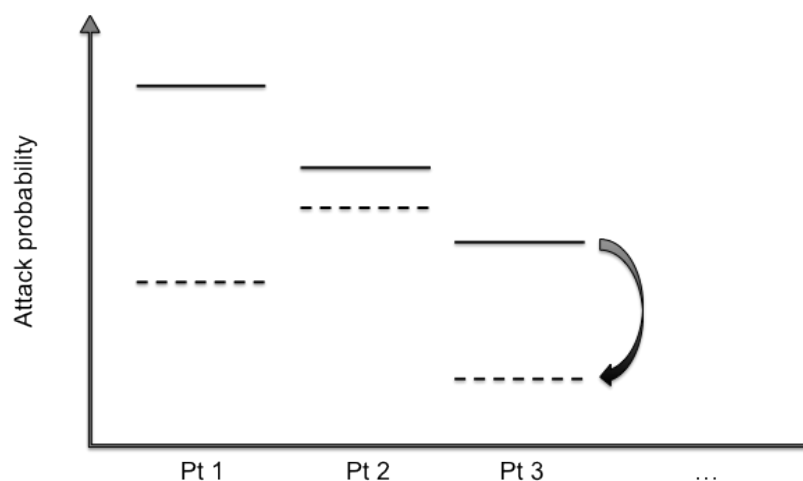


Figure 6 Concept of migraine as a threshold disorder. Genetic predisposition creates variation among patients concerning their threshold to develop a migraine attack (solid lines). Certain factors can temporarily decrease the personal threshold (dashed lines, e.g., hormone levels in female patients), as a result of which patients can be more prone to attacks. The threshold is not fixed within one patient and varies depending on the influencing factors. Finally, triggers (such as sleep deprivation, postponing a meal, etc) can push the patient above his “migraine threshold”.

Within one migraine patient, this threshold is a dynamic phenomenon, e.g., hormone levels in women can change their threshold. Any incidental trigger, such as stress, fasting, sleep disturbances, changing hormone levels, etc, or combinations of triggers may be crucial to exceeding the threshold and, consequently, the development of a migraine attack.

Given that the threshold is dynamic within one patient, a certain trigger will provoke an attack, but under different conditions the same trigger will not cause a threshold exceeding.

Strictly speaking, this concept of “vulnerable cortex” is not part of the ictal phase, but it explains the circumstances in which an attack can develop.

Chapter 2: Imaging in migraine

Several neuroimaging studies have tried to find structural and/or functional abnormalities in migraine patients. Generally speaking, structural imaging reveals no extensive structural changes compared to the normal brain, and review of the literature does not always yield concordant results. Ictal functional changes have been demonstrated with positron emission tomography (PET) and functional magnetic resonance imaging (fMRI) studies. Recently, interictal studies have been published as well.

1. Structural imaging in migraine

Magnetic Resonance Imaging (MRI) is the preferred modality for structural neuroimaging due to excellent soft tissue contrast. The technique itself is described in Chapter 3. Apart from the conventional acquisition sequences, diffusion tensor imaging (DTI) and voxel-based morphometry (VBM) analyses are also used to evaluate the migraine brain.

Since migraine is a primary headache disorder, by definition no major structural abnormalities are found in the migraine brain. Structural imaging is useful to exclude other problems that may cause (migrainous) headache. Yet subtle brain abnormalities are detected more often in migraine patients compared to controls. Many groups report on the increased risk of small cerebral white matter abnormalities (meta-analysis by Swartz et al. (105)) as well as abnormalities in brainstem and cerebellum, presenting as subclinical infarct-like lesions, typically hyperintense on T₂-weighted or FLAIR images (77, 106-111). A population-based MRI study reports on a higher incidence of brain infarcts particularly in the posterior circulation territory of the brain (112). Follow-up of patients suggests that

repeated migraine attacks are the cause of this damage, rather than vice versa (78, 113, 114).

Looking at grey matter changes, there is less concordance in the literature. Matharu et al. performed a VBM study on groups of patients with MWA and MwoA (115). In both patient groups no macroscopic and mesoscopic structural changes could be detected. The findings in this early VBM study are inconsistent with the studies by Rocca et al. (116-118). Both T₂-weighted MRI and DTI were used to detect structural changes in migraineurs. The studies concluded that patients had several areas of reduced grey matter densities, increased density of the PAG in the pons and anomalous mean diffusivity histogram peak heights in their grey matter. Regional grey matter volume loss was also reported by Kim et al. (119), Valfre et al. (120) and Schmidt-Wilke et al. (121). DaSilva et al. observed a lower fractional anisotropy for the ventrolateral PAG, indicating a more isotropic diffusion, due to loss of its microscopic structure (122). Cortical thickness measurements in migraineurs revealed a thicker somatosensory cortex (123) and thickening of motion-processing visual areas (124). On the contrary, recent advanced surface-based morphometry was not able to demonstrate significant differences in grey matter thickness between patients and controls (125).

Alterations in normal appearing brain tissue of migraineurs are probably induced by the repetitive exposure to pain: there is an association between chronic pain disorders, other than migraine, and morphologic grey matter changes (126). Several migraine studies mention a correlation between the amount and extent of abnormalities and attack frequency and duration of the disorder (77, 117, 119, 127).

T₂-weighted MR images can be used to evaluate the in vivo non-haem iron content by calculating R₂ relaxation maps (128). Their values are a measure of local free iron deposition.

Welch et al. (79) mentioned an increase in brain iron accumulation in the PAG of patients with MwoA and MWA. Later on, Kruit et al confirmed iron accumulations in putamen, globus pallidus and red nucleus in relatively young migraineurs (< 50 years)(129). Both studies found a positive correlation with the duration of the disorder, because repeated attacks would facilitate iron depositions.

To conclude, migraine patients are definitely more at risk to develop subclinical brain white matter hyperintensities, posterior circulation infarcts and local brain iron depositions, but it is under debate whether or not patients have grey matter changes more often than controls and what kind of changes they have.

2. Functional imaging in migraine

Structural imaging may show subtle brain abnormalities, e.g., migraineurs are more at risk for white matter lesions (78), however, such findings are not valid for all migraineurs. Imaging is generally non-contributing to the diagnosis (130), because migraine is a primary headache disorder. Several functional imaging techniques provide complementary information about the migraine brain.

2.1. Positron Emission Tomography (PET) and Single-Photon Emission Computed Tomography (SPECT)

PET and SPECT are very sensitive functional imaging techniques. Several PET and SPECT tracers have been used to investigate the brain during and between migraine attacks. The injection of a radiotracer probably limits the initiation of new PET and SPECT studies.

PET studies with ¹⁵O-water have reported increased cerebral blood flow (CBF) in several pain-related structures, brainstem activation and posterior cerebral hypoperfusion during

attacks (94, 100, 131). The brainstem activation persists after acute treatment, while clinical symptoms disappear (94, 132, 133). Dynamic ^{15}O -water PET scans in a patient with MwoA revealed a spreading decrease in CBF, which may be linked to a clinically silent CSD (98). A PET study with three ^{15}O -containing tracers confirmed the ictal decrease in global CBF and cerebral blood volume (CBV), but reported unchanged oxygen metabolism and oxygen extraction (134). An interictal ^{18}F -fluorodeoxyglucose (^{18}F -FDG) PET study revealed hypometabolism in pain-related cerebral regions, such as insula, cingulate cortex and somatosensory cortex (80). However, it should be mentioned that the concept of a “pain matrix”, i.e., a network of cortical regions specific for pain and nociception, is currently under debate, because pain-related regions are also involved in brain activation upon non-painful stimulation (135).

Injection of $^{99\text{m}}\text{Tc}$ -HMPAO or ^{133}Xe , SPECT tracers used to measure CBF, reveal asymmetric, locally impaired perfusion in migraineurs, both ictally (136) and interictally (137, 138).

2.2. Functional Magnetic Resonance Imaging (fMRI)

“Conventional” fMRI experiments are used to uncover those brain areas that are more (or less) actively involved during the execution of a specific task or exposure to a certain stimulus. Consequently, task-related results from fMRI measurements in patients with migraine may reveal brain regions that are significantly different from those seen in controls, either additionally activated regions or regions that do not seem to be activated during that particular task, whereas they are in controls.

To date, only few fMRI studies have been published investigating differences between migraineurs and healthy controls. The ictal phase of visually triggered migraine has been investigated with fMRI by Cao et al. to make inferences about changes in the oxygenation of

the occipital cortex and brainstem structures during the attack (139). In the previous paragraph it was mentioned that PET studies are able to detect ictal brainstem activation. Cao et al. confirmed this and reported additional activated brainstem regions, such as red nucleus and substantia nigra. In addition, a spreading suppression of the occipital cortical activation precedes the increased occipital oxygenation in the ictal phase (95).

These activations are in contrast with the interictal phase. An interictal multimodality study reported decreased activation levels in the visual cortex, which were inversely correlated to the attack frequency of the participating patients (140). Moulton et al. reported interictal brainstem abnormalities in migraineurs: the nucleus cuneiformis, part of a modulatory circuit in the brainstem, was found hypofunctional compared to controls in response to heat stimuli (141).

Recently, interictal resting-state fMRI measurements – which occur in the absence of an external task – revealed abnormal connectivity in several brain networks: increased connectivity was found in primary networks (visual, auditory, sensorimotor) and in the salience network, which these authors define as a network largely overlapping the pain network, while decreased connectivity was found in parts of the default mode network (142). The functional connectivity between the PAG and pathways related to nociception is increased and positively correlated to attack frequency, whereas its connectivity with regions involved in pain modulation is decreased (143).

Finally, the haemodynamic time course itself can be studied in migraineurs using the MR scanner. In an interictal, combined fMRI and DTI study, Rocca et al. compared BOLD-fMRI time courses following a finger flexion - extension task between patients and controls. They

could not detect significant changes in the shape, nor in the haemodynamic signal intensity changes (144).

2.3. Transcranial Doppler (TCD) and near-infrared spectroscopy (NIRS)

Static as well as dynamic cerebral blood properties can be assessed non-invasively. TCD, a technique based on ultrasound, can measure cerebral blood flow velocities, whereas NIRS is used to obtain information on haemoglobin content and oxygenation levels. Although these techniques do not offer images per se, they provide information on the haemodynamic response, described in more detail in Chapter 3.2.

In Chapter 1, it was already mentioned that interictal TCD studies reported mostly on increased blood flow velocities in cerebral arteries and increased cerebrovascular reactivity to carbon dioxide in migraineurs compared to controls (68-73). Analogous to this, Zaletel et al. (145) demonstrated an increase in cerebrovascular coupling in migraineurs using TCD and VEP. A combined TCD and NIRS study was also able to identify an increase in vasomotor reactivity and oxygen haemoglobin saturation in migraineurs (146). Results from NIRS studies are contradictory. Schytz et al. (147) could not identify differences in amplitude nor in latency of response curves during a cognitive task. Another functional NIRS study (148) reports on significantly lower amplitudes of the oxy- and deoxyhaemoglobin response curves in migraineurs compared to controls when performing a breath hold task. However, the latencies are unchanged in the migraine patients. In a more recent NIRS study, Coutts et al. (149) could not demonstrate differences in the amplitude of haemodynamic responses to visual stimuli, but they were able to differentiate between migraineurs and controls due to alterations in the latency of the responses. It should be noted that some of the above-

mentioned studies were performed in patients with MwA only, but obviously, no consensus has been reached so far.

In summary:

- Migraine is a primary disorder, so by definition, no major structural abnormalities are found in migraineurs.
- Epidemiologic studies demonstrate that specific structural imaging findings are associated with migraine patients, e.g., an increased risk for white matter lesions and/or posterior circulation infarcts.
- Several functional imaging studies link their findings to the migraine pathophysiology, such as decreased ATP concentrations, VBM abnormalities, local iron accumulations, etc. Some of them support the theory of a vulnerable cortex, prone to recurrent attacks (see Chapter 1, paragraph 3.5, § III). However, so far, no unifying hypothesis has been formulated.

Chapter 3: functional Magnetic Resonance Imaging (fMRI)

1. From NMR to fMRI: principles

1.1. Nuclear Magnetic Resonance (NMR)

The nuclei of certain atoms with an odd number of protons possess the NMR property: they have both a magnetic and an angular moment. Examples of such atoms are ^1H , ^{13}C , ^{19}F , ^{31}P , etc. Among these, hydrogen, with a single proton in its nucleus, is the most commonly used element in NMR and MRI because it is the most abundant atom in the body. When the term “proton” is used, it refers to a hydrogen proton. The use of the adjective “nuclear” is somewhat misleading and refers to the fact that the atomic nucleus is involved in the magnetic resonance phenomenon, not the surrounding electrons. MRI, based on the NMR principles, is different from the (functional) nuclear imaging techniques PET and SPECT, in which patients are exposed to ionizing radiation.

Protons – and other NMR sensitive nuclei – possess the intrinsic property called spin, due to their magnetic and angular moment. They behave like little magnets. They are randomly oriented in the absence of an external magnetic field and rotate around their axis. The macroscopic net magnetization M of these spins is 0. When a strong external magnetic field B_0 is applied (by convention along the Z-axis), the spins align along the axis of B_0 in a parallel (‘spin up’, lower energy) or antiparallel (‘spin down’, higher energy) state. Most spins cancel each other out, but there is a slight excess of spins (approximately 6 ppm at 1 tesla) in the preferred low-energy state. As a result the net magnetization M is now M_z along the Z-axis. The spins precess around their axis with a certain frequency, the Larmor frequency, which is

proportional to the magnetic field strength and dependent on the type of nucleus. Larmor frequencies are situated in the radiofrequency (RF) range of the electromagnetic spectrum.

When an external RF pulse with this Larmor frequency is sent through a transmit coil, an oscillating magnetic field B_1 is generated, the small excess of spins in the lower-energy state are excited and they will absorb the energy. They change to the high-energy state. Applying this RF pulse also causes a flip of the precession angle. Consequently, the net magnetization flips away from the longitudinal Z-axis and a transverse component M_{XY} arises. Once the RF pulse is switched off, the spins emit the energy with the same resonance frequency while they return to their original low-energy state. These emitted RF signals can be captured with one or more receiver coils positioned in the XY-plane. The net magnetization gradually loses its transverse component and returns to the equilibrium with only the longitudinal component. The spontaneous change of the magnetization over time once the RF pulse is switched off, is called relaxation. The spins in the transverse plane quickly lose their phase coherence due to spin-spin interactions. This fast decay process is called transverse relaxation and is characterized by the time constant T_2 : at time T_2 only 37% of the initial magnetization in the XY plane is left. The recovery of the M_z component is a slower process due to interactions with surrounding molecules (spin-lattice interactions), and is called the longitudinal relaxation, characterized by the time constant T_1 : at time T_1 the magnetization along the Z-axis has recovered for about 63%.

T_1 and T_2 relaxation processes are illustrated in Figure 7.

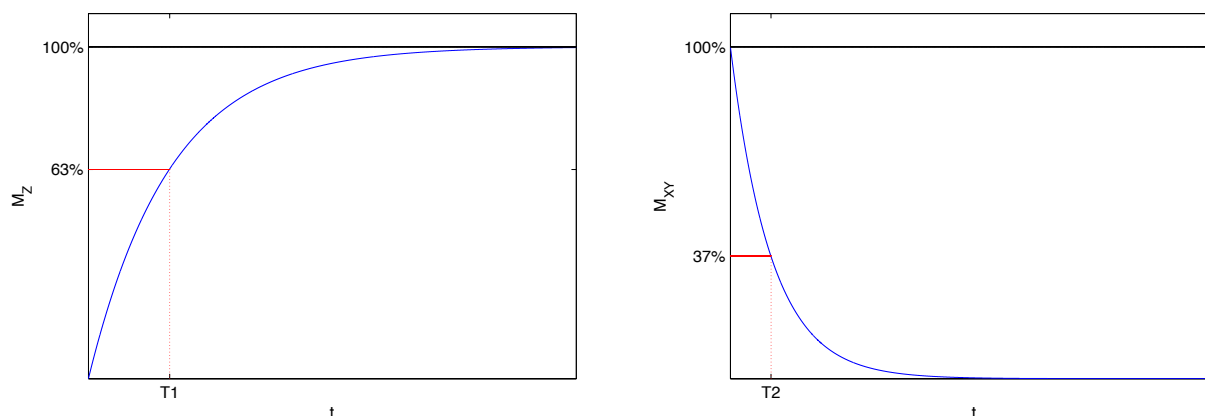


Figure 7 Relaxation processes are exponential processes, characterized by their time constant. Recovery of the macroscopic magnetization along the Z-axis is called longitudinal relaxation or T_1 relaxation (left). Decay of the macroscopic magnetization in the XY plane is called transverse relaxation or T_2 relaxation (right).

Both relaxation constants are field-dependent: T_1 increases with increasing B_0 , while T_2 only slightly decreases with increasing field strength. Furthermore, the time constants are tissue-specific. The proton density in tissue or in a biological sample and the local environment of the spins cause a range of T_1 s and T_2 s (Table 1, Figure 8). This property of tissue composition is used to create contrast differences in images (150).

	T_1 (in ms)	T_2 (in ms)
Brain white matter	830	80
Brain grey matter	1300	100
Cerebrospinal fluid / water	> 4000	> 2000

Table 1 T_1 and T_2 relaxation constants are tissue-specific and dependent on the magnetic field strength; the values given here are indicative at 3 tesla (151).

1.2. Magnetic Resonance Imaging

The amount of (water) protons in a given tissue and their surrounding molecules, thus the tissue composition, will determine the relaxation constants. Contrast in the image is obtained because different tissue types have different T_1 and T_2 values. However, different relaxation constants by themselves are insufficient to create an image. If the spatial origin of the different signals in a complex sample cannot be differentiated, the measured signal would be an inextricable tangle with contributions from all tissue types in the field of view of

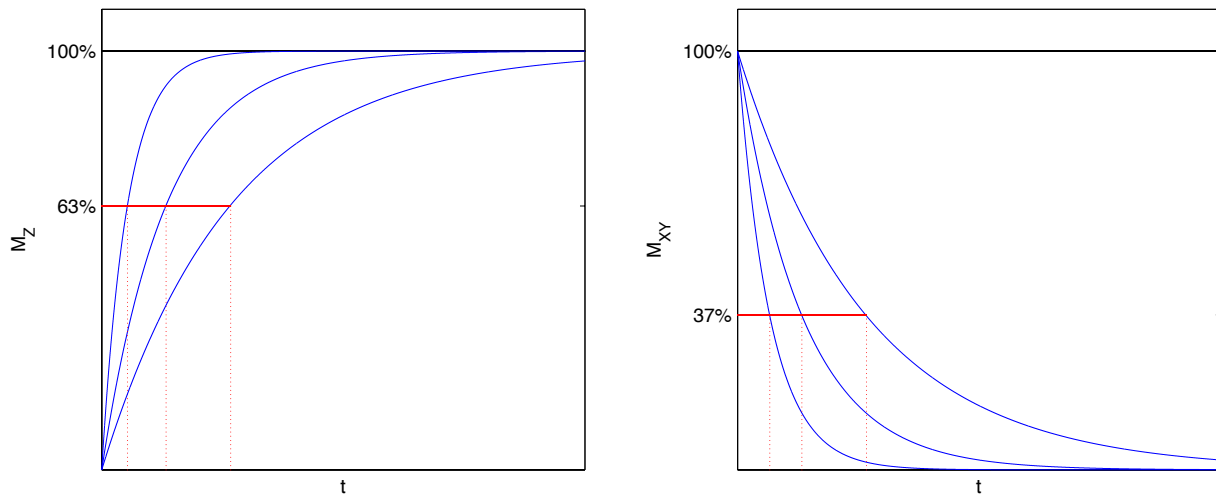


Figure 8 Different tissue types have different T_1 (left part) and T_2 (right part) time constants. Fatty tissues have shorter relaxation constants, whereas tissue types with more free water molecules have slower relaxation constants. These differences are the basis for image contrast, because at a well-chosen point in time (along the X-axis), the magnetization is different for different tissue types.

the system. Spatial localization can be provided by applying gradients in the three directions X (left – right), Y (anterior – posterior) and Z (head – feet). A gradient generates a linear, spatial variation in the magnetic field strength, thereby implicitly changing the corresponding resonance frequencies. The gradient along the longitudinal axis G_z is used for slice selection. Frequency-encoding, obtained by G_x , creates a gradient of frequencies along the left-right axis. Finally, applying a phase-encoding gradient G_y manipulates the phase of the spins along this axis (152).

Previously, transverse magnetization M_{xy} and T_2 relaxation, caused by spin-spin interactions, have been described. The measured signal decays even faster than the T_2 -based signal loss, due to local field inhomogeneities. This decay process is characterized by time constant T_2^* . However, the signal can partly be recalled, taking into account that the T_2 relaxation continues. The dephased spins can be refocussed to obtain an echo by applying a 180 degree RF pulse (spin echo, Figure 9) or applying a particular combination of gradients with opposite polarity (gradient echo). The time between the initial 90 degree RF pulse and the first echo is called the echo time (TE), an important acquisition parameter (153).

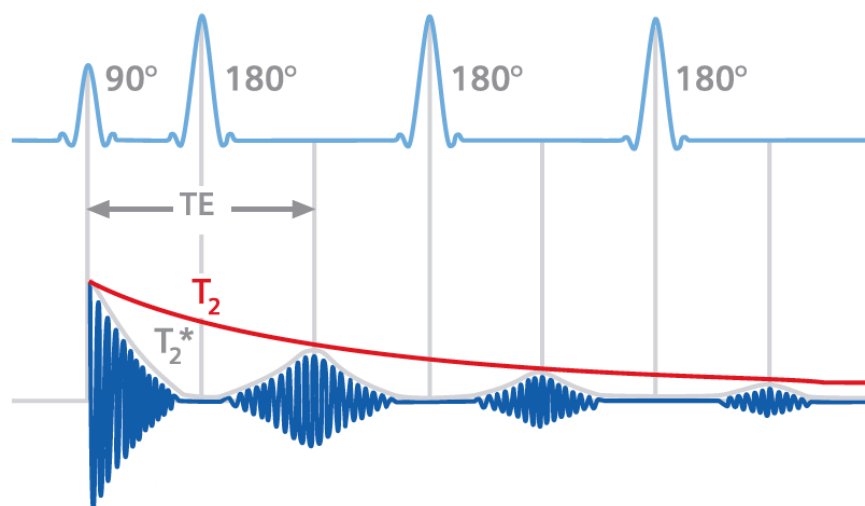


Figure 9 An initial 90 degree RF pulse flips the spins in the transverse plane. The signal measured in the receiver coil(s) placed next to this XY-plane quickly decays due local field inhomogeneities (T_2^*). By applying a 180 degree pulse the dephased spins can regain their phase coherence and regenerate the signal (spin echo), although the maximum signal amplitude of the successive echos also decays due to spin-spin interactions (T_2 relaxation) (150).

The other main parameter for controlling image contrast is the repetition time TR, defined by the time between the (initial) 90 degree pulses. The succession of RF pulses and gradients has to be repeated several times to obtain sufficient signals for image acquisition. TR and TE determine the contrast, the weighting of the image. With a long TR and a short TE, the image contrast is mainly determined by the proton density, i.e. a proton density weighted image. If a long TR is accompanied by a long TE, the influence of the T_2 relaxation is dominant. Images acquired with such parameter settings are T_2 -weighted images. Analogously, images with predominantly information about T_1 values – T_1 -weighted images – are obtained with short TR and short TE (150).

The combination of RF pulses and gradients, necessary for spin excitation, the generation of an echo, spatial localization and read-out of the signal is called a pulse sequence. They are schematically represented in pulse sequence diagrams. An example of a gradient echo (GE) pulse sequence diagram is given in Figure 10. Only one RF pulse is applied to flip the spins 90 degrees in the XY-plane. During the RF pulse a gradient for slice-selection is applied (G_z),

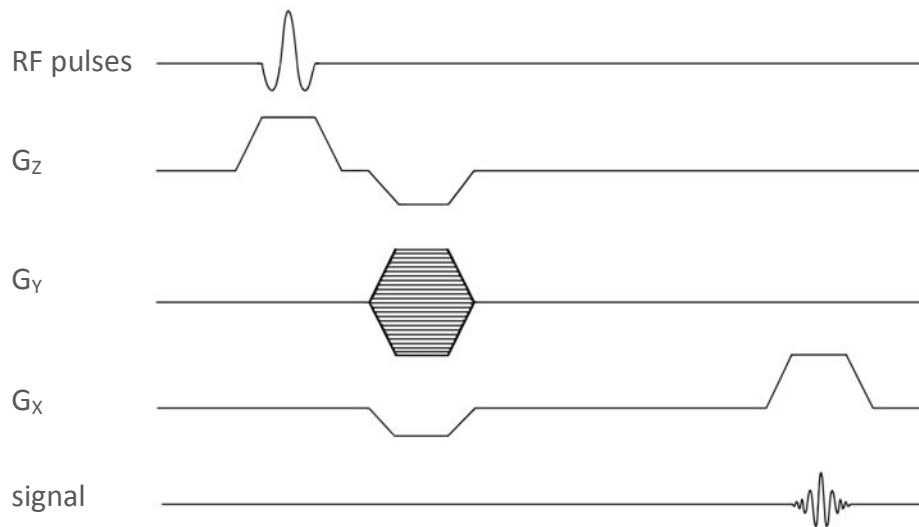


Figure 10 A pulse diagram of a simple gradient echo sequence. RF pulses and gradients applied during one TR are schematically given. Typically there is no 180 degree RF refocussing pulse in GE sequences. The echo is created by applying a rephasing gradient G_x with opposite polarity of the first G_x , yielding a signal that can be read out. After one TR, the cycle is repeated until all phase-encoding steps (different horizontal lines) are acquired.

followed by dephasing of the spins with frequency-encoding gradient G_x and the first phase-encoding step with G_y . The echo, created by applying a rephasing gradient G_x with the opposite polarity of the first G_x , yields a signal that can be read out. In this particular sequence, the cycle is repeated several times until all phase-encoding steps are acquired.

During every repetition the phase-encoding gradient is slightly altered. Total measurement time in this sequence is determined by the TR and the number of phase-encoding steps until all raw data are acquired.

Varying parameter settings (TR, TE, ...) and numerous combinations of RF pulses and gradient switching provide a wide range of pulse sequences with different contrasts, all with their specific applications. A single-shot T_2^* -weighted GE pulse sequence with echo planar imaging (EPI) read-out is an example of a fast imaging sequence often used in fMRI. Contrary to conventional sequences, where one phase-encoding step is acquired per TR, multiple echoes are created after a single excitation. Fast gradient switching and read out allow the collection of all raw data for one image within one TR (154). An example of such a pulse

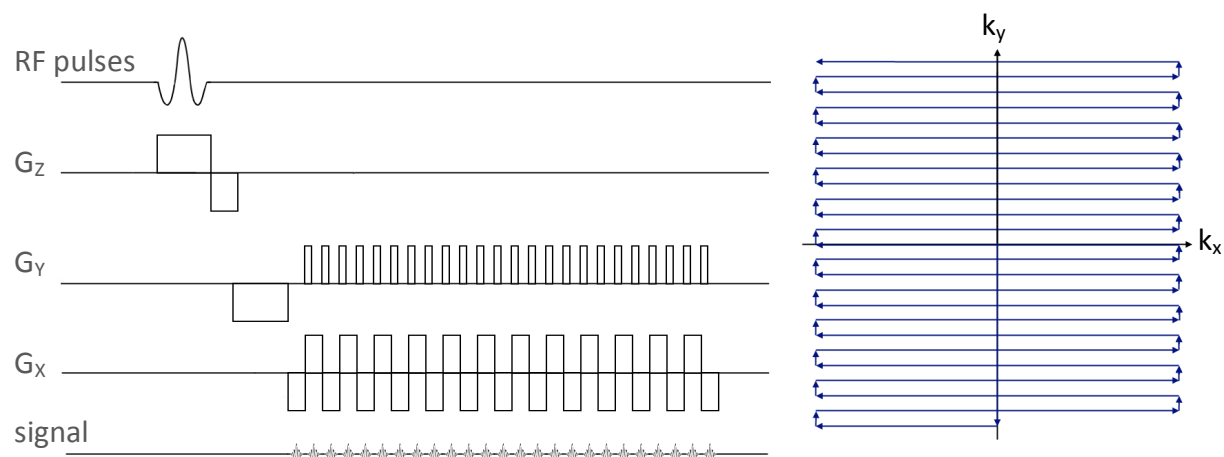


Figure 11 An example of a GE sequence with EPI readout (left). All k-space lines are filled within one TR (right) due to fast gradient switching. T_2^* weighting is obtained by choosing a long TE and long TR. The timing of the middle line, through the center of k-space, determines the (effective) echo time.

diagram is given in Figure 11. The TR is typically long enough to allow multi-slice imaging. As a consequence, images from the whole brain can be acquired within this cycle (typically 1 to 3 seconds). The resulting images have an excellent temporal resolution, but limited spatial resolution (see Figure 12). The application of this kind of T_2^* -weighted sequences is explained in more detail in paragraph 2.

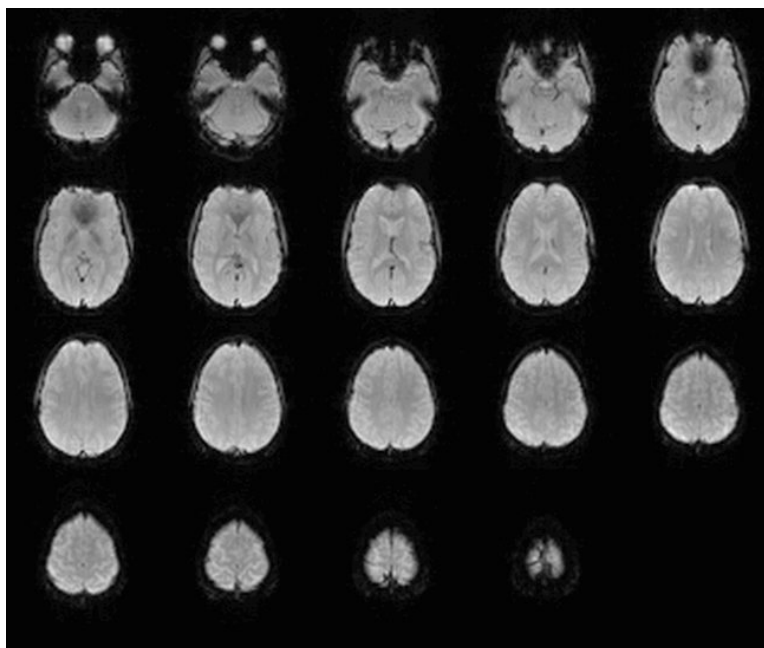


Figure 12 This mosaic image is composed of multiple slices which can cover a whole brain, all acquired during one TR. With a TR of one second, these images have an excellent temporal resolution, but the spatial resolution is rather limited (e.g., in this case: voxel size $3 \times 3 \text{ mm}^2$).

The signals measured with the receiver coil(s) are characterized by their amplitude and frequency. They are amplified and digitized and these raw data are stored in k-space, i.e., the 2D or 3D data matrix in the frequency domain. The information in k-space is reconstructed by a mathematical procedure – an inverse Fourier transformation – to obtain an image (152).

2. The BOLD signal

Besides providing structural information, MRI measurements can also be used to capture signals associated with physiological events. This paragraph explains how or why images provide functional rather than structural information, when they are acquired with T_2^* -weighted GE pulse sequences with EPI read-out.

Brain activity can indirectly be mapped by measuring haemodynamic responses. The main contributors to such responses are local changes in CBF, cerebral blood volume (CBV) and cerebral metabolic rate of oxygen consumption ($CMRO_2$), thereby altering the oxygen extraction fraction (OEF) and the proportion of oxyhaemoglobin in the blood (155, 156). Several invasive and non-invasive measurement techniques can be applied to measure haemodynamic responses, depending on the aim of the observer and desired resolution, either spatial or temporal. One of the possibilities is fMRI with blood-oxygenation-level-dependent (BOLD) contrast, a non-invasive technique providing direct information about the blood oxygenation level (157). The BOLD signal represents the ratio of oxyhaemoglobin to deoxyhaemoglobin. The first is a diamagnetic molecule, i.e. due to the absence of unpaired electrons there is no magnetic moment and hardly interaction with the magnetic field, while the latter is paramagnetic. Fully deoxygenated haemoglobin has sixteen unpaired electrons (four per haem group), resulting in a significant magnetic moment (158). The total amount of oxygen bound to the haem groups in haemoglobin determines the magnetic susceptibility of the molecule, i.e. its ability to become magnetized and change the magnetic field of the surrounding red blood cells. Changes in the oxygenation level of haemoglobin alter the MR relaxation constant T_2^* because the magnetic susceptibility differences provoke diffusion of water through local field gradients (159). Consequently, MRI pulse sequences sensitive to

changes in T_2^* can be used to capture haemodynamic changes associated with brain activity. T_2^* -weighted images, acquired with relatively fast pulse sequences such as GE EPI, are the most commonly used measurements in brain fMRI. Other fMRI techniques are based on changes in diffusion (160), perfusion (161) or extravascular proton density (162), but to date, BOLD is still the most commonly used fMRI technique.

Brain activity is a combination of very fast and slower events. At the neuronal level, the electrical signal changes have temporal properties on the millisecond scale. For example, a visual stimulus – such as a flashing light – provokes a positive potential difference in the primary visual cortex at approximately 100 ms after stimulus onset, flanked by two negative peaks at 75 and 135 ms, respectively. These fast signals can be measured with surface electrodes. In 2001, Logothetis et al. described a link between electrophysiological activity and BOLD signals (163). They measured single-unit activity, multi-unit activity (firing of a single or small group of neurons, respectively), and local field potentials (LFP, generated by postsynaptic activity) simultaneously with BOLD fMRI. During prolonged stimulus presentation the signals of single-unit and multi-unit recordings rapidly returned to baseline, while those of LFP remained elevated, just like the BOLD response. These results show that LFP are good predictors of the BOLD signal and suggest that it is primarily the postsynaptic activity that contributes to the HRF.

BOLD fMRI measurements in the absence of a particular task or stimulus yield data with – at first sight – no particular pattern. In the past, these data were considered as rather noisy and meaningless, however, recent combined fMRI/EEG studies with high spatial and temporal resolution demonstrated that the BOLD fluctuations significantly correspond to the EEG signals. Decomposing the latter signal into different nonoverlapping frequency bands shows

that the strongest, positive correlation with BOLD is found for gamma band oscillations (depending on the study ranging from 30 to 100 Hz) (164). Additionally, Logothetis' group has demonstrated that the fluctuations in these bands are not independent from each other: the relationship between alpha and gamma power is reflected in the amplitude of the BOLD response, whereas the latency of the response reflects the relationship between beta and gamma power (165). The high-frequency oscillations are also present during stimulus presentation. The importance of these gamma band oscillations manifests itself when comparing the BOLD signal to both EPs and the fast oscillations: it seems that the BOLD signal is more closely related to the latter than to the EPs (166).

The BOLD response that accompanies the electrical (and metabolic) activity following a stimulus is relatively slow and is described by the haemodynamic response function (HRF). Generally speaking, the HRF has a response peak at five to eight seconds after stimulus onset and full recovery to the initial baseline signal requires up to twenty-five seconds. These are slow changes compared to the electrical events, but certain measurement methods require signals with these temporal properties. Given the temporal resolution of most (structural) MRI acquisitions, BOLD fMRI measurements with T2*-weighted GE EPI sequences allow relatively fast acquisitions which are capable of gathering sufficient temporal information, to catch the varying signal intensities due to the local oxygenation changes.

It was previously mentioned that several parameters (e.g., CBV, CBF, OEF, ...) contribute to the HRF. A typical HRF in response to a short, single, neuronal stimulus is depicted in Figure 13. Several phases can be distinguished. The first change in the signal after stimulus onset is an early negative response, the initial dip. During this signal reduction, the oxygen extraction fraction is already increased, while the CBV and CBF are still unchanged (167). Due to its

limited duration and amplitude, it was under debate whether or not this dip really existed (168), and still, this initial dip cannot be detected without a proper temporal resolution. The initial dip is followed by the major positive response. Taking into account that the BOLD signal is a ratio with the amount of oxygenated blood in its numerator, the positive signal is an overcompensatory response. The regional increase in CBV and CBF in response to a stimulus is significantly larger than strictly necessary to cover the increased demands. Even with the persistently increased OEF, the local oxygenation level is augmented, causing the positive BOLD signal. It reaches its peak amplitude around five to eight seconds after stimulus onset. At that time, CBF and OEF tend to normalize and the BOLD signal decreases. However, the CBV, which is predominantly determined by the venous fraction of the total blood volume, remains increased for a while. This parameter is the main contributor to the post-stimulus undershoot, the last phase of the HRF. Once the diameter of the venous vessels has normalized, the HRF has fully recovered to its baseline.

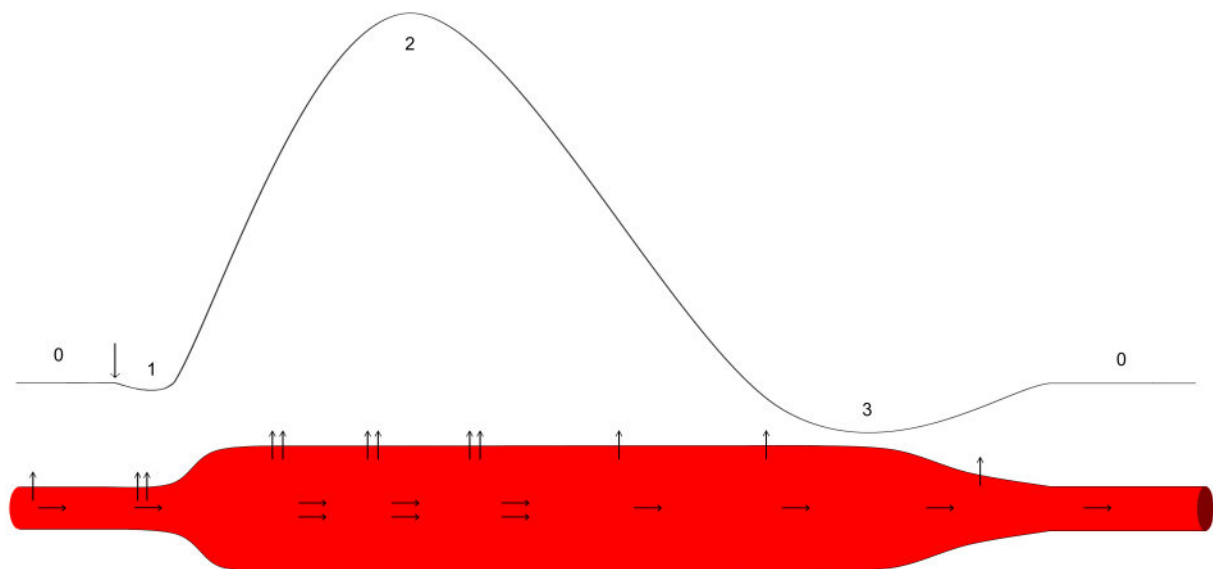


Figure 13 Schematic representation of the relationship between the haemodynamic events in the blood vessel (lower part) and the resulting haemodynamic response function (HRF, upper part) following a single stimulus (arrow down). The phases of the HRF – rest (phase 0), initial dip (phase 1), main response (phase 2) and post-stimulus undershoot (phase 3) – arise from the different timings of the haemodynamic parameter changes. An immediately increased oxygen extraction fraction (arrows up) is the main contributor to the initial dip; the decrease of the response peak is due to a normalizing cerebral blood flow (arrows to the right) and oxygen extraction fraction, while the post-stimulus undershoot is mainly caused by a prolonged increase in cerebral blood volume (blood vessel diameter remains increased).

It is somewhat misleading to talk about “the” HRF. The precise shape and temporal characteristics of the HRF are influenced by several factors, such as sequence-related factors, inter- as well as intrasubject variability, and stimulus-related factors. Voxel size, magnetic field strength and acquisition settings affect the BOLD signal strength, resulting in different HRFs. Intersubject variability is more distinct than intrasubject variability (169). Ageing affects the HRF, both in normal as well as in diseased states, e.g. reduction in resting CBF in healthy elderly (170, 171). Variability in the BOLD signal can partly be attributed to the extent of changes in CBV, CBF and OEF. Alterations in physiological conditions can alter the HRF. For example, CO₂ has a significant effect on the diameter of arterioles, more than on the diameter of the venules. Consequently, the amount of CO₂ in the blood influences the HRF. Hypercapnia can be used to induce increased BOLD responses, by breathholding or breathing a mixture of 5% CO₂ and 95% air or oxygen. The administration of any vasoactive substance can influence the HRF. An example of a commonly used molecule is caffeine, for instance leading to reductions in the time-to-peak of the BOLD signal (172). Given the average half-life of three to seven hours in healthy adults (173), this neurostimulant can affect the “normal” or “baseline” HRF for a long time. Therefore, participants in fMRI studies are sometimes asked to withdraw from caffeine-containing drinks for a certain time.

Depending on the stimulus type (e.g., auditory, visual, somatosensory, etc), different cortical regions are activated, with subtle regional variation in HRF shapes (174, 175). Differences in susceptibility across brain regions contribute to this phenomenon. Vulnerable regions are found in the neighbourhood of marked tissue type changes, e.g. bony structures or air (ear cavities, sinuses). The use of GE EPI sequences might be replaced by SE EPI sequences to avoid signal loss in these regions (176).

The HRF in response to a single stimulus is also largely dependent on stimulus characteristics such as amplitude, rate or frequency, intensity, and features such as luminance or contrast for visual or volume for auditory stimuli (177-179). Among these characteristics, the stimulus duration is a particular one. A shortly presented, single stimulus – often called a pulse stimulus – results in a single HRF. A visual stimulus with an ultrashort duration (even as short as 0.1 ms) can already provoke a HRF (179, 180). Extension of the stimulus duration causes a plateau in the response. In fact, the BOLD response to such a long stimulus is the convolution of a theoretical single HRF – an impulse response function – with the stimulus function. However, it is not always possible to make inferences on the shape of the HRF due to nonlinearities, which are discussed in the next paragraph.

3. Haemodynamic refractory effects and their nonlinearities

The nonlinearity of haemodynamic responses covers two aspects: the shape of the HRF in terms of *stimulus duration* on the one hand, and the shape of a second HRF rapidly following an earlier HRF in terms of the *interstimulus interval* on the other hand. The former is only briefly explained. We focus on the latter type of nonlinearity.

3.1. Effect of stimulus duration

As previously mentioned, the HRF evoked by a stimulus is the result of the convolution of the stimulus function with an impulse response function. This can be a synthetic HRF consisting of, for example, two Gamma functions. When it is assumed that the impulse response function is invariant, irrespective of the stimulus properties, then deconvolving the HRF would result in correct stimulus functions regarding features such as duration and amplitude. However, varying the stimulus duration results in varying HRFs. Investigating the effect of stimulus duration, ranging from a very short duration (millisecond scale) up to a block stimulus of sixteen seconds, was the topic in many studies (178-185). The overall conclusion was that the HRF is nonlinear for short stimulus durations: the impulse response function varies for brief stimuli, with a relatively increased peak amplitude and decreased response width for shorter stimuli. Figure 14 illustrates this type of nonlinearity. In addition, the extent of these nonlinearities is highly dependent on the cortical area. The assumption of linearity is only valid for durations of several seconds: in the auditory cortex for stimuli more than ten seconds, in primary visual cortex for stimuli more than three seconds (182). This type of nonlinearity makes it very difficult to predict the exact HRFs in response to stimuli with different timing properties, which was already observed in the earliest fMRI studies (186).

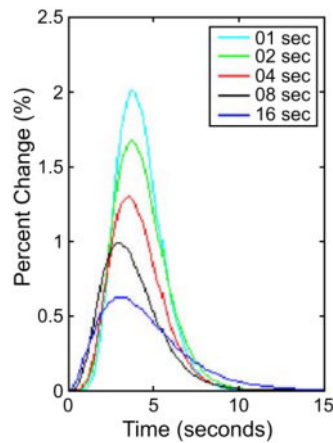


Figure 14 Different impulse functions are elucidated by deconvolving the nonlinear HRFs in response to stimuli with different durations (ranging from 1 up to 16 seconds). Adapted from Soltysik et al. (182).

3.2. Effect of limited interstimulus intervals

The other type of nonlinearity is about the shape of HRFs when stimuli are rapidly succeeding: the additivity of multiple HRFs is temporarily nonlinear as well. Dale and Buckner were one of the earliest researchers investigating the influence of the preceding stimulus on the haemodynamic response to a second visual stimulus with varying interstimulus intervals (ISI) (trials spaced two and five seconds apart) (187). Their results showed a roughly linear additivity for responses to these individual events. However, they also reported subtle departures from this linearity. When the ISI gets shorter, the assumption of linearity is not valid anymore. Despite the minor but consistent nonlinearities, Dale and Buckner held on to the theory of linearity. In their early papers on fMRI analysis Friston et al. assumed linearity of the fMRI response (188), but soon thereafter, they described the interaction over time of two stimuli that are rapidly succeeding and suggested that the haemodynamic response is not fully linear (189). The net haemodynamic response to a second stimulus in an auditory task (with words presented one second apart) was attenuated by the preceding stimulus. This nonlinearity turned out to be dependent on the stimulus presentation rate. Later on, studies were explicitly devoted on investigating the

nonlinearities. Huettel et al. studied the nonlinearity of paired stimuli for ISIs of one, two, four and six seconds (onset-to-onset) using a radial checkerboard pattern (190). Subtraction of the response to a single stimulus (i.e. the reference response) from the overall response reveals the net response to the second stimulus of the pair. For longer ISIs, this net response is identical to the reference response, but linearity disappears for short ISIs. The nonlinear effects, called haemodynamic refractory effects (HREs), are present during a limited refractory period. The extent of the refractory effects is a gradual phenomenon and dependent on the ISI: the amplitude is more attenuated and the delay in the time-to-peak is more pronounced for shorter ISIs. The poststimulus undershoot appears to be less affected. The HREs have nearly disappeared with ISIs of six seconds. The concept of HREs is illustrated in Figure 15.

HREs can also be described in a more quantitative way. Several parameters have to be determined to characterize these signals. Given the limited temporal resolution of the BOLD time series it is necessary to model the HRF to obtain a continuous function, which is then used to derive quantitative data. Many procedures have been developed for the estimation and modeling of the HRF, e.g. Poisson functions (188), Gamma functions (185), extensions to these Gamma functions (including noise and time shifts) (191), and Gaussian functions (192, 193). The SPM software package, for example, uses the canonical HRF which is a linear combination of two Gamma functions (189). Several mathematical models have tried to account for the nonlinearities in particular, because this would substantially increase the sensitivity of rapid event-related fMRI analyses (194), but the extent of those refractory BOLD effects have mostly been described qualitatively (185, 195, 196). In 2007, Lindquist and Wager have developed an algorithm comprising three inverse logit functions to fit HRFs (197).

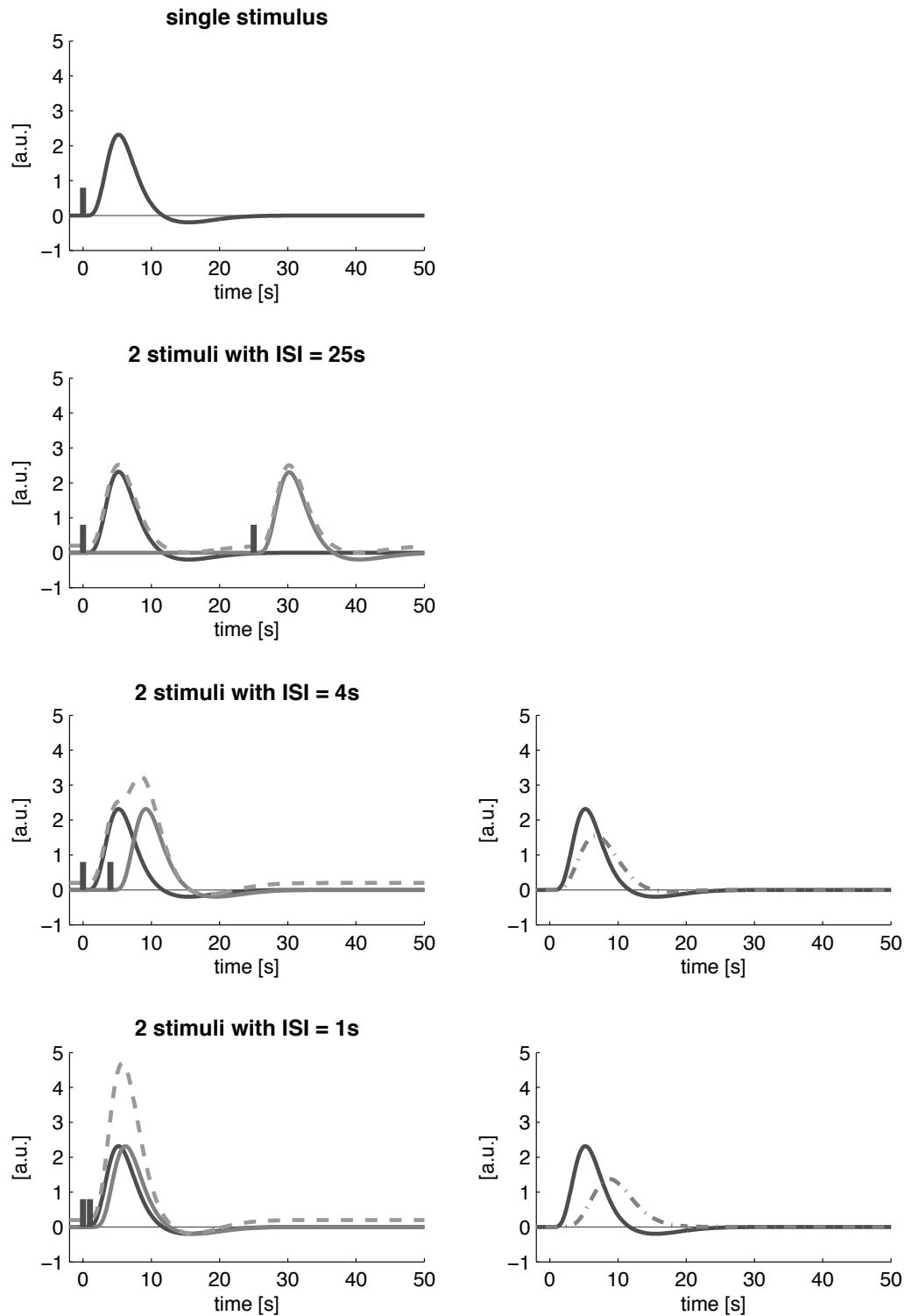


Figure 15 Haemodynamic refractory effects: the theoretical BOLD response to one (upper plot) or two stimuli with varying interstimulus intervals is illustrated on the left. Two separate, identical stimuli (with interstimulus interval > 20 seconds) provoke separate responses (second plot). When the interstimulus interval gets shorter, the responses are summed (third and fourth plot). In the left panel, the responses are linearly summed (dashed line): refractory effects are not taken into account. The right panel illustrates the nonlinear additivity of HRFs in healthy volunteers: for short interstimulus intervals the net response to the second stimulus in a pair is decreased in amplitude and delayed compared to the response to a single, isolated stimulus. Stimulus onsets are depicted in grey bars. The summed responses on the left are shifted 0.2 arbitrary units upwards for reasons of clarity.

To evaluate and quantify HREs, it is important to use a model in which data are not too much forced into a predetermined framework with constraints regarding timing and shape. Lindquist and Wager's method has no constraints concerning timing and comparison of their method with other methods using synthetic data yielded better results (198).

Once the data points of the HRFs are fitted with a continuous function, the following parameters may be calculated for characterization: peak amplitude, latency of the peak or time-to-peak, peak width measured at half of the peak amplitude (FWHM) and the latency of this FWHM or time-to-half-peak (Figure 16). During the refractory period, these parameters change as follows: amplitude decreases, time-to-peak and time-to-half peak increase and peak width decreases as well.

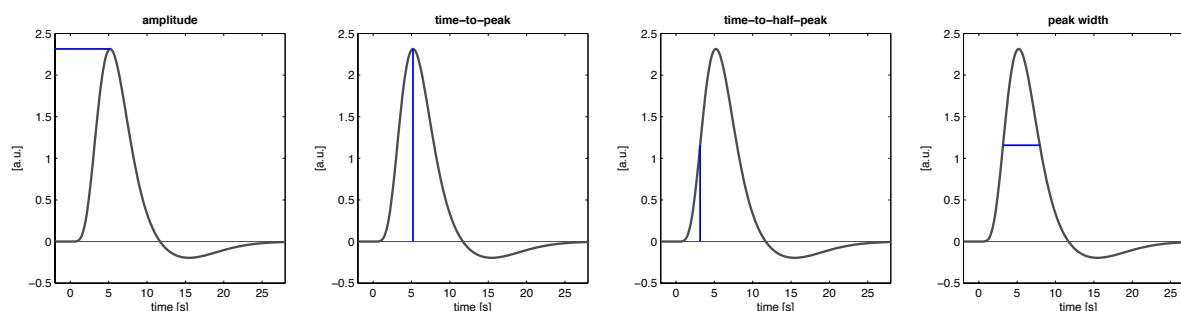


Figure 16 Four parameters typically measured to characterize HRFs: peak amplitude, peak latency or time-to-peak, latency of rise (measured at half of the maximum peak height, FWHM), and peak width (measured at FWHM).

Nearly all studies on BOLD haemodynamics are group studies, either to increase signal-to-noise ratios because data were collected at lower field strengths, or to cancel out noise, inherent to the signal type. However, when someone is interested to measure HRFs and refractory effects at the single-subject level, both in healthy volunteers or patients, it is necessary to use a reliable and robust fitting and quantification method, not prone to generalizing algorithms, risking smoothed data with loss of information.

On the neuronal level, effects resembling the HREs have been described: it is shown by means of EPs that neuronal adaptation (also referred to as repetition suppression) appears

when subjects are exposed to repeated stimuli. Given the close – albeit not exactly known – relationship between the neuronal and the vascular compartment, this neuronal repetition suppression is supposed to play a role in the origin of these refractory effects: neurons tend to decrease their activation when exposed to repeated stimuli, so does the haemodynamic response. Grill-Spector et al. reviewed the three theories that explain this increased neuronal efficiency (199). We briefly summarize them.

- The fatigue model: stimulus-responsive neurons show a mean proportional decrease in firing amplitude; they respond less due to a learning effect;
- The sharpening model: fewer neurons respond to perform the repeated task;
- The facilitation model: it costs less effort for neurons to respond to repeated stimulation, resulting in a reduced processing time (decreased latency or decreased duration of neuronal activation).

Although the repetition suppression is very likely, it is very difficult to attribute the haemodynamic events to one of these models (or potential other theories).

Other observations indirectly support the relationship between electrical and haemodynamic signals: the recently identified correlation between VEP and gamma band activity suggests their potential mediating role in the relationship between VEP and BOLD (200). Thus, VEP habituation may be a significant contributor to the HREs. However, it should not be overlooked that there are a couple of other contributors to the HRF, which potentially play a role in the origin of refractory effects, e.g., vascular changes during repeated stimulation: sustained neuronal activation, albeit discontinuous due to short ISIs, will cause a gradually increased amount of oxyhaemoglobin in the venous compartment, which considerably and continuously contributes to the BOLD signal. Furthermore, it is unclear

which metabolic messengers are involved in the HREs, nor where and when they are released.

Although BOLD haemodynamics have elaborately been studied, the precise mechanism of the nonlinearities remains unclear. Moreover, it is difficult to track the precise relationship between BOLD HREs and several electrophysiological observations, due to the characteristics and limitations of techniques involved in this research area.

Part 2 – Research work

Chapter 4: Aims of the research

Several structural and functional anomalies in the interical brain of patients with MwoA have already been described in the literature. However, until now, HREs have not been the object of study. Nevertheless, it is tempting as well as obvious to investigate whether haemodynamic anomalies can be measured in migraineurs, analogous the lack of habituation in the electrical signaling, assuming that healthy volunteers show both habituation in electrical signalling and HREs for short ISIs.

The first research objective is to develop a method to measure and quantify haemodynamic signals at the single-subject level for obtaining useful information from the particular subject. Performing all analysis steps at the single-subject level is necessary to provide insight into individual patient data rather than grouped data, to study certain disease states of the brain (including headache disorders) or pharmacological responses. Special notice will have to be taken for the choice of a proper fitting algorithm, to optimize information extraction from one data set, without forcing the data into any standardized model.

The second research objective is to apply the method on real patient data. Patient selection will have to occur on the basis of stringent inclusion criteria to create a homogeneous MwoA patient group. The patient data will be compared with reference data. It is hypothesized that patients lack HREs, given these patients' lack of habituation in EPs. Although HRFs and EPs are different types of signals (temporal characteristics, origin, contributing parameters), both types of time courses might be affected in patents with MwoA.

On the day of the fMRI-measurements, patients first underwent a resting MRS protocol to quantify several ^1H - and ^{31}P -metabolites. The aim of these measurements was to identify differences between patients with MwoA and controls using an absolute quantification strategy. MRS results were separately communicated in two peer-reviewed articles, which are part of Harmen Reyngoudt's PhD thesis (201).

The final aim of the current research was to investigate whether data from patients with MwoA are sufficiently different from controls: can a single-subject data set be used to determine – with high sensitivity and specificity – whether the scanned subject is a migraineur or not? This would imply that a set of MR measurements could derive parameters serving as a biomarker for MwoA. For this purpose the fMRI data will be combined with the metabolic data, obtained with MRS measurements in the same participants.

Chapter 5: Results

In this chapter, we summarize the results of the research work.

First, we elaborate on the methodology to determine the extent of HREs. Data acquisition, extraction, fitting and quantification at the single-subject level are described in detail.

Subsequently, we apply the method to a group of 21 patients with MwoA. The results are compared with healthy controls and we investigate the relationship between the findings and relevant literature.

For results of the MRS studies, performed with the same patient and reference population on the same day of the fMRI measurements, we refer to Appendix B (page 141) and C (page 159).

Finally, combining the results of both the haemodynamic (fMRI) and metabolic (MRS) studies is discussed in this chapter. A scientific communication concerning these findings is in preparation.

1. Quantifying haemodynamic refractory BOLD effects in normal subjects at the single-subject level using an inverse logit fitting procedure

Benedicte Descamps, Pieter Vandemaele, Harmen Reyngoudt, Karel Deblaere, Luc Leybaert, Koen Paemeleire, Eric Achten

J Magn Reson Imaging 2012, 35(3):723-30.

Original Research

Quantifying Hemodynamic Refractory BOLD Effects in Normal Subjects at the Single-Subject Level Using an Inverse Logit Fitting Procedure

Benedicte Descamps, MS,^{1,2*} Pieter Vandemaele, MS,^{1,2} Harmen Reyngoudt, MS, PhD,^{1,2} Karel Deblaere, MD, PhD,^{1,2} Luc Leybaert, MD, PhD,³ Koen Paemeleire, MD, PhD,^{3,4} and Eric Achten, MD, PhD^{1,2}

Purpose: To evaluate whether hemodynamic refractory effects provoked by repeated visual stimulation can be detected and quantified at the single-subject level using a recently described hemodynamic response function (HRF) fitting algorithm.

Materials and Methods: Hemodynamic refractory effects were induced with an easily applicable functional MRI (fMRI) paradigm. A fitting method with inverse logit (IL) functions was applied to quantify net HRFs at the single-subject level with three interstimulus intervals (ISI; 1, 2, and 6 s). The model yielded amplitude, latencies, and width for each HRF.

Results: HRF fitting was possible in 44 of 51 healthy volunteers, with excellent goodness-of-fit ($R^2 = 0.9745 \pm 0.0241$). Refractory effects were most pronounced for the 1-s ISI ($P < 0.001$) and had nearly disappeared for the 6-s ISI.

Conclusion: Quantifying refractory effects in individuals was possible in 86.3% of normal subjects using the IL fitting algorithm. This setup may be suitable to explore such effects in individual patients.

Key Words: BOLD-fMRI; hemodynamic response; refractory effects; single-subject quantification; adaptation

J. Magn. Reson. Imaging 2012;35:723-730.

© 2011 Wiley Periodicals, Inc.

BRAIN ACTIVITY CAN be mapped by measuring hemodynamic responses. One modality able to measure hemodynamic responses is functional MRI (fMRI), a noninvasive technique that provides direct information regarding blood oxygenation level, with signal contributions from local changes in cerebral blood flow, cerebral blood volume, and cerebral metabolic rate of oxygen consumption altering the oxygen extraction fraction and oxygenation level. The change in oxygenation level can be captured by MRI pulse sequences sensitive to blood-oxygenation-level-dependent (BOLD) contrast (1,2).

The hemodynamic response function (HRF) to a single, short, neuronal stimulus has a typical shape in which three major phases can be distinguished. The increase in the response leads to a response peak at 5–8 s (phase 1), followed by a decrease leading to a minimum below baseline (phase 2), and finally a recovery phase to baseline (phase 3). Full recovery to the initial baseline signal requires at least 20 s after presentation of a short-duration stimulus. The overall HRF to a succession of short neuronal stimuli is the summation of the HRFs of individual stimuli. When successive neuronal stimuli are roughly more than 6 s apart, i.e., when the interstimulus interval (ISI) is more than 6 s, the individual HRFs tend to be identical, whereas as the ISI becomes shorter, a clear attenuation of the successive HRFs has been described by several authors (3–5).

The study of such refractory effects, or hemodynamic adaptation, is used in neurocognitive research to explain the strategies used by the brain or to elucidate neural networks (6,7). Studying neural adaptation through refractory effects may also be of interest in certain disease states of the brain including epilepsy (8), headache disorders (9), and vascular dementia (10). To be useful in investigating these diseases, fMRI must provide insight into individual patient data (i.e., at the single-subject level). fMRI studies investigating refractory effects often use stimuli that activate a primary cortex, but the effects of repetitive stimulation have also been observed and

¹Department of Radiology and Nuclear Medicine, Ghent University, Ghent, Belgium.

²Ghent Institute for Functional and Metabolic Imaging (GfMI), Ghent University, Ghent, Belgium.

³Department of Basic Medical Sciences, Ghent University, Ghent, Belgium.

⁴Department of Neurology, Ghent University Hospital, Ghent, Belgium. Contract grant sponsor: Flemish Agency for Innovation by Science and Technology (IWT-Vlaanderen); Contract grant number: SB-51437/53437.

*Address reprint requests to: B.D., Ghent University, De Pintelaan 185, 9000 Ghent, Belgium. E-mail: benedicte.descamps@ugent.be

Received December 17, 2010; Accepted September 29, 2011.

DOI 10.1002/jmri.22868

View this article online at wileyonlinelibrary.com.

studied in higher-order cortical regions (e.g., face recognition areas (11)).

HRF shape is influenced by several factors including stimulus type (e.g., auditory, visual, somatosensory, motor), stimulus amplitude, stimulus rate, stimulus duration (12–17), and the brain region of interest (5,11), but is fairly consistent if these factors are kept constant. Fitting of BOLD responses is essential for quantification, and many studies have proposed procedures for HRF estimation and modeling, including Poisson functions (18), gamma functions (19), and Gaussian functions (20,21). In 2007, Lindquist and Wager (22) developed an algorithm comprising three inverse logit (IL) functions to fit HRFs, each corresponding to one of the HRF phases specified above. Lindquist and Wager compared their new method with other common models using simulated data based on empirical HRFs and concluded that the IL model was more suitable for fitting because it determines characterizing parameters with less error compared with other models, while preserving sufficient power and user flexibility (23).

To date, refractory effects have not been quantified at the single-subject level using the IL fitting algorithm. In the interest of acquiring single-subject data for patient studies, the aim of this work was to examine the usefulness of the IL model of Lindquist and Wager to quantify the extent of individual refractory effects in BOLD time series from the fusiform face area (FFA) (24) in normal subjects.

MATERIALS AND METHODS

Subjects

Fifty-one healthy volunteers (17 males) aged 29.8 ± 11.6 (mean \pm SD) years, participated in this study. The study was approved by the local Ethics Committee, and all participants provided written informed consent. Subjects were asked to abstain from caffeine the day of the examination.

Imaging

A 3 Tesla (T) Siemens Trio Tim system (Siemens AG, Erlangen, Germany) with an eight-channel head coil was used for image acquisition. Anatomical images were acquired using a T1-weighted sequence (MPRAGE) with isotropic voxels (voxel size $0.9 \times 0.9 \times 0.9$ mm³, repetition time (TR) = 1550 ms, echo time (TE) = 2.39 ms, matrix 256×256 , three-dimensional (3D) slab with 176 slices). For functional imaging, a T2*-weighted echo planar sequence was used, which is sensitive to BOLD contrast (voxel size $3.5 \times 3.5 \times 5.0$ mm³, TR = 1000 ms, TE = 27 ms, matrix 64×64 , 19 slices). Total protocol scanning time was 45 min 57 s and included two functional measurements: a localizer and the main experiment. All stimuli for these measurements were presented through MR-compatible goggles (Resonance Technology Inc., Los Angeles, CA) to minimize the possibility of eye movement.

Functional Localizer

To localize the subject-specific FFA (24), a block-designed visual paradigm was used (functional localizer) consisting of alternating blocks of faces, scenes, and a baseline rest condition with fixation cross hair (4×3 blocks of 16 s). Subjects were instructed to simply look at the stimuli.

Main Experiment

An event-related visual paradigm incorporating a one-back task was selected for the main experiment. Stimuli consisted of images of male faces presented for 500 ms. During the ISIs, a fixation cross-hair was presented. The face stimuli were smoothly blurred along the contours so that only the internal features of the face were visible to ensure that face-selective areas were activated (25). Subjects were instructed to look at the face images or the cross hair without moving their heads and to press a button if the present face was identical to the previous face (oddball). Subjects were also instructed that the ISI would be variable, between 1 and 26 s. Figure 1 shows the paradigm and timing used. Within the paradigm, four conditions could be distinguished. A single face followed by a 26-s rest served as reference condition (REF), and for the other three conditions faces were shown in pairs with 1-, 2-, or 6-s ISI (onset-to-onset; 1S, 2S, and 6S, respectively) and a 20-s rest before a new face was presented. The duration of REF was chosen to be equal to the total duration of the 6S condition (i.e., 26 s) to generate sufficient data for the subtraction step.

Five consecutive sessions of 7 min 38 s were acquired, with 19 trials per session of which three were oddball trials to ensure subjects' attention. All faces were different except for the faces in the oddball trials. For the one-back task, subjects were instructed to press a button when the current face was exactly the same as the previous face. The design was randomized for every subject to avoid a potential ordering effect.

Analysis

Preprocessing steps were performed on all data in SPM5 and included slice timing correction, realignment, coregistration of anatomy to functional images, spatial normalization to the MNI template (1- and 3-mm isotropic voxels for anatomical and functional images, respectively) (26), and spatial Gaussian smoothing (8-mm kernel). Preprocessed data from the functional localizer were further analyzed in SPM5 and provided information for defining the FFA as a region of interest (ROI). The ROI was derived for each individual participant. A mask image was created as the intersection of the fusiform gyrus, selected with the WFU PickAtlas (27,28), and the spmT image for the contrast "*faces* > (*scenes* & *rest*). Only those voxels with a *t* value higher than 80% of the maximum *t* value within this mask image were selected for further analysis.

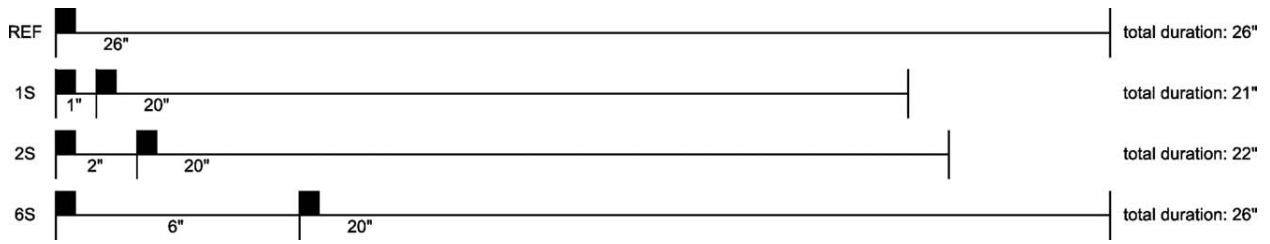


Figure 1. This diagram represents the four conditions: one reference condition (REF) and three paired trial types (1S, 2S, and 6S). Stimulus duration was 500 ms. Interstimulus and poststimulus intervals were measured onset-to-onset.

The smoothed images of the main experiment were analyzed with software built in-house and written in Matlab (The MathWorks, Inc.). Trials from the main experiment were excluded from analysis if subjects had pressed the button during that trial, to avoid a potential confounding effect caused by the motor response. If the subject had not pressed the button at all during a particular session, the subject was considered inattentive, and the entire session was excluded from further analysis. For each subject, several input parameters were required: (i) the random trial order for each of the five sessions for that particular subject, (ii) the trials and sessions to exclude, and (iii) the subject-specific ROI. Time courses from the selected voxels were averaged. Three data points before the presentation of every trial were used to calculate the baseline signal. This baseline calculation was repeated for every session to avoid the effect of intersession variations such as scanner drift. The baseline-corrected trials from each condition were averaged over all sessions.

Normalization was then performed by calculating percent signal changes for all conditions. Subsequently, the normalized mean response to REF was subtracted from the responses to the three paired conditions 1S, 2S, and 6S, yielding the net response to the second stimulus of the pair. For each participant, raw data with the hemodynamic responses both before and after subtraction were plotted and visually inspected. Plots of raw data revealed the additivity of the hemodynamic responses, whereas plots of the subtracted, net responses provided information on the quality of each subject's responses and a first indication of whether the net responses were linear. Only datasets of good quality, i.e., where the three HRF phases could clearly be discerned, were suitable for application of the fitting algorithm. Participants with fitted responses are referred to as "responders".

The net HRFs, four time series per subject, were semi-automatically fitted using a linear combination of three inverse logit functions (22,23):

$$h(t) = d_1 * \frac{e^{(A_1 * (t-T_1))}}{1 + e^{(A_1 * (t-T_1))}} + d_2 * \frac{e^{(A_2 * (t-T_2))}}{1 + e^{(A_2 * (t-T_2))}} + d_3 * \frac{e^{(A_3 * (t-T_3))}}{1 + e^{(A_3 * (t-T_3))}} \quad (1)$$

These three terms model the three phases of the HRF: the rising slope, the falling slope, and the recovery from undershoot, respectively. The fitting algo-

rithm requires seven parameters: angle of the slope (A_1), time-to-half-peak (T_1), and maximum amplitude (d_1) for the first IL function; angle of the slope (A_2, A_3) and time-to-half-peak (T_2, T_3) for both the second and third term; and d_2 and d_3 calculated in accordance with restrictions inherent to the algorithm (22). The initial fit was obtained with a set of seven predetermined values for these parameters and was visually evaluated and manually fine-tuned by applying subtle changes to the initial predetermined parameters. The goodness-of-fit was then determined for the interval containing the data points used in the subsequent parameter calculation. This validation was carried out by calculating the coefficient of determination R^2 :

$$R^2 = 1 - \frac{SS_{res}}{SS_{tot}} \quad (2)$$

$$\text{with } SS_{res} = \sum (y_i - \hat{y}_i)^2 \quad (3)$$

$$\text{and } SS_{tot} = \sum (y_i - \bar{y})^2 \quad (4)$$

where SS_{res} is the sum of squares of the residuals, SS_{tot} is the total sum of squares, y_i is the observed value, \hat{y}_i the estimated value, and \bar{y} the averaged value. For each properly fitted HRF, four parameters

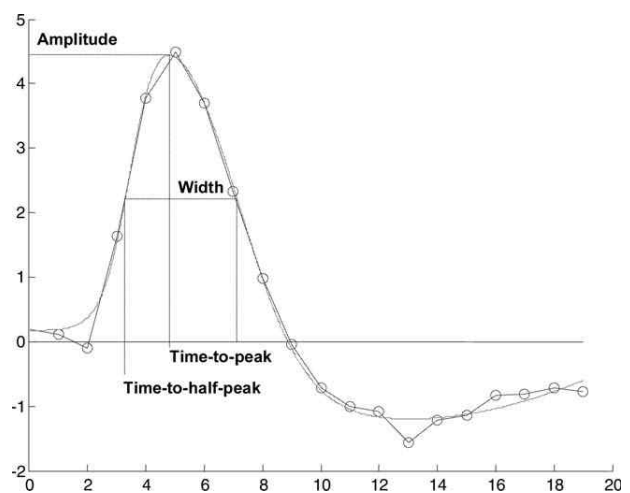


Figure 2. The fitted function is used for the calculation of the maximum amplitude, time-to-peak, time-to-half-peak measured at FWHM, and peak width. Note that fitting of all three phases is essential to ensure a reliable HRF parameter calculation, although this calculation is based on the fit of the first two phases.

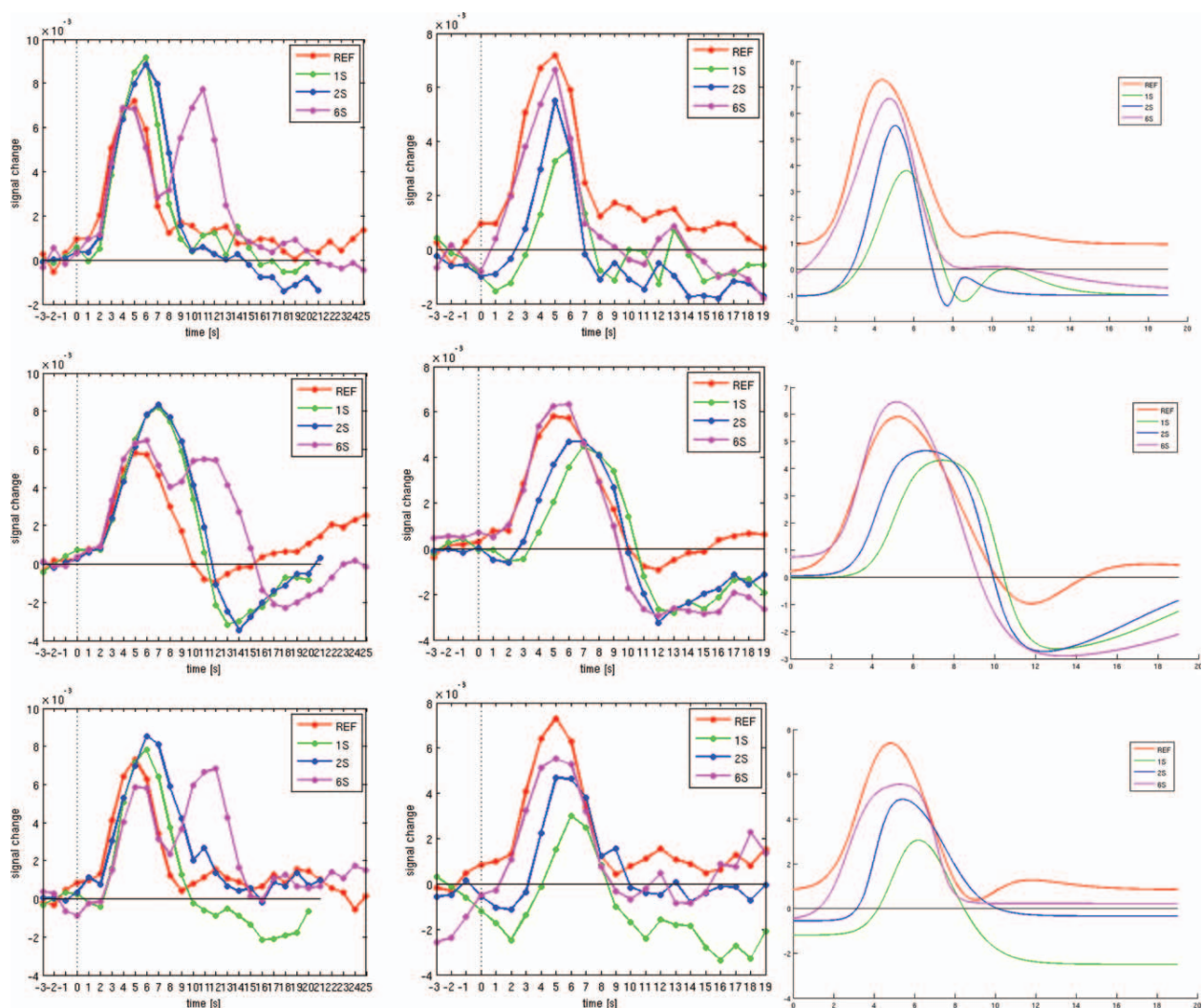


Figure 3. Time-courses from three subjects are shown, with responses to the four conditions (REF, 1S, 2S, 6S) both before (left) and after (middle) subtraction of the reference response. The fitted responses (right) were used to derive the characteristic parameters (amplitude, time-to-peak, time-to-half-peak, and peak width). The first three data points were used to calculate the baseline signal and omitted in the fitted plots. Note the wide variety of shapes across individuals.

were automatically calculated based on the fitted curve: maximum amplitude, latency in time-to-peak, latency in time-to-half-peak measured at full width at half maximum (FWHM), and peak width (see Fig. 2 for an example). Although only the first two phases of the fit may seem necessary for the calculation of the parameters, fitting of all three phases is absolutely essential to obtain the calculated values, because the third phase actively contributes to a reliable overall fit.

Absolute and relative differences in the parameters relative to the REF condition were calculated. The single-subject results were used to draw general conclusions about refractory effects in our group of healthy participants. An analysis of variance (ANOVA, repeated measures design) was applied to the absolute values for the four parameters using IBM SPSS Statistics 18. For each parameter, ANOVA tests were also used for the relative differences to identify statistically significant differences between the four condi-

tions. Bonferroni tests were used for multiple comparisons in the post hoc analysis to determine the ISI means that differed. The correlation between the number of included trials for a certain subject and the number of his/her fitted responses was investigated with Pearson's correlation. Results with P values less than 0.05 were considered to be significant.

RESULTS

On average, 72 ± 1.5 (mean \pm SEM) trials per subject (89.7%) were included (range: 45–80 trials). In four subjects, at least one entire session was omitted due to the absence of button presses; in seven subjects, at least two entire sessions were omitted.

In total, 161 of the 204 time series were fitted (78.9%). The mean R^2 for these fits was 0.9745 ± 0.0241 (mean \pm SD). Specifically, in data from 29 participants all four curves were fitted, and partial

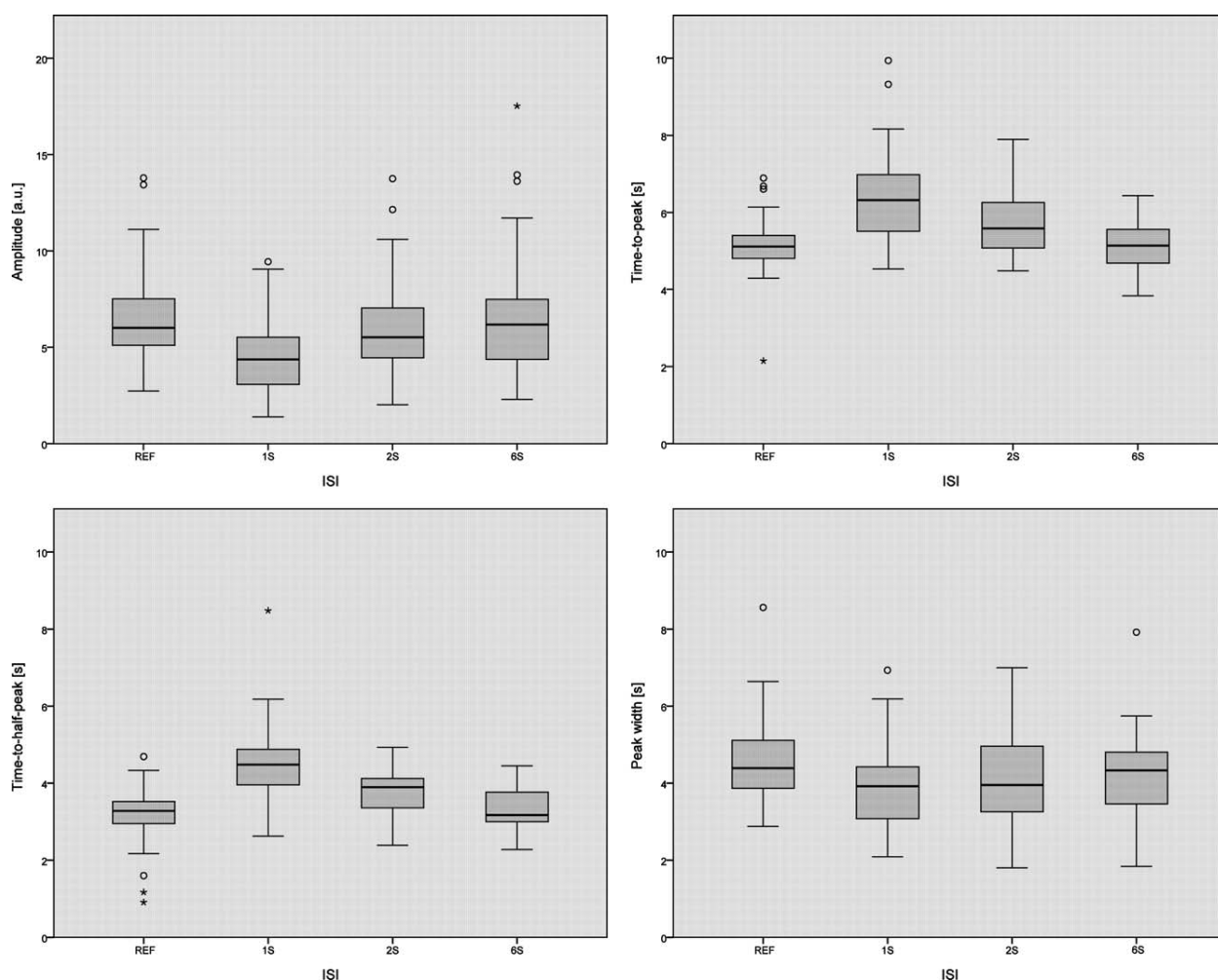


Figure 4. Box-and-whisker plots are given for the absolute values of the four conditions, sorted by parameter (including outliers [°] and extreme values [*]). Note the trend: the shorter the ISI, the larger the deviation from REF.

results were obtained for 15 participants. For seven participants (13.7%), fitting was impossible due to the inadequate shape of the reference condition. These seven subjects were not the same subjects with at least two omitted sessions. No correlation was observed between the number of included trials and the number of fitted responses ($P > 0.05$). In Figure 3, the raw responses of three subjects are plotted both before (left) and after (middle) subtraction of the REF

condition. Their fitted responses are included in the right panel of Figure 3.

The included participants' maximum t value in the ROI was 8.59 ± 0.32 (mean \pm SEM). The mean number of voxels in their ROIs was 299 ± 82 (mean \pm SEM). Box-and-whisker plots for the absolute values of each condition, sorted by parameter, are given in Figure 4. They provide a first indication of the trend for shorter ISI associated with larger deviation from REF.

Table 1
The Averaged Absolute Values (Mean \pm SEM)*

	REF Mean \pm SEM	1S Mean \pm SEM	2S Mean \pm SEM	6S Mean \pm SEM
Amplitude [a.u.]	6.51 ± 0.36	$4.73^{**} \pm 0.33$	6.08 ± 0.42	6.58 ± 0.54
Time-to-peak [s]	5.14 ± 0.11	$6.38^{**} \pm 0.19$	$5.73^{**} \pm 0.12$	5.11 ± 0.10
Time-to-half-peak [s]	3.18 ± 0.10	$4.49^{**} \pm 0.17$	$3.82^{**} \pm 0.09$	3.36 ± 0.08
Peak width [s]	4.59 ± 0.16	$3.86^{*} \pm 0.17$	4.12 ± 0.19	4.19 ± 0.18

*For each parameter, the ANOVA of absolute values was followed by post hoc comparisons with the reference condition (REF; Bonferroni tests, threshold for significance = 0.05):

* $P < 0.01$,

** $P < 0.001$.

Table 2
Results for the Percentages*

	1S		2S		6S	
	Mean \pm SEM	95% CI	Mean \pm SEM	95% CI	Mean \pm SEM	95% CI
Amplitude	-25.1* \pm 4.9	(-41.6, -8.7)	-7.0 \pm 5.2	(-23.2, 9.2)	-1.8 \pm 6.4	(-17.9, 14.4)
Time-to-peak	21.6* \pm 2.2	(16.2, 27.0)	10.9* \pm 1.4	(5.5, 16.2)	-1.6 \pm 1.7	(-6.9, 3.7)
Time-to-half-peak	42.4* \pm 6.4	(26.4, 58.4)	21.6* \pm 5.2	(5.9, 37.3)	5.7 \pm 4.6	(-9.9, 21.3)
Peak width	-10.0 [‡] \pm 4.4	(-23.8, 3.8)	-3.9 \pm 5.1	(-17.4, 9.7)	-3.8 \pm 4.4	(-17.2, 9.7)

*Relative differences in comparison with the reference condition (REF; mean percentages \pm SEM, Bonferroni tests, threshold for significance = 0.05; 95% confidence intervals):

* $P < 0.001$,

[‡] $P = 0.06$.

For each parameter, the ANOVA of the absolute values revealed significantly different values for at least one ISI ($P < 0.001$ for all parameters except peak width: $P < 0.05$). Detailed results of the ANOVA and post hoc Bonferroni tests are included in Table 1 and show that the 1S condition significantly differed from REF in all parameters. For the net responses in 2S, some parameters significantly differed from REF. Refractory effects disappeared in the 6S condition: no significant differences were found.

Appreciation of the refractory effects is more intuitive with percentages, i.e., relative differences in relation to the REF condition. The mean normalized values of the responders are shown in Table 2 (mean \pm SEM and 95% confidence intervals). Percentage analysis provided comparable results to analysis with absolute values, with a decrease in maximum amplitude, an increase in the time-to-peak, an increase in the time-to-half-peak, and a decreased peak width, all of them more pronounced for shorter ISIs.

Taking into account the standard errors of the mean values (Table 2), these findings demonstrate that the refractory effects disappear with a 6-s ISI. No significant deviations from REF were calculated for the 6S condition.

DISCUSSION

In this study, refractory effects were induced with paired brief stimuli using varying interstimulus intervals (1, 2, and 6 s onset-to-onset). Previous work has reported hemodynamic adaptation for group results based on averaged time series (5); however, in the present study results were obtained with all analysis steps and parameter extraction performed at the single-subject level. This may be useful for the study of individual brain physiology in normal versus abnormal aging (29); to measure pharmacological responses to specific drugs; or in conditions of cortical hyperexcitability such as epilepsy (30,31) and primary neurovascular headaches (32), metabolic disorders such as MELAS (33), and vascular disorders such as hypertension and vascular dementia (10,34). To achieve a setup that can eventually be used in individual patients, several issues must be addressed: the brain region to study, acquisition time, compliance of the participants, quality assurance of the data, and the fitting algorithm.

The actual paradigm to measure refractory effects was preceded by a functional localizer, which was used for the determination of the subject-dependent FFA. This face recognition area was selected because it is a higher-order cortical area, with neurons having viewpoint-invariant properties to any face in the visual field (6). Other studies have also observed refractory effects and priming effects in this region (11,35).

Acquiring data during long scanning sessions is challenging, because subjects may begin moving their heads or become less attentive to the stimuli due to tiredness. Therefore, several measures were taken to ensure good data quality. Data were acquired over five separate sessions of 7 min 38 s each. During each session, the subject's attention to the faces was primed by a combination of using an ecologically valid stimulus, e.g., images of faces, and the one-back task with the use of many different new faces. To avoid tiredness, each subject was able to set the pace to start each subsequent session. If the subject did not report any of the oddballs in a session, data from that entire session were excluded from analysis, because attentive vision of the paradigm could not be ensured. Using this procedure, refractory effects could be investigated in 86.3% of the subjects.

Since the first measurement of HRFs, researchers have been interested in estimating and modeling these signals. Several procedures have been investigated. Poisson (18), gamma (19,36–38), and Gaussian (20,21,39) functions have been implemented to model the HRF. Currently, gamma and Gaussian functions are still used often in models. In the analysis of most fMRI data sets they have proven to work adequately. However, these fitting algorithms have some drawbacks that make them unfavorable for the aim of this work. They rely too heavily on a specific model of the HRF, with assumptions about its shape and timing, and too few degrees of freedom.

In this work, a superposition of three inverse logit functions was used for curve fitting (22,23). This algorithm only assumes the presence of the three major HR phases: a rise, a fall, and a recovery from under-shoot. It places no constraints on timing or steepness of the phases. We applied this model in the present study on the basis of a simulation study that tested and compared this algorithm with other methods (23). The simulation study concluded that the IL model was more suitable for fitting HRFs because the parameters were determined with less error compared

with other models, while preserving sufficient power and user flexibility. The above-mentioned fitting algorithms have not been formally compared with this method.

To apply the fitting algorithm, a data set of “good quality” is required, which is described as a HRF where rise, fall, and recovery to baseline can be distinguished. The algorithm cannot fit the HRF when the three phases are not distinguishable or if the fall of the HRF does not extend below half of the rise (i.e., FWHM becomes infinite). After the subtraction step, we may obtain HRFs with such a shape that the subsequent fitting step cannot be run properly. This issue may occur, for example, when too many trials must be excluded for one particular condition. If the criterion was not fulfilled, no fitting was performed, leaving us with missing HRFs and, in turn, missing extracted parameters that are calculated using the fitted HRFs.

The quality of the raw data was first assessed by viewing the extracted time curves. Omission of this quality assurance step and automatic feeding of curves in the fitting algorithm can yield useless results for those time series where no normal HRF pattern is discernible for REF. When the shape of the reference condition does not meet the criterion, the subtraction to calculate the three related net responses yields inadequate, non-HRF shapes. As a consequence, the ability to obtain a well-fitted HRF is affected, and fitting may become impossible for those net responses. At the end of the discussion, we comment on how to increase the number of successfully fitted HRFs.

The software developed in-house comprises the fitting algorithm and the subsequent validation. Several interventions of the user are necessary; for example, acceptance of the fitting is required before the R^2 is calculated. Manual fine-tuning of the predefined parameter set is optional and suggests that the user cannot directly determine the optimal fitting parameters. The algorithm will always use a predefined set (whether or not slightly modified and fine-tuned by the user) to compute the optimal fitting parameters. The user-friendliness of the software can be highly improved without affecting the core of the algorithm. For instance, the R^2 could be calculated automatically, without the user's acceptance, and ask for fine-tuning only when the R^2 is below a certain threshold (e.g., 0.95). Another improvement is the introduction of two or three additional predefined parameter sets that can be invoked when the standard predefined set is not sufficient to compute the optimal fitting parameters (e.g., when R^2 never exceeds the threshold). This software modification will avoid the intervention of manual fine-tuning.

The main goal of this study was to quantify hemodynamic refractory BOLD effects in individuals. For statistical analysis with a random sample of the overall subject population, one must take into account that subjects' observations with different ISIs are not independent. Therefore, an ANOVA repeated measures design is preferable to a one-way ANOVA. The data set was split on the basis of the parameters, and the ISI

was considered to be the fixed factor of interest. In this way, the study design corrected for intersubject variability, and a comparison with REF is justified. It is important to keep in mind that BOLD signal changes are relatively small (approximately 3–5% at 3T) and susceptible to noise. Nevertheless, this study managed to demonstrate that even in the data set with absolute values, refractory effects could be detected.

The research presented here could be extended with combined visual evoked potential measurements using a visual stimulation paradigm (whether simultaneous or not with fMRI data acquisition) to correlate electrical cortical activity with fMRI signal changes. Future research could also focus on the 13.7% rate of nonresponders (with inadequate REF shape). How can the paradigm sensitivity or yield of the analysis procedure be augmented or improved? Changing hardware devices (e.g., 32-channel head coil) is feasible, while increasing the number of measurements is not. Trying to obtain more data points by adding more trials to the paradigm is not advisable because the total scanning time already exceeds 45 min. Prolonging the paradigm would decrease attentiveness and increase tiredness, probably resulting in a higher dropout rate (40). Furthermore, because no obvious correlation was detected between the number of included trials for a particular subject and the number of his fitted responses, extending the paradigm would not be meaningful. To use the analysis of refractory effects at the single-subject level in applications such as clinical settings, the ability to detect and quantify those effects should preferably be close to 100%. Alternatively, a clear indication of what can go wrong in the measurement should be available from the data (quality assessment).

In future studies, investigators may pay more attention to the subjects' focus to maximize the percentage of responders; for example, by using an eye-tracking system in addition to the oddball trials. The participant's performance may be enhanced when receiving accurate feedback between the sessions based on objective eye-tracking information. The simple fMRI paradigm and accompanying analysis at the single-subject level can then also be used to test whether the HRF of patients differs from controls and to test the influence of drugs on HRF, either in a therapeutic scheme or in new pharmacological studies. However, it should be mentioned that one of the drawbacks of fMRI, inherent to the technique, is the subject's compliance, which suggests that further decreasing the number of nonresponders will be difficult.

When subjects are assessed to determine their individual refractory effects in future studies, their results can be compared with the known relative values for each parameter. Due to the substantial sample size of this study, the mean relative difference per parameter and their corresponding 95% confidence intervals may serve as such a reference. Because the refractory effects are most pronounced for the shortest ISI, the relative values for 1S ISI will be most relevant to determine whether the effects are present in each particular subject.

In conclusion, this work demonstrates the ability to detect and quantify refractory effects caused by short interstimulus intervals in the hemodynamic responses of healthy individuals, using single and paired brief stimuli in an event-related paradigm of 5×7 min 38 s. Inverse logit functions have been found suitable to fit the subtracted, net time points.

ACKNOWLEDGMENT

The authors thank Prof. Dr. M.T. Ysebaert for her statistical input.

REFERENCES

- Ogawa S, Lee TM, Kay AR, Tank DW. Brain magnetic resonance imaging with contrast dependent on blood oxygenation. *Proc Natl Acad Sci U S A* 1990;87:9868-9872.
- Buxton RB, Uludag K, Dubowitz DJ, Liu TT. Modeling the hemodynamic response to brain activation. *Neuroimage* 2004;23:S220-S233.
- Dale AM, Buckner RL. Selective averaging of rapidly presented individual trials using fMRI. *Human Brain Mapping* 1997;5:329-340.
- Friston KJ, Josephs O, Rees G, Turner R. Nonlinear event-related responses in fMRI. *Magn Reson Med* 1998;39:41-52.
- Huettel SA, McCarthy G. Evidence for a refractory period in the hemodynamic response to visual stimuli as measured by MRI. *Neuroimage* 2000;11:547-553.
- Grill-Spector K, Malach R. fMRI-adaptation: a tool for studying the functional properties of human cortical neurons. *Acta Psychol* 2001;107:293-321.
- Weigelt S. Functional magnetic resonance adaptation in visual neuroscience. *Rev Neurosci* 2008;19:363-380.
- Jacobs J, Levan P, Moeller F, et al. Hemodynamic changes preceding the interictal EEG spike in patients with focal epilepsy investigated using simultaneous EEG-fMRI. *Neuroimage* 2009;45:1220-1231.
- Arjona A, Perula de Torres LA, Serrano-Castro PJ, Guardado-Santervas PL, Olivares J, Rubi-Callejon J. A transcranial Doppler study in interictal migraine and tension-type headache. *J Clin Ultrasound* 2007;35:372-375.
- Goto H, Ishii K, Uemura T, et al. Differential diagnosis of dementia with Lewy bodies and Alzheimer disease using combined MR imaging and brain perfusion single-photon emission tomography. *AJNR Am J Neuroradiol* 2010;31:720-725.
- Huettel SA, McCarthy G. Regional differences in the refractory period of the hemodynamic response: an event-related fMRI study. *Neuroimage* 2001;14:967-976.
- Friston KJ, Fletcher P, Josephs O, Holmes A, Rugg MD, Turner R. Event-related fMRI: characterizing differential responses. *Neuroimage* 1998;7:30-40.
- Vazquez AL, Noll DC. Nonlinear aspects of the BOLD response in functional MRI. *Neuroimage* 1998;7:108-118.
- Singh M, Kim S, Kim TS. Correlation between BOLD-fMRI and EEG signal changes in response to visual stimulus frequency in humans. *Magn Reson Med* 2003;49:108-114.
- Pfeuffer J, McCullough JC, Van de Moortele PF, Ugurbil K, Hu XP. Spatial dependence of the nonlinear BOLD response at short stimulus duration. *Neuroimage* 2003;18:990-1000.
- Soltysik DA, Peck KK, White KD, Crosson B, Briggs RW. Comparison of hemodynamic response nonlinearity across primary cortical areas. *Neuroimage* 2004;22:1117-1127.
- Yesilyurt B, Ugurbil K, Uludag K. Dynamics and nonlinearities of the BOLD response at very short stimulus durations. *Magn Reson Imaging* 2008;26:853-862.
- Friston KJ, Jezzard P, Turner R. Analysis of Functional MRI Time-Series. *Hum Brain Mapp* 1994;1:153-171.
- Miller KL, Luh WM, Liu TT, et al. Nonlinear temporal dynamics of the cerebral blood flow response. *Hum Brain Mapp* 2001;13:1-12.
- Rajapakse JC, Kruggel F, Maisog JM, von Cramon DY. Modeling hemodynamic response for analysis of functional MRI time-series. *Hum Brain Mapp* 1998;6:283-300.
- Chen HF, Yao DZ, Liu ZX. A study on asymmetry of spatial visual field by analysis of the fMRI BOLD response. *Brain Topogr* 2004;17:39-46.
- Lindquist MA, Wager TD. Validity and power in hemodynamic response modeling: a comparison study and a new approach. *Hum Brain Mapp* 2007;28:764-784.
- Lindquist MA, Meng Loh J, Atlas LY, Wager TD. Modeling the hemodynamic response function in fMRI: efficiency, bias and mis-modeling. *Neuroimage* 2009;45:S187-S198.
- Kanwisher N, McDermott J, Chun MM. The fusiform face area: a module in human extrastriate cortex specialized for face perception. *J Neurosci* 1997;17:4302-4311.
- Rissman J, Gazzaley A, D'Esposito M. The effect of non-visual working memory load on top-down modulation of visual processing. *Neuropsychologia* 2009;47:1637-1646.
- Evans AC, Collins DL, Mills SR, Brown ED, Kelly RL, Peters TM. 3D statistical neuroanatomical models from 305 MRI volumes. In: *Proceedings of the IEEE Conference Record Nuclear Science Symposium and Medical Imaging Conference*, San Francisco, 1993. p 1813-1817.
- Maldjian JA, Laurienti PJ, Burdette JH. Precentral gyrus discrepancy in electronic versions of the Talairach atlas. *Neuroimage* 2004;21:450-455.
- Maldjian JA, Laurienti PJ, Kraft RA, Burdette JH. An automated method for neuroanatomic and cytoarchitectonic atlas-based interrogation of fMRI data sets. *Neuroimage* 2003;19:1233-1239.
- Kannurpatti SS, Motes MA, Rypma B, Biswal BB. Neural and vascular variability and the fMRI-BOLD response in normal aging. *Magn Reson Imaging* 2010;28:466-476.
- Badawy RAB, Harvey AS, Macdonell RAL. Cortical hyperexcitability and epileptogenesis: understanding the mechanisms of epilepsy - Part 1. *J Clin Neurosci* 2009;16:355-365.
- Badawy RAB, Harvey AS, MacDonell RAL. Cortical hyperexcitability and epileptogenesis: understanding the mechanisms of epilepsy - Part 2. *J Clin Neurosci* 2009;16:485-500.
- van der Kamp W, Maassen VanDenBrink A, Ferrari MD, van Dijk JG. Interictal cortical hyperexcitability in migraine patients demonstrated with transcranial magnetic stimulation. *J Neurol Sci* 1996;139:106-110.
- Wilichowski E, Pouwels PJW, Frahm J, Hanefeld F. Quantitative proton magnetic resonance spectroscopy of cerebral metabolic disturbances in patients with MELAS. *Neuropediatrics* 1999;30:256-263.
- Shi J, Perry G, Smith MA, Friedland RP. Vascular abnormalities: the insidious pathogenesis of Alzheimer's disease. *Neurobiol Aging* 2000;21:357-361.
- Henson RNA, Price CJ, Rugg MD, Turner R, Friston KJ. Detecting latency differences in event-related BOLD responses: application to words versus nonwords and initial versus repeated face presentations. *Neuroimage* 2002;15:83-97.
- Boynton GM, Engel SA, Glover GH, Heeger DJ. Linear systems analysis of functional magnetic resonance imaging in human V1. *J Neurosci* 1996;16:4207-4221.
- Chen HF, Yao DZ, Yang L. An extended convolution dynamic model of fMRI BOLD response. *Neurocomputing* 2004;61:395-400.
- Jung KJ. A nonlinear BOLD model accounting for refractory effect by applying the longitudinal relaxation in NMR to the linear BOLD model. *Magn Reson Imaging* 2009;27:907-912.
- Kruggel F, von Cramon DY. Modeling the hemodynamic response in single-trial functional MRI experiments. *Magn Reson Med* 1999;42:787-797.
- Haller S, Bartsch AJ. Pitfalls in fMRI. *Eur Radiol* 2009;19:2689-2706.

2. Absence of haemodynamic refractory effects in patients with migraine without aura – an interictal fMRI study

Benedicte Descamps, Pieter Vandemaele, Harmen Reyngoudt, Karel Deblaere, Luc Leybaert, Koen Paemeleire, Eric Achten

Cephalalgia 2011, 31(11): 1220-31.

Absence of haemodynamic refractory effects in patients with migraine without aura – an interictal fMRI study

Benedicte Descamps, Pieter Vandemaele, Harmen Reyngoudt, Karel Deblaere, Luc Leybaert, Koen Paemeleire and Eric Achten

Cephalalgia

31(11) 1220–1231

© International Headache Society 2011

Reprints and permissions:

sagepub.co.uk/journalsPermissions.nav

DOI: 10.1177/0333102411415881

cep.sagepub.com



Abstract

Background: In healthy controls, haemodynamic refractory effects are observed with blood-oxygenation-level dependent (BOLD) functional MRI (fMRI): the haemodynamic response function (HRF) to the second stimulus in a pair of stimuli with short interstimulus interval (ISI) shows a decreased amplitude and an increased time-to-peak. We hypothesize that there may be interictal haemodynamic abnormalities in migraineurs.

Methods: An event-related fMRI design with paired face stimuli and varying ISIs was used to measure interictal HRFs in the face recognition area of patients with migraine without aura (MwoA) and controls. Net responses to the second stimulus in a pair were calculated and averaged per participant. Several characterizing parameters of the net responses were quantified and examined within each group.

Results: Refractory effects were not observed in our patient group. There are no changes in the net responses compared with the reference situation in patients, irrespective of the ISI, whereas in controls all HRF parameters are decreased or delayed for an ISI of 1 second.

Conclusion: This is the first fMRI study investigating the haemodynamic refractory effects in MwoA patients. Unlike in controls, these effects are not observed in migraineurs. Although currently unclear, it is tempting to speculate that this observation reflects the neurovascular correlate of lack of habituation measured with evoked potentials in migraineurs.

Keywords

Migraine without aura, interictal, BOLD-fMRI, haemodynamic refractory effects

Date received: 14 December 2010; revised: 8 June 2011; accepted: 10 June 2011

Introduction

During the interictal phase of migraine, some differences in brain functioning between patients and healthy controls can be demonstrated. In 1995, Schoenen et al. were the first to describe the lack of habituation in patients with migraine, demonstrated with visual evoked potential (VEP) measurements (1). Habituation is a phenomenon of a decreasing response amplitude to repetitive stimulation in healthy controls (2). Migraineurs do not show this phenomenon; on the contrary, even a transient potentiation of their responses has been observed. The lack of habituation of evoked brain potentials (EP) is not exclusively related to VEP measurements, and has been described with other types of stimuli, such as auditory, somatosensory and pain stimuli (reviewed by Coppola et al. (2)).

A hyperventilation study indicated that the lack of habituation in patients with MwoA is worsened by hypocapnia (low blood carbon dioxide) (3). Transcranial Doppler (TCD) studies mostly reported increased mean blood flow velocities in cerebral arteries and increased cerebrovascular reactivity to carbon dioxide in migraineurs compared with controls (4–9). Furthermore, patients are more sensitive to nitric oxide, such as

Ghent University, Belgium.

Corresponding author:

Benedicte Descamps, Ghent University Hospital, Department of Radiology, MR Department (-1K12IB), De Pintelaan 185, B-9000 Ghent, Belgium

Email: Benedicte.Descamps@UGent.be

by infusion of nitroglycerin. Both patients and controls develop a headache immediately after infusion, but patients also develop a delayed headache with migraine characteristics (10). A recent study with ^{31}P -magnetic resonance spectroscopy (^{31}P -MRS) demonstrated interictal reductions in ATP and phosphocreatine (PCr) concentrations in patients with MwoA compared with controls (11). Glucose hypometabolism had been reported in episodic migraine using ^{18}F -fluorodeoxyglucose positron emission tomography (FDG-PET). This hypometabolism was more pronounced with increasing disease duration and increasing attack frequency (12). Despite these interictal findings, a coherent theory to explain migraine neurobiology, culminating in episodic headache attacks, is lacking.

Haemodynamic changes in response to stimuli can be measured non-invasively with functional magnetic resonance imaging (fMRI) to map brain activity. Externally applied stimuli provoke neuronal activity and local changes in cerebral blood flow (CBF), cerebral blood volume (CBV) and cerebral metabolic rate of oxygen consumption (CMRO_2), thereby altering the blood oxygenation level. Information about local changes in oxygenation level are directly captured by MRI pulse sequences sensitive to blood-oxygenation-level dependent (BOLD) contrast (13). BOLD-fMRI is by far the most commonly used non-invasive functional imaging method. The BOLD response to a single stimulus is described as the haemodynamic response function (HRF). Single, short, successive stimuli with an interstimulus interval (ISI) of more than 20 s generate separate HRFs. When the ISI is shortened, the overall HRF is the summed response of the successive stimuli (Figure 1, left panel). This summation is linear to a certain extent: subtraction of a reference HRF (the HRF in response to a single stimulus) from the overall HRF reveals the net HRF to the second stimulus in the pair, which is identical to the reference HRF. However, when the ISI is very short (less than 6 seconds), the net HRF to the second stimulus is not identical to the reference HRF (Figure 1, right panel). The response amplitude gradually decreases and the time-to-peak is delayed with shorter ISIs. Consequently, the net HRF to the second stimulus cannot be predicted based on a single HRF. Such nonlinear properties of the HRF are called refractory effects and the short time frame after a stimulus during which refractory effects will appear in subsequent responses is referred to as the refractory period (14,15). Linear responses recur for an ISI of 6 seconds or more.

To date, only a few fMRI studies have been published investigating differences between migraineurs and healthy controls. The ictal phase of visually triggered migraine has been investigated with fMRI by Cao

et al. (16,17) to make inferences about changes in the oxygenation of the occipital cortex and brainstem structures during the attack. Moulton et al. reported interictal brainstem abnormalities in migraineurs: the nucleus cuneiformis, part of a modulatory circuit in the brainstem, was found to be hypofunctional compared with controls (18). Recently, work from Stankewitz et al. suggested that the migraine attack might be predictable with fMRI measurements because of increasing preictal activation in spinal trigeminal nuclei following nociceptive stimulation (19), and interictal resting-state fMRI measurements revealed abnormal connectivity in several brain networks (20). To our knowledge, no fMRI activation studies have been published investigating the cerebrum of patients with MwoA interictally, nor on the haemodynamic response characteristics of such activations.

The aim of this fMRI study was to examine whether there are interictal haemodynamic abnormalities in patients with MwoA and to quantify the degree of the haemodynamic refractory effects or the lack of it. We focused on patients with MwoA, to avoid interference of the aura biology. An event-related fMRI study was set up to measure haemodynamic responses to single and paired face stimuli in the face recognition area of the brain, that is, the fusiform face area (FFA), a small higher-order cortical area in which haemodynamic refractory effects in normal participants have been demonstrated (21). Net HRFs were calculated, fitted and quantified per participant. The analysis procedure was applied on data from patients with MwoA and healthy controls.

Methods

Subjects

Twenty-one patients with MwoA (1 male, aged 18–53 years, mean 32.9 ± 12.2) and 51 age-matched healthy volunteers (17 males, aged 18–60 years, mean 29.8 ± 11.7) participated in this study. We allowed a gender imbalance between the groups, because a previous study failed to show differences in the HRF between men and women (22). Patients were recruited at the local outpatient headache clinic. They were all diagnosed according to criteria of the International Classification of Headache Disorders (23), had 2–8 attacks per month (mean 3.4 ± 1.1), were not taking any prophylactic treatment and were at least 48 hours attack-free before the scanning procedure. None of the patients experienced a migraine attack within 24 h after the study. Candidates with epilepsy or MRI contraindications were excluded. All participants were generally healthy, had no neurological history (other than migraine in the patient group) and were asked to

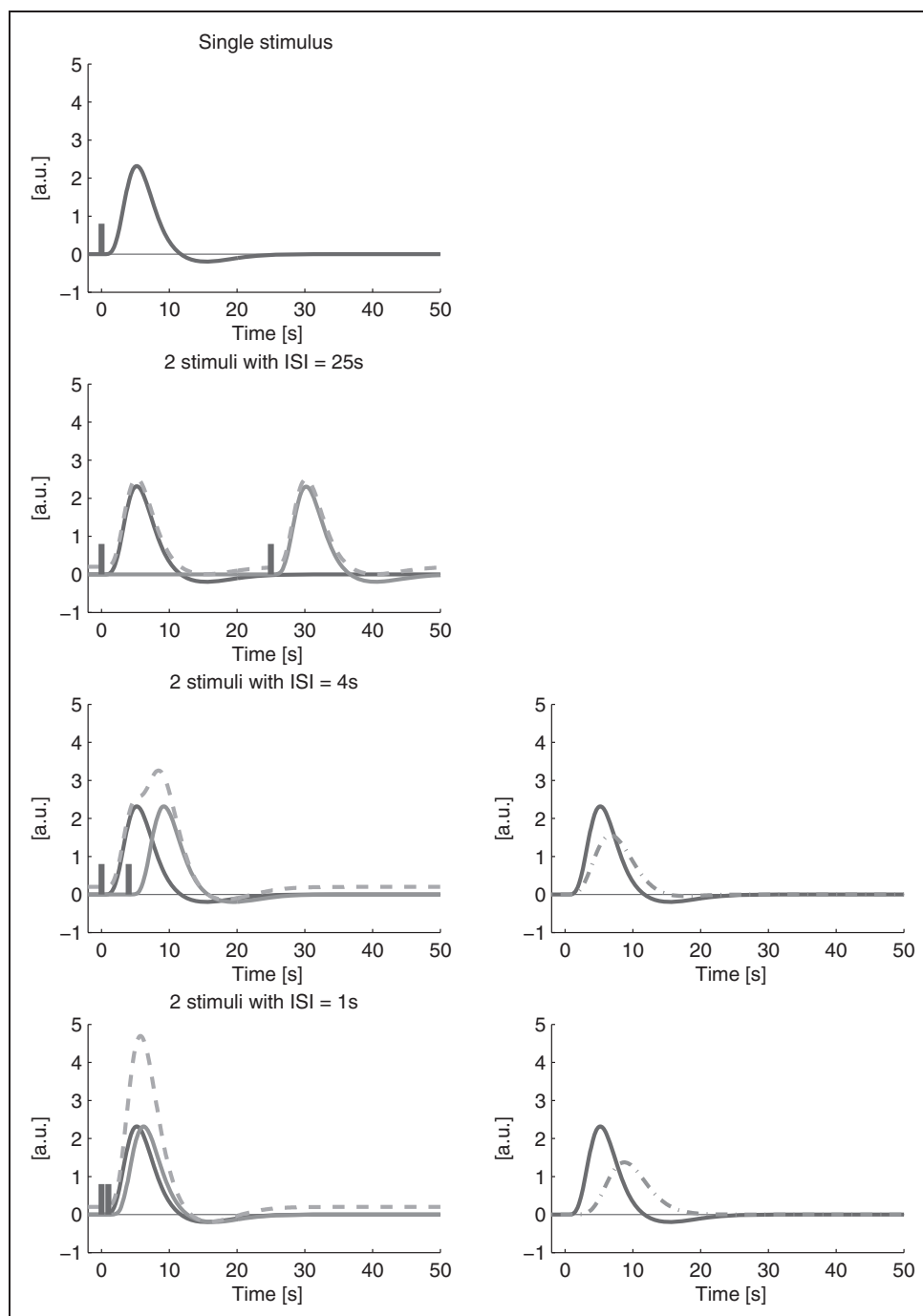


Figure 1. The theoretical BOLD response to one (upper plot) or two stimuli with varying interstimulus intervals is illustrated in the left panel. Two separate stimuli (interstimulus interval >20 s) provoke separate responses (second plot). When the interstimulus interval gets shorter, the responses are summed (third and fourth plot). In the left panel of this schematic representation, the responses are linearly summed (dashed line): refractory effects are not taken into account. Stimulus onsets are depicted with grey bars. For reasons of clarity the summed responses are shifted 0.2 arbitrary units (a.u.) upwards. The right panel illustrates what haemodynamic refractory effects in healthy volunteers are: for short ISIs, the net response to the second stimulus in a pair is decreased in amplitude and delayed compared to the response to a single stimulus.

abstain from caffeine 24 h before the examination. The study was approved by the local ethics committee and all participants provided written informed consent.

Imaging and experimental setup

A 3 T Siemens Trio Tim system (Siemens AG, Erlangen, Germany) with an 8-channel head coil was used for image acquisition. Anatomical images were acquired using a T1-weighted sequence (MPRAGE) with isotropic voxels (voxel size $0.9 \times 0.9 \times 0.9 \text{ mm}^3$, TR = 1550 ms, TE = 2.39 ms, matrix 256×256 , 3D slab with 176 slices). For functional imaging, a T2*-weighted echo planar sequence was used, which is sensitive to BOLD contrast (voxel size $3.5 \times 3.5 \times 5.0 \text{ mm}^3$, TR = 1000 ms, TE = 27 ms, matrix 64×64 , 19 slices).

Total protocol scanning time was 45 min 57 s and included two functional measurements: a functional localizer and the main experiment. The block-designed functional localizer comprised three conditions (looking at faces, scenes and a fixation cross hair as rest) and was necessary to determine the subject-specific FFA. The main experiment was an event-related study. The global paradigm design and its four conditions are shown in Figure 2. We acquired five consecutive sessions with 19 trials per session. Each trial belonged to one of the four conditions and consisted of one or two male faces with blurred contours. The faces were presented for 500 ms. A single face followed by 26 seconds rest served as reference condition (REF); for the three

other conditions faces were shown in pairs with 1, 2 or 6 seconds ISI (onset-to-onset; called 1S, 2S and 6S, respectively) and a fixed post-stimulus interval of 20 seconds rest before a new face was presented, to allow the HRF to return to baseline. Within one session, each condition was randomly displayed four times and between them three random 'oddball' trials of type REF, 1S, 2S or 6S were added to keep the subject attentive. One session took 7 min 38 s ($4 \times (26 \text{ s} + 21 \text{ s} + 22 \text{ s} + 26 \text{ s}) + 3 \times \text{max. } 26 \text{ s}$). The difference in trial lengths is related to the subtraction step in the analysis (see below). Participants were instructed to look at the face images or the cross hair, without moving the head, and to press a button if the present face was identical to the previous one (oddball). The order of appearance of the trials, including the oddball trials, was randomly assigned and different for each participant to avoid a potential ordering effect. All stimuli were supplied by Mark D'Esposito and are cited in Rissman et al. (24).

Analysis

All data were preprocessed in SPM5 (Wellcome Trust Centre for Neuroimaging Functional Imaging Laboratory, London, UK) comprising slice timing, realignment, co-registration of anatomy to functional images, spatial normalization to 1 and 3 mm isotropic voxels for anatomical and functional images, respectively, and spatial Gaussian smoothing (8 mm kernel).

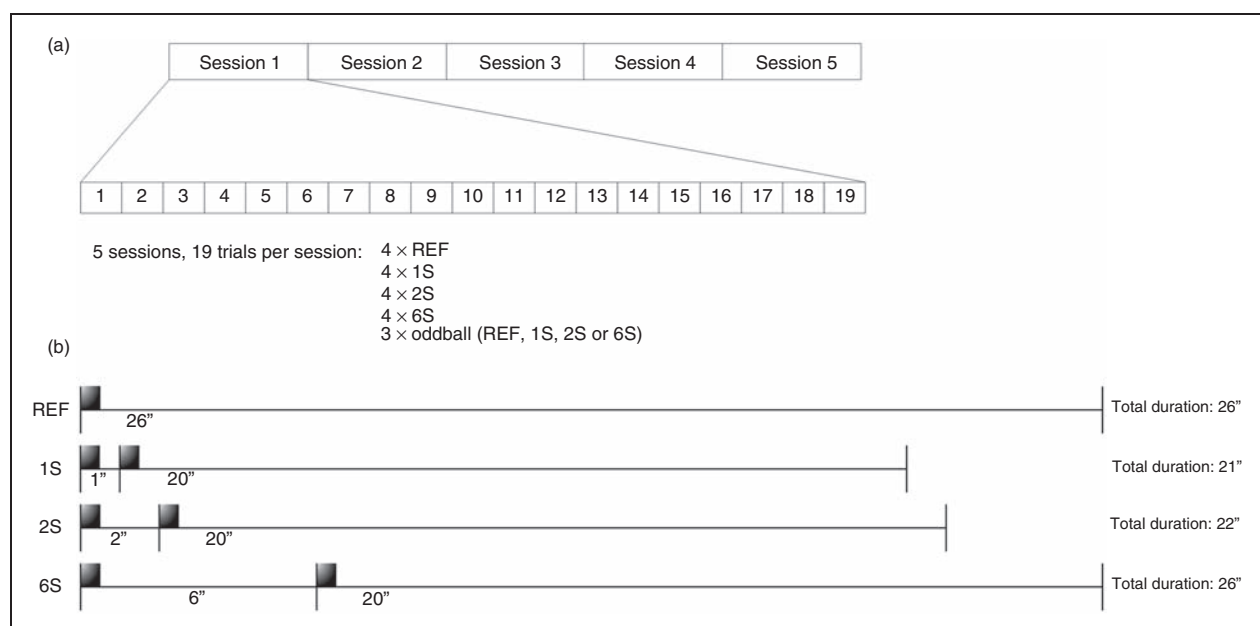


Figure 2. The global paradigm design (a) and a detail of the four conditions (b). One reference condition (REF) and three paired trial types (1S, 2S, and 6S respectively). Each stimulus is presented for 500 ms. Interstimulus (1S, 2S, and 6S) and poststimulus intervals (20S, 26S) are measured onset-to-onset.

Preprocessed data from the functional localizer were further analysed in SPM5 and provided information for defining each individual's FFA as a region-of-interest (ROI). The ROI was the intersection of the fusiform gyrus, selected with the WFU PickAtlas (25,26), and the subject-specific spmT image, which contains the t -values for the contrast '*faces > (scenes & rest)*'. Only those voxels with a t -value higher than 80% of the maximum t -value within this mask image were selected for further analysis. The number of voxels in the ROI of patients and controls were compared with a two-tailed two-sample t -test.

Processing of the smoothed images from the main experiment was as follows: first, trials were excluded from analysis when participants had pressed during a trial, indicating oddball detection, to prevent confounding effects caused by the motor responses. If the subject had not pressed at all during a particular session, the subject was considered inattentive and the entire session was also excluded from further analysis. Remaining responses from all voxels in the ROI above the threshold were averaged per condition. The response to the single stimulus (REF) was subtracted from the overall responses to the paired stimuli (1S, 2S and 6S). To execute this subtraction, the two arrays with data points from REF and the paired condition must have the same length, otherwise an error due to different array length will prevent the software from continuing. This is why the REF duration equals the duration of the longest paired condition (i.e. 26s). For the 1S and 2S conditions the last time points of REF are not necessary, and were thus omitted.

Net haemodynamic responses to the second stimulus in the pair were semi-automatically fitted using a recently developed algorithm (27), which uses the linear combination of three inverse logit functions – sigmoid curves, in fact – followed by a validation of the fits by calculating the R^2 . Fitted responses were used to determine four characterizing parameters of the haemodynamic responses: peak amplitude, time-to-peak, time-to-half-peak and peak width (measured at full-width-at-half-maximum (FWHM)). These absolute values were used to calculate relative differences, defined as a percentage in relation to REF, because these percentages are more intuitive for assessing the refractory effects.

Statistical analysis was performed with SPSS 18 (IBM SPSS Inc., Chicago, IL, USA). A repeated measures analysis of variance (ANOVA) – including Levene's test to assess equality of variances – was carried out separately on the absolute and relative values. Each of these ANOVAs had a fixed factor with four levels (the ISI) and a random factor (the participants), to correct for subject-to-subject variability. As separate ANOVAs were calculated for migraineurs and controls,

a total of sixteen ANOVAs was carried out: one each for the four parameters (peak amplitude, time-to-peak, time-to-half-peak, peak width), separately for absolute and relative values in each group. Sixteen Bonferroni tests were used for triple comparisons in the post hoc analysis, where the ISI is under investigation, to determine which means differ.

Spearman's rank-correlation coefficients were calculated for each parameter to test whether patient results are correlated with the available clinical data (attack frequency).

Finally, mean absolute values from patients and controls of the REF condition were additionally compared for every separate parameter using Student's t -tests (uncorrected, two-tailed two-sample t -tests). These comparisons are helpful, for example to check whether the reference amplitude is equal in patients with MwoA and controls.

For all statistical tests, results with p -values less than 0.05 were considered to be significant.

Results

Screening of the high resolution T1-weighted anatomical images by a neuroradiologist revealed no clinically relevant abnormalities.

The comparison of the subject-specific ROIs between patients with MwoA and controls revealed no differences for the number of voxels in the ROI (mean \pm SEM: 192 ± 39 and 299 ± 82 voxels, respectively, $p > 0.05$) and the maximum t -values (mean \pm SEM: $t_{\max} = 8.678 \pm 0.344$ and $t_{\max} = 8.587 \pm 0.323$, respectively).

For some participants, not all HRFs could be fitted. Table 1 summarizes the total number of fitted HRFs per condition in migraineurs and controls. Eleven patients out of 21 (52.4%) had a full dataset (four well-fitted HRFs), in seven patients (33.3%) one HRF was missing (a 1S, 2S or 6S response), and from three patients (14.3%) we obtained no useful data. In the control group, comparable ratios were observed: all four HRFs from 29 participants out of 51 (56.9%) were fitted and partial results were obtained for 15 participants (29.4%). For seven participants (13.7%), fitting was impossible for any HRF. The mean R^2 of the fitted HRFs to assess the goodness-of-fit was high for both groups (0.954 ± 0.006 and 0.974 ± 0.002 in migraineurs and controls, respectively).

An example of the four plotted HRFs from a patient and a healthy control is given in Figure 3. There, refractory effects are seen in the net responses for shorter ISIs in the healthy participants, but not in the patient with MwoA. The four parameters which characterize the HRFs are averaged per condition and per group. These mean values are presented in clustered bar

Table 1. List with the number of fitted HRFs per condition for the 21 patients and 51 controls

Condition	Patients	Controls
REF	21 (100%)	46 (90.2%)
1S	15 (71.4%)	37 (72.5%)
2S	15 (71.4%)	38 (74.5%)
6S	17 (81.0%)	39 (76.5%)

diagrams (Figure 4). Whether amplitude, latencies and width change significantly as a result of the varying ISIs is investigated with the ANOVA. For each parameter, results from the ANOVA and post hoc Bonferroni test of the absolute values are shown in Table 2. For 1S, all parameters were significantly different from REF in controls, but this was not the case for the patients, except for the 1S time-to-half-peak.

The relative values of the four parameters are averaged and shown in Figure 5. ANOVA and post hoc Bonferroni test results of these percentages are comparable to the absolute ones (Table 3). Those values that were significantly different from REF in the ANOVA with absolute values are also significantly different from REF in the ANOVA with relative values, and vice versa, except for three values out of the 24, where there is no agreement with the absolute values. In the migraine patient group, the time-to-peak (1S) and the time-to-half-peak (2S) are additionally significantly different from REF; in the controls, the width in 1S is not significantly different from REF, whereas with absolute values it is.

There is no relationship between the available clinical information of the patients (the attack frequency) and the values of the parameters characterizing the haemodynamic responses ($p > 0.05$ for all percentages per parameter and per ISI, data not shown).

The results of the Student's t -test for the additional comparisons of REF values reveal no significant differences between patients and controls. The REF-amplitude difference between patients and controls has a borderline p -value of 0.07 (uncorrected).

Discussion

In this study, the interictal haemodynamic refractory effects in patients with MwoA were investigated using BOLD-fMRI. Refractory effects have been extensively studied in healthy controls, but to date no studies have examined these effects in migraineurs. We hypothesized refractory effects to be altered in migraine, based on several observations in the interictal migrainous brain, such as lack of habituation (EP), altered haemodynamics (TCD), ATP and PCr reductions (^{31}P -MRS),

glucose hypometabolism (FDG-PET), abnormal brain network connectivity (resting-state fMRI) and anomalous brainstem activations (fMRI). The nonlinear properties of the HRF in controls appear when short ISIs are applied in the fMRI paradigm, that is, less than 6 s, and gradually decrease when the ISI increases. We demonstrate that these refractory effects are not present in our well-selected group of patients with MwoA.

In this section, we comment on the paradigm set up and the analysis steps, elaborate on the results, discuss the relevance of our findings and relate them to the current knowledge.

Faces were chosen as ecologically valid stimuli to provoke haemodynamic refractory effects. The face stimuli were smoothly blurred along the contours, so that only the internal features of the face were visible, to make sure that the face-selective areas were activated (24) and the subject was not focusing on hair style, face shape or background. The face recognition area was selected to investigate haemodynamic refractory effects, because it is a higher-order cortical area in which haemodynamic refractory effects have already been observed (21,28) and its neurons have size- and position-invariant properties to any face in the visual field (29). This means that neurons remain in an adapted state when new stimuli have a slightly different size or position.

The visual task 'looking at faces' first provokes BOLD changes in primary visual areas. The same visual stimulus activates different brain regions involved in processing visual information. Huettel et al. investigated the characteristics of haemodynamic responses and refractory effects in different regions with different visual stimuli (15,21). They reported regional differences in both the haemodynamic responses and the refractory effects and stipulated that their characteristics are stimulus-specific. This means that haemodynamic responses to a basic alternating checkerboard are more pronounced in primary visual cortical areas, whereas faces provoke more pronounced responses in the face recognition areas. In other words, haemodynamic responses to certain stimuli should be investigated in the corresponding stimulus-specific region of activation. Consequently, for the present study comparisons with different regions are rather pointless. We decided to focus on one region, the FFA, to investigate haemodynamic refractory effects in patients with MwoA and healthy controls because faces were used to provoke HRFs. Volumes acquired during motor responses were omitted because of the possible confounding effect. The oddball task might in theory introduce an additional confounding effect, a difference in working memory load, owing to the difference between the 1 s ISI and 6 s ISI. The connectivity between the hippocampus and the FFA and its potential dynamic

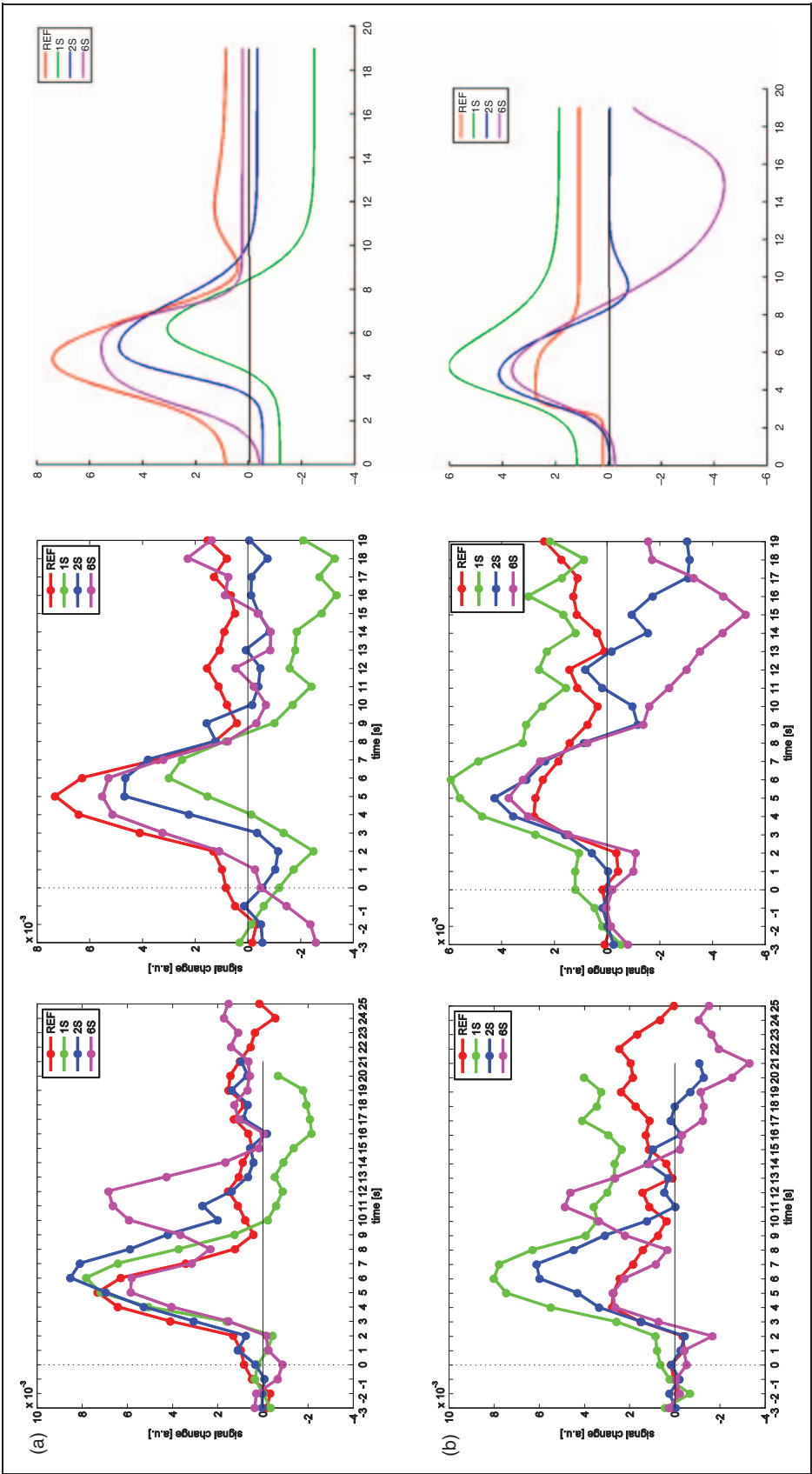


Figure 3. Time-courses from one healthy volunteer (a) and one patient (b), with responses to the four conditions (REF, 1S, 2S, 6S) both before (left) and after (middle) subtraction of the reference response. The fitted responses (right) were used to derive the characteristic parameters (amplitude, time-to-peak, time-to-half-peak and peak width). Parameters are quantified at the single-subject level. Afterwards, the data are put together to perform an ANOVA. The first three data points are used to calculate the baseline signal and are omitted in the fitted plots.

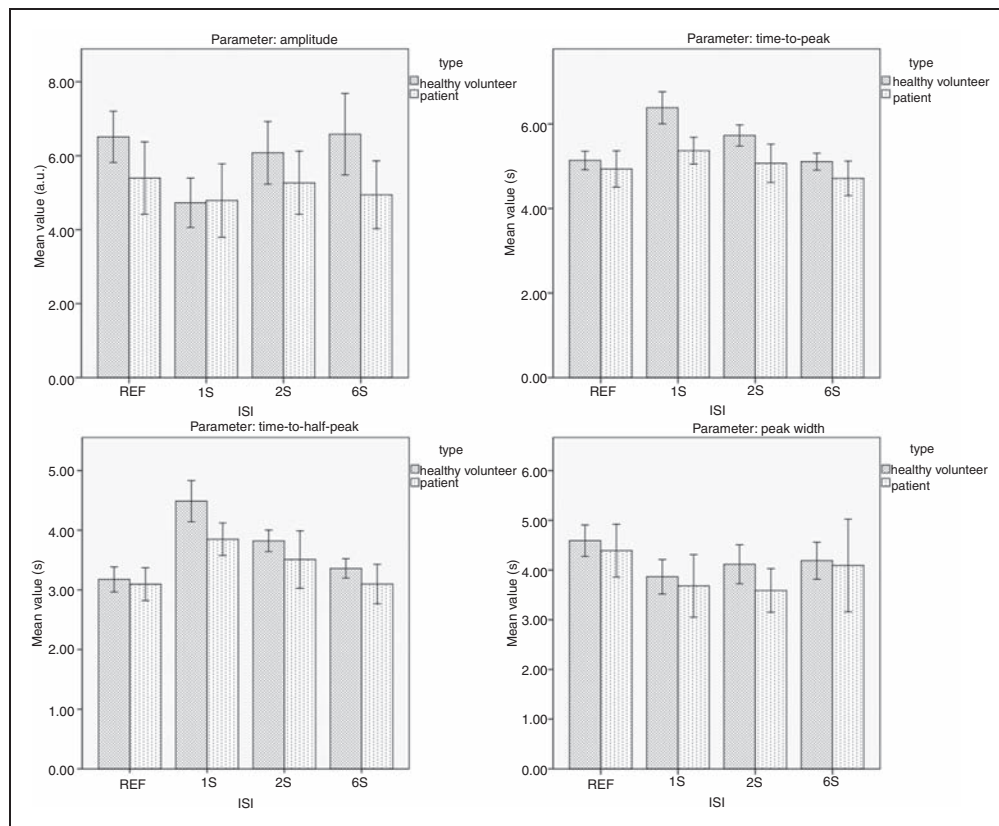


Figure 4. Graphs showing the mean absolute values for each parameter (amplitude, time-to-peak, time-to-half-peak and peak width) in patients and healthy controls. Error bars represent 95% confidence intervals. The shorter the ISI, the larger the deviation from the reference condition. Only for controls are all IS parameters significantly different from REF. The significant differences are listed in Table 2.

Table 2. F-values of the ANOVAs with absolute values and p-values for post hoc comparisons with the reference condition following the ANOVAs

Parameter	Patients				Controls			
	F	IS	2S	6S	F	IS	2S	6S
Amplitude	0.396	n.s.	n.s.	n.s.	4.161*	<0.001	n.s.	n.s.
Time-to-peak	1.829	n.s.	n.s.	n.s.	20.594*	<0.001	<0.001	n.s.
Time-to-half-peak	5.011*	<0.001	n.s.	n.s.	25.730*	<0.001	<0.001	n.s.
Width	1.430	n.s.	n.s.	n.s.	3.095*	<0.01	n.s.	n.s.

Post hoc Bonferroni tests, threshold for significance = 0.05 for both groups. For each parameter, absolute values for at least one ISI are significantly different from REF in healthy controls, whereas nearly all these differences are not observed in patients.

adjustments might affect the remaining HRFs (30). Another point of discussion is the gender imbalance in the groups. For this, we can refer to one study, which failed to show statistically significant differences in the HRF between men and women, $p > 0.10$ (22). However, small sample sizes were used as well as different stimuli and a different brain region. Therefore, we mention the possibility of a confounding effect.

One of the crucial steps involved in this study is the curve fitting. We incorporated a recently developed algorithm into the analysis procedure. The choice for the inverse logit model to fit the HRFs is based on the information provided by Lindquist and Wager (27,31). The only criterion for this fitting method is the presence of the three phases of the haemodynamic response: the rise, the fall and the recovery from undershoot (the negative signal in the HRF due to the combination of

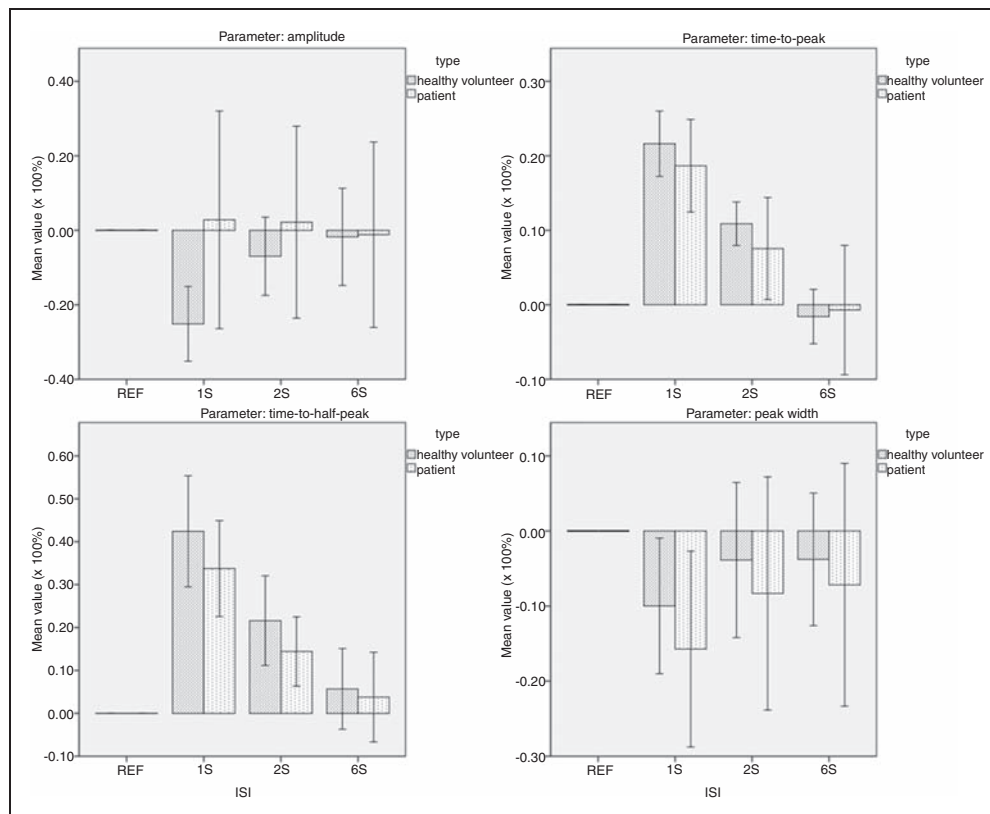


Figure 5. Graphs showing the mean percentages for each parameter (amplitude, time-to-peak, time-to-half-peak and peak width) in patients and healthy controls. The shorter the ISI, the larger the deviation from the reference condition, which is added only for clarity on these graphs. Error bars indicate 95% confidence intervals. A remarkable difference can be clearly observed for parameter amplitude: controls show an amplitude decrease of 25% for the net IS response, whereas there is no significant difference from REF in patients with this ISI. Only for controls are all IS parameters significantly different from REF. Significant differences are listed in Table 3.

Table 3. F-values of the ANOVAs with relative values and mean relative differences for the three net responses in relation to REF for the four parameters for both patients and controls

Parameter	Patients				Controls			
	F	IS	2S	6S	F	IS	2S	6S
Amplitude	0.034	2.8%	2.2%	-1.2%	6.388*	-25.1%*	-7.0%	-1.8%
Time-to-peak	9.950*	18.7%*	7.5%	-0.7%	53.114*	21.6%*	10.9%*	-1.6%
Time-to-half-peak	15.831*	33.7%*	14.4%*	3.8%	19.201*	42.4%*	21.6%*	5.7%
Width	1.330	-15.7%	-8.3%	-7.2%	1.252*	-10.0%	-3.9%	-3.8%

Post hoc Bonferroni tests are used with the threshold for significance at 0.05, indicated with an asterisk.

decreased CBF and increased CBV). Contrary to other methods, assumptions about timing and steepness of the phases are not required. This has the advantage that the parameter calculation is based on fitted curves that are as close to the raw data as possible. The algorithm cannot fit the HRF when rise, fall and recovery to baseline are not distinguishable or if the fall of the HRF does not go below half of the rise (i.e. if FWHM becomes infinite). After the subtraction step we may get HRFs with such a shape that the

subsequent fitting step cannot be run properly. This may happen when, for example, too many trials had to be excluded for a particular condition. If the criterion is not fulfilled, no fitting was performed and we end up with missing HRFs. The extracted parameters, which are calculated on the fitted HRFs, will also be missing.

The origin of the haemodynamic refractory effects is difficult to trace. Neuronal as well as vascular mechanisms may be involved, and we discuss both below.

Neuronal activity contributes to the BOLD signal, albeit indirectly. The BOLD signal directly reflects the blood oxygenation level, which is an indirect measure of neuronal activity. The BOLD signal changes are indisputably correlated with the neuronal compartment, because the initial triggers for the haemodynamic changes are the higher regional oxygen and glucose demand from neurons and astrocytes during neuronal activation. Several studies, including electrophysiological and fMRI studies, have investigated the cortical responsiveness of patients with migraine (32–35). The fMRI studies all included patients with MwA and were focusing on the implications of their findings for the aura phenomenon. The widely accepted phenomenon of habituation has been considered a protective mechanism against cortical hyperexcitability. The assumption is that patients with both MwA and MwoA show increased cortical excitability as they lack this protective mechanism (36). Given that the refractory period of the haemodynamic response is a sign of temporary neural adaptation and believed to be a protective phenomenon (29,37), the lack of habituation in migraineurs could be the basis of the absence of refractory effects. However, the cortical hyperexcitability hypothesis in migraine has been refuted (35). A reduction in the cortical pre-activation level of migraine patients has been suggested as an alternative explanation and it is inferred from the initial lower amplitude of the P100 in the first averaged block of VEP measurements (38,39). The reduced cortical pre-activation level could be due to abnormalities in thalamocortical networks (40) or hypoactivation in subcortico-cortical aminergic pathways (41). This observation might be reflected in the haemodynamic data presented in our study: the amplitude of a single response (REF) in patients seems on average lower than the REF amplitude in controls (Figure 4, parameter amplitude, condition REF). However, the mean difference we have found is only borderline non-significant ($p = 0.07$).

Another point of view to explain the observed lack of haemodynamic refractory effects in patients is that the effects are related to the vascular compartment. Vascular-related parameters (CBF, CBV, oxygen extraction fraction, etc) directly contribute to the BOLD signal. The interictal vascular reactivity in patients might be affected (either increased or decreased). However, a recent near infra-red spectroscopy study demonstrated that the interictal neurovascular coupling in patients with MwoA seems to be intact (42). Simultaneous measurements of BOLD, CBV and CBF with a dedicated MR-sequence could add further strength to this hypothesis (43,44).

Taking into account the fact that successive stimuli applied to induce the measured HRF provoke local electrical changes, it is tempting to see a link between

the electrophysiological habituation and haemodynamic refractory effects. However, there are some major differences between these two phenomena. A first involves the different temporal properties. The electrophysiological peak latencies are detected at the millisecond scale after stimulus onset, whereas the peak of the HRF is reached at 5 to 8 seconds after stimulus onset. Furthermore, the stimuli used in electrophysiology are presented at a high rate (typically 2–8 Hz), whereas the stimuli in this BOLD-fMRI paradigm should be considered as single events (viewing faces) presented for 500 ms with limited ISIs (1–6 s onset-to-onset).

Often, inferences in fMRI studies are based on group results, similar to EP data: first, individual data are averaged, followed by the determination of the derived group parameters. One strength of the paradigm applied in this study is that the data have first been analysed and quantified at the single-subject level. A visual evaluation of the net HRFs in individuals may already suggest the lack of haemodynamic refractory effects in individual patients with MwoA, which is illustrated by the examples in Figure 3. However, measuring haemodynamic refractory effects is not suitable as a biomarker for migraine in individual patients. The sensitivity of the measurements is unsatisfactory for discriminating between healthy controls and patients owing to an overlap in observations. Averaging of the extracted data per group is needed to make statistical inferences.

There is no relationship between available clinical information of the patients, that is, the attack frequency, and their values characterizing the haemodynamic responses, lacking refractory effects. Migraine can be considered as a threshold disorder. Lack of haemodynamic refractory effects, decreased ATP concentration (11), genetic susceptibility (45), and so on can all contribute to a lowered migraine threshold. It is impossible to link each of these factors to, for example, the attack frequency. One predisposing factor is not generalizable to the whole population of migraine patients, which is an additional argument why the absence of haemodynamic refractory effects in migraineurs is unsuitable as biomarker for migraine.

Finally, it is impossible to determine the exact link between the two abovementioned signal types (vascular vs. neuronal) when data from simultaneous measurements are missing. Habituation to repetitive stimulation has been investigated in the face recognition region using intracranial event-related potentials (with, for example, significant habituation of the face-specific P350) in patients with medically intractable epilepsy (46). However, habituation in face perception areas in healthy controls and patients with migraine has not been investigated directly, because of the invasive

character of the intracranial recordings. Therefore, we do not wish to state conclusively that the lack of haemodynamic refractory effects in patients caused by a face recognition task also means that they really show a lack of habituation during that task. A subsequent, interesting step in this research would be applying a paradigm to measure combined EEG-fMRI, to define a more precise relationship between the electrophysiological and the haemodynamic observations. From a practical point of view, a basic visual paradigm with MR-compatible surface electrodes is the most realistic experimental set up.

Besides combined EEG-fMRI or simultaneous BOLD, CBV and CBF measurements, it would also be interesting to try to link our findings to the genotype of the participants. Recently, a genome-wide association study identified a minor allele on chromosome 8q22.1 (rs1835740) to be associated with migraine (45). One of the strengths of this study was the selection of a well-defined patient group (only patients with MwoA, no prophylactic treatment, 2–8 attacks per month, 48 h attack free before scan session, and so on). However, genotyping might reveal additional divergences or uncover a sub-group in the patient population, in line with a proposal by Schoenen et al. (47) and a recent ^{31}P -MRS study (11).

Irrespective of the origin of the observations in the present study, one implication is worth mentioning. fMRI is widely used to investigate cognitive functions and physiological brain processes in healthy volunteers, and several exclusion criteria are therefore applied, such as MRI incompatible devices and neurological conditions such as stroke and epilepsy. However, migraine is hardly ever mentioned. Our findings suggest that studies with event-related fMRI paradigms using stimuli with short ISIs should add migraine (without aura) to the exclusion criteria for candidate participants, because including data from these patients may considerably influence the results of these studies.

In summary, this work is the first fMRI study that has measured BOLD haemodynamics interictally in patients with MwoA. The net HRFs of healthy controls have nonlinear properties for very short ISIs, but these refractory effects are not observed in patients with MwoA. Conclusive statements about the origin of the absence of refractory effects are difficult to make without additional, coupled measurements.

Acknowledgements

The authors are grateful to all patients and healthy volunteers for their participation and want to thank MT Ysebaert for her statistical input. This research was funded by a PhD grant of the Flemish Agency for Innovation by Science and Technology (IWT-Vlaanderen, grant SB-51437/53437).

References

1. Schoenen J, Wang W, Albert A and Delwaide PJ. Potentiation instead of habituation characterizes visual-evoked potentials in migraine patients between attacks. *Eur J Neurol* 1995; 2: 115–122.
2. Coppola G, Pierelli F and Schoenen J. Habituation and migraine. *Neurobiol Learn Mem* 2009; 92: 249–259.
3. Coppola G, Currà A, Sava SA, Alibardi A, Parisi V, Pierelli F and Schoenen J. Changes in visual-evoked potential habituation induced by hyperventilation in migraine. *J Headache Pain* 2010; 11: 497–503.
4. Thie A, Fuhlenndorf A, Spitzer K and Kunze K. Transcranial Doppler evaluation of common and classic migraine. 1. Ultrasound features during the headache-free period. *Headache* 1990; 30: 201–208.
5. Harer C and Vonkummer R. Cerebrovascular CO₂ reactivity in migraine -assessment by transcranial Doppler ultrasound. *J Neurol* 1991; 238: 23–26.
6. Abernathy M, Donnelly G, Kay G, Wieneke J, Morris S, Bergeson S, et al. Transcranial Doppler sonography in headache-free migraineurs. *Headache* 1994; 34: 198–203.
7. Fiermonte G, Pierelli F, Pauri F, Cosentino FII, Soccorsi R and Giacomini P. Cerebrovascular CO₂ reactivity in migraine with aura and without aura -a transcranial Doppler study. *Acta Neurol Scand* 1995; 92: 166–169.
8. Valikovics A, Olah L, Fulesdi B, Kaposzta Z, Ficzer A, Bereczki D and Csiba L. Cerebrovascular reactivity measured by transcranial Doppler in migraine. *Headache* 1996; 36: 323–328.
9. Arjona A, de Torres LAP, Serrano-Castro PJ, Guardado-Santervas PL, Olivares J and Rubi-Callejon J. A Transcranial Doppler study in interictal migraine and tension-type headache. *J Clinical Ultrasound* 2007; 35: 372–375.
10. Olesen J. The role of nitric oxide (NO) in migraine, tension-type headache and cluster headache. *Pharmacol Ther* 2008; 120: 157–171.
11. Reyngoudt H, Paemeleire K, Descamps B, De Deene Y and Achten E. ^{31}P -MRS demonstrates a reduction in high-energy phosphates in the occipital lobe of migraine without aura patients. *Cephalalgia* 2011. E-pub ahead of print, DOI: 10.1177/0333102410394675.
12. Kim JH, Kim S, Suh SI, Koh SB, Park KW and Oh K. Interictal metabolic changes in episodic migraine: A voxel-based FDG-PET study. *Cephalalgia* 2010; 30: 53–61.
13. Kwong KK, Belliveau JW, Chesler DA, Goldberg IE, Weisskoff RM, Poncelet BP, et al. Dynamic magnetic resonance imaging of human brain activity during primary sensory stimulation. *Proc Natl Acad Sci USA* 1992; 89: 5675–5679.
14. Friston KJ, Josephs O, Rees G and Turner R. Nonlinear event-related responses in fMRI. *Magn Reson Med* 1998; 39: 41–52.
15. Huettel SA and McCarthy G. Evidence for a refractory period in the hemodynamic response to visual stimuli as measured by MRI. *Neuroimage* 2000; 11: 547–553.
16. Cao Y, Aurora SK, Nagesh V, Patel SC and Welch KM. Functional MRI-BOLD of brainstem structures during visually triggered migraine. *Neurology* 2002; 59: 72–78.

17. Cao Y, Welch KM, Aurora S and Vikingstad EM. Functional MRI-BOLD of visually triggered headache in patients with migraine. *Arch Neurol* 1999; 56: 548–554.
18. Moulton EA, Burstein R, Tully S, Hargreaves R, Becerra L and Borsook D. Interictal Dysfunction of a Brainstem Descending Modulatory Center in Migraine Patients. *PLoS One* 2008; 3: e3799.
19. Stankewitz A, Aderjan D, Eippert F and May A. Trigeminal Nociceptive Transmission in Migraineurs Predicts Migraine Attacks. *J Neurosci* 2011; 31: 1937–1943.
20. Sprenger T, Seifert CL, Valet M, Staehle K, Tölle TR, Foerschler A, et al. Abnormal interictal large-scale brain network connectivity in episodic migraine. *Headache* 2010; 50: S71.
21. Huettel SA and McCarthy G. Regional differences in the refractory period of the hemodynamic response: an event-related fMRI study. *Neuroimage* 2001; 14: 967–976.
22. Huettel SA, Singerman JD and McCarthy G. The effects of aging upon the hemodynamic response measured by functional MRI. *Neuroimage* 2001; 13: 161–175.
23. The International Classification of Headache Disorders: 2nd edition. *Cephalalgia* 2004; 24 Suppl 1: 9–160.
24. Rissman J, Gazzaley A and D'Esposito M. The effect of non-visual working memory load on top-down modulation of visual processing. *Neuropsychologia* 2009; 47: 1637–1646.
25. Maldjian JA, Laurienti PJ and Burdette JH. Precentral gyrus discrepancy in electronic versions of the Talairach atlas. *Neuroimage* 2004; 21: 450–455.
26. Maldjian JA, Laurienti PJ, Kraft RA and Burdette JH. An automated method for neuroanatomic and cytoarchitectonic atlas-based interrogation of fMRI data sets. *Neuroimage* 2003; 19: 1233–1239.
27. Lindquist MA and Wager TD. Validity and power in hemodynamic response modeling: a comparison study and a new approach. *Human Brain Mapp* 2007; 28: 764–784.
28. Henson RNA, Price CJ, Rugg MD, Turner R and Friston KJ. Detecting latency differences in event-related BOLD responses: application to words versus nonwords and initial versus repeated face presentations. *Neuroimage* 2002; 15: 83–97.
29. Grill-Spector K and Malach R. fMR-adaptation: a tool for studying the functional properties of human cortical neurons. *Acta Psychologica* 2001; 107: 293–321.
30. Rissman J, Gazzaley A and D'Esposito M. Dynamic adjustments in prefrontal, hippocampal, and inferior temporal interactions with increasing visual working memory load. *Cereb Cortex* 2008; 18: 1618–1629.
31. Lindquist MA, Meng Loh J, Atlas LY and Wager TD. Modeling the hemodynamic response function in fMRI: efficiency, bias and mis-modeling. *Neuroimage* 2009; 45: S187–S198.
32. Bramanti P, Grugno R, Vitetta A, Di Bella P, Muscara N and Nappi G. Migraine with and without aura: electrophysiological and functional neuroimaging evidence. *Funct Neurol* 2005; 20: 29–32.
33. Huang J, Cooper TG, Satana B, Kaufman DI and Cao Y. Visual distortion provoked by a stimulus in migraine associated with hyperneuronal activity. *Headache* 2003; 43: 664–671.
34. Vincent M, Pedra E, Mourao-Miranda J, Bramati I, Henrique A and Moll J. Enhanced interictal responsiveness of the migraineous visual cortex to incongruent bar stimulation: a functional MRI visual activation study. *Cephalalgia* 2003; 23: 860–868.
35. Huang J, DeLano M and Cao Y. Visual cortical inhibitory function in migraine is not generally impaired: evidence from a combined psychophysical test with an fMRI study. *Cephalalgia* 2006; 26: 554–560.
36. Aurora SK and Wilkinson F. The brain is hyperexcitable in migraine. *Cephalalgia* 2007; 27: 1442–1453.
37. Huettel SA, Obembe OO, Song AW and Woldorff MG. The BOLD fMRI refractory effect is specific to stimulus attributes: evidence from a visual motion paradigm. *Neuroimage* 2004; 23: 402–408.
38. Afra J, Cecchini AP, Sandor PS and Schoenen J. Comparison of visual and auditory evoked cortical potentials in migraine patients between attacks. *Clinical Neurophysiology* 2000; 111: 1124–1129.
39. Ambrosini A, de Noordhout AM, Sandor P and Schoenen J. Electrophysiological studies in migraine: a comprehensive review of their interest and limitations. *Cephalalgia* 2003; 23: 13–31.
40. Coppola G, Ambrosini A, Di Clemente L, Magis D, Fumal A, Gerard P, et al. Interictal abnormalities of gamma band activity in visual evoked responses in migraine: an indication of thalamocortical dysrhythmia? *Cephalalgia* 2007; 27: 1360–1367.
41. Fumal A and Schoenen J. Cortical hypoactivity or reduced efficiency of cortical inhibition in migraine? Reply. *Cephalalgia* 2007; 27: 188–189.
42. Schytz HW, Ciftci K, Akin A, Ashina M and Bolay H. Intact neurovascular coupling during executive function in migraine without aura: Interictal near-infrared spectroscopy study. *Cephalalgia* 2010; 30: 457–466.
43. Yang Y, Gu H and Stein EA. Simultaneous MRI acquisition of blood volume, blood flow, and blood oxygenation information during brain activation. *Magn Reson Med* 2004; 52: 1407–1417.
44. Gu H, Stein EA and Yang Y. Nonlinear responses of cerebral blood volume, blood flow and blood oxygenation signals during visual stimulation. *Magn Reson Imaging* 2005; 23: 921–928.
45. Anttila V, Stefansson H, Kallela M, Todt U, Terwindt GM, Calafato MS, et al. Genome-wide association study of migraine implicates a common susceptibility variant on 8q22.1. *Nat Genet* 2010; 42: 869–873.
46. Puce A, Allison T and McCarthy G. Electrophysiological studies of human face perception. III: Effects of top-down processing on face-specific potentials. *Cereb Cortex* 1999; 9: 445–458.
47. Schoenen J, Ambrosini A, Sandor PS and de Noordhout AM. Evoked potentials and transcranial magnetic stimulation in migraine: published data and viewpoint on their pathophysiological significance. *Clin Neurophysiol* 2003; 114: 955–972.

3. Combining haemodynamic and metabolic patient data reveals the presence of subgroups

A scientific communication on this topic is in preparation.

On the day of the fMRI scans, patients first underwent an MRS protocol to quantify several ^1H - and ^{31}P -metabolites. These data have led to two peer-reviewed articles (83, 202), added in Appendix B and C, and are part of Harmen Reyngoudt's PhD thesis.

Interictal ^1H - and ^{31}P -MRS measurements during resting-state revealed decreased PCr- and ATP-concentrations compared to controls (83). In one fifth of the patients, a deviation of twice the standard deviation (SD) was observed. Interestingly, these patients had the highest attack frequency, which points towards latent metabolic abnormalities in at least a subgroup of patients. On the other hand, lactate was not quantifiable in our MwoA patients (202), which might be attributed to the introduction of a more correct quantification strategy with the phantom replacement technique. Later, a stimulation protocol demonstrated that lactate concentrations remain close to the detection limit during intensive visual stimulation (203), hence, no lactate increase could be detected, which is in contrast to earlier studies in controls and patients (204, 205). Results of both resting-state MRS protocols are available in Appendix B and C.

Given that the haemodynamic and metabolic data are consecutively gathered in the individual participants, combining the data may result in additional valuable information.

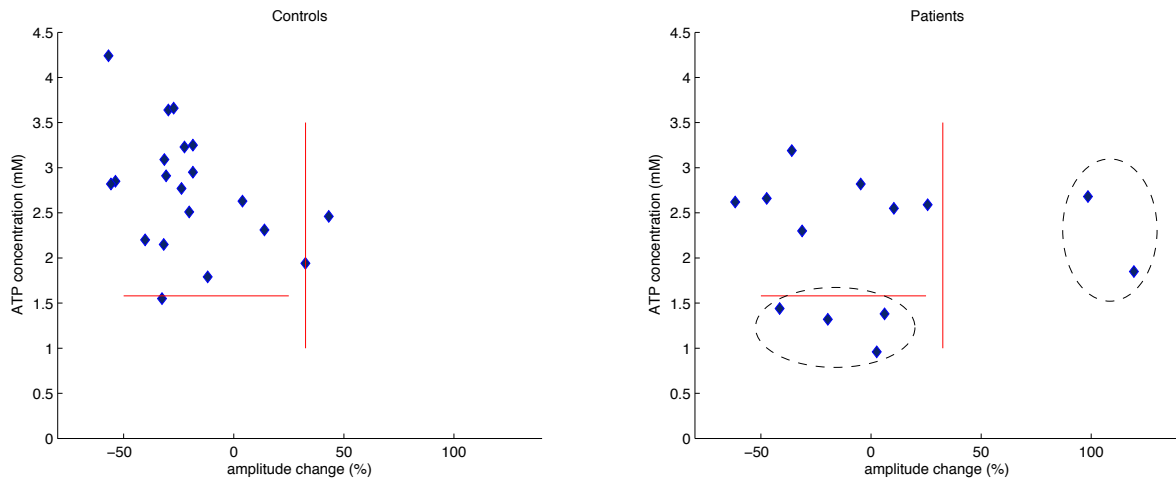


Figure 17 Scatter plots from controls (left pane) and patients (right pane) giving single subject data for both a metabolic (ATP concentration on y-axis) and a haemodynamic parameter (amplitude changes for the 1S ISI on x-axis). The horizontal and vertical red lines indicate the 2 SD borders, displayed for one side only. In the patients population, 2 subgroups are identified, one with significantly lower ATP concentrations, one with significantly increased amplitude changes. Note that not all the participants are present in their respective scatter plot because of some missing data in both measurements.

The most striking parameters from both studies, namely the amplitude of the 1S condition and the ATP-concentration, are combined in Figure 17. Only those participants with a complete dataset can be included, which results in a slight data reduction.

Nevertheless, the scatter plot clearly demonstrates that a subgroup of patients is not only present in the MRS-results: within the group of patients with normal ATP-concentrations, there is another subgroup of patients who have outlying amplitude changes. None of these subgroups are present in the pool of controls.

Given that there is still a relative large group of patients that cannot be assigned to a specific subgroup, this combination of MR-related measurements is not sensitive enough to support a migraine diagnosis.

We elaborate more on the finding of subgroups in the general discussion of this thesis.

Chapter 6: General discussion

1. Discussion and future perspectives

The main aim of this thesis was to study neurovascular properties in patients with migraine, thereby focusing on their cerebral haemodynamic behaviour. All measurements were performed using fMRI as a safe, non-invasive imaging technique. First, a measurement method was developed to measure HREs at the single-subject level. The method was tested and validated in a large group of 51 healthy volunteers. In a second phase of this research, the method was applied on a group of 21 patients with MwoA. Their results were compared with the large reference group. The haemodynamic results are also combined with metabolic data obtained in the same patient group with MRS. Options towards the use of the measurements as biomarkers are investigated.

In Chapter 3, it was explained that the basic, unprocessed signals from fMRI measurements are interesting to investigate. The haemodynamic response following a single stimulus is characterized by a particular time-course and successive stimuli alter its intrinsic properties. HREs are revealed by the presence of nonlinearities in the net haemodynamic response for very short ISIs. These nonlinearities have been described in studies with healthy volunteers and at the group level, mostly on 1.5T MRI systems (190). Initially, we had tried to detect these refractory effects in individuals during a pilot study (six healthy volunteers), using a 3T MRI system (206). It was expected that the stronger magnetic field would allow us to extract nonlinear signal differences at the single-subject level, which was confirmed by the pilot results.

A flashing checkerboard is often used to provoke HRFs with visual stimuli (for example in (187) and (190)). Although this is an easily standardized and reproducible way of presenting visual stimuli, the flashing checkerboard mainly activates a primary cortical area (V1) and the event itself does not resemble a common daily life situation. For the present research, faces were chosen as ecologically valid stimuli to provoke HREs. Face-selective areas in the brain were activated because only the internal features of the faces were visible through blurring the face stimuli along their contours. That way the participant could not focus on hair style, face shape or background. This fusiform face area (FFA) is a higher-order cortical area in which HREs have already been observed (207-209). Moreover, its neurons have size- and position-invariant properties to any face in the visual field (210). This means that neurons remain in an adapted state when new stimuli have a slightly different size or position. The FFA is easily activated through a block-designed functional localizer paradigm, described in Chapter 5, paragraph 1.

The participants' responses may be sensitive to their level of attentiveness and mood. To prevent influences from anxiety and/or lack of attention to the maximum possible extent, participants were extensively informed before the MR acquisition, followed by a (subjective) post-acquisition inquiry. Furthermore, given the possible effect of emotional faces on the participants' mood, faces with a neutral, instead of a fearful expression were chosen for presentation. Finally, sessions were entirely excluded from further analysis when the participant had not pressed during that particular session.

Besides proper data acquisition, the methodological aspect of this thesis also comprised the need for an adequate fitting and validation method. Therefore, the core of Lindquist and Wager's algorithm was used (197). In Chapter 5, paragraph 1, we elaborate on the

usefulness of the fitting algorithm, which is based on a linear combination of inverse logit functions. This algorithm was very suitable for our purpose, since it implements all processing on raw data, without accepting too many indulgences. From our point of view, an appropriate fitting method cannot force the data into a straitjacket, but has to remain as close to the raw data as possible to obtain reasonable fits. The IL approach requires only few assumptions for the fitting: requirements toward the overall HRF shape (rise, fall, rise), not towards timing of the peak, nor steepness of the signals. We applied a derivative of this algorithm on real data, while Lindquist and Wager had tested and compared their fitting procedure on simulated data.

The pool of 51 healthy volunteers was used for the determination of 95% confidence intervals for each parameter and each ISI. This results in a useful reference framework, which allows to test measurements from patients (or controls) for the absence or presence of HREs. Evaluating the absence or presence of HREs is most straightforward for the parameters obtained for the 1s ISI in comparison with REF. The 95% confidence intervals for three relative HRF parameters (i.e., amplitude, time-to-peak and time-to-half-peak) under 1S are useful to evaluate whether or not the net responses show refractoriness (Chapter 5.1, table 2). When the newly calculated parameters of a subject are within these boundaries, it is reasonable to accept the presence of refractory effects. With the current group of volunteers, these boundaries could not be determined for the peak width, in spite of a tendency towards a decreased width in the presence of HREs.

Using the current confidence interval boundaries for the reference pool evokes a point of criticism: there is no real gold standard to determine whether or not subjects show HREs. Consequently, the sensitivity and specificity for the proposed method is hard to define.

Particularly for this thesis, such group of patients whose HRFs are measured, are migraineurs, recruited in the outpatient Headache Clinic at the Department of Neurology of the Ghent University Hospital. Candidate-patients were carefully screened before they were included in the study. It was the intention to apply all measurements on a homogeneous group of patients with MwoA, assessed using the ICHD-II criteria. In paragraph 2 of Chapter 5, the results of the patient study are presented. On average, the MwoA patients lack HREs; in other words, the averaged, net 1S HRF with all its derived parameters is in migraineurs not statistically different from the reference HRF.

Since simultaneous electrophysiological data have not been acquired, it is currently difficult to assess the implications of our findings. Given that migraineurs also show lack of electrophysiological habituation, it is tempting to pursue the comparison. Our observation could fit in both theories mentioned in Chapter 1. The hypothesis of dysexcitability can be supported by our data through the absence of the HREs in migraineurs. These patients do not show HREs, because their cortex is hyperexcitable. The other hypothesis of reduced preactivation levels can also be applied onto our data: the amplitude of the reference HRF in migraineurs seems on average lower than in controls (upper left pane of Figure 4 in Chapter 5, paragraph 2), albeit a borderline nonsignificant difference ($p = 0.07$). Controls seem to show on average a decreased amplitude for the net 1S HRF, i.e. a distinct HRE, while patients with MwoA show on average the same amplitude compared to their REF HRF. These reduced preactivation levels are schematically explained in Figure 18. Adding haemodynamic information to related electrophysiological data sets provides a new point of view for future research on this topic.

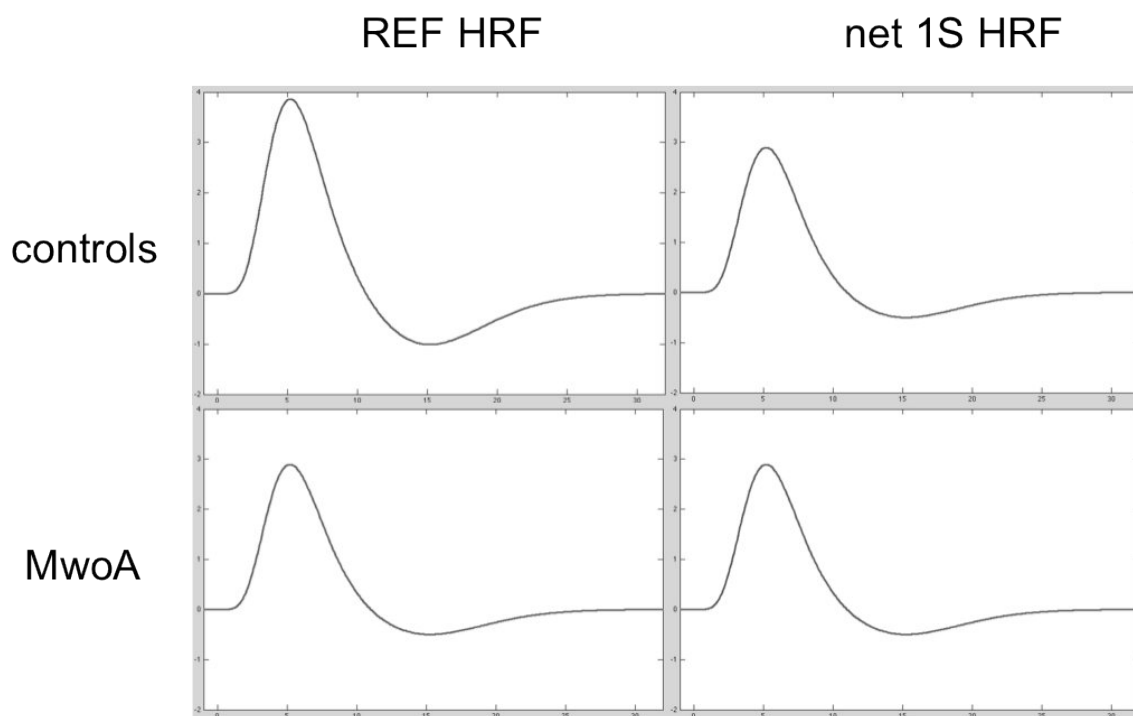


Figure 18 These plots show how the theory of reduced preactivation levels in migraineurs may explain one of our observations. A characteristic of HREs is observed in controls: the amplitude of the net 1S HRF (upper right) is reduced compared to their REF HRF (upper left). On the contrary, patients with MwoA seem to have on average a lower amplitude, even for their REF HRF (lower left). In other words: their baseline or reference or preactivation levels are reduced. The amplitude of their averaged net 1S HRF is not significantly different from their REF HRF (lower left) and lies in the same range of that corresponding amplitude in controls. All axes have the same scale (Y axes in arbitrary units, X axes in seconds).

Despite the absence of electrophysiological data, we are able to correlate our haemodynamic data to other – metabolic – information, namely interictal resting-state ^1H - and ^{31}P -MRS measurements consecutively acquired during the same day in the same patients. A scatter plot with ATP-concentrations versus amplitude changes for 1S clearly demonstrates two subgroups of patients: a subgroup of patients has significantly lowered ATP-concentrations (at least twice the SD) and within the group of patients with normal ATP-concentrations, there is another subgroup of patients who have outlying amplitude changes. None of these subgroups are present in the pool of controls.

Contrary to the ATP-findings, the fMRI-observations could not be related to the patients' attack frequency. Also, the differentiation into subgroups could not be attributed to patients

being in the peri-attack period. It is known that habituation in patients tends to normalize approximately one day before and during an attack (66). However, all patients in the study were at least 48 hours attack-free before the scanning procedure and none of the patients experienced a migraine attack within 24 hours after the study.

It would be very interesting to measure the EPs in the patients with increased HRF amplitudes to see whether their EP amplitude is increased as well, which has been described as a potentiation instead of a habituation in migraine patients (48). However, to our knowledge, the face-specific P350 cannot be measured in a non-invasive manner, to obtain truly simultaneous EP-fMRI data. During epilepsy-related surgery, intracranial EPs have demonstrated habituation of this P350 (211).

The assumption that the lack of HREs is related to habituation deficits is not too far-fetched, given the evidence that the lack of VEP habituation in migraineurs is accompanied by habituation deficits of their gamma band oscillations (64), and secondly, that there is a strong correlation with (event-related) gamma band activity and BOLD (164).

Despite the tempting resemblance, we want to stress that there are considerable differences between (V)EP habituation and HREs: temporal scale (milliseconds vs. seconds), signal source (electrical vs. haemodynamic), presentation rate (often 8 Hz vs. 2 Hz), (V)EP amplitude changes in the second block with tens of stimuli vs. 2 stimuli out of max. 20 averaged signals, etc. Furthermore, in Chapter 3, paragraph 3, current literature demonstrates that the exact link between HREs and electrophysiological findings under terms of repeated stimuli are not that straightforward.

Rather than deriving generalizing conclusions which apply to all patients, our combined fMRI and MRS data suggest that patients can be divided into subgroups, although the selection

criteria for creating a homogeneous patient pool were already stringent. Logically, one could wonder whether the other patients that are currently not (yet) assigned to a particular subgroup, also differ from healthy controls or from each other at other levels. As long as measurements (or combinations of measurements) do not provide a sufficiently high sensitivity and specificity, which is the case for our relatively small patient group, these measurements can not be used to support migraine diagnosis in any patient.

Three recent genome-wide association studies (43-45) report genetic susceptibility variants in large migraine populations. The presence of particular SNPs indicate an increased risk for migraine. Future genetic studies may reveal additional polymorphisms in migraine susceptibility genes. Studying the migraine phenotype may evolve more and more toward genetic research, starting from observations in patients of objectively measurable parameters. Presumably, this procedure provides a faster chance of success due to its goal-oriented base, rather than extensive genome screenings which seem more like looking for a needle in a haystack. Our haemodynamic and metabolic findings provide a clue for future genetic research. Finally, the observation that patients can be divided into subgroups supports the thesis that patients with migraine share a common phenotype hiding different genotypes.

From a radiological point of view, it seems hard, though not impossible, to optimize the fMRI measurements. Increasing the number of experiments to obtain a higher signal-to-noise ratio (SNR) would have an adverse effect: a higher dropout rate is expected due to tiredness and loss of attentiveness (212). On the other hand, shortening of the acquisition time introduces the risk of ending up without enough data due to a low SNR or due to a lack of included sessions. Improving the amount of responders, i.e., subjects with fitted

responses, could be obtained by using state-of-the-art hardware: recently, the MR-equipment at Ghent University Hospital has been upgraded to 32 channels, while all participants were scanned with a 8-channel birdcage head coil. An increase in SNR is to be expected.

Structural imaging does not contribute to the diagnosis of migraine, nor is imaging mentioned in the current diagnostic criteria (ICHD-II) (4). However, conventional structural MR imaging may be helpful to exclude other underlying pathologies, such as brain tumor or hydrocephalus. Advanced imaging techniques are not routinely used in daily practice to corroborate a clinical diagnosis. Although the combination of our fMRI and MRS measurements may provide objective data to support a migraine diagnosis in some patients, we cannot conclude that these measurements are sensitive and specific enough to serve as a biomarker, no more than other findings (213). Therefore, the value of combined MR-measurements is rather situated in further stratification of migraine disorders. Our data illustrate that an apparently homogeneous group can be subdivided based on multiple MR-derived parameters.

Future research with this kind of combined measurements may also be helpful in prophylactic studies. To date, the choice for a certain prophylactic drug is more or less based on trial and error, for lack of obvious indications to link a particular drug to the patient's profile. Predicting the efficacy of preventive drugs will save time and money for the patient presenting in daily clinical practice. For example, vitamin B2 (riboflavin) supplementation may be preferred for migraine patients with metabolic anomalies (14), while patients who lack HREs may benefit from anti-epileptic drugs.

2. Conclusion

The conclusion of this doctoral thesis is twofold.

In the first place, we have demonstrated that HREs can be extracted and quantified at the single-subject level, thereby using non-invasive fMRI measurements with a high field, clinical MR system in combination with an adjusted processing strategy. In addition, IL functions are well suited to perform time-course fitting with minimal restrictions and assumptions.

Secondly, application of this measurement technique has led to the observation that patients with MwoA show anomalies in their haemodynamic responses, which is conceivably related to the well-known lack of habituation in migraineurs. The absence of HREs is not observed in all migraineurs. However, together with the outcome of the MRS study in the same patient group, functional parameters are revealed to evaluate the brain of migraine patients and subgroups of patients can be identified. These results may be helpful in future research on understanding the effectiveness of prophylactic treatments.

Once more, functional imaging demonstrates that the migraine disorder stretches beyond episodic symptoms and the interictal migraine brain is not so normal as it often looks on structural images.

References

1. Stovner LJ, Hagen K, Jensen R, Katsarava Z, Lipton RB, Scher AI, et al. The global burden of headache: a documentation of headache prevalence and disability worldwide. *Cephalalgia*. 2007;27(3):193-210.
2. IDEWE. Studie van IDEWE meldt meer dan 1 150 000 ziektedagen in Vlaanderen en in het Brussels gewest door migraine. 2006; Available from: http://www.idewe.be/jahia/webdav/site/internet/shared/persberichten/NL/PB_Migraine_finaal_100706.pdf.
3. WHO. The Global Burden of Disease: 2004 update. 2008. Report No.: ISBN 978 92 4 156371 0.
4. The International Classification of Headache Disorders: 2nd edition. *Cephalalgia*. 2004;24 Suppl 1:9-160.
5. Lipton RB, Diamond S, Reed M, Diamond ML, Stewart WF. Migraine diagnosis and treatment: Results from the American Migraine Study II. *Headache*. 2001;41(7):638-45.
6. Leão AAP. Spreading depression of activity in the cerebral cortex. *Journal of Neurophysiology*. 1944;7(6):359-90.
7. Milner PM. Note on a possible correspondence between the scotomas of migraine and spreading depression of Leao. *Electroen Clin Neuro Suppl*. 1958;10(4):705.
8. Lauritzen M. Pathophysiology of the Migraine Aura: the Spreading Depression Theory. *Brain*. 1994;117(1):199-210.
9. Lauritzen M. Cortical spreading depression in migraine. *Cephalalgia*. 2001;21(7):757-60.
10. Lauritzen M, Olsen TS, Lassen NA, Paulson OB. Changes in Regional Cerebral Blood Flow during the Course of Classic Migraine Attacks. *Annals of Neurology*. 1983;13(6):633-41.
11. Hadjikhani N, Sanchez DR, Wu O, Schwartz D, Bakker D, Fischl B, et al. Mechanisms of migraine aura revealed by functional MRI in human visual cortex. *Proc Natl Acad Sci U S A*. 2001;98(8):4687-92.
12. Lashley KS. Patterns of Cerebral Integration Indicated by the Scotomas of Migraine. *Archives of Neurology and Psychiatry*. 1941;46:331-9.

13. Tfelt-Hansen P, Saxena PR, Dahlof C, Pascual J, Lainez M, Henry P, et al. Ergotamine in the acute treatment of migraine - A review and European consensus. *Brain*. 2000;123:9-18.
14. Schoenen J, Jacquy J, Lenaerts M. Effectiveness of high-dose riboflavin in migraine prophylaxis. A randomized controlled trial. *Neurology*. 1998;50(2):466-70.
15. Olesen J, Goadsby PJ, Ramadan NM, Tfelt-Hansen P, Welch KMA. *The Headaches*. 3rd Edition ed: Lippincott Williams & Wilkins; 2006.
16. Paemeleire K, De Brabandere C. *Hoofdpijn. Oorzaken, symptomen en behandelingen: Davidsfonds Uitgeverij*; 2011.
17. Van den Bergh V, Amery WK, Waelkens J. Trigger Factors in Migraine: a Study Conducted by the Belgian Migraine Society. *Headache*. 1987;27(4):191-6.
18. Rasmussen BK. Migraine and Tension-Type Headache in a General Population: Precipitating Factors, Female Hormones, Sleep Pattern and Relation to Lifestyle. *Pain*. 1993;53(1):65-72.
19. Robbins L. Precipitating Factors in Migraine: a Retrospective Review of 494 Patients. *Headache*. 1994;34(4):214-6.
20. Kelman L. The triggers or precipitants of the acute migraine attack. *Cephalalgia*. 2007;27(5):394-402.
21. Giffin NJ, Ruggiero L, Lipton RB, Silberstein SD, Tvedskov JF, Olesen J, et al. Premonitory symptoms in migraine - An electronic diary study. *Neurology*. 2003;60(6):935-40.
22. Villalon CM, Olesen J. The role of CGRP in the pathophysiology of migraine and efficacy of CGRP receptor antagonists as acute antimigraine drugs. *Pharmacology & Therapeutics*. 2009;124(3):309-23.
23. Blau JN. Migraine - Theories of Pathogenesis. *Lancet*. 1992;339(8803):1202-7.
24. Goadsby PJ, Charbit AR, Andreou AP, Akerman S, Holland PR. Neurobiology of migraine. *Neuroscience*. 2009;161(2):327-41.
25. Goadsby PJ, Lipton RB, Ferrari MD. Migraine--current understanding and treatment. *N Eng J Med*. 2002;346(4):257-70.
26. Akerman S, Holland PR, Goadsby PJ. Diencephalic and brainstem mechanisms in migraine. *Nature Reviews Neuroscience*. 2011;12(10):570-84.

27. Sherman SM. Thalamocortical loops and information processing. In: Schmidt RF, Willis WD, editors. *Encyclopedia of Pain*. Heidelberg, Germany: Springer-Verlag; 2007. p. 2427-31.
28. Pellerin L, Magistretti PJ. Glutamate uptake into astrocytes stimulates aerobic glycolysis: a mechanism coupling neuronal activity to glucose utilization. *Proc Natl Acad Sci U S A*. 1994;91(22):10625-9.
29. Kasischke KA, Vishwasrao HD, Fisher PJ, Zipfel WR, Webb WW. Neural activity triggers neuronal oxidative metabolism followed by astrocytic glycolysis. *Science*. 2004;305(5680):99-103.
30. Magistretti PJ, Pellerin L, Rothman DL, Shulman RG. Energy on demand. *Science*. 1999;283(5401):496-7.
31. Leybaert L. Neurobarrier coupling in the brain: a partner of neurovascular and neurometabolic coupling? *J Cereb Blood Flow Metab*. 2005;25(1):2-16.
32. Brady ST, Siegel GJ, Albers RW, Price DL. *Basic Neurochemistry*. Eighth ed: Academic press, Elsevier; 2012.
33. Shmuel A. Locally Measured Neuronal Correlates of Functional MRI Signals. In: Mulert C, Lemieux L, editors. *EEG-fMRI Physiological Basis, Technique, and Applications*: Springer; 2010.
34. Tsacopoulos M, Magistretti PJ. Metabolic coupling between glia and neurons. *J Neurosci*. 1996;16(3):877-85.
35. Gervil M, Ulrich V, Kyvik KO, Olesen J, Russell MB. Migraine without aura: A population-based twin study. *Annals of Neurology*. 1999;46(4):606-11.
36. Ulrich V, Gervil M, Kyvik KO, Olesen J, Russell MB. Evidence of a genetic factor in migraine with aura: A population-based Danish twin study. *Annals of Neurology*. 1999;45(2):242-6.
37. Kallela M, Wessman M, Farkkila M, Palotie A, Koskenvuo M, Honkasalo ML, et al. Clinical characteristics of migraine concordant monozygotic twin pairs. *Acta Neurol Scand*. 1999;100(4):254-9.
38. Ophoff RA, Terwindt GM, Vergouwe MN, van Eijk R, Oefner PJ, Hoffman SM, et al. Familial hemiplegic migraine and episodic ataxia type-2 are caused by mutations in the Ca²⁺ channel gene CACNL1A4. *Cell*. 1996;87(3):543-52.
39. De Fusco M, Marconi R, Silvestri L, Atorino L, Rampoldi L, Morgante L, et al. Haploinsufficiency of ATP1A2 encoding the Na⁺/K⁺ pump alpha 2 subunit associated with familial hemiplegic migraine type 2. *Nat Genet*. 2003;33(2):192-6.

40. Moseley AE, Lieske SP, Wetzel RK, James PF, He SW, Shelly DA, et al. The Na,K-ATPase alpha 2 isoform is expressed in neurons, and its absence disrupts neuronal activity in newborn mice. *Journal of Biological Chemistry*. 2003;278(7):5317-24.
41. Dichgans M, Freilinger T, Eckstein G, Babini E, Lorenz-Depiereux B, Biskup S, et al. Mutation in the neuronal voltage-gated sodium channel SCN1A in familial hemiplegic migraine. *Lancet*. 2005;366(9483):371-7.
42. de Vries B, Frants RR, Ferrari MD, van den Maagdenberg A. Molecular genetics of migraine. *Human Genetics*. 2009;126(1):115-32.
43. Anttila V, Stefansson H, Kallela M, Todt U, Terwindt GM, Calafato MS, et al. Genome-wide association study of migraine implicates a common susceptibility variant on 8q22.1. *Nat Genet*. 2010;42(10):869-73.
44. Chasman DI, Schurks M, Anttila V, de Vries B, Schminke U, Launer LJ, et al. Genome-wide association study reveals three susceptibility loci for common migraine in the general population. *Nat Genet*. 2011;43(7):695-U116.
45. Ligthart L, de Vries B, Smith AV, Ikram MA, Amin N, Hottenga J-J, et al. Meta-analysis of genome-wide association for migraine in six population-based European cohorts. *European Journal of Human Genetics*. 2011;19(8):901-7.
46. Schürks M. Genetics of migraine in the age of genome-wide association studies. *Journal of Headache and Pain*. 2012;13(1):1-9.
47. Nyholt DR, LaForge KS, Kallela M, Alakurtti K, Anttila V, Farkkila M, et al. A high-density association screen of 155 ion transport genes for involvement with common migraine. *Human Molecular Genetics*. 2008;17(21):3318-31.
48. Schoenen J, Wang W, Albert A, Delwaide PJ. Potentiation Instead of Habituation Characterizes Visual-Evoked Potentials in Migraine Patients Between Attacks. *Eur J Neurol*. 1995;2(2):115-22.
49. Coppola G, Pierelli F, Schoenen J. Habituation and migraine. *Neurobiology of Learning and Memory*. 2009;92(2):249-59.
50. Katsarava Z, Giffin N, Diener HC, Kaube H. Abnormal habituation of 'nociceptive' blink reflex in migraine evidence for increased excitability of trigeminal nociception. *Cephalalgia*. 2003;23(8):814-9.
51. Evers S, Quibeldey F, Grotemeyer KH, Suhr B, Husstedt IW. Dynamic changes of cognitive habituation and serotonin metabolism during the migraine interval. *Cephalalgia*. 1999;19(5):485-91.

-
52. Coppola G, Currà A, Sava SA, Alibardi A, Parisi V, Pierelli F, et al. Changes in visual-evoked potential habituation induced by hyperventilation in migraine. *Journal of Headache and Pain*. 2010;11:497-503.
53. Welch KMA, Dandrea G, Tepley N, Barkley G, Ramadan NM. The Concept of Migraine as a State of Central Neuronal Hyperexcitability. *Neurologic Clinics*. 1990;8(4):817-28.
54. Aurora SK, Ahmad BK, Welch KMA, Bhardhwaj P, Ramadan NM. Transcranial magnetic stimulation confirms hyperexcitability of occipital cortex in migraine. *Neurology*. 1998;50(4):1111-4.
55. Aurora SK, Wilkinson F. The brain is hyperexcitable in migraine. *Cephalalgia*. 2007;27(12):1442-53.
56. Mulleners WM, Chronicle EP, Palmer JE, Koehler PJ, Vredeveld JW. Visual cortex excitability in migraine with and without aura. *Headache*. 2001;41(6):565-72.
57. Chronicle E, Mulleners W. Might Migraine Damage the Brain. *Cephalalgia*. 1994;14(6):415-8.
58. Huang J, DeLano M, Cao Y. Visual cortical inhibitory function in migraine is not generally impaired: evidence from a combined psychophysical test with an fMRI study. *Cephalalgia*. 2006;26(5):554-60.
59. Afra J, Mascia A, Gerard P, de Noordhout AM, Schoenen J. Interictal cortical excitability in migraine: A study using transcranial magnetic stimulation of motor and visual cortices. *Annals of Neurology*. 1998;44(2):209-15.
60. Afra J, Ambrosini A, Genicot R, Albert A, Schoenen J. Influence of colors on habituation of visual evoked potentials in patients with migraine with aura and in healthy volunteers. *Headache*. 2000;40(1):36-40.
61. Coppola G, Vandenheede M, Di Clemente L, Ambrosini A, Fumal A, De Pasqua V, et al. Somatosensory evoked high-frequency oscillations reflecting thalamo-cortical activity are decreased in migraine patients between attacks. *Brain*. 2005;128:98-103.
62. Afra J, Cecchini AP, Sandor PS, Schoenen J. Comparison of visual and auditory evoked cortical potentials in migraine patients between attacks. *Clin Neurophysiol*. 2000;111(6):1124-9.
63. Ambrosini A, de Noordhout AM, Sandor P, Schoenen J. Electrophysiological studies in migraine: a comprehensive review of their interest and limitations. *Cephalalgia*. 2003;23:13-31.

64. Coppola G, Ambrosini A, Di Clemente L, Magis D, Fumal A, Gerard P, et al. Interictal abnormalities of gamma band activity in visual evoked responses in migraine: an indication of thalamocortical dysrhythmia? *Cephalalgia*. 2007;27:1360-7.
65. Fumal A, Schoenen J. Cortical hypoactivity or reduced efficiency of cortical inhibition in migraine? Reply. *Cephalalgia*. 2007;27(2):188-9.
66. Afra J, Sandor PS, Schoenen J. Habituation of visual and intensity dependence of auditory evoked cortical potentials tends to normalize just before and during the migraine attack. *Cephalalgia*. 2000;20(8):714-9.
67. Sandor PS, Afra J, Cecchini AP, Albert A, Schoenen J. From neurophysiology to genetics: Cortical information processing in migraine underlies familial influences - A novel approach. *Funct Neurol*. 2000;15(3):68-72.
68. Thie A, Fuhlendorf A, Spitzer K, Kunze K. Transcranial Doppler evaluation of common and classic migraine. 1. Ultrasound features during the headache- free period. *Headache*. 1990;30(4):201-8.
69. Harer C, Vonkummer R. Cerebrovascular CO₂ reactivity in migraine - assessment by transcranial Doppler ultrasound. *J Neurol*. 1991;238(1):23-6.
70. Abernathy M, Donnelly G, Kay G, Wieneke J, Morris S, Bergeson S, et al. Transcranial Doppler sonography in headache-free migraineurs. *Headache*. 1994;34(4):198-203.
71. Fiermonte G, Pierelli F, Pauri F, Cosentino FII, Soccorsi R, Giacomini P. Cerebrovascular CO₂ reactivity in migraine with aura and without aura - a transcranial Doppler study. *Acta Neurol Scand*. 1995;92(2):166-9.
72. Valikovics A, Olah L, Fulesdi B, Kaposzta Z, Ficzer A, Bereczki D, et al. Cerebrovascular reactivity measured by transcranial Doppler in migraine. *Headache*. 1996;36(5):323-8.
73. Arjona A, de Torres LAP, Serrano-Castro PJ, Guardado-Santervas PL, Olivares J, Rubi-Callejon J. A Transcranial Doppler study in interictal migraine and tension-type headache. *Journal of Clinical Ultrasound*. 2007;35(7):372-5.
74. Olesen J. The role of nitric oxide (NO) in migraine, tension-type headache and cluster headache. *Pharmacology & Therapeutics*. 2008;120(2):157-71.
75. Thomsen LL, Kruuse C, Iversen HK, Olesen J. A nitric oxide donor (nitroglycerin) triggers genuine migraine attacks. *Eur J Neurol*. 1994;1(1):73-80.

-
76. Christiansen I, Thomsen LL, Daugaard D, Ulrich V, Olesen J. Glyceryl trinitrate induces attacks of migraine without aura in sufferers of migraine with aura. *Cephalalgia*. 1999;19(7):660-7.
77. Kruit MC, van Buchem MA, Hofman PA, Bakkers JT, Terwindt GM, Ferrari MD, et al. Migraine as a risk factor for subclinical brain lesions. *JAMA*. 2004;291(4):427-34.
78. Kruit MC, van Buchem MA, Launer LJ, Terwindt GM, Ferrari MD. Migraine is associated with an increased risk of deep white matter lesions, subclinical posterior circulation infarcts and brain iron accumulation: The population-based MRI CAMERA study. *Cephalalgia*. 2010;30(2):129-36.
79. Welch KMA, Nagesh V, Aurora SK, Gelman N. Periaqueductal gray matter dysfunction in migraine: Cause or the burden of illness? *Headache*. 2001;41(7):629-37.
80. Kim JH, Kim S, Suh SI, Koh SB, Park KW, Oh K. Interictal metabolic changes in episodic migraine: A voxel-based FDG-PET study. *Cephalalgia*. 2010;30(1):53-61.
81. Montagna P, Sacquegna T, Martinelli P, Cortelli P, Bresolin N, Moggio M, et al. Mitochondrial abnormalities in migraine. Preliminary findings. *Headache*. 1988;28(7):477-80.
82. Montagna P, Cortelli P, Monari L, Pierangeli G, Parchi P, Lodi R, et al. P-31-Magnetic Resonance Spectroscopy in Migraine Without Aura. *Neurology*. 1994;44(4):666-9.
83. Reyngoudt H, Paemeleire K, Descamps B, De Deene Y, Achten E. (31)P-MRS demonstrates a reduction in high-energy phosphates in the occipital lobe of migraine without aura patients. *Cephalalgia*. 2011;31(12):1243-53.
84. Lodi R, Lotti S, Cortelli P, Pierangeli G, Cevoli S, Clementi V, et al. Deficient energy metabolism is associated with low free magnesium in the brains of patients with migraine and cluster headache. *Brain Res Bull*. 2001;54(4):437-41.
85. Sanchez-del-Rio M, Reuter U, Moskowitz MA. New insights into migraine pathophysiology. *Curr Opin Neurol*. 2006;19(3):294-8.
86. Schoenen J. Pathogenesis of Migraine: the Biobehavioral and Hypoxia Theories Reconciled. *Acta Neurol Belg*. 1994;94(2):79-86.
87. May A, Goadsby PJ. The trigeminovascular system in humans: Pathophysiologic implications for primary headache syndromes of the neural influences on the cerebral circulation. *J Cereb Blood Flow Metab*. 1999;19(2):115-27.
88. Goadsby PJ, Edvinsson L, Ekman R. Vasoactive Peptide Release in the Extracerebral Circulation of Humans during Migraine Headache. *Annals of Neurology*. 1990;28(2):183-7.

89. Gallai V, Sarchielli P, Floridi A, Franceschini M, Codini M, Glioti G, et al. Vasoactive Peptide Levels in the Plasma of Young Migraine Patients With and Without Aura Assessed both Interictally and Ictally. *Cephalalgia*. 1995;15(5):384-90.
90. Schelstraete C, Paemeleire K. CGRP antagonists: hope for a new era in acute migraine treatment. *Acta Neurol Belg*. 2009;109(4):252-61.
91. Schoonman GG, van der Grond J, Kortmann C, van der Geest RJ, Terwindt GM, Ferrari MD. Migraine headache is not associated with cerebral or meningeal vasodilatation - a 3T magnetic resonance angiography study. *Brain*. 2008;131:2192-200.
92. Wolff HG. Headache and Other Head Pain. New York: Oxford University Press; 1948.
93. Goadsby PJ, Akerman S. The trigeminovascular system does not require a peripheral sensory input to be activated - migraine is a central disorder. *Cephalalgia*. 2012;32(1):3-5.
94. Weiller C, May A, Limmroth V, Juptner M, Kaube H, Schayck RV, et al. Brain stem activation in spontaneous human migraine attacks. *Nat Med*. 1995;1(7):658-60.
95. Cao Y, Welch KM, Aurora S, Vikingstad EM. Functional MRI-BOLD of visually triggered headache in patients with migraine. *Arch Neurol*. 1999;56(5):548-54.
96. Olesen J, Larsen B, Lauritzen M. Focal Hyperemia Followed by Spreading Oligemia and Impaired Activation of rCBF in Classic Migraine. *Annals of Neurology*. 1981;9(4):344-52.
97. Tfelt-Hansen PC. History of migraine with aura and cortical spreading depression from 1941 and onwards. *Cephalalgia*. 2010;30(7):780-92.
98. Woods RP, Iacoboni M, Mazziotta JC. Bilateral Spreading Cerebral Hypoperfusion during Spontaneous Migraine Headache. *N Eng J Med*. 1994;331(25):1689-92.
99. Blau J. Migraine With Aura and Migraine Without Aura are not Different Entities. *Cephalalgia*. 1995;15(3):186-90.
100. Denuelle M, Fabre N, Payoux P, Chollet F, Geraud G. Posterior cerebral hypoperfusion in migraine without aura. *Cephalalgia*. 2008;28(8):856-62.
101. Moskowitz MA, Nozaki K, Kraig RP. Neocortical Spreading Depression Provokes the Expression of c-fos Protein-like Immunoreactivity within Trigeminal Nucleus Caudalis via Trigemino-vascular Mechanisms. *Journal of Neuroscience*. 1993;13(3):1167-77.

-
102. Bolay H, Reuter U, Dunn AK, Huang ZH, Boas DA, Moskowitz MA. Intrinsic brain activity triggers trigeminal meningeal afferents in a migraine model. *Nat Med*. 2002;8(2):136-42.
103. Zhang X, Levy D, Kainz V, Nosedà R, Jakubowski M, Burstein R. Activation of Central Trigemino-vascular Neurons by Cortical Spreading Depression. *Annals of Neurology*. 2011;69(5):855-65.
104. Zhang X, Levy D, Nosedà R, Kainz V, Jakubowski M, Burstein R. Activation of Meningeal Nociceptors by Cortical Spreading Depression: Implications for Migraine with Aura. *Journal of Neuroscience*. 2010;30(26):8807-14.
105. Swartz RH, Kern RZ. Migraine is associated with magnetic resonance imaging white matter abnormalities - A meta-analysis. *Arch Neurol*. 2004;61(9):1366-8.
106. Igarashi H, Sakai F, Kan S, Okada J, Tazaki Y. Magnetic Resonance Imaging of the Brain in Patients with Migraine. *Cephalalgia*. 1991;11(2):69-74.
107. Pavese N, Canapicchi R, Nuti A, Bibbiani F, Lucetti C, Collavoli P, et al. White-Matter MRI Hyperintensities in a 129 Consecutive Migraine Patients. *Cephalalgia*. 1994;14(5):342-5.
108. De Benedittis G, Lorenzetti A, Sina C, Bernasconi V. Magnetic-Resonance-Imaging in Migraine and Tension-Type Headache. *Headache*. 1995;35(5):264-8.
109. Cooney BS, Grossman RI, Farber RE, Goin JE, Galetta SL. Frequency of magnetic resonance imaging abnormalities in patients with migraine. *Headache*. 1996;36(10):616-21.
110. Swartz RH, Kern RZ. Migraine Is Associated with MRI White Matter Abnormalities: Meta-Analysis. *Arch Neurol*. 2004;61(9):1366-8.
111. Kruit MC, Launer LJ, Ferrari MD, van Buchem MA. Brain Stem and Cerebellar Hyperintense Lesions in Migraine. *Stroke*. 2006;37(4):1109-12.
112. Kruit MC, Launer LJ, Ferrari MD, van Buchem MA. Infarcts in the posterior circulation territory in migraine. The population-based MRI CAMERA study. *Brain*. 2005;128:2068-77.
113. Palm-Meinders IH, Koppen H, Terwindt GM, Launer LJ, van Buchem MA, Ferrari MD, et al. Progression of brain white matter lesions in migraine? The 9-year follow-up population-based CAMERA-2 study. *Cephalalgia*. 2009;29(12):1351-2.
114. Trautinger A, Leel-Ossy E, Kamson DO, Poto L, Aradi M, Kover F, et al. Risk factors of migraine-related brain white matter hyperintensities: an investigation of 186 patients. *Journal of Headache and Pain*. 2011;12(1):97-103.

115. Matharu MS, Good CD, May A, Bahra A, Goadsby PJ. No change in the structure of the brain in migraine: a voxel-based morphometric study. *Eur J Neurol*. 2003;10(1):53-7.
116. Rocca MA, Colombo B, Inglese M, Codella M, Comi G, Filippi M. A diffusion tensor magnetic resonance imaging study of brain tissue from patients with migraine. *J Neurol Neurosurg PS*. 2003;74(4):501-3.
117. Rocca MA, Ceccarelli A, Falini A, Colombo B, Tortorella P, Bernasconi L, et al. Brain Gray Matter Changes in Migraine Patients With T2-Visible Lesions: A 3-T MRI Study. *Stroke*. 2006;37(7):1765-70.
118. Rocca MA, Ceccarelli A, Falini A, Tortorella P, Colombo B, Pagani E, et al. Diffusion tensor magnetic resonance imaging at 3.0 tesla shows subtle cerebral grey matter abnormalities in patients with migraine. *J Neurol Neurosurg PS*. 2006;77(5):686-9.
119. Kim J, Suh SI, Seol H, Oh K, Seo WK, Yu SW, et al. Regional grey matter changes in patients with migraine: a voxel-based morphometry study. *Cephalalgia*. 2008;28(6):598-604.
120. Valfre W, Rainero I, Bergui M, Pinessi L. Voxel-based morphometry reveals gray matter abnormalities in migraine. *Headache*. 2008;48(1):109-17.
121. Schmidt-Wilcke T, Ganssbauer S, Neuner T, Bogdahn U, May A. Subtle grey matter changes between migraine patients and healthy controls. *Cephalalgia*. 2008;28(1):1-4.
122. DaSilva AFM, Granziera C, Tuch DS, Snyder J, Vincent M, Hadjikhani N. Interictal alterations of the trigeminal somatosensory pathway and periaqueductal gray matter in migraine. *Neuroreport*. 2007;18(4):301-5.
123. DaSilva AFM, Granziera C, Snyder J, Hadjikhani N. Thickening in the somatosensory cortex of patients with migraine. *Neurology*. 2007;69(21):1990-5.
124. Granziera C, DaSilva AFM, Snyder J, Tuch DS, Hadjikhani N. Anatomical alterations of the visual motion processing network in migraine with and without aura. *Plos Medicine*. 2006;3(10):1915-21.
125. Datta R, Detre JA, Aguirre GK, Cucchiara B. Absence of changes in cortical thickness in patients with migraine. *Cephalalgia*. 2011;31(14):1452-8.
126. May A. Chronic pain may change the structure of the brain. *Pain*. 2008;137(1):7-15.

-
127. Schmitz N, Admiraal-Behloul F, Arkink EB, Kruit MC, Schoonman GG, Ferrari MD, et al. Attack frequency and disease duration as indicators for brain damage in migraine. *Headache*. 2008;48(7):1044-55.
128. Gelman N, Gorell JM, Barker PB, Savage RM, Spickler EM, Windham JP, et al. MR imaging of human brain at 3.0 T: Preliminary report on transverse relaxation rates and relation to estimated iron content. *Radiology*. 1999;210(3):759-67.
129. Kruit MC, Launer LJ, Overbosch J, van Buchem MA, Ferrari MD. Iron accumulation in deep brain nuclei in migraine: a population-based magnetic resonance imaging study. *Cephalalgia*. 2009;29(3):351-9.
130. Paemeleire K. Brain lesions and cerebral functional impairment in migraine patients. *J Neurol Sci*. 2009;283(1-2):134-6.
131. Afridi SK, Giffin NJ, Kaube H, Friston KJ, Ward NS, Frackowiak RSJ, et al. A positron emission tomographic study in spontaneous migraine. *Arch Neurol*. 2005;62(8):1270-5.
132. Bahra A, Matharu MS, Buchel C, Frackowiak RSJ, Goadsby PJ. Brainstem activation specific to migraine headache. *Lancet*. 2001;357(9261):1016-7.
133. Afridi SK, Matharu MS, Lee L, Kaube H, Friston KJ, Frackowiak RSJ, et al. A PET study exploring the laterality of brainstem activation in migraine using glyceryl trinitrate. *Brain*. 2005;128:932-9.
134. Bednarczyk EM, Remler B, Weikart C, Nelson AD, Reed RC. Global cerebral blood flow, blood volume, and oxygen metabolism in patients with migraine headache. *Neurology*. 1998;50(6):1736-40.
135. Iannetti GD, Mouraux A. From the neuromatrix to the pain matrix (and back). *Experimental Brain Research*. 2010;205(1):1-12.
136. Lauritzen M, Olesen J. Regional Cerebral Blood-Flow during Migraine Attacks by Xe-133 Inhalation and Emission Tomography. *Brain*. 1984;107(JUN):447-61.
137. Mirza M, Tutus A, Erdogan F, Kula M, Tomar A, Silov G, et al. Interictal SPECT with tc-99m HMPAO studies in migraine patients. *Acta Neurol Belg*. 1998;98(2):190-4.
138. Levine SR, Welch KMA, Ewing JR, Robertson WM. Asymmetric Cerebral Blood-Flow Patterns in Migraine. *Stroke*. 1986;17(1):147-.
139. Cao Y, Aurora SK, Nagesh V, Patel SC, Welch KM. Functional MRI-BOLD of brainstem structures during visually triggered migraine. *Neurology*. 2002;59(1):72-8.

140. Bramanti P, Grugno R, Vitetta A, Di Bella P, Muscara N, Nappi G. Migraine with and without aura: electrophysiological and functional neuroimaging evidence. *Funct Neurol*. 2005;20(1):29-32.
141. Moulton EA, Burstein R, Tully S, Hargreaves R, Becerra L, Borsook D. Interictal Dysfunction of a Brainstem Descending Modulatory Center in Migraine Patients. *Plos One*. 2008;3(11).
142. Sprenger T, Seifert CL, Valet M, Staehle K, Tölle TR, Foerschler A, et al. Abnormal interictal large-scale brain network connectivity in episodic migraine. Abstract presented at the 52nd Annual Scientific Meeting of the American Headache Society. 2010.
143. Mainero C, Boshyan J, Hadjikhani N. Altered functional magnetic resonance imaging resting-state connectivity in periaqueductal gray networks in migraine. *Annals of Neurology*. 2011;70(5):838-45.
144. Rocca MA, Colombo B, Pagani E, Falini A, Codella M, Scotti G, et al. Evidence for cortical functional changes in patients with migraine and white matter abnormalities on conventional and diffusion tensor magnetic resonance imaging. *Stroke*. 2003;34(3):665-70.
145. Zaletel M, Strucl M, Bajrovic FF, Pogacnik T. Coupling between visual evoked cerebral blood flow velocity responses and visual evoked potentials in migraineurs. *Cephalalgia*. 2005;25(8):567-74.
146. Vernieri F, Tibuzzi F, Pasqualetti P, Altamura C, Palazzo P, Rossini PM, et al. Increased cerebral vasomotor reactivity in migraine with aura: an autoregulation disorder? A transcranial Doppler and near-infrared spectroscopy study. *Cephalalgia*. 2008;28(7):689-95.
147. Schytz HW, Ciftci K, Akin A, Ashina M, Bolay H. Intact neurovascular coupling during executive function in migraine without aura: Interictal near-infrared spectroscopy study. *Cephalalgia*. 2010;30(4):457-66.
148. Akin A, Bilensoy D, Emir UE, Gulsoy M, Candansayar S, Bolay H. Cerebrovascular dynamics in patients with migraine: Near-infrared spectroscopy study. *Neurosci Lett*. 2006;400(1-2):86-91.
149. Coutts LV, Cooper CE, Elwell CE, Wilkins AJ. Time course of the haemodynamic response to visual stimulation in migraine, measured using near-infrared spectroscopy. *Cephalalgia*. 2012;32(8):621-9.
150. Hendrix A. Magnets, Spins, and Resonances - An introduction to the basics of Magnetic Resonance: Siemens Medical Solutions; 2003.
151. Wansapura JP, Holland SK, Dunn RS, Ball WS. NMR relaxation times in the human brain at 3.0 tesla. *J Magn Reson Imaging*. 1999;9(4):531-8.

-
152. Haacke EM, Brown RW, Thompson MR, Venkatesan R. Magnetic Resonance Imaging - Physical Principles and Sequence Design: Wiley; 1999.
153. Kuperman V. Magnetic Resonance Imaging - Physical Principles and Applications. Mayergoyz I, editor: Academic Press; 2000.
154. Bernstein MA, King KF, Zhou XJ. Handbook of MRI Pulse Sequences: Elsevier; 2004.
155. Buxton RB, Uludag K, Dubowitz DJ, Liu TT. Modeling the hemodynamic response to brain activation. *NeuroImage*. 2004;23:S220-S33.
156. Fox PT, Raichle ME. Focal Physiological Uncoupling of Cerebral Blood-Flow and Oxidative-Metabolism During Somatosensory Stimulation in Human-Subjects. *Proc Natl Acad Sci U S A*. 1986;83(4):1140-4.
157. Ogawa S, Lee TM, Kay AR, Tank DW. Brain magnetic resonance imaging with contrast dependent on blood oxygenation. *Proc Natl Acad Sci U S A*. 1990;87(24):9868-72.
158. Pauling L, Coryell C. The Magnetic Properties and Structure of Hemoglobin, Oxyhemoglobin and Carbonmonoxyhemoglobin. *Proc Natl Acad Sci U S A*. 1936;22(4):210-6.
159. Thulborn KR, Waterton JC, Matthews PM, Radda GK. Oxygenation Dependence of the Transverse Relaxation-Time of Water Protons in Whole-Blood at High-Field. *Biochimica Et Biophysica Acta*. 1982;714(2):265-70.
160. Le Bihan D, Urayama S, Aso T, Hanakawa T, Fukuyama H. Direct and fast detection of neuronal activation in the human brain with diffusion MRI. *Proc Natl Acad Sci U S A*. 2006;103(21):8263-8.
161. Williams DS, Detre JA, Leigh JS, Koretsky AP. Magnetic resonance imaging of perfusion using spin inversion of arterial water. *Proc Natl Acad Sci U S A*. 1992;89(1):212-6.
162. Stroman PW, Krause V, Malisza KL, Frankenstein UN, Tomanek B. Extravascular proton-density changes as a Non-BOLD component of contrast in fMRI of the human spinal cord. *Magn Reson Med*. 2002;48(1):122-7.
163. Logothetis NK, Pauls J, Augath M, Trinath T, Oeltermann A. Neurophysiological investigation of the basis of the fMRI signal. *Nature*. 2001;412(6843):150-7.
164. Scheeringa R, Fries P, Petersson K-M, Oostenveld R, Grothe I, Norris DG, et al. Neuronal Dynamics Underlying High- and Low-Frequency EEG Oscillations Contribute Independently to the Human BOLD Signal. *Neuron*. 2011;69(3):572-83.

165. Magri C, Schridde U, Murayama Y, Panzeri S, Logothetis NK. The Amplitude and Timing of the BOLD Signal Reflects the Relationship between Local Field Potential Power at Different Frequencies. *Journal of Neuroscience*. 2012;32(4):1395-407.
166. Foucher JR, Otzenberger H, Gounot D. The BOLD response and the gamma oscillations respond differently than evoked potentials: an interleaved EEG-fMRI study. *Bmc Neuroscience*. 2003;4.
167. Menon RS, Ogawa S, Hu XP, Strupp JP, Anderson P, Ugurbil K. BOLD Based Functional MRI at 4 Tesla Includes a Capillary Bed Contribution: Echo-Planar Imaging Correlates with Previous Optical Imaging Using Intrinsic Signals. *Magn Reson Med*. 1995;33(3):453-9.
168. Ances BM. Coupling of changes in cerebral blood flow with neural activity: What must initially dip must come back up. *J Cereb Blood Flow Metab*. 2004;24(1):1-6.
169. Aguirre GK, Zarahn E, D'Esposito M. The variability of human, BOLD hemodynamic responses. *NeuroImage*. 1998;8(4):360-9.
170. D'Esposito M, Zarahn E, Aguirre GK, Rypma B. The variability of bold hemodynamic responses in young and elderly subjects: Implications for FMRI studies of normal aging. *Journal of Cognitive Neuroscience*. 1999:72-.
171. Buckner RL, Snyder AZ, Sanders AL, Raichle ME, Morris JC. Functional brain imaging of young, nondemented, and demented older adults. *Journal of Cognitive Neuroscience*. 2000;12:24-34.
172. Liu TT, Behzadi Y, Restom K, Uludag K, Lu K, Buracas GT, et al. Caffeine alters the temporal dynamics of the visual BOLD response. *NeuroImage*. 2004;23(4):1402-13.
173. <http://www.drugbank.ca/drugs/DB00201 - pharmacology>. Drug Bank; 2010 [updated 27 December 2010].
174. Marrelec G, Benali H, Ciuciu P, Pelegrini-Issac M, Poline JB. Robust Bayesian estimation of the hemodynamic response function in event-related BOLD fMRI using basic physiological information. *Hum Brain Mapp*. 2003;19(1).
175. Handwerker DA, Ollinger JM, D'Esposito M. Variation of BOLD hemodynamic responses across subjects and brain regions and their effects on statistical analyses. *NeuroImage*. 2004;21(4):1639-51.
176. Schwarzbauer C, Mildner T, Heinke W, Brett M, Deichmann R. Dual echo EPI - The method of choice for fMRI in the presence of magnetic field inhomogeneities? *NeuroImage*. 2010;49(1):316-26.

-
177. Singh M, Kim S, Kim TS. Correlation between BOLD-fMRI and EEG signal changes in response to visual stimulus frequency in humans. *Magn Reson Med*. 2003;49(1):108-14.
178. Vazquez AL, Noll DC. Nonlinear aspects of the BOLD response in functional MRI. *NeuroImage*. 1998;7(2):108-18.
179. Yesilyurt B, Ugurbil K, Uludag K. Dynamics and nonlinearities of the BOLD response at very short stimulus durations. *Magn Reson Imaging*. 2008;26(7):853-62.
180. Yesilyurt B, Whittingstall K, Ugurbil K, Logothetis NK, Uludag K. Relationship of the BOLD signal with VEP for ultrashort duration visual stimuli (0.1 to 5 ms) in humans. *J Cereb Blood Flow Metab*. 2010;30(2):449-58.
181. Pfeuffer J, McCullough JC, Van de Moortele PF, Ugurbil K, Hu XP. Spatial dependence of the nonlinear BOLD response at short stimulus duration. *NeuroImage*. 2003;18(4):990-1000.
182. Soltysik DA, Peck KK, White KD, Crosson B, Briggs RW. Comparison of hemodynamic response nonlinearity across primary cortical areas. *NeuroImage*. 2004;22(3):1117-27.
183. Birn RM, Saad ZS, Bandettini PA. Spatial heterogeneity of the nonlinear dynamics in the fMRI BOLD response. *NeuroImage*. 2001;14(4):817-26.
184. Gu H, Stein EA, Yang Y. Nonlinear responses of cerebral blood volume, blood flow and blood oxygenation signals during visual stimulation. *Magn Reson Imaging*. 2005;23(9):921-8.
185. Miller KL, Luh WM, Liu TT, Martinez A, Obata T, Wong EC, et al. Nonlinear temporal dynamics of the cerebral blood flow response. *Hum Brain Mapp*. 2001;13(1):1-12.
186. Boynton GM, Engel SA, Glover GH, Heeger DJ. Linear systems analysis of functional magnetic resonance imaging in human V1. *J Neurosci*. 1996;16(13):4207-21.
187. Dale AM, Buckner RL. Selective averaging of rapidly presented individual trials using fMRI. *Hum Brain Mapp*. 1997;5(5):329-40.
188. Friston KJ, Jezzard P, Turner R. Analysis of Functional MRI Time-Series. *Hum Brain Mapp*. 1994;1(2):153-71.
189. Friston KJ, Josephs O, Rees G, Turner R. Nonlinear event-related responses in fMRI. *Magn Reson Med*. 1998;39(1):41-52.

190. Huettel SA, McCarthy G. Evidence for a refractory period in the hemodynamic response to visual stimuli as measured by MRI. *NeuroImage*. 2000;11(5):547-53.
191. Chen HF, Yao DZ, Yang L. An extended convolution dynamic model of fMRI BOLD response. *Neurocomputing*. 2004;61:395-400.
192. Chen HF, Yao DZ, Liu ZX. A study on asymmetry of spatial visual field by analysis of the fMRI BOLD response. *Brain Topogr*. 2004;17(1):39-46.
193. Rajapakse JC, Kruggel F, Maisog JM, von Cramon DY. Modeling hemodynamic response for analysis of functional MRI time-series. *Hum Brain Mapp*. 1998;6(4):283-300.
194. Wager TD, Vazquez A, Hernandez L, Noll DC. Accounting for nonlinear BOLD effects in fMRI: parameter estimates and a model for prediction in rapid event-related studies. *NeuroImage*. 2005;25(1):206-18.
195. Johnston LA, Duff E, Mareels I, Egan GF. Nonlinear estimation of the BOLD signal. *NeuroImage*. 2008;40(2):504-14.
196. Jung KJ. A nonlinear BOLD model accounting for refractory effect by applying the longitudinal relaxation in NMR to the linear BOLD model. *Magn Reson Imaging*. 2009;27(7):907-12.
197. Lindquist MA, Wager TD. Validity and power in hemodynamic response modeling: A comparison study and a new approach. *Hum Brain Mapp*. 2007;28(8):764-84.
198. Lindquist MA, Meng Loh J, Atlas LY, Wager TD. Modeling the hemodynamic response function in fMRI: Efficiency, bias and mis-modeling. *NeuroImage*. 2009;45(1, Supplement 1):S187-S98.
199. Grill-Spector K, Henson R, Martin A. Repetition and the brain: neural models of stimulus-specific effects. *Trends Cogn Sci*. 2006;10(1):14-23.
200. Porcaro C, Ostwald D, Hadjipapas A, Barnes GR, Bagshaw AP. The relationship between the visual evoked potential and the gamma band investigated by blind and semi-blind methods. *Neuroimage*. 2011;56(3):1059-71.
201. Reyngoudt H. *In Vivo Quantitative Nuclear Magnetic Resonance Spectroscopy and the Neurobiology of Migraine*. Ghent: Ghent University; 2011.
202. Reyngoudt H, De Deene Y, Descamps B, Paemeleire K, Achten E. (1)H-MRS of brain metabolites in migraine without aura: absolute quantification using the phantom replacement technique. *Magn Reson Mater Phys*. 2010;23(4):227-41.

203. Reyngoudt H, Paemeleire K, Dierickx A, Descamps B, Vandemaele P, De Deene Y, et al. Does visual cortex lactate increase following photic stimulation in migraine without aura patients? A functional (1)H-MRS study. *Journal of Headache and Pain*. 2011;12(3):295-302.
204. Watanabe H, Kuwabara T, Ohkubo M, Tsuji S, Yuasa T. Elevation of cerebral lactate detected by localized 1H-magnetic resonance spectroscopy in migraine during the interictal period. *Neurology*. 1996;47(4):1093-5.
205. Sappey-Marinié D, Calabrese G, Fein G, Hugg JW, Biggins C, Weiner MW. Effect of photic stimulation on human visual cortex lactate and phosphates using 1H and 31P magnetic resonance spectroscopy. *J Cereb Blood Flow Metab*. 1992;12(4):584-92.
206. Descamps B, Vandemaele P, Paemeleire K, Leybaert L, Achten E. Single-Subject Hemodynamic Refractory Effects in Healthy Volunteers. *Proceedings of the International Society for Magnetic Resonance in Medicine*. 2008;16th Annual Scientific Meeting and Exhibition:389 (n° 2353).
207. Huettel SA, McCarthy G. Regional differences in the refractory period of the hemodynamic response: An event-related fMRI study. *NeuroImage*. 2001;14(5):967-76.
208. Henson RNA, Price CJ, Rugg MD, Turner R, Friston KJ. Detecting latency differences in event-related BOLD responses: Application to words versus nonwords and initial versus repeated face presentations. *NeuroImage*. 2002;15(1):83-97.
209. Kanwisher N, McDermott J, Chun MM. The fusiform face area: A module in human extrastriate cortex specialized for face perception. *J Neurosci*. 1997;17(11):4302-11.
210. Grill-Spector K, Malach R. fMR-adaptation: a tool for studying the functional properties of human cortical neurons. *Acta Psychol*. 2001;107(1-3):293-321.
211. Puce A, Allison T, McCarthy G. Electrophysiological studies of human face perception. III: Effects of top-down processing on face-specific potentials. *Cerebral Cortex*. 1999;9(5):445-58.
212. Haller S, Bartsch AJ. Pitfalls in fMRI. *European Radiology*. 2009;19(11):2689-706.
213. Gantenbein AR, Sandor PS. Physiological Parameters as Biomarkers of Migraine. *Headache*. 2006;46(7):1069-74.

Appendices

A. International Classification of Headache Disorders, 2nd Edition (ICHD-II), according to the International Headache Societyⁱ

Part I – The primary headaches

1. Migraine

- 1.1. Migraine without aura
- 1.2. Migraine with aura
 - 1.2.1. Typical aura with migraine headache
 - 1.2.2. Typical aura with non-migraine headache
 - 1.2.3. Typical aura without headache
 - 1.2.4. Familial hemiplegic migraine
 - 1.2.5. Sporadic hemiplegic migraine
 - 1.2.6. Basilar-type migraine
- 1.3. Childhood periodic syndromes that are commonly precursors of migraine
 - 1.3.1. Cyclical vomiting
 - 1.3.2. Abdominal migraine
 - 1.3.3. Benign paroxysmal vertigo of childhood
- 1.4. Retinal migraine
- 1.5. Complications of migraine
 - 1.5.1. Chronic migraine
 - 1.5.2. Status migrainosus
 - 1.5.3. Persistent aura without infarction
 - 1.5.4. Migrainous infarction
 - 1.5.5. Migraine-triggered seizure
- 1.6. Probable migraine
 - 1.6.1. Probable migraine without aura
 - 1.6.2. Probable migraine with aura
 - 1.6.3. Probable chronic migraine

2. Tension-type headache

- 2.1. Infrequent episodic tension-type headache
 - 2.1.1. Infrequent episodic tension-type headache associated with pericranial tenderness
 - 2.1.2. Infrequent episodic tension-type headache not associated with pericranial tenderness
- 2.2. Frequent episodic tension-type headache
 - 2.2.1. Frequent episodic tension-type headache associated with pericranial tenderness

ⁱ http://ihs-classification.org/_downloads/mixed/ihc_II_main_no_print.pdf

- 2.2.2. Frequent episodic tension-type headache not associated with pericranial tenderness
- 2.3. Chronic tension-type headache
 - 2.3.1. Chronic tension-type headache associated with pericranial tenderness
 - 2.3.2. Chronic tension-type headache not associated with pericranial tenderness
- 2.4. Probable tension-type headache
 - 2.4.1. Probable infrequent episodic tension-type headache
 - 2.4.2. Probable frequent episodic tension-type headache
 - 2.4.3. Probable chronic tension-type headache
- 3. Cluster headache and other trigeminal autonomic cephalalgias**
 - 3.1. Cluster headache
 - 3.1.1. Episodic cluster headache
 - 3.1.2. Chronic cluster headache
 - 3.2. Paroxysmal hemicrania
 - 3.2.1. Episodic paroxysmal hemicrania
 - 3.2.2. Chronic paroxysmal hemicrania
 - 3.3. Short-lasting Unilateral Neuralgiform headache attacks with Conjunctival injection and Tearing (SUNCT)
 - 3.4. Probable trigeminal autonomic cephalalgia
 - 3.4.1. Probable cluster headache
 - 3.4.2. Probable paroxysmal hemicrania
 - 3.4.3. Probable SUNCT
- 4. Other primary headaches
 - 4.1. Primary stabbing headache
 - 4.2. Primary cough headache
 - 4.3. Primary exertional headache
 - 4.4. Primary headache associated with sexual activity
 - 4.4.1. Preorgasmic headache
 - 4.4.2. Orgasmic headache
 - 4.5. Hypnic headache
 - 4.6. Primary thunderclap headache
 - 4.7. Hemicrania continua
 - 4.8. New daily-persistent headache

Part II – The secondary headaches

- 5. Headache attributed to head and/or neck trauma
 - 5.1. Acute post-traumatic headache
 - 5.1.1. Acute post-traumatic headache attributed to moderate or severe head injury
 - 5.1.2. Acute post-traumatic headache attributed to mild head injury
 - 5.2. Chronic post-traumatic headache
 - 5.2.1. Chronic post-traumatic headache attributed to moderate or severe head injury
 - 5.2.2. Chronic post-traumatic headache attributed to mild head injury
 - 5.3. Acute headache attributed to whiplash injury
 - 5.4. Chronic headache attributed to whiplash injury
 - 5.5. Headache attributed to traumatic intracranial haematoma
 - 5.5.1. Headache attributed to traumatic epidural haematoma

- 5.5.2. Headache attributed to subdural haematoma
- 5.6. Headache attributed to other head and / or neck traumata
 - 5.6.1. Acute headache attributed to other head and / or neck traumata
 - 5.6.2. Chronic headache attributed to other head and / or neck traumata
- 5.7. Post-craniotomy headache
 - 5.7.1. Acute post-craniotomy headache
 - 5.7.2. Chronic post-craniotomy
- 6. Headache attributed to cranial or cervical vascular disorder
 - 6.1. Headache attributed to ischaemic stroke or transient ischaemic attack
 - 6.1.1. Headache attributed to ischaemic stroke (cerebral infarction)
 - 6.1.2. Headache attributed to transient ischaemic attack
 - 6.2. Headache attributed to non-traumatic intracranial haemorrhage
 - 6.2.1. Headache attributed to intracerebral haemorrhage
 - 6.2.2. Headache attributed to subarachnoid haemorrhage
 - 6.3. Headache attributed to unruptured vascular malformation
 - 6.3.1. Headache attributed to saccular aneurysm
 - 6.3.2. Headache attributed to arteriovenous malformation
 - 6.3.3. Headache attributed to dural arteriovenous fistula
 - 6.3.4. Headache attributed to cavernous angioma
 - 6.3.5. Headache attributed to encephalotrigeminal or leptomeningeal angiomatosis (Sturge Weber syndrome)
 - 6.4. Headache attributed to arteritis
 - 6.4.1. Headache attributed to giant cell arteritis
 - 6.4.2. Headache attributed to primary central nervous system angiitis
 - 6.4.3. Headache attributed to secondary central nervous system angiitis
 - 6.5. Carotid or vertebral artery pain
 - 6.5.1. Headache or facial or neck pain attributed to arterial dissection
 - 6.5.2. Post-endarterectomy headache
 - 6.5.3. Carotid angioplasty headache
 - 6.5.4. Headache attributed to intracranial endovascular procedures
 - 6.5.5. Angiography headache
 - 6.6. Headache attributed to cerebral venous thrombosis
 - 6.7. Headache attributed to other intracranial vascular disorder
 - 6.7.1. Cerebral Autosomal Dominant Arteriopathy with Subcortical Infarcts and Leukoencephalopathy (CADASIL)
 - 6.7.2. Mitochondrial Encephalopathy, Lactic Acidosis and Stroke-like episodes (MELAS)
 - 6.7.3. Headache attributed to benign angiopathy of the central nervous system
 - 6.7.4. Headache attributed to pituitary apoplexy
- 7. Headache attributed to non-vascular intracranial disorder
 - 7.1. Headache attributed to high cerebrospinal fluid pressure
 - 7.1.1. Headache attributed to idiopathic intracranial hypertension
 - 7.1.2. Headache attributed to intracranial hypertension secondary to metabolic, toxic or hormonal causes
 - 7.1.3. Headache attributed to intracranial hypertension secondary to hydrocephalus
 - 7.2. Headache attributed to low cerebrospinal fluid pressure
 - 7.2.1. Post-dural puncture headache

- 7.2.2. CSF fistula headache
- 7.2.3. Headache attributed to spontaneous (or idiopathic) low CSF pressure
- 7.3. Headache attributed to non-infectious inflammatory disease
 - 7.3.1. Headache attributed to neurosarcoidosis
 - 7.3.2. Headache attributed to aseptic (non-infectious) meningitis
 - 7.3.3. Headache attributed to other non-infectious inflammatory disease
 - 7.3.4. Headache attributed to lymphocytic hypophysitis
- 7.4. Headache attributed to intracranial neoplasm
 - 7.4.1. Headache attributed to increased intracranial pressure or hydrocephalus caused by neoplasm
 - 7.4.2. Headache attributed directly to neoplasm
 - 7.4.3. Headache attributed to carcinomatous meningitis
 - 7.4.4. Headache attributed to hypothalamic or pituitary hyper- or hyposecretion
- 7.5. Headache attributed to intrathecal injection
- 7.6. Headache attributed to epileptic seizure
 - 7.6.1. Hemicrania epileptica
 - 7.6.2. Post-seizure headache
- 7.7. Headache attributed to Chiari malformation type I
- 7.8. Syndrome of transient Headache and Neurological Deficits with cerebrospinal fluid Lymphocytosis (HaNDL)
- 7.9. Headache attributed to other non-vascular intracranial disorder
- 8. Headache attributed to a substance or its withdrawal
 - 8.1. Headache induced by acute substance use or exposure
 - 8.1.1. Nitric oxide (NO) donor-induced headache
 - 8.1.1.1. Immediate NO donor-induced headache
 - 8.1.1.2. Delayed NO donor-headache
 - 8.1.2. Phosphodiesterase (PDE) inhibitor-induced headache
 - 8.1.3. Carbon monoxide-induced headache
 - 8.1.4. Alcohol-induced headache
 - 8.1.4.1. Immediate alcohol-induced headache
 - 8.1.4.2. Delayed alcohol-induced headache
 - 8.1.5. Headache induced by food components and additives
 - 8.1.5.1. Monosodium glutamate-induced headache
 - 8.1.6. Cocaine-induced headache
 - 8.1.7. Cannabis-induced headache
 - 8.1.8. Histamine-induced headache
 - 8.1.8.1. Immediate histamine-induced headache
 - 8.1.8.2. Delayed histamine-induced headache
 - 8.1.9. Calcitonin gene-related peptide (CGRP)-induced headache
 - 8.1.9.1. Immediate CGRP-induced headache
 - 8.1.9.2. Delayed CGRP-induced headache
 - 8.1.10. Headache as an acute adverse event attributed to medication used for other indications
 - 8.1.11. Headache induced by other acute substance use or exposure
 - 8.2. Medication-overuse headache (MOH)
 - 8.2.1. Ergotamine-overuse headache
 - 8.2.2. Triptan-overuse headache

- 8.2.3. Analgesic-overuse headache
- 8.2.4. Opioid-overuse headache
- 8.2.5. Combination medication-overuse headache
- 8.2.6. Headache attributed to other medication overuse
- 8.2.7. Probable medication-overuse headache
- 8.3. Headache as an adverse event attributed to chronic medication
 - 8.3.1. Exogenous hormone-induced headache
- 8.4. Headache attributed to substance withdrawal
 - 8.4.1. Caffeine-withdrawal headache
 - 8.4.2. Opioid-withdrawal headache
 - 8.4.3. Oestrogen-withdrawal headache
 - 8.4.4. Headache attributed to withdrawal from chronic use of other substances
- 9. Headache attributed to infection
 - 9.1. Headache attributed to intracranial infection
 - 9.1.1. Headache attributed to bacterial meningitis
 - 9.1.2. Headache attributed to lymphocytic meningitis
 - 9.1.3. Headache attributed to encephalitis
 - 9.1.4. Headache attributed to brain abscess
 - 9.1.5. Headache attributed to subdural empyema
 - 9.2. Headache attributed to systemic infection
 - 9.2.1. Headache attributed to systemic bacterial infection
 - 9.2.2. Headache attributed to systemic viral infection
 - 9.2.3. Headache attributed to other systemic infection
 - 9.3. Headache attributed to HIV / aids
 - 9.4. Chronic post-infection headache
 - 9.4.1. Chronic post-bacterial meningitis headache
- 10. Headache attributed to disorder of homoeostasis
 - 10.1. Headache attributed to hypoxia and / or hypercapnia
 - 10.1.1. High-altitude headache
 - 10.1.2. Diving headache
 - 10.1.3. Sleep apnoea headache
 - 10.2. Dialysis headache
 - 10.3. Headache attributed to arterial hypertension
 - 10.3.1. Headache attributed to pheochromocytoma
 - 10.3.2. Headache attributed to hypertensive crisis without hypertensive encephalopathy
 - 10.3.3. Headache attributed to hypertensive encephalopathy
 - 10.3.4. Headache attributed to pre-eclampsia
 - 10.3.5. Headache attributed to eclampsia
 - 10.3.6. Headache attributed to acute pressor response to an exogenous agent
 - 10.4. Headache attributed to hypothyroidism
 - 10.5. Headache attributed to fasting
 - 10.6. Cardiac cephalgia
 - 10.7. Headache attributed to other disorder of homoeostasis
- 11. Headache or facial pain attributed to disorder of cranium, neck, eyes, ears, nose, sinuses, teeth, mouth or other facial or cranial structures
 - 11.1. Headache attributed to disorder of cranial bone

- 11.2. Headache attributed to disorder of neck
 - 11.2.1. Cervicogenic headache
 - 11.2.2. Headache attributed to retropharyngeal tendonitis
 - 11.2.3. Headache attributed to craniocervical dystonia
- 11.3. Headache attributed to disorder of the eyes
 - 11.3.1. Headache attributed to acute glaucoma
 - 11.3.2. Headache attributed to refractive errors
 - 11.3.3. Headache attributed to heterophoria or heterotropia (latent or manifest squint)
 - 11.3.4. Headache attributed to ocular inflammatory disorder
- 11.4. Headache attributed to disorder of ears
- 11.5. Headache attributed to rhinosinusitis
- 11.6. Headache attributed to disorder of teeth, jaws or related structures
- 11.7. Headache or facial pain attributed to temporomandibular joint disorder
- 11.8. Headache attributed to other disorder of cranium, neck, eyes, ears, nose, sinuses, teeth, mouth or other facial or cervical structures
- 12. Headache attributed to psychiatric disorder
 - 12.1. Headache attributed to somatisation disorder
 - 12.2. Headache attributed to psychotic disorder

Part III – Cranial neuralgias, central and primary facial pain and other headaches

- 13. Cranial neuralgias and central causes of facial pain
 - 13.1. Trigeminal neuralgia
 - 13.1.1. Classical trigeminal migraine
 - 13.1.2. Symptomatic trigeminal neuralgia
 - 13.2. Glossopharyngeal neuralgia
 - 13.2.1. Classical glossopharyngeal neuralgia
 - 13.2.2. Symptomatic glossopharyngeal neuralgia
 - 13.3. Nervus intermedius neuralgia
 - 13.4. Superior laryngeal neuralgia
 - 13.5. Nasociliary neuralgia
 - 13.6. Supraorbital neuralgia
 - 13.7. Other terminal branch neuralgias
 - 13.8. Occipital neuralgia
 - 13.9. Neck-tongue syndrome
 - 13.10. External compression headache
 - 13.11. Cold-stimulus headache
 - 13.11.1. Headache attributed to external application of a cold stimulus
 - 13.11.2. Headache attributed to ingestion or inhalation of a cold stimulus
 - 13.12. Constant pain caused by compression, irritation or distortion of cranial nerves or upper cervical roots by structural lesions
 - 13.13. Optic neuritis
 - 13.14. Ocular diabetic neuropathy
 - 13.15. Head or facial pain attributed to herpes zoster
 - 13.15.1. Head or facial pain attributed to acute herpes zoster
 - 13.15.2. Post-herpetic neuralgia
 - 13.16. Tolosa-Hunt syndrome

- 13.17. Ophtalmoplegic 'migraine'
- 13.18. Central causes of facial pain
 - 13.18.1. Anaesthesia dolorosa
 - 13.18.2. Central post-stroke pain
 - 13.18.3. Facial pain attributed to multiple sclerosis
 - 13.18.4. Persistent idiopathic facial pain
 - 13.18.5. Burning mouth syndrome
- 13.19. Other cranial neuralgia or other centrally mediated facial pain
- 14. Other headache, cranial neuralgia, central or primary facial pain
 - 14.1. Headache not elsewhere classified
 - 14.2. Headache unspecified

**B. ^1H -MRS of brain metabolites in migraine without aura: absolute quantification
using the phantom replacement technique**

Harmen Reyngoudt, Yves De Deene, **Benedicte Descamps**, Koen Paemeleire, Eric Achten

Magn Reson Mater Phy 2010, 23(4): 227-41.

RESEARCH ARTICLE

^1H -MRS of brain metabolites in migraine without aura: absolute quantification using the phantom replacement technique

Harmen Reyngoudt · Yves De Deene ·
 Benedicte Descamps · Koen Paemeleire · Eric Achten

Received: 12 April 2010 / Revised: 21 June 2010 / Accepted: 23 June 2010 / Published online: 13 August 2010
 © ESMRMB 2010

Abstract

Objective Several studies have demonstrated differences in migraine patients when performing ^1H -MRS; however, no studies have performed ^1H -MRS in migraine without aura (MwoA), the most common migraine subtype. The aim of this ^1H -MRS study was to elucidate whether any differences could be found between MwoA patients and controls by performing absolute quantification.

Materials and methods ^1H -MRS was performed in 22 MwoA patients and 25 control subjects. Absolute quanti-

fication was based on the phantom replacement technique. Corrections were made for T_1 and T_2 relaxation effects, CSF content, coil loading and temperature. The method was validated by phantom measurements and in vivo measurements in the occipital visual cortex.

Results After calibration of the quantification procedure and the implementation of the required correction factors, measured absolute concentrations in the visual cortex of MwoA patients showed no significant differences compared to controls, in contrast to relative results obtained in earlier studies.

Conclusion In this study, we demonstrate the implementation of quantitative in vivo ^1H -MRS spectroscopy in migraine patients. Despite rigorous quantification, no spectroscopic abnormalities could be found in patients with migraine without aura.

Keywords Absolute quantification · ^1H -MRS · migraine without aura · correction factors · phantom replacement technique

H. Reyngoudt · B. Descamps · E. Achten (✉)
 Department of Radiology and Nuclear Medicine,
 Ghent Institute for Functional and Metabolic Imaging,
 Ghent University, Ghent, Belgium
 e-mail: rik.achten@ugent.be

H. Reyngoudt · B. Descamps · E. Achten
 MR-department, Ghent University Hospital,
 De Pintelaan 185, 9000 Ghent, Belgium

H. Reyngoudt
 e-mail: harmen.reyngoudt@ugent.be

Y. De Deene
 Department of Radiation Oncology and Experimental
 Cancer Research, Laboratory for Quantitative Nuclear
 Magnetic Resonance in Medicine and Biology,
 Ghent University, Ghent, Belgium

Y. De Deene
 Department of Nuclear Medicine and Radiobiology,
 University of Sherbrooke, Sherbrooke, Quebec, Canada

K. Paemeleire
 Department of Basic Medical Sciences,
 Ghent University, Ghent, Belgium

K. Paemeleire
 Department of Neurology, Ghent University Hospital,
 Ghent, Belgium

Introduction

Migraine is a common, chronic, disabling neurovascular disorder, with episodic manifestations, characterized by attacks of headache lasting 4–72 h, and associated symptoms such as photophobia, phonophobia, nausea and/or vomiting [1–4]. In 20–30% of the patients, aura symptoms are experienced [1, 2]. Migraine has a 1-year prevalence of at least 11% worldwide [5], affects women three times more than men [5] and has a high socio-economic impact [6]. It has been ranked nineteenth as worldwide cause of years lived with disability, according to the World Health Organization [7]. Migraine is a primary headache disorder, with an important genetic background and can be divided into two major subtypes: migraine

Table 1 Literature survey of ^1H -MRS studies in migraine (n is the number of patients included)

Study	Migraine type (n)	Brain region	Quantification	Results
Watanabe et al. [19]	MwA/other ^a (3/3)	Occipital	Relative	Lac/NAA ↑
Macri et al. [26]	MwA (8)	Cerebellum	Relative	Ins/tCr ↓, Cho/tCr ↓
Sandor et al. [20] ^b	MwA/MwpA (5/5)	Occipital	Relative	Lac/NAA ↑
Dichgans et al. [22]	FHM ^d (15)	Cerebellum	Absolute	Glu ↓, NAA ↓, Ins ↑
Sarchielli et al. [21] ^c	MwA/MwoA (22/22)	Occipital	Relative	NAA/tCr ↓
Jacob et al. [23]	SHM ^e (1)	Temporo-parietal	Relative	NAA/tCr ↓, Ins/tCr ↓
Schulz et al. [24]	MwA (21)	Basal ganglia	Relative	No changes
Gu et al. [25]	MwoA (22)	Thalamus	Relative	NAA/tCr ↓
Grimaldi et al. [28]	FHM (4)	Parieto-occipital	Relative	Lac ↑

^a Basilar migraine, migrainous infarction and MwpA^b Visual stimulation was performed by projection of a blue/yellow flickering checkerboard (8 Hz)^c Familial hemiplegic migraine^d Visual stimulation was performed by projection of a flashing red light (14 Hz)^e Sporadic hemiplegic migraine

without aura (MwoA) and migraine with aura (MwA), previously known as common and classic migraine, respectively [4]. Despite the high prevalence of migraine in the general population, the causes are still unknown. One hypothesis is that migraine is a disorder that might be caused by the concurrence of two pathophysiological components: excessive cortical activation due to lack of habituation during repetitive stimulation as well as a decreased brain mitochondrial energy reserve [8,9].

In the last 20 years several magnetic resonance spectroscopy (MRS) studies, in particular phosphorus magnetic resonance spectroscopy (^{31}P -MRS), suggested an energy disturbance in the brain of migraine patients during interictal periods [10–18]. Recent studies emphasized more on proton magnetic resonance spectroscopy (^1H -MRS) with a lot of heterogeneous, sometimes contradictory, results (Table 1). ^1H -MRS studies showed elevated interictal levels of cerebral lactate (Lac) in the occipital visual cortex of a heterogeneous group of migraine patients [19]. These results suggested a deranged oxidative glycolysis. In functional ^1H -MRS studies, visual stimulation resulted in a Lac increase in the visual cortex of patients with migraine with prolonged aura (MwpA) but not in MwA patients, in which Lac was already higher than normal [20] and N-acetylaspartate (NAA) was found to be reduced in the visual cortex of MwA patients [21]. A reduced NAA concentration was also found in several other brain regions of MwA patients without stimulation [22,23,25]. In other than occipital regions, significant differences for other metabolites such as myo-inositol (Ins), total creatine (tCr), choline (Cho) and glutamate/glutamine (Glx) have been found between migraineurs and controls [22,23,26,27].

Very few studies have quantified proton metabolites in the subgroup of MwoA patients. From these studies in which ^1H -MRS was performed, only relative quantification was

applied and/or spectra were acquired following visual stimulation (Table 1). From this point of view, we took a great interest in verifying whether there was indeed a basal interictal metabolic deficiency in the occipital visual cortex of these migraine patients. In order to confirm if there are subtle differences compared to controls, robust absolute quantification of these metabolites is necessary. In this study, we first describe the rigorous methodological setup of absolute quantification of metabolites in the visual cortex using ^1H -MRS, based on the phantom replacement technique. Important methodological parameters of absolute quantification were considered and taken into account, including reproducibility, stability, B_0 homogeneity, B_1 homogeneity, relaxation effect correction, temperature correction and cerebrospinal fluid content correction. Absolute quantification using the internal water reference was also performed. The optimized method was then applied to address the question of interictal metabolite abnormalities in the occipital visual cortex of MwoA patients when compared to normal controls.

Materials and methods

Acquisition, voxel placement, subjects and phantoms

Measurements were taken on a 3 Tesla Siemens Trio-Tim whole-body MR scanner (Erlangen, Germany), using a 26.5-cm-diameter quadrature dual-tuned (^{31}P - ^1H) birdcage transmit/receive head coil (Rapid Biomedical, Würzburg-Rimpar, Germany). Spectra were acquired using a single voxel point-resolved spin echo sequence (PRESS), with CHESS pulses for water suppression. Manual shimming of the B_0 magnetic field and manual optimization of the transmitter pulse power was applied. Twenty-two MwoA patients (33.3 ± 12.2 years, 1 man) were recruited by the local Headache Clinic of the Ghent University Hospital. The control

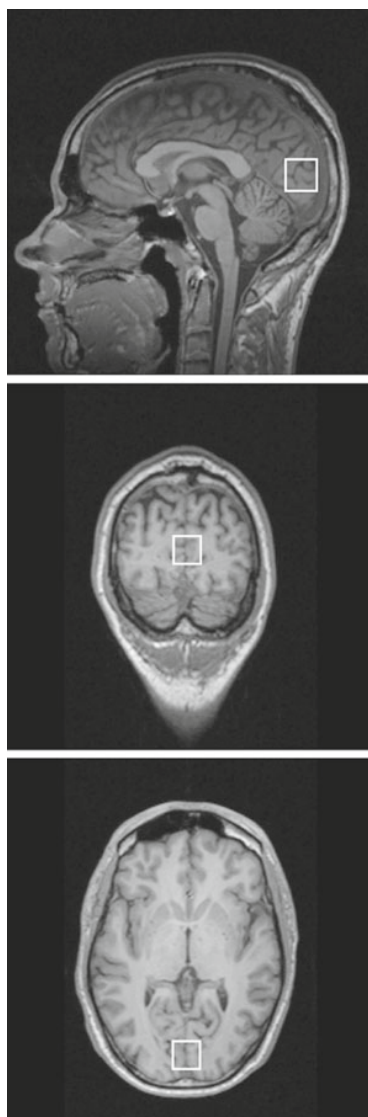


Fig. 1 Sagittal, coronal and axial T_1 -weighted images with a 20 mm cubic VOI localized in the occipital visual cortex

group (27.6 ± 12 years, 10 men) consisted of twenty-five volunteers which were matched in age but not in gender. All subjects have given written consent, and the study was approved by the local ethics committee. The migraine patients were diagnosed with MwoA according to the criteria of the International Headache Society [4]. On average, patients experienced 3.4 ± 1.1 attacks per month, were not using any prophylactic medication and were attack free for at least 48 h. A possible attack after the measurement was verified by e-mail.

The volume of interest (VOI) was placed in the primary visual cortex (Brodmann area 17), centered on the calcarine fissure (Fig. 1), localized on T_1 -weighted gradient-echo images in three orthogonal planes with a slice thickness of 1 mm, a TR of 1,550 ms and a TE of 2.37 ms. VOI size was

$20 \times 20 \times 20 \text{ mm}^3$. For each subject, six water-suppressed spectra at different TE (30, 60, 90, 120, 144 and 288 ms) with a TR of 4,000 ms and 64 averages, one water-suppressed spectrum with a TE of 30 ms, a TR of 2,000 ms and 96 averages and ten water-unsuppressed spectra (TE = 30, 50, 70, 90, 110, 150, 200, 300, 500, 1000 ms, TR = 10,000 ms, 1 average) were acquired. The raw data of each acquisition consisted of 1,024 complex-valued data points, at a sampling interval of 0.833 ms. The corresponding bandwidth was 1,200 Hz. The total duration of the examination was approximately 50 min.

The phantoms contained an aqueous solution (pH 7) of NAA, tCr, Cho and Ins (Sigma Aldrich) in different concentrations and combinations. Sodium chloride (NaCl) and sodium azide (NaN_3) were added to change the conductivity and as an antimycotic agent, respectively. Phantoms were made of plastic, were spherical and had a diameter of 10.4 cm. One of the phantoms consisted of an aqueous solution of 12 mM NAA, 10 mM tCr, 3 mM Cho and 6 mM Ins, to which 1% NaCl was added to simulate the physiological NaCl concentration, referred to further as the standard metabolite solution.

Spectral analysis

Water-unsuppressed spectra were processed without apodization and fitted by a single component using HLSVD, a method based on the Lanczos algorithm and included in the jMRUI package [29], yielding an estimation of the water signal amplitude. The residual water resonance was removed by HLSVD [30]. The signals of Lac, NAA, tCr and Cho were referenced at 1.31, 2.01, 3.03 and 3.19 ppm, respectively. The strongly coupled signal of Ins is referenced at 3.55 and 3.61 (Fig. 2). Following apodization (Lorentzian filter of 5 Hz), zero-filling (adding 1,024 zeros) and baseline correction, the water-suppressed spectra were fitted by the time-domain algorithm AMARES [31,32], software that is also included in the jMRUI package. This nonlinear least-squares algorithm fits a time-domain model function, using a singlet approach at a priori predefined resonance frequencies. The AMARES algorithm also includes other prior knowledge such as lower and upper bounds of the spectral parameters (frequency, linewidth, phase), Gaussian instead of Lorentzian lineshape for each peak and modulation of the background signal. In this study, Gaussian lineshapes and a least-squares fit were used in order to avoid problems from occasional minimal overlap of Cho and tCr peaks (Fig. 2c). Quantification of short TE in vivo signals is often hampered by a background signal originating mainly from macromolecules and lipids (Fig. 2b). In order to minimize the signals of macromolecules and lipids of water-suppressed spectra, AMARES gives the opportunity to truncate the initial data points [31].

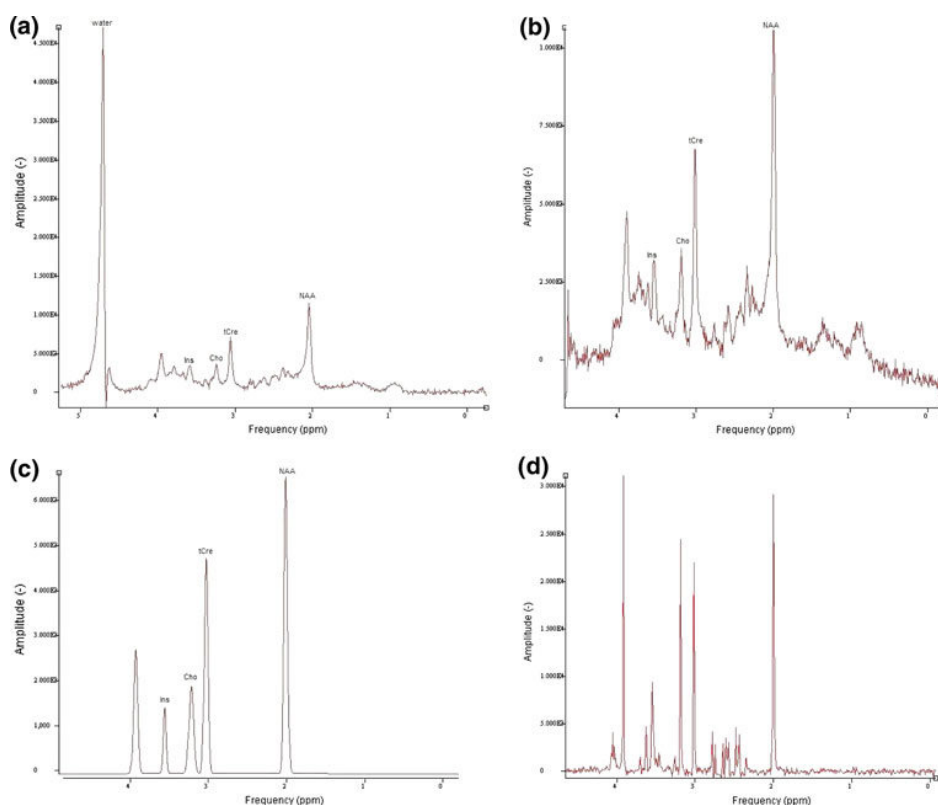


Fig. 2 Spectrum obtained in a patient with a water-suppressed PRESS sequence with a TE of 30 ms, a TR of 2,000 ms and 128 averages before (a) and after (b) removal of the residual water resonance. Notice the significant background signal in the in vivo spectra. c An estimation of

the in vivo metabolites based on spectrum b with removal of the macromolecular background signal by AMARES. d Spectrum obtained in a 20 mm cubic VOI in a phantom containing 12 mM NAA, 10 mM tCr, 3 mM Cho and 6 mM Ins

We truncated the first 20 data points, in order not to influence the quantification of the metabolites.

Reproducibility and stability

Before using the phantom for calibration of the in vivo signals, the influence of several scanning factors on signal amplitude, such as reproducibility and stability of the signal, was investigated.

Stability of the scanner, repeatability and reproducibility of the measurements were verified in both phantom and in vivo experimental setups. Repeatability and reproducibility both refer to the precision of the measurement and the ability to repeat and reproduce the experiment. In this study, repeatability is interpreted as consecutive measurements without repositioning and reshimming of the phantom, and reproducibility is interpreted as measurements with repositioning and reshimming of the phantom. In the phantom containing the standard metabolite solution, fifteen measurements were taken in the same voxel ($\text{VOI} = 20 \times 20 \times 20 \text{ mm}^3$) without repositioning and reshimming, followed by five additional measurements each time with repositioning and

reshimming of the phantom. The VOI was placed in the center of the phantom. This experiment was also repeated after one week, one month, six months and one year. In ten controls, two consecutive measurements were taken in the same voxel ($\text{VOI} = 20 \times 20 \times 20 \text{ mm}^3$) without repositioning and reshimming. Finally, we verified the in vivo reproducibility by repeating the experiment 16 times during one year in a single healthy volunteer (male, 29 years).

B_0 homogeneity

When a phantom or a subject is scanned, the magnetized object or body distorts the net magnetic field. Especially in heterogeneous media, composed of tissue with different magnetic susceptibilities, significant errors may be induced in the spectra [33]. Local B_0 inhomogeneities widen and distort the spectral lines from the ideal Lorentzian form [34]. The homogeneity of the B_0 field can be optimized by automatic and manual shimming. Manual shimming was performed until the linewidth or full-width-at-half-maximum (FWHM) was equal to or lower than 0.1 ppm or 12 Hz for $B_0 = 3 \text{ T}$ and the time-domain signal showed an exponential decay [33,35].

We verified the effect of incomplete shimming in a phantom containing an aqueous solution of 20 mM tCr (1% NaCl, pH 7). A first measurement was taken with optimized shim settings, followed by several other measurements with intentionally insufficient shimming (i.e. inhomogeneous B_0 field). The FWHM of the spectral peaks of all metabolites and water were verified in every volunteer.

B_1 homogeneity

It is assumed that in spectral quantification based on the phantom replacement technique, spatial sensitivity remains the same for the phantom and the in vivo measurement. In practice, there may be unexpected variations in signal intensity due to B_1 inhomogeneity, effects related to loading, eddy currents and standing waves [36]. These variations may depend on the size of the phantom, the electrical properties of the phantom and the corresponding properties of the human head. The spatial distribution of the B_1 field was investigated by the double-angle method, which measures the flip angle distribution within the sample [37]. This is an indirect measure of the B_1 field and can reveal standing waves in the coil. Two gradient-echo images, I_1 and I_2 , with corresponding flip angles θ and 2θ were recorded. The flip angle distribution is given by:

$$\theta = \arccos\left(\frac{I_2}{I_1}\right). \quad (1)$$

These images were obtained in two water-filled phantoms by a gradient-echo pulse sequence with a TE of 4.15 ms, a TR of 10,000 ms, slice thickness of 5 mm and a nominal θ of 35° . The two phantoms contained a 0 and 1% NaCl solution, respectively.

We further evaluated the potential presence of standing waves by positioning the voxel in different locations (central and off-center) in phantoms with different NaCl concentration (0, 0.5, 1, 1.5 and 2%) in order to change the dielectric properties of the phantom.

The effect of coil-related inhomogeneity was investigated by placing a water-filled phantom with 20 mm cubic VOIs at the system isocenter and at offsets of ± 30 , ± 60 and ± 90 mm along the x -, y - and z -axes. Spectra were acquired with the phantom repositioned between each acquisition with the VOI always located in the center of the phantom. A single-shot acquisition was used, with a TE of 30 ms, a TR of 10,000 ms and no water suppression. Each measurement was taken with separate optimization of the transmitter pulse voltage (V_{tra}).

Absolute quantification

The complete equation for calculating the absolute in vivo concentrations, using the phantom replacement technique, is

given by [33]:

$$[C_i] = [C_r] \frac{S_i V_r N_r c_{T1r} c_{T2r} T_i \rho_i c_{\text{load}}}{S_r V_i N_i c_{T1i} c_{T2i} T_r \rho_r c_{\text{csf}}} \quad (2)$$

where subscripts i and r correspond with in vivo and the reference phantom, respectively, $[C]$ is the metabolite concentration, the tCr metabolite concentration $[C_r]$ in the reference phantom was 10 mM, S is the signal strength, V is the volume of the voxel from which the signal is acquired, N is the number of protons that contribute to the spectral line ($N = 3$ for NAA and tCr, $N = 9$ for Cho and $N = 2$ for Ins and water), c_{T1} and c_{T2} are correction factors for the signal loss caused by T_1 and T_2 , respectively, T is the absolute temperature ($T_i = 37^\circ\text{C}$ in the human subject and $T_r = 21^\circ\text{C}$ in the reference phantom), ρ is the density of water, c_{load} is a correction factor that accounts for different coil loading (i.e. the respective V_{tra} s) and c_{csf} is the correction factor for partial volume effects (i.e. the fraction of CSF compared to the fraction of water in the brain parenchyma in the VOI). The volume ratio V_r/V_i cancels from the equation since V was the same in the reference phantom and in vivo, i.e. $20 \times 20 \times 20 \text{ mm}^3$.

When using the internal water reference for absolute quantification, the equation has to be adjusted for the reference concentration, being 55 M [38], and for T_1 and T_2 of water. The corrections for temperature and coil loading cancel from the equation, when the internal water signal is used as a reference.

Relaxation times

The acquired signal must be corrected for T_1 and T_2 decay as the measurement was performed with a TE of 30 ms and a TR of 2,000 ms, corresponding with a considerable loss of signal in the transverse plane and a not fully relaxed signal in the longitudinal direction, respectively. The relaxation decay times were determined in the phantom and in vivo. The phantom containing the standard metabolite solution was used. For the phantom measurement T_1 relaxation times, a water-suppressed PRESS sequence was used with thirty different repetition times (between 1,120 and 30,000 ms), a TE of 30 ms and 128 averages. For the measurement of the phantom T_2 relaxation times, a water-suppressed PRESS sequence was used with twenty-four different echo times (between 30 and 1,500 ms), a TR of 10,000 ms and 128 averages.

The determination of T_2 was performed in all volunteers (MwoA patients and controls) with the same water-suppressed PRESS sequence with six different echo times (TE = 30, 60, 90, 120, 144 and 288 ms), a TR of 4,000 ms and 64 averages. In order not to expose the MwoA patients and the controls to excessive scan times, the measurement of in vivo T_1 relaxation times was performed in an additional group of age- and gender-matched healthy volunteers ($n = 12$,

men/women = 5/7, age = 28.5 ± 4.8 years). The same water-suppressed PRESS sequence was used with eight different repetition times (TR = 1,500, 2,000, 2,500, 3,000, 3,500, 4,000, 6,000 and 10,000 ms), a TE of 30 ms and 64 averages. T_1 and T_2 relaxation times were calculated by fitting the peak areas determined by AMARES, to single-exponential functions, using a Levenberg-Marquardt algorithm in MATLAB (Mathworks, Natick, MA):

$$S = S_0 e^{-TE/T_2} \quad (3)$$

$$S = S_0 (1 - e^{-TR/T_1}) \quad (4)$$

The correction factors are given by:

$$c_{T2} = e^{-TE/T_2} \quad (5)$$

$$c_{T1} = (1 - e^{-TR/T_1}) \quad (6)$$

Temperature

Temperature has to be taken into account as it has an influence on the spin populations, according to the Boltzmann distribution. A 5 % difference between the in vivo signal (i.e. body temperature) and the reference signal (i.e. room temperature) is found [33, 39]. Temperature has also an influence on the water density; however, in the temperature range from 20 to 37°C, this influence is negligible. Temperature in the phantoms was verified regularly.

Coil loading

When applying the phantom replacement technique for absolute quantification, a correction is needed to compensate for the change in coil loading between volunteer and the phantom [40–42]. The change in coil loading is related to the difference in electrical conductivity and shape of the scanned subject or phantom [33]. The correction method is based on the principle of reciprocity, which states that (for combined transmit/receive coils) the external voltage needed to produce a certain B_1 at a given location is inversely proportional to the voltage induced by a predefined B_1 [43]. A measure of the local B_1 in a certain VOI can be derived from the V_{tra} required to obtain a 90° excitation pulse. According to the principle of reciprocity, the product of the received signal and V_{tra} is constant, under varying loading conditions [33]. This was verified by measuring a set of phantoms containing an aqueous solution of 10 mM tCr with varying NaCl concentration (0, 0.5, 1, 1.5 and 2%), simulating differential coil loading. The correction factor c_{load} used in Eq. 2 is calculated by the following correction factor:

$$c_{load} = \frac{V_{tra, in vivo}}{V_{tra, phantom}} \quad (7)$$

where $V_{tra, in vivo}$ and $V_{tra, phantom}$ are the transmitter voltages, determined in vivo and in the reference phantom, respectively.

Partial volume effects

Brain tissue consists of different compartments (gray matter, white matter, CSF, blood), and this compartmentalization is spatially dependent [44]. Metabolite concentrations are often underestimated when the contribution of cerebrospinal fluid is not accounted for [45]. There are several segmentation approaches, all of which are based on differences in relaxation properties. Next to image segmentation [46], the determination of the CSF compartment can also be accomplished by a series of spectra in which the signal amplitude of water is measured as a function of TE, yielding T_2 [42, 47]. Based on the differences in T_2 between CSF and brain tissue water, the CSF contribution can be easily determined [40, 44]. The double-exponential decay of the water signal was measured using a single shot water-unsuppressed PRESS sequence with ten different echo times (TE = 30, 50, 70, 90, 110, 150, 200, 300, 500 and 1,000 ms) and a TR of 10,000 ms. The signal amplitudes of CSF and brain tissue water were extracted using a Levenberg-Marquardt algorithm in MATLAB, using the following equation:

$$S = S_{0,csf} e^{-TE/T_{2,csf}} (1 - e^{-TR/T_{1,csf}}) + S_{0,bw} e^{-TE/T_{2,bw}} (1 - e^{-TR/T_{1,bw}}) \quad (8)$$

with $T_{1,csf}$, $T_{2,csf}$, $T_{1,bw}$ and $T_{2,bw}$ the longitudinal and transverse relaxation times of CSF and brain water (bw), respectively and $S_{0,csf}$ and $S_{0,bw}$ the unrelaxed signal amplitudes of CSF and brain water, respectively. The signal intensity with the longer T_2 was assigned to CSF. The correction factor c_{csf} used in equation 2 is determined by the following ratio:

$$c_{csf} = 1 - \frac{S_{0,csf}}{S_{0,bw} + S_{0,csf}} \quad (9)$$

Statistical analysis

Statistical analysis was performed using the SPSS software (SPSS 15.0 for Windows, Chicago, IL). Descriptive statistics were calculated for age, sex, T_1 , T_2 , V_{tra} , c_{csf} , absolute metabolite concentrations and metabolite ratios. The t -test for unpaired data was applied. Analyses were done on T_1 , T_2 , V_{tra} , c_{csf} , absolute metabolite concentrations and metabolite ratios between MwoA patients and controls, and between men and women. Results were considered to be significant at $P < 0.05$. For V_{tra} and c_{csf} , a nonparametric test for unpaired data (Mann-Whitney U -test) was applied. Coefficients of variation (CV), defined as the ratio of standard deviation and mean (in %), were calculated for repeatability, reproducibility, B_0 homogeneity, the inter-subject variation of T_1 and T_2

Table 2 Repeatability, reproducibility and signal amplitudes: CV (%)

	NAA	tCr	Cho	Ins
15 Consecutive measurements in 1 phantom	1.83	1.44	1.53	3.23
30 Measurements spread over 1 year in 1 phantom	4.62	4.01	5.63	12.45
2 Consecutive measurements in 10 healthy subjects	1.99	3.59	8.23	5.58
18 Measurements spread over 1 year in 1 healthy subject	3.42	4.65	11.99	8.56

relaxation times and the errors on the absolute metabolite concentrations.

Results

Reproducibility and stability

Accuracy of the single voxel spectroscopy measurement can be verified by both repeatability and reproducibility (Table 2). When performing consecutive measurements (= repeatability) in the same voxel without repositioning the phantom, the V_{tra} -value had a CV of 0.16%. Variation of the metabolite signals, corrected for coil loading, ranged from 1.44% for tCr to 3.23% for Ins. Variation of these metabolite signals, again corrected for coil loading, measured within the same phantom at several times spread over a timespan of a year (= reproducibility), ranged from 4.62% for NAA to 12.45% for Ins. V_{tra} had a CV of 1.33% (Table 2; Fig. 3a).

The average CV of the metabolite signals when performing consecutive measurements in ten healthy subjects ranged from 1.99% for NAA to 8.23% for Cho. Finally, the CV of the metabolite signals when performing measurements on regular time points during the year in one healthy subject ranged from 3.42% for NAA to 11.99% for Cho (Table 2; Fig. 3b).

B_0 homogeneity

Upon shimming, a spectral width of 3–5 Hz could easily be achieved for the water resonance in phantoms. When deliberately increasing the FWHM of the water resonance in increments of 5 Hz to about 35 Hz, we observed a CV of $12.86 \pm 6.39\%$ for the tCr signal in a phantom, when comparing to the optimally shimmed water resonance of 5 Hz. In vivo we achieved on average a spectral width of 15.42 ± 1.48 Hz for water in the occipital visual cortex. The FWHM for the main metabolites in vivo ranged from 8.34 ± 1.80 Hz for NAA to 10.87 ± 3.13 Hz for Cho.

B_1 homogeneity

Figure 4 shows the signal intensity profiles of the water resonance, obtained in a small spherical phantom. Spatial variation has been calculated from signal intensities measured

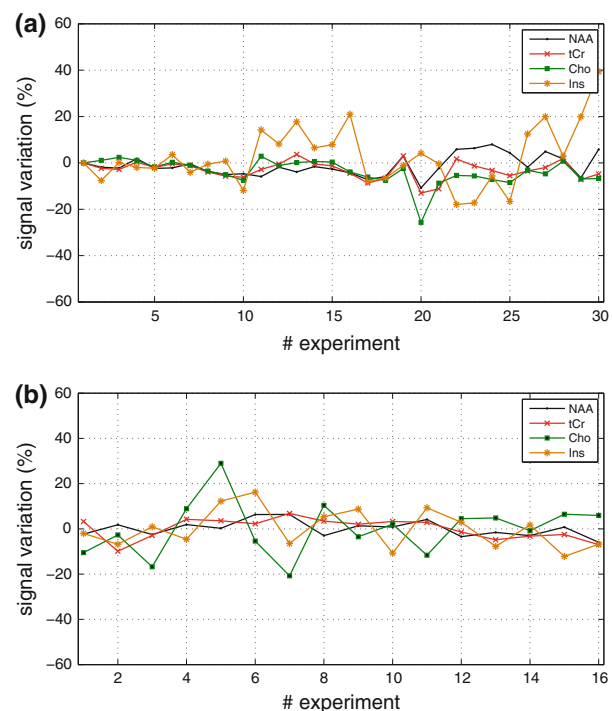


Fig. 3 **a** Signal variation in a phantom measured at different time points during the year (with the value of the first measured time point normalized to 0%). **b** Signal variation in one subject measured at different time points during the year (with the average value normalized to 0%). Experiments are shown chronologically

within 20 mm cubic VOIs with offsets along all three Cartesian axes of up to 90 mm. Signal intensity is defined to be 0% at the isocenter, so significant deviation of mean signal intensities from this value indicates variation in response along one or more axes. Different spatial variations were observed along different axes (as shown in Fig. 4). A signal intensity variation of 5.40, 3.04 and 4.97% was observed in the z-, y- and x-directions, respectively.

The variation in signal intensity was quite similar in all phantoms with different NaCl concentrations with the highest variation closest to the edge of the phantoms (Fig. 5). The smallest variation (2.76%) was found in the 1%-NaCl-doped phantom. Figure 6 shows the flip angle images in the axial plane obtained in the phantoms containing 0 and 1% NaCl. The mean flip angle and the corresponding standard deviation

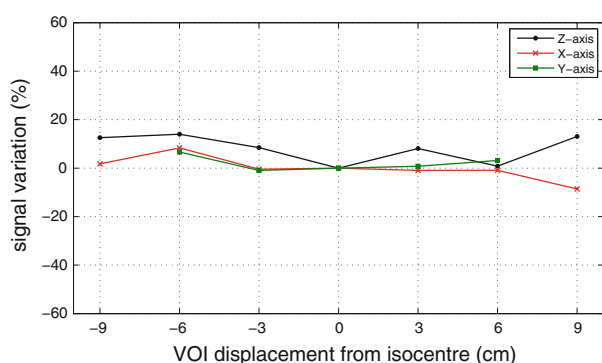


Fig. 4 Spatial variation in the water signal intensity with respect to the value at the isocenter (normalized to 0% at the isocenter) in a small water-filled phantom. The excitation pulse flip angle was optimized at each VOI location

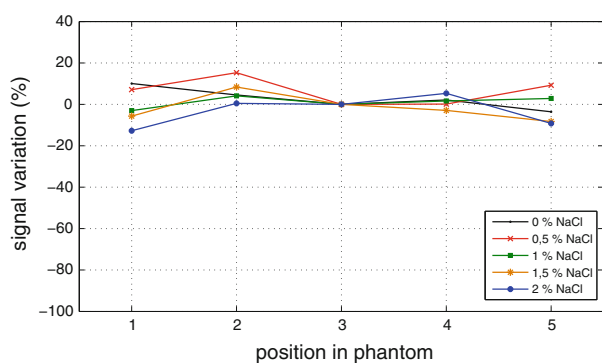


Fig. 5 Spatial variation in signal intensity for different NaCl concentrations (normalized to 0% at the central position in the phantom), with optimization of the excitation pulse flip angle at isocenter at each VOI. Positions 1 and 5 are VOIs closest to the edge of the phantom

were $32.87 \pm 2.21^\circ$ and $37.74 \pm 2.34^\circ$, respectively. As can be seen, there are no significant deviations from the nominal flip angle in both phantoms.

Relaxation times

Relaxation times of the metabolites, both in the phantom and in vivo, are listed in Table 3. The tCr signal was used as the external reference standard for absolute quantification of the in vivo metabolites. T_1 and T_2 relaxation times of brain water and CSF are listed separately in Table 3 and were also derived from the double-exponential fit of the water decay. There were no significant differences in relaxation times between MwoA patients and controls ($P \geq 0.113$), nor between men and women ($P \geq 0.100$). The T_2 -value of Ins could not be determined since the signal of Ins does not follow a single- or double-exponential with multiple echo times.

Table 3 Relaxation times

	T_1 (ms, \pm SD)	T_2 (ms, \pm SD)
Phantom^a		
H ₂ O	$2,860 \pm 177$	$2,275 \pm 77$
NAA	$1,267 \pm 84$	$1,247 \pm 84$
tCr	$1,825 \pm 95$	$1,385 \pm 108$
Cho	$1,934 \pm 76$	$1,882 \pm 101$
Ins	$1,117 \pm 51$	—
In vivo		
H ₂ O (CSF)	$2,897 \pm 701^b$	670 ± 120^b
H ₂ O (bw)	484 ± 113^b	70 ± 6^b
NAA	$1,448 \pm 99^c$	224 ± 27^b
tCr	$1,424 \pm 146^c$	146 ± 23^b
Cho	$1,380 \pm 232^c$	148 ± 38^b
Ins	$1,113 \pm 201^c$	—

^a All values were the average of six identical measurements

^b These values were the average 22 MwoA patients and 25 controls

^c These values were the average of an additional group of 12 controls

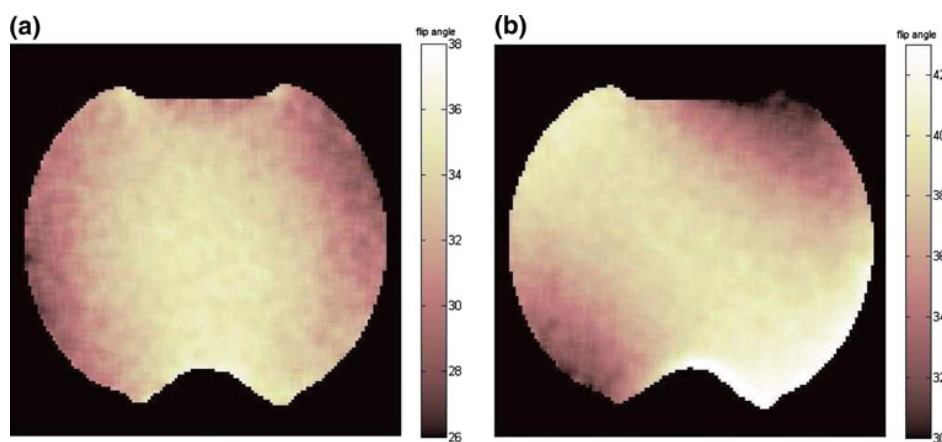


Fig. 6 Axial flip angle images for phantoms containing 0 % (a) and 1% NaCl (b), respectively. The nominal flip angle (θ) was 35°

Temperature

No significant temperature variations were observed over the phantom measurements during the study. Temperature was always $20 \pm 0.7^\circ\text{C}$.

Coil loading

The effect of different coil loading on the acquired signal in a phantom is demonstrated in Fig. 7. Signal amplitudes decrease with increasing NaCl concentration (and hence increased coil loading). Since V_{tra} is a direct measure of coil loading, Fig. 7 also illustrates an increase of V_{tra} with increasing NaCl concentration.

V_{tra} was 168.03 ± 8.06 V and 176.88 ± 12.86 V for MwoA patients and controls ($P = 0.001$), respectively. Whereas the V_{tra} in vivo was on average 170 V, the V_{tra} -value was 138.5 V when scanning the phantom.

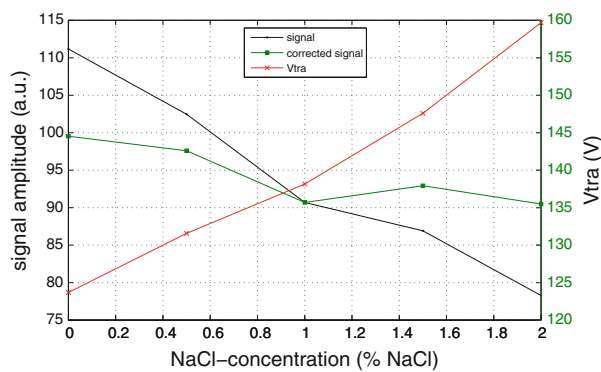


Fig. 7 Relation between the signal intensity (before and after correction), NaCl concentration and the V_{tra}

Partial volume effects

The CSF content is on average $11.84 \pm 4.17\%$. The CSF fraction does not show any significant differences both between MwoA patients ($12.00 \pm 4.70\%$) and controls ($12.58 \pm 4.10\%$) and between men ($13.00 \pm 4.36\%$) and women ($12.00 \pm 4.38\%$), respectively. The P -values were 0.719 and 0.927, respectively.

Absolute quantification

The quantification protocol was evaluated using a phantom containing an aqueous solution of 15 mM NAA (pH 7) and 2% NaCl to simulate a different coil loading. The phantom containing the standard metabolite solution was used as a reference. After taking into account correction factors for T_1 , T_2 and coil loading, the absolute concentration of NAA was found to be 15.22 mM NAA, which results in an error of 1.01%. There was no temperature difference between these phantoms.

Table 4 shows the absolute concentrations of NAA, tCr, Cho and Ins, with their corresponding standard deviations, in the occipital visual cortex of 22 MwoA patients and 25 controls. These values were obtained after applying corrections for T_1 , T_2 (except for Ins in vivo), coil loading, temperature and CSF, as described above. Absolute metabolite concentrations based on the internal water reference method and metabolite ratios are also listed in Table 4. For all concentrations and ratios, there were no significant differences between MwoA patients and controls ($P \geq 0.550$, Table 4). In addition, because the study population was age- but not gender-matched, a similar analysis was performed to compare male and female volunteers. This showed no significant differences in metabolite concentrations between men and women in the occipital visual cortex ($P \geq 0.100$).

Table 4 Absolute concentration values in mmol/(kg wet weight) and metabolite ratios (mean \pm SD)^a

	MwoA patients	Controls	Absolute quantification method
[NAA] (mmol/(kg ww))	11.39 ± 1.55	11.39 ± 1.35	Phantom replacement technique
	12.21 ± 1.78	11.56 ± 1.66	Internal water reference
[tCr] (mmol/(kg ww))	8.78 ± 1.59	8.96 ± 1.37	Phantom replacement technique
	9.37 ± 1.53	9.03 ± 1.46	Internal water reference
[Cho] (mmol/(kg ww))	1.59 ± 0.41	1.58 ± 0.47	Phantom replacement technique
	1.70 ± 0.43	1.62 ± 0.43	Internal water reference
[Ins] (mmol/(kg ww))	2.44 ± 0.46	2.46 ± 0.65	Phantom replacement technique
	2.63 ± 0.58	2.52 ± 0.64	Internal water reference
NAA/tCr	1.44 ± 0.13	1.42 ± 0.18	–
Cho/tCr	0.18 ± 0.03	0.18 ± 0.05	–
Ins/tCr	0.38 ± 0.06	0.38 ± 0.09	–
Cho/NAA	0.12 ± 0.02	0.12 ± 0.03	–
Ins/NAA	0.27 ± 0.03	0.27 ± 0.05	–

^a Significance level: $P < 0.05$

Discussion

In migraine, several magnetic resonance spectroscopy studies, in particular ^{31}P -MRS and a few ^1H -MRS studies, have been performed. Most of these studies suggested a metabolic disturbance in the brain of MwA patients and, to a lesser extent, of MwoA patients, which is evident even in the interictal period [10–18].

In MwoA, ^1H -MRS has only been performed following visual stimulation and using relative quantification. As already mentioned, only a few number of studies emphasized on MwoA. Only one study reports measurements from the occipital visual cortex. Sarchielli et al. observed no changes in the occipital cortex between MwoA patients and controls before visual stimulation; however, following stimulation, the NAA signal amplitude was found to be downregulated (unsignificantly) [21].

One other study (Gu et al.) found a significant decrease in NAA/tCr in the left thalamus of MwoA patients compared to controls [25].

Several other studies also performed ^1H -MRS in the occipital cortex, however, in other migraine subgroups. Sarchielli et al. found a significantly decreased NAA signal amplitude in MwA patients, both before and after visual stimulation [21]. Lactate was found increased in MwA and MwpA patients in several other studies [19–21]. In a few other studies, significant changes have been observed in other brain regions of MwA patients.

Because of the lack of quantitative ^1H -MRS data in MwoA patients and the assumption of a possible deficiency in the energy metabolism of the brain in these patients, in which tCr plays a vital role, a firm interest grew to perform absolute quantification with ^1H -MRS in this migraine subgroup.

In this study, we searched for possible interictal differences in metabolic concentrations in the occipital visual cortex between healthy subjects and MwoA patients by use of quantitative absolute ^1H -MRS. The assumption of a constant in vivo water concentration of 55 mM, as used with internal water referencing, was an important reason to prefer the phantom replacement technique for obtaining absolute concentrations [38]. To utilize a robust methodological ^1H -MRS protocol in this migraine study, several scanner properties such as reproducibility, B_0 and B_1 homogeneity were assessed in both phantom and in vivo situations. Absolute quantification also involves the determination of several correction factors such as relaxation times, coil loading effects and temperature. One of the big advantages of absolute quantification when compared to relative quantification is that it does not assume a constant metabolite concentration (e.g. tCr). Indeed, several studies have shown significant changes in both tCr and Cho [48, 49]. In addition, if patients have global metabolic defects, comparisons with contralateral brain regions (which are assumed to be metabolically

normal) are not possible [50, 51]. To our knowledge, this was the first study in which absolute quantification was applied with ^1H -MRS in MwoA and migraine in general.

Quality assessment

When performing consecutive measurements in the same voxel of a phantom, without repositioning and reshimming, CVs were small for all metabolites (around 3% maximal). When repeating this experiment but now with repositioning and reshimming of the phantom, the CV increased for all metabolites and for V_{tra} . The reproducibility was also assessed by repeating the experiment after one week, one month, six months and one year, each time with repositioning and reshimming of the phantom. The CV for all metabolites during this period amounted to around 4 or 5% for NAA, tCr and Cho and 12.45% for Ins. V_{tra} had a CV of 1.33% during a 1-year period. No systematic trend was found in the variations with respect to time. Possible reasons for this variation are the deviating stability of the scanner and the phantom composition. No degradation of metabolites was found.

When performing consecutive measurements in ten healthy control subjects, the CV ranged from 1.99% for NAA to 8.23% for Cho, indicating an inherent signal variation of the system. For Cho, this was somewhat higher than for the other metabolites, which can be attributed to underlying J-coupling evolutions and small metabolic fluctuations [39, 52]. So far, all variation could be attributed to variation in the methodological setup, which includes the influence of spectral noise, data analysis, repositioning of the subject, the phantom and voxel volume. Signal variation was also verified in a longitudinal experiment in which a male healthy volunteer was followed up during one year with CVs smaller than 5% for NAA and tCr and smaller than 10% for Ins. Again, signal variation for Cho was the highest ($\pm 12\%$). Intra-subject variation was similar to that reported in the literature [53]. Inter-subject variation varied from approximately 10% for NAA and tCr to approximately 20% for Cho and Ins, which were values that were somewhat higher than in a previous report [53]. Next to the methodological variation described above, there is also the inherent biological variation, which can be further complicated by pathology.

In both phantoms and human subjects, following shimming, the FWHM of the metabolites was always less than 12 Hz except in the case of the in vivo water resonance (± 15 Hz). The somewhat higher, yet acceptable linewidth of the water resonance is probably due to the central occipital localization of the voxel with a high contribution of CSF, affecting the B_0 homogeneity. The VOI (8 ml) was placed in the primary visual cortex close to the skull and the subcutaneous fat, all contributing to susceptibility issues and B_0 inhomogeneities. Phantom experiments demonstrated the importance of shimming and B_0 homogeneity.

Table 5 The different errors on the absolute metabolite concentrations (of the 25 control subjects) when the correction factors were not taken into account, using the phantom replacement technique

	$[c_i]$ (mmol/(kg ww), \pm SD)	CV of error on absolute metabolite concentration (% , \pm SD)						
	All corrections	No c_{T2}	No c_{T1}	No c_{csf}	No c_{load}	No c_{temp}	No corrections	Int. wat. ^a
NAA	11.39 \pm 1.35	−11.55 \pm 2.14	14.49				−33.05 \pm 6.07	1.5
tCr	8.96 \pm 1.37	−18.16 \pm 3.86	12.34	−11.06	−21.44	−5.48	−39.24 \pm 5.84	0.8
Cho	1.58 \pm 0.47	−19.22 \pm 8.78	13.95	\pm 3.15	\pm 5.28		−39.17 \pm 8.49	2.5
Ins	2.46 \pm 0.65	–	24.20				−16.53 \pm 5.41	2.4

^a The CV is based on the average differences in concentration between both quantification methods, as seen in Table 4

The water signal intensity did not show significant variation with respect to the VOI position. The spatial uniformity has important implications for quantification methods involving external standards. Signal variation at greater distances from the coils isocenter is of relevance to techniques in which an external reference is placed adjacent to the head of the subject. The results shown in Fig. 7 indicate signal intensity variations of 4.47% on average. Large signal variations can be caused by standing radiofrequency waves [36]. Standing waves can be compensated by using a small and/or doped water phantom [36,54,55], as used in our study. Signal variations were quite similar between different NaCl-doped phantoms and with the smallest signal variation in the 1%NaCl-doped phantom which corresponded to the physiological NaCl concentration. Highest variation was found closest to the edge of the phantoms, because of susceptibility artifacts. Other contributions to signal variations are related to eddy currents and coil loading, as well as the intrinsic inhomogeneity of the B_1 field of the RF coil. Most variation was found away from the isocenter. These coil-dependent signal variations are present in in vivo and phantom measurements. The external calibration method used in this study relies on the ratio of the in vivo signal and the phantom signal obtained at the same location with respect to the coil and given the small signal variation in the center of the coil, it is expected that the error caused by these coil-related variations will be minimal. Separate optimization of the excitation pulse angle at each VOI location had little effect on the signal profile, and this alone is not a satisfactory approach to the problem of spatial variation in signal intensity.

Correction factors

A first correction was applied for T_1 and T_2 relaxation effects. The T_2 -values were measured in all subjects separately and also compensated individually. Except for the T_2 -value of Cho, all in vivo values corresponded well with literature values [52,56]. The T_2 -values of Cho (i.e. 148 \pm 38 ms) in this study were significantly lower than in previous reports [52,56]. A potential reason for this could be the interference with underlying J-coupled resonances which are dependent on the

echo time [52]. Due to T_2 -decay, the signal was reduced by 1.7% in the phantom and 18.6% in vivo, indicating a correction for T_2 -relaxation was only needed for the in vivo data. The inter-subject variation for the T_2 of NAA, tCr and Cho was approximately 12, 16 and 26%, respectively, indicating a substantial biological variation, especially for Cho and Ins. When using an average T_2 -value or a literature value, the error in the quantified concentration might have been as high as 0.13 mmol/(kg wet weight) in the case of Cho, which is not negligible. For resonances of coupled spin systems such as Ins, J-modulation strongly affects both the signal intensity and the spectral lineshape and hence, complicating the determination of reproducible T_2 -values. The signal of Ins does not follow a single- or double-exponential with multiple echo times, so the T_2 -value of Ins could not be determined. There is a lack of literature values concerning the in vivo T_2 of Ins, and only a few studies report values varying from 110 to 279 ms in the occipital cortex; however, these values were obtained at a field strength of 1.5 T [57–59]. It also has to be emphasized that T_2 decreases with increasing field strength. So taking all this into consideration, absolute Ins concentration was not corrected for T_2 in vivo, resulting in an error on the actual concentration. This would explain the discrepancy in absolute Ins concentration between this study and previous studies [39]. When not correcting for T_2 , the error on the concentration could amount to 19.22%, as was the case for Cho (Table 5; Fig. 8).

In vivo T_1 relaxation times were also measured, although in a separate group of age- and gender-matched subjects. These values were similar to literature values [52,56]. A relatively short TR (i.e. 2,000 ms) was used in the experiments, so T_1 correction was necessary since the tCr signal was reduced to 64.6% in the phantom and 75% in vivo because of incomplete longitudinal magnetization recovery. The inter-subject variation for the T_1 -value of NAA, tCr, Cho and Ins was approximately 7, 10, 17 and 18%, respectively, indicating a substantial biological variation for Cho and Ins. There were no significant differences in relaxation times between MwoA patients and controls. Both T_1 and T_2 relaxation times of NAA, tCr, Cho, Ins and water were also measured in a phantom. These values can be used for relaxation time corrections

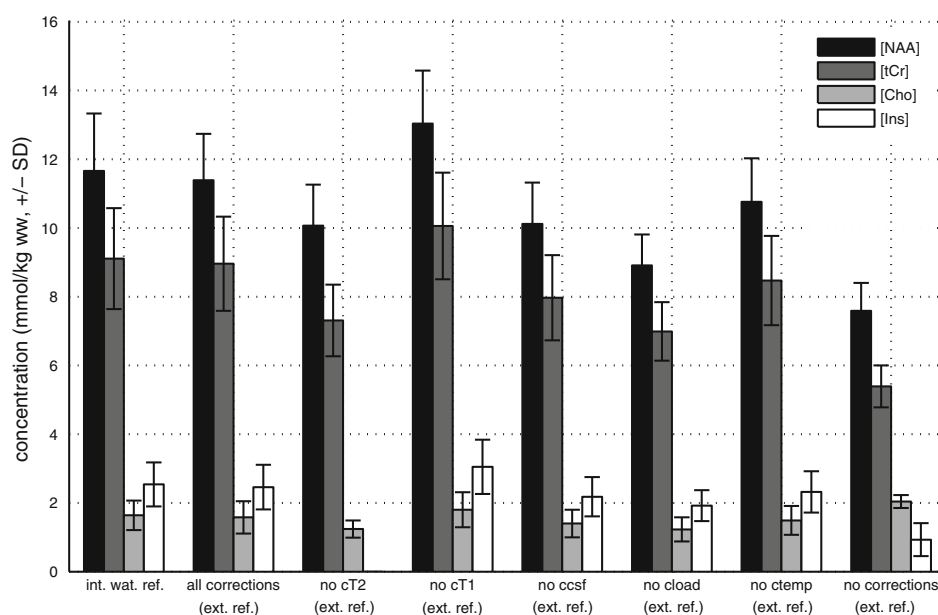


Fig. 8 Absolute metabolite concentrations (mmol/(kg wet weight) \pm SD) when the different correction factors are not applied, using the phantom replacement technique (ext. ref.). The bars on the extreme

left illustrate the absolute metabolite concentrations, obtained with the internal water reference (int. wat. ref.)

when using an external reference standard. In contrast to the in vivo values, phantom T_2 -values are much higher. When not correcting for T_1 , the error on the concentration could amount to 24.20%, as was the case for Ins (Table 5; Fig. 8).

The partial volume effect of CSF is derived by fitting a double-exponential function to the water-unsuppressed signal as a function of TE. On average, the CSF content was 11.84% and thus had a significant effect on the ultimate metabolite concentrations (Table 5; Fig. 8). When not accounted for, this would have led to an underestimation of the metabolite concentrations. This high contribution of CSF was due to the central occipital localization of the voxel and was in accordance with CSF values in a previous study in the same brain region [56]. No significant differences were found between MwoA patients and controls. When not using a correction for the partial volume effect, the error in the quantified concentration might have been as high as 1.32 mmol/(kg wet weight) in the case of NAA.

A fourth correction was made for the different coil loading between the phantom and the in vivo measurement. Coil loading has a large influence on the final absolute concentration values when comparing with an external reference phantom. When not correcting for coil loading, the error on the concentration was 21.44% (Table 5; Fig. 8).

The fifth and final correction factor concerned the temperature difference between the human subjects and the external reference phantom. Since no significant variations were observed over the phantom measurements, a constant cor-

rection factor of approximately 5% was attributed to all in vivo measurements. When not correcting for temperature, the error on the concentration was 5.48% (Table 5; Fig. 8).

Patients vs controls

In this work, we performed absolute quantification of proton metabolites in the occipital visual cortex of 22 MwoA patients and 25 control subjects. Effects of signal relaxation, CSF contribution, coil loading and temperature difference between the external reference phantom and in vivo were compensated for.

No significant differences in absolute metabolite concentrations nor in metabolite ratios were found between MwoA patients and controls. This confirms the earlier results of Sarchielli et al., although they did not perform a quantitative ^1H -MRS study [21]. We did not observe a decreased NAA or increased Lac concentration as seen in several studies, performed in Mwa [19–21]. Sarchielli et al. observed a decrease in NAA (even before visual stimulation) in Mwa patients [21]. More specifically, NAA is considered a neuronal marker, synthesized and located prevalently in neuronal mitochondria, and it is assumed to be involved in mitochondrial/cytosolic carbon transport [60]. In migraine patients, both Mwa and MwoA, a disturbance of the interictal energy metabolism has been demonstrated [10–16] and the finding of a NAA decrease in Mwa patients would, according to Sarchielli et al., indicate a less efficient mitochondrial

functioning in MwA patients compared to MwoA patients and controls [21]. This decrease in occipital NAA could not be confirmed by another study in which no significant differences were found between FHM patients, a rare type of MwA, and controls [20].

In addition, when using the internal water reference, the absolute values were very similar to the concentrations obtained with the phantom replacement technique. We can therefore conclude that both methods, with their own specific inherent difficulties, lead to comparable data (Table 5; Fig. 8).

Limitations

In this study, we did not consider the quantification of other metabolites such as Lac and Glx.

Because of both the chemical shift displacement artifact and anomalous J-modulation at 3 T and using a PRESS sequence, the Lac resonance showed a reduced or absent signal intensity at an echo time of 144 ms [61], which can lead to a severe underestimation of Lac. The extent of the signal loss due to anomalous J-modulation can vary considerably depending on the field strength, the used coil and the sequence parameters. A recommendation is to acquire also a spectrum at an echo time of 288 ms but the Lac peak, however, was only detected in a few subjects, including both patients and controls. A possible reason could have been the decreased sensitivity due to T_2 relaxation at longer echo times. Strategies to reduce the signal loss due to anomalous J-modulation usually requires changes in the sequence programming.

Glx signal strengths were also processed, but due to the unreliable quantification in unedited spectra, the values were not included in this study. We did, however, perform an initial AMARES analysis of Glx and did not observe any differences between MwoA patients and controls (data not shown). Since the partial overlap of NAA and Glx resonances can interfere with the NAA quantification at low TE and in the presence of possible Glx changes between MwoA patients and controls, a similar analysis was performed at longer TE [62]. Still no differences were observed between MwoA patients and controls. A possible solution to exclude these ambiguities in the future is to use the QUEST algorithm, as demonstrated in a previous study [63].

Conclusion

In this study, absolute quantification with ^1H -MRS was performed in an experimental migraine study in a homogeneous patient group. To obtain reliable absolute concentrations, however, several methodological aspects were investigated in depth and compensated for. Absolute quantification showed

no differences in metabolite concentrations in the occipital visual cortex between MwoA patients and controls, in contrast to results obtained by relative quantification in earlier studies. When no corrections were applied for relaxation times, CSF, temperature and coil loading, absolute concentration errors could amount to approximately 40%, emphasizing the importance of these correction factors.

Acknowledgments This research is funded by the Special Research Fund PhD-grant B/07768/02 and performed at GifMI. The Department of Radiotherapy is also greatly acknowledged for the use of the Radio-physics lab.

References

1. Lance JW, Goadsby PJ (1998) Mechanism and management of headache. Butterworth-Heinemann, Boston
2. Silberstein SD, Lipton RB, Goadsby PJ (1998). In: Goadsby PJ (ed) Headache in clinical practice, edn. Isis Medical Media, Oxford, pp 69–112
3. Olesen J, Tfelt-Hansen P, Welch KMA (2000) The headaches. Williams & Wilkins, Philadelphia
4. The International Headache Society Classification Subcommittee (2004) The international classification of headache disorders. 2. Cephalalgia 24(S1):1–160
5. Stovner LJ, Zwart JA, Hagen K, Terwindt GM, Pascual J (2006) Epidemiology of headache in Europe. Eur J Neurol 13(4):333–345
6. Edmeads J, Mackell JA (2002) The economic impact of migraine: an analysis of direct and indirect costs. Headache 42(6):501–509
7. Leonardi M, Steiner TJ, Scher AT, Lipton RB (2005) The global burden of migraine: measuring disability in headache disorders with WHO's classification of functioning, disability and health (ICF). J Headache Pain 6(6):429–440
8. Schoenen J (1994) Pathogenesis of migraine: the biobehavioural and hypoxia theories reconciled. Acta Neurol Belg 94(2):79–86
9. Schoenen J (1998) Cortical electrophysiology in migraine and possible pathogenic implications. Clin Neurosci 5(1):10–17
10. Welch KM, Levine SR, D'Andrea G, Helpert JA (1988) Brain pH in migraine: an in vivo phosphorus-31 magnetic resonance spectroscopy study. Cephalalgia 8(4):273–277
11. Welch KM, Levine SR, D'Andrea G, Schultz LR, Helpert JA (1989) Preliminary observations on brain energy metabolism in migraine studied by in vivo phosphorus 31 NMR spectroscopy. Neurology 39(4):538–541
12. Barbiroli B, Montagna P, Cortelli P, Martinelli P, Sacquegnia T, Zaniol P, Lugaesi E (1990) Complicated migraine studied by phosphorus magnetic resonance spectroscopy. Cephalalgia 10(5):263–272
13. Sacquegnia T, Lodi R, De Carolis P, Tinuper P, Cortelli P, Zaniol P, Funicello R, Montagna P, Barbiroli B (1992) Brain energy metabolism studied by 31P-MR spectroscopy in a case of migraine with prolonged aura. Acta Neurol Scand 86(4):376–380
14. Barbiroli B, Montagna P, Cortelli P, Funicello R, Iotti S, Monari L, Pierangeli G, Zaniol P, Lugaesi E (1992) Abnormal brain and energy metabolism shown by 31P magnetic resonance spectroscopy in patients affected by migraine with aura. Neurology 42(6):1209–1214
15. Montagna P, Cortelli P, Monari L, Pierangeli G, Parchi P, Lodi R, Iotti S, Frassinetti C, Zaniol P, Lugaesi E, Barbiroli B (1994) 31P-Magnetic resonance spectroscopy in migraine without aura. Neurology 44(4):666–669
16. Uncini A, Lodi R, Di Muzio A, Silvestri G, Servidei S, Lugaesi A, Iotti S, Zaniol P, Barbiroli B (1995) Abnormal brain

- and muscle energy metabolism shown by 31P-MRS in familial hemiplegic migraine. *J Neurol Sci* 129(2):214–222
17. Lodi R, Montagna P, Soriani S, Iotti S, Arnaldi C, Cortelli P, Pierangeli G, Patuelli A, Zaniol P, Barbiroli B (1997) Deficit of brain and skeletal muscle bioenergetics and low brain magnesium in juvenile migraine: an in vivo 31P magnetic resonance spectroscopy interictal study. *Pediatr Res* 42(6):866–871
 18. Boska MD, Welch KM, Barker PB, Nelson JA, Schultz L (2002) Contrasts in cortical magnesium, phospholipid and energy metabolism between migraine syndromes. *Neurology* 58(8):1227–1233
 19. Watanabe H, Kuwabara T, Ohkubo M, Tsuji S, Yuasa T (1996) Elevation of cerebral lactate detected by localized 1H-magnetic resonance spectroscopy in migraine during the interictal period. *Neurology* 47(4):1093–1095
 20. Sandor PS, Dydak U, Schoenen J, Kollias SS, Hess K, Boesiger P, Agosti RM (2005) MR-spectroscopic imaging during visual stimulation in subgroups of migraine with aura. *Cephalalgia* 25(7):507–518
 21. Sarchielli P, Tarducci R, Preciutti O, Gobbi G, Pelliccioli GP, Stipa G, Alberti A, Capocchi G (2005) Functional 1H-MRS findings in migraine patients with and without aura assessed interictally. *Neuroimage* 24(4):1025–1031
 22. Dichgans M, Herzog J, Freilinger T, Wilke M, Auer DP (2005) 1H-MRS alterations in the cerebellum of patients with familial hemiplegic migraine type 1. *Neurology* 64(4):608–613
 23. Jacob A, Mahavish K, Bowden A, Smith ET, Enevoldson P, White RP (2006) Imaging abnormalities in sporadic hemiplegic migraine on conventional MRI, diffusion and perfusion MRI and MRS. *Cephalalgia* 26(8):1004–1009
 24. Schulz UG, Blamire AM, Corkill RG, Davies P, Styles P, Rothwell PM (2007) Association between cortical metabolite levels and clinical manifestations of migrainous aura: an MR-spectroscopy study. *Brain* 130(Pt12):3102–3110
 25. Gu T, Ma XX, Xu YH, Xiu JJ, Li CF (2008) Metabolite concentration ratios in thalami of patients with migraine and trigeminal neuralgia measured with 1H-MRS. *Neurol Res* 30(3):229–233
 26. Macri MA, Garreffa G, Giove F, Ambrosini A, Guardati M, Pierelli F, Schoenen J, Colonnese C, Maraviglia B (2003) Cerebellar metabolite alterations detected in vivo by proton MR spectroscopy. *Magn Reson Imaging* 21(10):1201–1206
 27. Ma Z, Wang SJ, Li CF, Ma XX, Gu T (2008) Increased metabolite concentration in migraine rat model by proton MR spectroscopy in vivo and ex vivo. *Neurol Sci* 29(5):337–342
 28. Grimaldi D, Tonon C, Cevoli S, Pierangeli G, Malucelli E, Rizzo G, Soriani S, Montagna P, Barbiroli B, Lodi R, Cortelli P (2010) Clinical and neuroimaging evidence of interictal cerebellar dysfunction in FHM2. *Cephalalgia* 30(5):552–559
 29. Naressi A, Couturier C, Castang I, de Beer R, Graveron-Demilly D (2001) Java-based graphical user interface for MRUI, a software package for quantitation of in vivo/medical magnetic resonance spectroscopy signals. *Comput Biol Med* 31(4):269–286
 30. Laudadio T, Mastroradi N, Vanhamme L, Van Hecke P, Van Huffel S (2002) Improved Lanczos algorithms for blackbox MRS data quantitation. *J Magn Reson* 157(2):292–297
 31. Vanhamme L, van den Boogaart A, Van Huffel S (1997) Improved method for accurate and efficient quantification of MRS data with use of prior knowledge. *J Magn Reson* 129(1):35–43
 32. Cavassila S, van Ormondt D, Graveron-Demilly D (2001) Cramer-rao bound analysis of spectroscopic signal processing methods. In: Yan H (ed) *Signal processing for magnetic resonance imaging and spectroscopy*, edn. Marcel Dekker, New York, pp 613–640
 33. Tofts PS (2004) Spectroscopy: 1H metabolite concentrations. In: Tofts P (ed) *Quantitative MRI of the brain: measuring changes caused by disease*. John Wiley, Chichester, pp 299–340
 34. Drost DJ, Riddle WD, Clarke GDAAPM MR Task Group #9 (2002) Proton magnetic resonance spectroscopy in the brain: report of AAPM MR Task Group #9. *Med Phys* 29(9):2177–2197
 35. Kreis R (2004) Issues of spectral quality in clinical 1H magnetic resonance spectroscopy and a gallery of artifacts. *NMR Biomed* 17(6):361–381
 36. Tofts PS (1994) Standing waves in uniform water phantoms. *J Magn Reson B* 104(2):143–147
 37. Insko EK, Bolinger L (1993) Mapping of the radiofrequency field. *J Magn Reson A* 103(1):82–85
 38. Helms G (2008) The principles of quantification applied to in vivo proton MR spectroscopy. *Eur J Radiol* 67(2):218–229
 39. Kreis R (1997) Quantitative localized 1H MR spectroscopy for clinical use. *Prog Nucl Mag Res Sp* 31:155–195
 40. Hennig J, Pfister H, Ernst T, Ott D (1992) Direct absolute quantification of metabolites in the human brain with in vivo localized proton spectroscopy. *NMR Biomed* 5(4):193–199
 41. Soher BJ, van Zijl PC, Duyn JH, Barker PB (1996) Quantitative proton MR spectroscopic imaging of the human brain. *Magn Reson Med* 35(3):356–363
 42. Helms G (2000) A precise and user-independent quantification technique for regional comparison of single volume proton MR spectroscopy of the human brain. *NMR Biomed* 13(7):398–406
 43. Hoult DI, Richards RE (1976) The signal-to-noise ratio of the nuclear magnetic resonance experiment. *J Magn Reson* 24(1):71–85
 44. Ernst T, Kreis R, Ross BD (1993) Absolute quantitation of water and metabolites in the human brain. I. Compartments and water. *J Magn Reson B* 102(1):1–8
 45. Lynch J, Peeling J, Auty A, Sutherland GR (1993) Nuclear magnetic resonance study of cerebrospinal fluid from patients with multiple sclerosis. *Can J Neurol Sci* 20(3):194–198
 46. Hetherington HP, Pan JW, Mason GF, Adams D, Vaughn MJ, Twieg DB, Pohost GM (1996) Quantitative 1H spectroscopic imaging of human brain at 4.1 T using image segmentation. *Magn Reson Med* 36(1):21–29
 47. Helms G (2003) T2-based segmentation of periventricular paragraph sign volumes for quantification of proton magnetic paragraph sign resonance spectra of multiple sclerosis lesions. *Magn Reson Mater Phys* 16(1):10–16
 48. Connelly A, Jackson GD, Duncan JS, King MD, Gadian DG (2004) Magnetic resonance spectroscopy in temporal lobe epilepsy. *Neurology* 44(8):1411–1417
 49. Lundbom N, Gaily E, Vuori K, Paetau R, Liukkonen E, Rajapakse JC, Valanne L, Hakkinen AM, Granstrom ML (2001) Proton spectroscopic imaging shows abnormalities in glial and neuronal cell pools in frontal lobe epilepsy. *Epilepsia* 42(12):1507–1514
 50. Mathews VP, Barker PB, Blackband SJ, Chatham JC, Bryan RN (1995) Cerebral metabolites in patients with acute and subacute strokes: concentrations determined by quantitative proton MR spectroscopy. *AJR Am J Roentgenol* 165(3):633–638
 51. Chang L, Ernst T, Tornatore C, Aronow H, Melchor R, Walot I, Singer E, Conford M (2001) Metabolite abnormalities in progressive multifocal leukoencephalopathy by proton magnetic resonance spectroscopy. *Neurology* 48(4):836–845
 52. Mlynarik V, Gruber S, Moser E (2001) Proton T1 and T2 relaxation times of human brain metabolites at 3 Tesla. *NMR Biomed* 14(5):325–331
 53. Schirmer T, Auer DP (2000) On the reliability of quantitative clinical magnetic resonance spectroscopy of the human brain. *NMR Biomed* 13(1):28–36
 54. Ozdemir MS, Reynoudt H, De Deene Y, Sazak HS, Fieremans E, Delpitte S, D'Asseler Y, Derave W, Lemahieu I, Achten E (2007) Absolute quantification of carnitine in human calf muscle by proton magnetic resonance spectroscopy. *Phys Med Biol* 52(23):6781–6794

55. Keevil SF, Barbiroli B, Brooks JC, Cady EB, Canese R, Carlier P, Collins DJ, Gilligan P, Gobbi G, Hennig J, Kugel H, Leach MO, Metzler D, Mlynarik V, Moser E, Newbold MC, Payne GS, Ring P, Roberts JN, Rowland IJ, Thiel T, Tkac I, Topp S, Wittsack HJ, Wylezinska M, Zaniol P, Henriksen O, Podo F (1998) Absolute metabolite quantification by in vivo NMR spectroscopy: II. A multicentre trial of protocols for in vivo localised proton studies of human brain. *Magn Reson Imaging* 16(9):1093–1106
56. Ethofer T, Mader I, Seeger U, Helms G, Erb M, Grodd W, Ludolph A, Klose U (2003) Comparison of longitudinal metabolite relaxation times in different regions of the human brain at 1.5 and 3 Tesla. *Magn Reson Med* 50(6):1296–1301
57. Frahm J, Bruhn H, Gyngell ML, Merboldt KD, Hanicke W, Sauter R (1989) Localized proton NMR spectroscopy in different regions of the human brain in vivo. Relaxation times and concentrations of cerebral metabolites. *Magn Reson Med* 11(1):47–63
58. Kreis R, Fusch C, Maloca P, Felbinger J, Boesch C (1994) Supposed pathology may be individuality: interindividual and regional differences of brain metabolite concentration determined by ¹H MRS. In Proceedings of 2nd meeting of the society of magnetic resonance. San Francisco, USA, 45pp
59. Kreis R, Ernst T, Ross BD (1993) Absolute quantitation of water and metabolites in the human brain. II. Metabolite concentrations. *J Magn Reson B* 102(1):9–19
60. Clark JB (1998) N-acetyl aspartate: a marker for neuronal loss or mitochondrial dysfunction. *Dev Neurosci* 20(4–5):271–276
61. Lange T, Dydak U, Roberts TP, Rowley HA, Bjeljac M, Boesiger P (2006) Pitfalls in lactate measurements at 3T. *AJNR Am J Neuroradiol* 27(4):895–901
62. Clementi V, Tonon C, Lodi R, Malucelli E, Barbiroli B, Iotti S (2005) Assessment of glutamate and glutamine contribution to in vivo N-acetylaspartate quantification in human brain by ¹H-magnetic resonance spectroscopy. *Magn Reson Med* 54(6):1333–1339
63. Malucelli E, Manners DN, Testa C, Tonon C, Lodi R, Barbiroli B, Iotti S (2009) Pitfalls and advantages of different strategies for the absolute quantification of N-acetylaspartate, creatine and choline in white and grey matter by ¹H-MRS. *NMR Biomed* 22(10):1003–1013

C. ^{31}P -MRS demonstrates a reduction in absolute concentrations of high-energy phosphates in the occipital lobe of migraine without aura patients.

Harmen Reyngoudt, Koen Paemeleire, **Benedicte Descamps**, Yves De Deene, Eric Achten

Cephalalgia 2011, 31(12): 1243-53.

³¹P-MRS demonstrates a reduction in high-energy phosphates in the occipital lobe of migraine without aura patients

**Harmen Reyngoudt¹, Koen Paemeleire¹,
Benedicte Descamps¹, Yves De Deene^{1,2} and Eric Achten¹**

Cephalalgia

31(12) 1243–1253

© International Headache Society 2010

Reprints and permissions:

sagepub.co.uk/journalsPermissions.nav

DOI: 10.1177/0333102410394675

cep.sagepub.com



Abstract

Background: Differences in brain energy metabolism have been found between migraine patients and controls in previous phosphorus magnetic resonance spectroscopy (³¹P-MRS) studies, most of them emphasizing migraine with aura (MwA). The aim of this study was to verify potential changes in resting-state brain energy metabolism in patients with migraine without aura (MwoA) compared to control subjects by ³¹P-MRS at 3 tesla.

Methods: Quantification was performed using the phantom replacement technique. MRS measurements were performed interictally and in the medial occipital lobe of 19 MwoA patients and 26 age-matched controls.

Results: A significantly decreased phosphocreatine concentration ([PCr]) was found as in previous studies. While adenosine triphosphate concentration ([ATP]) was considered to be constant in previously published work, this study found a significant decrease in the measured [ATP] in MwoA patients. The inorganic phosphate ([P_i]) and magnesium ([Mg²⁺]) concentrations were not significantly different between MwoA patients and controls.

Conclusions: The altered metabolic concentrations indicate that the energy metabolism in MwoA patients is impaired, certainly in a subgroup of patients. The actual decrease in [ATP] adds further strength to the theory of the presence of a mitochondrial component in the pathophysiology of migraine.

Keywords

³¹P-MRS, creatine kinase reaction, migraine without aura, mitochondria, phantom replacement technique

Date received: 26 August 2010; revised: 28 September 2010; 18 October 2010; accepted: 26 October 2010

Introduction

Migraine is a common, disabling, primary headache disorder, with episodic manifestations, affecting women three times more than men (1). Migraine is subdivided into two major subtypes: migraine without aura (MwoA) and migraine with aura (MwA), previously known as common and classic migraine, respectively (2). The aura is characterized by a gradual development of transient and reversible focal neurological symptoms, most often visual, and may be related to cortical spreading depression (3). The headache attack suggests a significant role of the activation of the trigeminovascular system (4). Migraine attacks are often triggered by external factors, with psychological stress, hormones and fasting being the most common (5).

Despite the high prevalence of migraine in the general population, its pathophysiology is still

largely unknown. The current assumption is that subcortical structures, probably including the brain stem, hypothalamus and thalamus, are involved in the generation of migraine attacks (6). Even more puzzling are the mechanisms at the basis of the interictal brain disorder that predisposes migraine patients to develop an attack. Until now no integrative model has been formulated that accounts for all the factors that may play a role in migraine neurobiology. Some of these

¹Ghent University, Belgium.

²Sherbrooke University, Canada.

Corresponding author:

Harmen Reyngoudt, Ghent University Hospital, MR Department—
IK12B, De Pintelaan 185, 9000 Ghent, Belgium

Email: harmen.reyngoudt@ugent.be

factors include genetic background, nitric oxide hypersensitivity (7), lack of cortical habituation (8,9) and a disturbed energy metabolism. Genetic background and disturbed energy metabolism are discussed below.

Twin studies and familial aggregation studies strongly suggest that migraine is genetically determined (10). The mode of inheritance is most likely multifactorial in both MwA and MwoA (11). No genetic mutations have been found in the common forms of migraine, but a variety of gene polymorphisms, most often irreproducible, have been described (12). Recently though, the first genetic risk factor for migraine (MwA and MwoA) has been described (13). Molecular genetic studies have not detected specific mitochondrial DNA (mtDNA) mutations in patients with migraine, but other studies suggest that particular genetic markers (i.e. neutral polymorphisms or secondary mtDNA mutations) might be present in some migraineurs (10,14). For instance, in migraineurs with occipital stroke (15) as well as in children with MwoA or cyclic vomiting, which can be a migraine equivalent (16), an increased number of mutations was detected in the noncoding control regions of mtDNA. The noncoding region of mtDNA has an extremely high mutation rate and is therefore highly polymorphic. Collections of mtDNA mutations derived from the same ancestor (i.e. haplogroups) can influence oxidative phosphorylation performance and could thus play a more subtle role in migraine pathogenesis, predisposing subjects to the disorder (14). A monogenic subtype of migraine is familial hemiplegic migraine (FHM), a rare form of MwA, in which three known different missense mutations have been found, all causing ionopathies, affecting ion homeostasis and eventually leading to cortical hyperexcitability by increasing synaptic glutamate levels, involved in the generation of an aura (17). No convincing evidence, however, has been obtained that these same genes play a major role in the common forms of migraine (12).

In vivo energy metabolism can be studied by phosphorus magnetic resonance spectroscopy (^{31}P -MRS). This technique allows for the noninvasive quantification of phosphorylated compounds, including high-energy phosphates such as adenosine triphosphate (ATP) and phosphocreatine (PCr) and low-energy phosphates such as inorganic phosphate (P_i). ^{31}P -MRS can also determine intracellular pH (pH_i) and intracellular magnesium (Mg^{2+}). In addition, adenosine diphosphate (ADP) and the phosphorylation potential (PP) can be calculated based on the creatine kinase equilibrium. Figure 1 shows resting-state brain energy metabolism and the corresponding metabolites that can be detected by ^{31}P -MRS (18). In the past 20 years, several ^{31}P -MRS studies suggested an abnormal cerebral energy metabolism in migraine patients during ictal and interictal periods (see Table 1 for a review) (19–29). These alterations

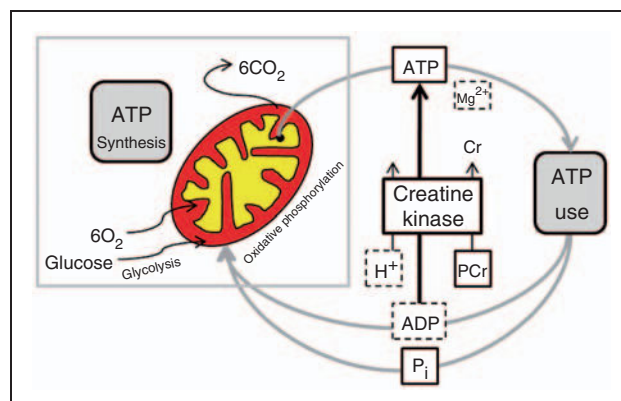


Figure 1. Resting-state brain energy metabolism, adapted from Kemp et al., 2000 (18). In the resting state, intracellular adenosine triphosphate (ATP) results from the balance between ATP use and ATP synthesis. ATP is derived almost exclusively from mitochondrial oxidative phosphorylation, depending on glucose and oxygen supply. Changes in phosphocreatine (PCr) reflect the time integral of the mismatch between ATP usage and supply, as adenosine diphosphate (ADP) can be rephosphorylated through the creatine kinase reaction, with conversion from PCr to creatine (Cr). Magnesium (Mg^{2+}) is bound to ATP in order for ATP to be biologically active. The metabolites in boxes can be detected by ^{31}P -MRS.

concern energy metabolism and are not limited to the brain but have also been observed in muscle (22–24,27,30). The reduced energy potential was interpreted as being indicative of a reduced mitochondrial reserve and was hypothesized to be the biochemical substrate of the susceptibility to migraine attacks (28,31). As summarized in Table 1, studies have been performed in a wide variety of migraine subtypes, during either the ictal or interictal period, mostly localized in the occipital lobe and mostly in patients who did not undergo prophylactic treatment. In several of these studies, the migraine patient group was heterogeneous and information about the attack frequency was scarce. These studies were performed at different field strengths and provided little information, if any, about the procedure for quantification of the metabolites. Most importantly, the ATP concentration ($[\text{ATP}]$) was always assumed constant and equal to that of normal controls, being 3 mM (32), or was not mentioned at all. However, cortical ATP levels can be decreased, as was demonstrated with ^{31}P -MRS in other pathologies, such as systemic lupus erythematosus (33), episodic ataxia type 2 (34), progressive supranuclear palsy (35) and Parkinson's disease (36).

In this study, the aim was to revisit quantitative ^{31}P -MRS at 3 tesla in the medial occipital lobe in patients with migraine without aura in the interictal phase, using quantification based on the phantom replacement technique.

Table 1. Literature survey of ^3P -MRS studies performed in the brain of migraine patients

Study	Migraine type (N)	Ictal/ interictal study	Brain region	Prophylaxis at time of study?	Field strength (T)	[ATP] (mM)	Results
Welch et al., 1988 (19); Welch et al., 1989 (20)	MwoA (12), MwA (8)	Ictal	Occipital	Yes	1.89	— ^b	PCr/P _i ↓
Barbiroli et al., 1990 (21)	MwpA (4), MS (4)	Interictal	Occipital	No	1.5	— ^b	PCr/P _i ↓
Sacquegnia et al., 1992 (22)	MwpA (1)	Interictal	Occipital	— ^b	1.5	3	[P _i] ↓, PP ↓
Barbiroli et al., 1992 (23)	MwA (12)	Interictal	Occipital	No	1.5	3	pH ↓, [PCr] ↓, [ADP] ↓, PP ↓
Montagna et al., 1994 (24); Montagna et al., 1995 (25)	MwoA (22), MwA (18), other ^a (15)	Interictal	Occipital	No	1.5	3	[PCr] ↓, [ADP] ↑, PP ↓
Uncini et al., 1995 (26)	FHM (5)	Interictal	Occipital	— ^b	1.5	3	[PCr] ↓, [P _i] ↑, PP ↓, [ADP] ↑
Lodi et al., 1997 (27)	MwA (12), MwpA (3)	Interictal	Occipital	No	1.5	3	[PCr] ↓, [P _i] ↑, [ADP] ↑, PP ↓ [Mg ²⁺] ↓, pH ↑
Boska et al., 2002 (28)	MwoA (19), MwA (19), FHM (8)	Interictal	Occipital	No	3	3	[Mg ²⁺] ↓, [PDE] ↑
Schulz et al., 2007 (29)	MwA (22)	Interictal	Basal ganglia	— ^b	2	— ^b	PCr/P _i ↓, P _i /ATP ↑

MwpA = migraine with prolonged aura. MS = migrainous stroke. N = number of included patients. PCr = phosphocreatine. P_i = inorganic phosphate. PP = phosphorylation potential. ADP = adenosine diphosphate. ATP = adenosine triphosphate. Mg²⁺ = magnesium. PDE = phosphodiesterase. [] are molar concentrations. PCr/P_i and P_i/ATP are ratios. ^aOther = MS or MwA, ^b— = information not mentioned in the study.

Table 2. Participant characteristics

Characteristic	Patients (N = 19)	Controls (N = 26)
Age (years, mean ± SD)	32.3 ± 12.1	27.6 ± 10.9
Males	1	11
Females	18	15
Attack frequency per month (mean ± SD)	3.6 ± 1.1	—

SD = standard deviation.

Materials and methods

Patients and control subjects

Nineteen MwoA patients fulfilling all required inclusion criteria (vide infra) were recruited by the local headache clinic. The control group consisted of 26 volunteers who were matched in age but not in gender. The details of the MwoA patients and the controls are given in Table 2.

The study was approved by the local ethics committee and all subjects gave written informed consent. The migraine patients were diagnosed with MwoA according to the criteria of the International Headache Society (2). Patients experienced two to eight attacks per month, were not using any prophylactic medication and were attack-free for at least 48 hours. None of the 19 patients experienced a migraine attack within 24 hours after the spectroscopy study.

^3P -MRS and region of interest

All measurements were performed on a 3 tesla Siemens TrioTim whole-body scanner (Erlangen, Germany), using a 26.5-cm-diameter quadrature dual tuned (^3P - ^1H) transmit/receive birdcage head coil (Rapid Biomedical, Würzburg-Rimpar, Germany). Spectra were acquired using a two-dimensional chemical shift imaging (CSI) phase-encoding scheme applying a pulse-free induction decay sequence. Manual shimming of the B_0 magnetic field and manual optimization of the transmitter pulse power were used.

The field of view (FOV) was placed occipitally, covering the visual cortex (Figures 2a and 2b), localized on T_1 -weighted gradient-echo images in three orthogonal planes with a slice thickness of 1 mm, a repetition time (TR) of 1550 ms and an echo time (TE) of 2.37 ms.

A $240 \times 240 \times 30 \text{ mm}^3$ two-dimensional CSI slice was recorded. Phase encoding was used with a weighted acquisition scheme, resulting in an axial slice with a nominal thickness of 30 mm and $30 \times 30 \text{ mm}^2$ in plane resolution (four averages, flip angle of 90° , TR of 4000 ms and TE of 2.3 ms). The raw data of each

acquisition consisted of 1024 complex-valued data points, at a sampling period of 0.4 ms. The corresponding bandwidth was 2500 Hz. The total duration of the measurement was approximately 10 minutes.

External calibration

Signal intensities were quantified in terms of arbitrary units (a.u.) by using the phantom replacement technique. The reference phantom contained an aqueous solution (pH 7) of 10 mM PCr (Sigma Aldrich).

Sodium chloride (NaCl) and sodium azide (NaN_3) were added to change the conductivity and to avoid mycotic growth, respectively. The phantom was made of plastic, was spherical and had a diameter of 10.4 cm.

The complete equation for calculating the in vivo concentrations is given by:

$$[C_i] = [C_r] \frac{S_i V_r N_r T_i}{S_r V_i N_i T_r} c_{load} \quad (1)$$

with subscripts i and r corresponding with the in vivo measurement and the reference phantom

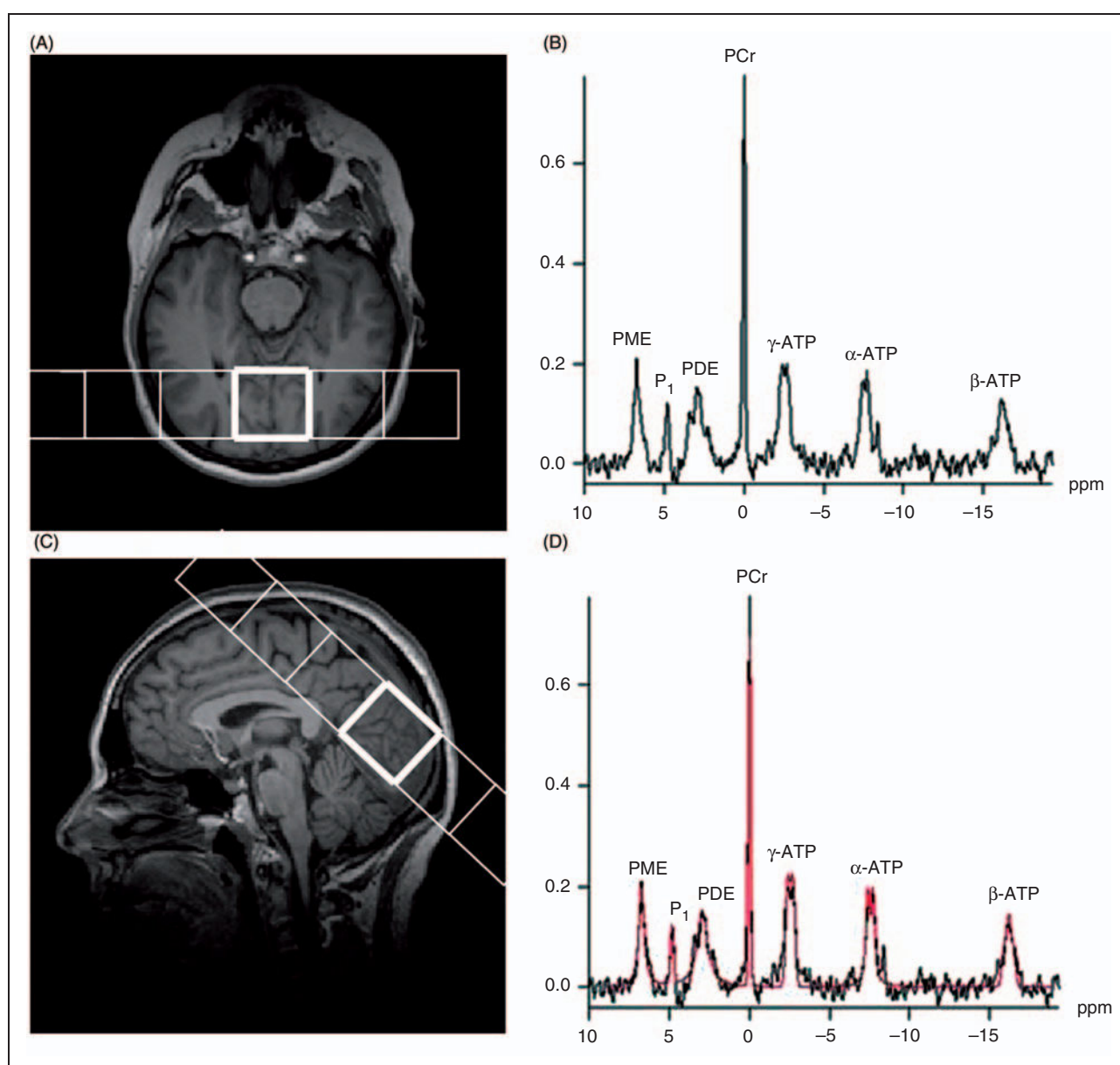


Figure 2. (a) Axial T_1 -weighted image and (b) sagittal T_1 -weighted image with the field of view and the voxel in the medial occipital lobe. (c) Spectrum acquired in the highlighted voxel. (d) The same spectrum with curve fitting. A CSI (chemical shift imaging) slice of $(240 \times 240 \times 30) \text{ mm}^3$ was placed and the nominal voxel volume was 30 ml.

measurement, respectively. $[C]$ is the metabolite concentration, S is the signal strength, V is the volume of the voxel from which the signal is acquired, N is the number of phosphorus atoms that contribute to the spectral line ($N=1$ in all cases), T is the absolute temperature ($T_i=310.16$ K in the human subject and $T_r=294.16$ K in the reference phantom), c_{load} is a correction factor for different coil loading (i.e. the respective transmitter voltages, V_{tra}). The volume ratio V_r/V_i cancels from the equation because V was the same in the reference phantom and in vivo, (i.e. 30 ml). All concentrations are expressed in a.u..

Spectral analysis

Figure 2c shows a typical ^{31}P -spectrum. The ^{31}P resonances can be allocated to ATP, PCr, phosphodiester (PDE), phosphomonoesters (PME) and P_i . The ^{31}P -MRS spectra for ATP contain three signals corresponding to the three phosphorus nuclei of the molecule: the α -ATP resonance contains contributions from both NADH and α -ADP, the γ -ATP resonance contains contributions from β -ADP, and β -ATP is proportional to the total cellular ATP content. We therefore used the β -ATP resonance to quantify [ATP] (37). Following apodization (exponential filter, width = 110 ms) and zero-filling, the Fourier transformed free induction decays were phase and baseline corrected. Peak areas were obtained by the classical Levenberg-Marquardt frequency domain-fitting method, using the software on the scanner (syngoMR B15, Numaris 4 [Siemens]) (Figure 2d).

Creatine kinase reaction

pH_i was calculated from the chemical shift of P_i in relation to PCr (38). Brain cytosolic free $[\text{Mg}^{2+}]$ was assessed by a semi-empirical equation that correlates the chemical shift of the β -ATP signal from PCr to the free $[\text{Mg}^{2+}]$ (39).

The biochemical equation for the creatine kinase reaction is as follows:



where Cr is creatine.

Based on this equilibrium, the cytosolic ADP concentration ($[\text{ADP}]$) was calculated as follows:

$$[\text{ADP}] = \frac{[\text{Cr}][\text{ATP}]}{K_{ck}[\text{PCr}][\text{H}^+]} \quad (3)$$

where the in vitro value of $1.66 \cdot 10^9 \text{ M}^{-1}$ is used for the creatine kinase equilibrium constant K_{ck} (40). $[\text{Cr}]$ is calculated from the measured PCr concentration

($[\text{PCr}]$), and $[\text{H}^+]$ is the proton concentration derived from the measured pH. The tCr concentration, measured with proton MRS (^1H -MRS), contains both contributions from both Cr and PCr. For tCr, no significant changes have been found between MwoA patients and controls in a recent ^1H -MRS study by our group (41). [ATP] is calculated from the β -ATP resonance (37). In addition, the PP, an index of free available energy per ATP, was calculated as follows:

$$PP = \frac{[\text{ATP}]}{[\text{ADP}][\text{P}_i]} \quad (4)$$

Statistical analysis

Statistical analysis was performed using the SPSS software (SPSS 15.0 for Windows; Chicago, IL, USA). Descriptive statistics was applied for age, V_{tra} , metabolite concentrations and calculated values. Wilcoxon's rank-sum test was applied to compare V_{tra} , metabolite concentrations and calculated values between MwoA patients and controls. Results were considered to be significant at $p < .05$.

Results

Table 3 shows the concentrations of PCr, P_i and ATP as well as calculated values for pH_i , ADP, PP and Mg^{2+} with their corresponding standard deviations, in the medial occipital lobe of 19 MwoA patients and 26 healthy volunteers. These values were obtained after applying corrections for coil loading and temperature.

First, no significant differences were observed for any of the variables between males and females in the control group (data not shown).

A significantly low PCr content was found in MwoA patients ($p = .001$). We also fitted the β -ATP signal to calculate [ATP]. On average, the ATP content was found to be significantly lower in MwoA patients

Table 3. Concentration values in a.u. and calculated values (mean \pm SD)

	MwoA patients	Controls	p
pH_i	7.03 ± 0.09	7.03 ± 0.03	.702
$[\text{PCr}](\text{a.u.})$	$4.09 \pm 0.58^*$	4.85 ± 0.60	.001*
$[\text{P}_i](\text{a.u.})$	1.32 ± 0.50	1.06 ± 0.36	.129
$[\text{ATP}](\text{a.u.})$	$2.33 \pm 0.63^*$	2.76 ± 0.59	.023*
$[\text{ADP}](\text{a.u.})$	0.020 ± 0.006	0.018 ± 0.009	.735
$\text{PP}(\text{a.u.}^{-1})$	$88.71 \pm 21.95^*$	144.35 ± 18.12	.001
$[\text{Mg}^{2+}](\text{a.u.})$	0.135 ± 0.058	0.156 ± 0.038	.254

*a.u. = arbitrary units. SD = standard deviation. *Level of significance, $p < .05$.

compared to controls ($p = .023$). This corresponds with an average reduction of [ATP] by approximately 15%. A subgroup of the MwoA patients (i.e. 20 %) demonstrates [ATP] values at least 2 standard deviations (SD) beneath the average [ATP] of controls, as illustrated in Figure 3. This subgroup corresponds with those patients who had the highest attack frequency.

Mean $[P_i]$ showed no significant difference between the MwoA patient group and the controls ($p = .129$). Calculated values of pH_i and [ADP] showed no differences between MwoA patients and controls ($p = .702$

and $p = .735$, respectively). The PP was significantly decreased in the MwoA patient group ($p = 0.001$). Finally, the Mg^{2+} content did not demonstrate a significant difference between MwoA patients and controls ($p = .254$).

Discussion

^{31}P -MRS provides a reliable noninvasive tool for the in vivo assessment of mitochondrial functionality by measuring cytosolic [ATP], [PCr], and $[P_i]$ and by

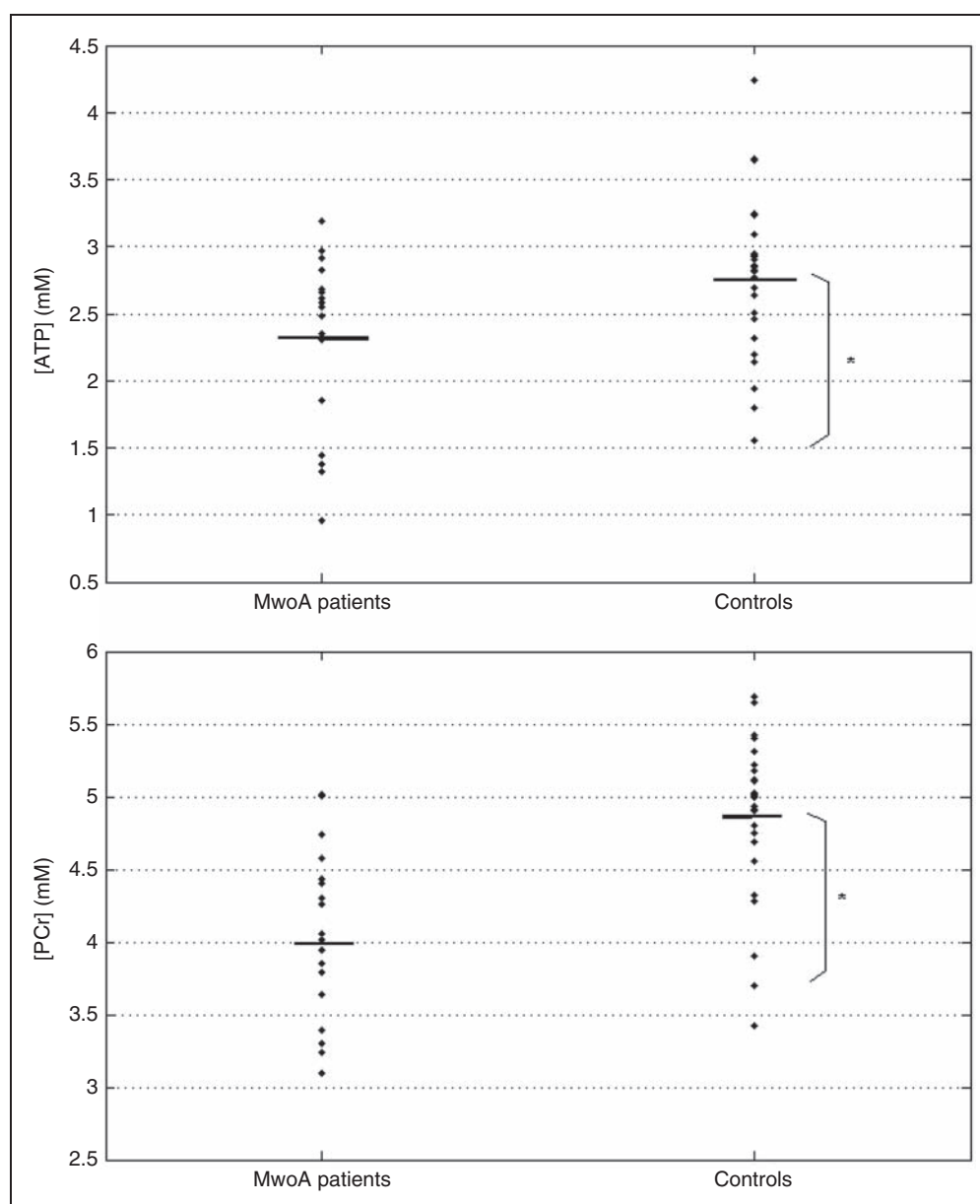


Figure 3. Distribution of the concentrations of the high-energy phosphates adenosine triphosphate (ATP) and phosphocreatine (PCr). Mean concentrations are illustrated with a horizontal line. The mean minus 2x the standard deviation is also shown. Note that in every plot, four patients have concentrations beneath this threshold. These patients are not the same for the two plots. In the case of [ATP], these values correspond with the patients who had the highest attack frequency.

calculating [ADP], PP, pH and $[Mg^{2+}]$, all playing crucial roles in the creatine kinase equilibrium (Figure 1).

In migraine, several magnetic resonance spectroscopy studies, in particular ^{31}P -MRS, have been performed. These studies were the first to document intrinsic biochemical abnormalities in migraine. In most of these studies, data was obtained in patients with migraine with prolonged aura (MwPA) and MwA patients, including patients with FHM (Table 1). Only two studies emphasized MwoA; in these, measurements were performed interictally (24,28).

To assess the resting-state brain energy metabolism, we performed ^{31}P -MRS on a 3 tesla high-field scanner in the medial occipital lobe of MwoA patients, who were attack-free and were not using any prophylactic medication, and compared the results with those of previous ^{31}P -MRS studies. It is worth underlining that the aim was to study a very homogeneous group of migraine patients who experienced a well-defined number of attacks (two to eight per month). This is in contrast to several other studies, in which a heterogeneous group of migraine patients was examined and in which information about the attack frequency is not always available (21,25). By focusing on MwoA, the potential influence of the predisposition to aura, which is most often visual and thus related to the occipital cortex too, was avoided in this study. The chance of migraine attack-related brain disturbances was minimized by examining the patients interictally, by assuring patients were at pain-free for at least 48 hours before the procedure and pain-free for at least 24 hours after the procedure.

We calibrated the *in vivo* spectra to an external standard to quantify metabolite concentrations rather than using raw signal intensities.

Because we were looking for metabolic disturbances, measurements were performed in the occipital lobe, as it has been found that the regional cerebral metabolic oxygen rate (CMRO₂) is significantly higher in this brain area compared to other cortical regions (42). Additionally, the regional cerebral metabolic glucose rate (CMR_{gl}) has been found to be the highest in occipital white matter and the visual cortex (43). An additional advantage is that the visual cortex remains metabolically unchanged with advancing age (44).

High-energy phosphate metabolism was found to be altered in MwoA patients in the medial occipital lobe. The average PCr concentrations were decreased significantly, which is comparable with previous data (24). However, others could not confirm this (28). In contrast to all other ^{31}P -MRS studies in migraine, in this study [ATP] was calculated from the spectrum. All other ^{31}P -MRS studies in migraine assumed a constant [ATP] of 3 mM (22–28). This assumption

was based on a ^{31}P -MRS study in healthy subjects (32). We observed a significant decrease in the average [ATP] of approximately 15% in MwoA patients as compared to controls.

The PP is an index of mitochondrial functionality and of the energy status of the cell. The higher the PP, the more free energy is available in the cell. The PP was significantly decreased in MwoA patients compared to controls. This is in concordance with the findings of previous studies (23,24). ADP is the major driving force for mitochondrial energy production. The concentration of free cytosolic ADP is in the micromolar range and is below the sensitivity of MRS *in vivo*. However, [ADP] can be calculated from the creatine kinase equilibrium. In contrast to most other studies, we did not find a difference between MwoA patients and controls. In all other studies, [ADP] was derived assuming an ATP concentration of 3 mM in both MwoA patients and controls. When calculating [ADP] assuming a constant [ATP] in our subjects, there was still no significant difference in [ADP] between MwoA patients and controls.

No cytosolic pH difference was found between MwoA patients and controls, as was also the case in previous studies (24,28).

Mg^{2+} is an important enzymatic cofactor and can influence the equilibrium constant of several biochemical reactions, including the creatine kinase reaction. Brain cytosolic free $[Mg^{2+}]$ was not significantly different in MwoA patients compared to controls. In a previous study, a significant decrease in interictal $[Mg^{2+}]$ was found in MwA patients (27). In another study, whereas a significantly reduced brain $[Mg^{2+}]$ was observed ictally in both MwA and MwoA patients, this was not the case for interictal brain $[Mg^{2+}]$ in some of the patients (45). The absence of a significant interictal reduction of $[Mg^{2+}]$ may be attributed to the large heterogeneity of the patient group, the variability of the examined brain area examined, or the semi-empirical method to calculate $[Mg^{2+}]$.

The decrease in high-energy phosphates suggests a mitochondrial component in the neurobiology of migraine. The brain is one of the most energy-expensive tissues and although it comprises only 2–3 % of the total body weight (46), it utilizes approximately 25% of the total glucose. The baseline metabolic rate of the brain is very high and most energy is thought to support glutamatergic neurotransmission, at least in the cortical grey matter (47). The brain at rest relies almost entirely on aerobic metabolism with glucose as the principal fuel (48). Glycogen can also be used but is only found in small amounts in the astrocytes (49). Lactate, an indicator of anaerobic glycolysis, accumulating in case of mitochondrial dysfunction, can be detected by 1H -MRS (50). A recent resting state

¹H-MRS study did not show any quantifiable lactate in the visual cortex of MwoA patients (41). The observed decrease in [ATP], often called the 'molecular unit of currency' of intracellular energy transfer, might thus be explained by a decrease in ATP production through aerobic glycolysis and oxidative phosphorylation (Figure 1). We emphasize that the decrease of high-energy phosphates in MwoA was detected at rest (interictally), implying the constant nature of this energy disturbance rather than being a transient phenomenon. This cannot be explained by hypermetabolism, as a recent [18]fluorodeoxyglucose-positron emission tomography (PET) study in migraine patients failed to show any hypermetabolic brain regions, including in the occipital lobe (51).

Is the reduction of interictal [ATP] related to a decrease in the number of mitochondria or to a decrease in mitochondrial efficiency? It is very difficult to draw conclusions in this regard since the brain is not readily accessible for histological and biochemical studies. There is, however, additional evidence for a mitochondrial component in migraine pathophysiology.

With ³¹P-MRS, a decreased postexercise recovery of high-energy phosphates was found in the gastrocnemius muscle of MwoA patients compared to controls (24,52). Platelet mitochondrial enzyme activities were found significantly lower in MwoA patients than in controls (53). Plasma lactate and pyruvate levels were found significantly increased in migraine patients compared to controls (54). Alterations comparable to those in migraine have been found in mitochondrial encephalomyopathies, and could conceivably result either from errors in energetic, oxidative pathways limiting the energy supply of cells, or to defects in ionic conductances or some specific neurotransmitters, responsible for neuronal excitability, whose failure increases energy expenditure in excitable cells (55). Stroke-like episodes and migraine are the predominant symptoms of mitochondrial encephalomyopathy with lactic acidosis and stroke-like episodes (MELAS), but the mtDNA point mutations at bp 3243 and 3271, generally associated with this syndrome, were not found in migraine (56). ³¹P-MRS studies in mitochondrial diseases such as MELAS show similar results as in migraine both in brain (57) and in muscle (58). In both aforementioned studies, no data concerning [ATP] is shown or [ATP] is, surprisingly, assumed constant, respectively. An occasional mtDNA mutation has been found in one study (59); however, this was not the case in systematic studies (60). Additionally, another study showed mitochondrial abnormalities in muscle biopsies of some migraine patients compared to controls (30). Mitochondrial metabolic enhancers such as riboflavin (61) and coenzyme Q10 (62) have a prophylactic effect in a subgroup of migraine patients.

Response to riboflavin seems to be related to a specific mitochondrial haplotype (14).

Stress, female hormones and fasting are the most common trigger factors for migraine attacks (5). Normobaric hypoxia is able to trigger a migraine attack (63), as well as hypoglycemia (5) in a subgroup of patients. It is intuitive to think that such specific triggers, having a direct effect on oxygen and glucose metabolism, respectively, would put a significant strain on the mitochondria. The hormones progesterone and estrogen regulate oxidative metabolism in brain mitochondria (64). It has also been shown, albeit in cardiac myocytes, that noradrenaline, a typical stress mediator, causes calcium overload and results in a decreased mitochondrial respiration (65). Stress activates the noradrenergic locus coeruleus (66), which projects widely to the cortex, including the occipital visual cortex (67).

A mitochondrial defect may reduce the threshold for migraine. The hypothesis of migraine being a "biobehavioural" (68) or a threshold disorder (69) states that it is a disorder in which an intrinsic metabolic defect renders the brain more susceptible to various factors that trigger an attack. It is hypothesized that trigger factors would act by increasing the metabolic energy demand or decreasing the metabolic energy supply. When a certain metabolic threshold is reached in the brain, which is already near to its maximum energetic capabilities, a metabolic crisis could be induced which is responsible for the headache attack. Our data show that [ATP] is profoundly reduced in a subgroup of MwoA patients. Rather than being a generic component of migraine neurobiology, we hypothesize that a reduced mitochondrial energy reserve may be one of the many factors determining the migraine threshold. This hypothesis is in line with the observation that a subgroup of migraine patients respond to mitochondrial enhancers, such as riboflavin (61) and coenzyme Q10 (62), and that this response may be related to a specific mitochondrial haplotype (14).

In conclusion, a significant depletion of high-energy phosphates, both ATP and PCr, was found at rest in the medial occipital lobe of MwoA patients, compared to controls. This suggests a decrease in oxidative phosphorylation and implies a mitochondrial component in the pathophysiology of migraine without aura. A decreased mitochondrial energy reserve is pivotal in lowering the threshold for a migraine attack, at least in a subgroup of patients. It has to be emphasized that also other factors such as a lack of cortical habituation, NO hypersensitivity and genetic aspects play crucial roles in migraine pathophysiology. ³¹P-MRS is sensitive enough to reveal defects of cell energy production of MwoA patients even in the absence of any symptoms and signs.

Acknowledgements

This research is funded by the Special Research Fund PhD grant B/07768/02 and performed at the Ghent Institute for Functional and Metabolic Imaging. The Ghent University Department of Radiation Oncology and Experimental Cancer Research is also greatly acknowledged for the use of the radiophysics laboratory

References

1. Stovner LJ, Hagen K, Jensen R, et al. The global burden of headache: a documentation of headache prevalence and disability worldwide. *Cephalalgia* 2007; 27: 193–210.
2. Classification Committee of the International Headache Society. The international classification of headache disorders. 2nd ed. *Cephalalgia* 2004; 24(Suppl 1): 9–160.
3. Olesen J, Larsen B and Lauritzen M. Focal hyperemia followed by spreading oligemia and impaired activation of rCBF in classic migraine. *Ann Neurol* 1981; 9: 344–352.
4. Goadsby PJ, Charbit AR, Andreou AP, Akerman S and Holland PR. Neurobiology of migraine. *Neuroscience* 2009; 161: 327–341.
5. Kelman L. The triggers of precipitants of the acute migraine attack. *Cephalalgia* 2007; 27: 394–402.
6. Goadsby PJ. Pathophysiology of migraine. *Neurol Clin* 2009; 27: 335–360.
7. Olesen J. The role of nitric oxide (NO) in migraine, tension-type headache and cluster headache. *Pharmacol Ther* 2008; 120: 157–171.
8. Schoenen J. Pathogenesis of migraine: the biobehavioural and hypoxia theories reconciled. *Acta Neurol Belg* 1994; 94: 79–86.
9. Schoenen J. Cortical electrophysiology in migraine and possible pathogenic implications. *Clin Neurosci* 1998; 5: 10–17.
10. Russell MB and Olesen J. The genetics of migraine without aura and migraine with aura. *Cephalalgia* 1993; 13: 245–248.
11. Russell MB, Iselius L and Olesen J. Inheritance of migraine investigated by complex segregation analysis. *Hum Genet* 1995; 96: 726–730.
12. De Vries B, Frants RR, Ferrari MD and Van Den Maagdenberg AM. Molecular genetics of migraine. *Hum Genet* 2009; 126: 115–132.
13. Antilla V, Stefansson H, Kallela M, et al. (International Headache Genetics Consortium). Genome-wide association study of migraine implicates a common susceptibility variant on 8q22.1. *Nat Genet* 2010; 42(10): 869–873.
14. Di Lorenzo C, Pierelli F, Coppola G, et al. Mitochondrial DNA haplogroups influence the therapeutic response to riboflavin in migraineurs. *Neurology* 2009; 72: 1588–1594.
15. Majamaa K, Finnila S, Turkka J and Hassinen IE. Mitochondrial DNA haplogroup U as a risk factor for occipital stroke in migraine. *Lancet* 1998; 352: 455–456.
16. Wang Q, Ito M, Adams K, et al. Mitochondrial DNA control region sequence variation in migraine headache and cyclic vomiting syndrome. *Am J Med Genet A* 2004; 131: 50–58.
17. Barrett CF, Van Den Maagdenberg AM, Frants RR and Ferrari MD. Familial hemiplegic migraine. *Adv Genet* 2008; 63: 57–83.
18. Kemp GJ. Non-invasive methods for studying brain energy metabolism: what they show and what it means. *Dev Neurosci* 2000; 22: 418–428.
19. Welch KM, Levine SR, D'Andrea G and Helpert JA. Brain pH in migraine: An in vivo phosphorus-31 magnetic resonance spectroscopy study. *Cephalalgia* 1988; 8: 273–277.
20. Welch KM, Levine SR, D'Andrea G, Schultz LR and Helpert JA. Preliminary observations on brain energy metabolism in migraine studied by in vivo phosphorus 31 NMR spectroscopy. *Neurology* 1989; 39: 538–541.
21. Barbiroli B, Montagna P, Cortelli P, et al. Complicated migraine studied by phosphorus magnetic resonance spectroscopy. *Cephalalgia* 1990; 10: 263–272.
22. Sacquegnia T, Lodi R, De Carolis P, et al. Brain energy metabolism studied by ³¹P-MR spectroscopy in a case of migraine with prolonged aura. *Acta Neurol Scand* 1992; 86: 376–380.
23. Barbiroli B, Montagna P, Cortelli P, et al. Abnormal brain and energy metabolism shown by ³¹P magnetic resonance spectroscopy in patients affected by migraine with aura. *Neurology* 1992; 42: 1209–1214.
24. Montagna P, Cortelli P, Monari L, et al. ³¹P-Magnetic resonance spectroscopy in migraine without aura. *Neurology* 1994; 44: 666–669.
25. Montagna P. Magnetic resonance spectroscopy in migraine. *Cephalalgia* 1995; 15: 323–327.
26. Uncini A, Lodi R, Di Muzio A, et al. Abnormal brain and muscle energy metabolism shown by ³¹P-MRS in familial hemiplegic migraine. *J Neurol Sci* 1995; 129: 214–222.
27. Lodi R, Montagna P, Soriani S, et al. Deficit of brain and skeletal muscle bioenergetics and low brain magnesium in juvenile migraine: an in vivo ³¹P magnetic resonance spectroscopy interictal study. *Pediatr Res* 1997; 42: 866–871.
28. Boska MD, Welch KM, Barker PB, Nelson JA and Schultz L. Contrasts in cortical magnesium, phospholipid and energy metabolism between migraine syndromes. *Neurology* 2002; 58: 1227–1233.
29. Schulz UG, Blamire AM, Corkill RG, Davies P, Styles P and Rothwell PM. Association between cortical metabolite levels and clinical manifestations of migrainous aura: an MR-spectroscopy study. *Brain* 2007; 130: 3102–3110.
30. Montagna P, Sacquegnia T, Martinelli P, et al. Mitochondrial abnormalities in migraine. *Preliminary findings. Headache* 1988; 28: 477–480.
31. Lodi R, Iotti S, Cortelli P, et al. Deficient energy metabolism is associated with low free magnesium in the brains of patients with migraine and cluster headache. *Brain Res Bull* 2001; 54: 437–441.
32. Bottomley PA and Hardy CJ. Rapid, reliable in vivo assay of human phosphate metabolites by nuclear magnetic resonance. *Clin Chem* 1989; 35: 392–395.
33. Griffey RH, Brown MS, Bankhurst AD, Sibbitt RR and Sibbitt WL. Depletion of high-energy phosphates in the central nervous system of patients with systemic lupus

- erythematosus, as determined by phosphorus-31 nuclear magnetic resonance spectroscopy. *Arthritis Rheum* 1990; 33: 827–833.
34. Sappey-Marinié D, Vighetto A, Peyron R, Broussolle E and Bonmartin A. Phosphorus and proton magnetic resonance spectroscopy in episodic ataxia type 2. *Ann Neurol* 1999; 46: 256–259.
 35. Stamelou M, Pilatus U, Reuss A, et al. In vivo evidence for cerebral depletion in high-energy phosphates in progressive supranuclear palsy. *J Cereb Blood Flow Metab* 2009; 29: 861–870.
 36. Hattingen E, Magerkurth J, Pilatus U, et al. Phosphorus and proton magnetic resonance spectroscopy demonstrates mitochondrial dysfunction in early and advanced Parkinson's disease. *Brain* 2009; 132: 3285–3297.
 37. Pietz J, Rupp A, Ebinger F, et al. Cerebral energy metabolism in phenylketonuria: findings by quantitative in vivo ³¹P-MR spectroscopy. *Pediatr Res* 2003; 53: 654–662.
 38. Petroff OA, Prichard JW, Behar KL, Alger JR, Den Hollander JA and Shulman RG. Cerebral intracellular pH by ³¹P nuclear magnetic resonance spectroscopy. *Neurology* 1985; 35: 781–788.
 39. Iotti S, Frassinetti C, Alderighi L, Sabatini A, Vacca A and Barbiroli B. In vivo assessment of free magnesium concentration in human brain by ³¹P-MRS. A new calibration curve based on a mathematical algorithm. *NMR Biomed* 1996; 9: 24–32.
 40. Kemp GJ, Roussel M, Bendahan B, Le Fur Y and Cozzzone PJ. Interrelations of ATP synthesis and proton handling in ischaemic exercise studied by ³¹P magnetic resonance spectroscopy. *J Physiol* 2001; 535: 901–928.
 41. Reyngoudt H, De Deene Y, Descamps B, Paemeleire K and Achten E. ¹H-MRS of brain metabolites in migraine without aura: absolute quantification using the phantom replacement technique. *Magn Reson Mater Phys* 2010; 23: 227–241.
 42. Ishii K, Sasaki M, Kitagaki H, Sakamoto S, Yamaji S and Maeda K. Regional difference in cerebral blood flow and oxidative metabolism in human cortex. *J Nucl Med* 1996; 37: 1086–1088.
 43. Reivich M, Kuhl D, Wolf A, et al. The [18]fluorodeoxyglucose method for the measurement of local cerebral glucose utilization in man. *Circ Res* 1979; 44: 127–137.
 44. Loessner A, Alavi A, Lewandrowski KU, Mozley D, Souder E and Gur RE. Regional cerebral function determined by FDG-PET in healthy volunteers: normal pattern and changes with age. *J Nucl Med* 1995; 36: 1141–1149.
 45. Ramadan NM, Halvorson H, Vande-Linde A, Levine SR, Helpert JA and Welch KM. Low brain magnesium in migraine. *Headache* 1989; 29: 590–593.
 46. Wiesinger H, Hamprecht B and Dringen R. Metabolic pathways for glucose in astrocytes. *Glia* 1997; 21: 22–34.
 47. Sibson NR, Dhankhar A, Mason GF, Rothman DL, Behar KL and Shulman RG. Stoichiometric coupling of brain glucose metabolism and glutamatergic neuronal activity. *Proc Natl Acad Sci USA* 1998; 95: 316–321.
 48. Siesjö BK. Utilisation of substrates by brain tissues. In: *Brain energy metabolism*. New York: John Wiley & Sons, 1978, pp.101–130.
 49. Benarroch EE. Glycogen metabolism: metabolic coupling between astrocytes and neurons. *Neurology* 2010; 74: 919–923.
 50. Prichard J, Rothman D, Novotny E, et al. Lactate rise detected by ¹H NMR in human visual cortex during physiologic stimulation. *Proc Natl Acad Sci USA* 1991; 88: 5829–5831.
 51. Kim J, Kim S, Suh SI, Koh SB, Park KW and Oh K. Interictal metabolic changes in episodic migraine: a voxel-based FDG-PET study. *Cephalalgia* 2009; 30: 53–61.
 52. Lodi R, Kemp GJ, Montagna P, et al. Quantitative analysis of skeletal muscle bioenergetics and proton efflux in migraine and cluster headache. *J Neurol Sci* 1997; 146: 73–80.
 53. Sangiorgi S, Mochi M, Riva R, et al. Abnormal platelet mitochondrial function in patients affected by migraine with and without aura. *Cephalalgia* 1994; 14: 21–23.
 54. Okada H, Araga S, Takeshima T and Nakashima K. Plasma lactic acid and pyruvic acid levels in migraine and tension-type headache. *Headache* 1997; 38: 39–42.
 55. Eleff SM, Barker PB, Blackband SJ, et al. Phosphorous magnetic resonance spectroscopy of patients with mitochondrial cytopathies demonstrates decreased levels of brain phosphocreatine. *Ann Neurol* 1990; 27: 626–630.
 56. Di Mauro S and Moraes CT. Mitochondrial encephalomyopathies. *Arch Neurol* 1993; 50: 1197–1208.
 57. Kato T, Murashita J, Shioiri T, Terada M, Inubushi T and Kato N. Photostimulation-induced alteration of brain energy metabolism measured by ³¹P-MR spectroscopy in patients with MELAS. *J Neurol Sci* 1998; 155: 182–185.
 58. Möller HE, Kurlmann G, Pützler M, Wiedermann D, Hilbich T and Fiedler B. Magnetic resonance spectroscopy in patients with MELAS. *J Neurol Sci* 2005; 229/230: 131–139.
 59. Bresolin N, Martinelli P, Barbiroli B, et al. Muscle mitochondrial DNA deletion and ³¹P-NMR spectroscopy alterations in a migraine patient. *J Neurol Sci* 1991; 104: 182–189.
 60. Klopstock T, May A, Seibel P, Papagiannuli E, Diener HC and Reichmann H. Mitochondrial DNA in migraine with aura. *Neurology* 1996; 46: 1735–1738.
 61. Schoonen J, Jacquy J and Lenaerts M. Effectiveness of high-dose riboflavin in migraine prophylaxis. A randomized controlled trial. *Neurology* 1998; 50: 466–470.
 62. Sandor PS, Di Clemente L, Coppola G, et al. Efficacy of coenzyme Q10 in migraine prophylaxis: a randomized trial. *Neurology* 2005; 64: 713–715.
 63. Schoonman GG, Sandor PS, Agosti RM, et al. Normobaric hypoxia and nitroglycerin as trigger factors for migraine. *Cephalalgia* 2006; 26: 816–819.
 64. Irwin RW, Yao J, Hamilton RT, Cadenas E, Brinton RD and Nilsen J. Progesterone and estrogen regulate oxidative metabolism in brain mitochondria. *Endocrinology* 2008; 149: 3167–3175.
 65. Sone T, Miyazaki Y, Ogawa K and Satake T. Effects of excessive noradrenaline on cardiac mitochondrial calcium transport and oxidative phosphorylation. *Jpn Circ J* 1984; 48: 492–497.

66. Valentino RJ, Curtis AL, Page ME, Pavcovich LA and Florin-Lechner SM. Activation of the locus ceruleus brain noradrenergic system during stress: circuitry, consequences, and regulation. *Adv Pharmacol* 1998; 42: 781–784.
67. Sato H, Fox K and Daw NW. Effect of electrical stimulation of locus coeruleus on the activity of neurons in the cat visual cortex. *J Neurophysiol* 1989; 62: 946–958.
68. Welch KM. Migraine: a biobehavioural disorder. *Arch Neurol* 1987; 44: 323–327.
69. Mochi M, Sangiorgi S, Cortelli P, Riva R, Crisci M and Monari L. Migraine with aura: a threshold character with mitochondrial enzyme deficiency. *Neurology* 1991; 41(Suppl 1): 1–254.

Acknowledgements

Eindelijk is het zover. Eindelijk ligt hét boekje voor u. En daar hoort natuurlijk een woordje van dank bij. Zonder de hulp en steun van heel wat mensen zou me dit immers nooit gelukt zijn!

Eerst en vooral wil ik mijn promotoren prof. dr. Rik Achten en prof. dr. Koen Paemeleire bedanken. Halfweg vorig decennium rijpte het idee om in Gent een migraineproject op poten te zetten. Jullie vonden elkaar als enthousiaste partners en werkten een omvangrijk project uit, waardoor uiteindelijk zelfs twee doctoraatsstudenten op het project konden werken. Rik, ik zat nog maar net in mijn laatste jaar toen ik kwam informeren om onderzoek te doen rond beeldvorming. Je enthousiasme tijdens de lessen neuroradiologie had mijn interesse in MR nog aangewakkerd. Enkele maanden later, net afgestudeerd, voelde ik me meteen welkom. Dankzij jou zat ik aan de bron om volop en in alle vrijheid onderzoek te kunnen en mogen doen. Het was niet altijd makkelijk de balans te vinden tussen openstaan voor nieuwe ideeën en lopende projecten finaliseren, maar vandaag blijkt dat we toch geslaagd zijn in deel 1 van het migraineproject. En zo is de cirkel weer rond. Koen, jouw inzet, werklust en aanstekelijk enthousiasme hebben me enorm vooruitgeduwd, niet in het minst wanneer het soms wat minder vlot verliep dan gehoopt. Ik apprecieer enorm dat je zelfs met een volle agenda nog tijd wou maken voor een bespreking hier, een discussie daar, de een soms wat filosofischer dan de ander. Een oprechte “merci!” is dus wel op zijn plaats. Ik hoop dat je nog verder kan bouwen aan het research-luik van je carrière en wie weet kruisen onze wegen nog eens. Als er ooit een migraine-model in Gent komt, weet je alvast de weg naar de preklinische beeldvorming te vinden.

Ik wil de leden van mijn IWT-commissie danken omdat zij geloofden in het project en in mij. De leden van de examen- en leescommissie bedank ik omdat hun inzicht en opmerkingen dit werk nog vollediger gemaakt hebben. Fien, bedankt voor het vertaalwerk! Ook een oprechte “dank je wel” voor alle migrainepatiënten en controlepersonen die we gescand hebben.

Prof. dr. Luc Leybaert, bedankt voor je heldere kijk op en inbreng in het project als een van de leden van mijn begeleidingscommissie. Door de technische beperkingen zijn we uiteindelijk (nog) niet geraakt waarvan het oorspronkelijk de bedoeling was, maar toch was je een belangrijke schakel in de neurofysiologische overpeinzingen.

Prof. dr. Karel Deblaere, beste Karel, toen ik als groentje binnenwaaide op -1K12 was je nog assistent en zelf pas gedoctoreerd, en net door die ervaring was je uitstekend geplaatst om me te begeleiden op het PhD-pad. Zelfs toen de researchers al verhuisd waren naar de bokaal in het dwarsgebouw, bleef ik steeds welkom om kleine en grote beslommingen te bespreken. Bedankt voor alles!! En zoals we afgelopen anderhalf jaar al gemerkt hebben: het is maar een kleine afstand van -1K12 naar -1P8 en van de klinische naar de preklinische

beeldvorming, dus onze samenwerking houdt vast niet op na vandaag. Pieter, mijn bureaugenoot van 't eerste uur: ik kijk met plezier terug op onze samenwerking die me menig maal tot lachbuien heeft beroerd. Waar is de tijd dat ik door jou en Karel, die zeker tijdens mijn eerste jaren op radiologie jouw partner in crime was, willens nillens werd gekist? Of zwarte mazelen werd bezorgd? Los van de fun werd er – voor alle duidelijkheid – ook wel gewerkt. Je bent de technische man die ik altijd mocht storen om een of ander computerprobleem op te lossen. Veel van mijn skills heb ik aan jou te danken. Linux, Matlab, DAQ-kaarten, je noemt het maar. Je introduceerde me in die voor mij toen nog onbekende wereld en door jou is het allemaal wat minder Chinees geworden. Harmen, jij was dan weer mijn partner in crime als het over het hoofdpijnproject ging. Samen uren zitten scannen, tientallen patiënten screenen en informeren, het mag gezegd: het heeft ons liters zweet gekost. Je was een betrouwbare collega met een schitterend en apart gevoel voor humor waaraan ik nu nog regelmatig terugdenk. Een jaar geleden ging je me voor, dus ik kon de laatste weken met al m'n vragen over praktische beslommeringen steeds bij jou terecht. Heel erg bedankt voor je snelle respons, elke keer opnieuw. Als mijn stress-niveau over die “bijkomstigheden” binnen de perken bleef, was dat mede daaraan te wijten. Verder zijn er ook nog Leslie & Sam (ik hoop dat jullie het goed stellen in jullie carrière na de passage op de GE16), Elke (de drijvende kracht achter de “Let’s go out”s), Laura (de eeuwige examensupervisor), Marjan (met de hartverwarmende schaterlach en steeds paraat om een beeldje te evalueren – veel succes trouwens met jouw onderzoek, Dr. Acou), de technologen van -1K12B: fijn dat jullie allen de middag-, koffie-, en andere pauzes mee opgevrolijkt hebben. Katrien, bedankt voor het opvolgen van de admin door de jaren heen!

Ik wil ook al mijn huidige collega's van Medisip bedanken (Anne-Marie, Bert, Carmen, Ewout, Faruk, Gregor, Hendrik, Inge, Karel, Karen, Lara, Nathalie, Pieter M, Pieter vM, Radek, Roel, Roma, Samuel, Saskia, Shandra, Victoria, Vincent, ...). Hoewel ik steeds getracht heb jullie niet op te zadelen met mijn PhD-die-maar-niet-af-geraakt, vermoed ik dat jullie er vroeg of laat wel eens “last” van hadden. Bedankt voor jullie begrip en geduld, en alle afleiding, zowel mentaal als tijdens de after-work momenten. Dit is de gelegenheid om een paar mensen heel uitdrukkelijk te bedanken en me bij hen te verontschuldigen voor de onvermijdelijke interferentie. Stefaan, Chris, Scharon en Aaike: zonder jullie eindeloos geduld en de steun en aanmoediging om door te zetten en af te werken zaten we hier vandaag nog steeds niet. Chris & Scharon, bedankt om jullie in bochten te plooiën wanneer ik er niet kon zijn omdat ik thuis zat te schrijven. Jullie zijn fantastische collega's!

Els, de eerste en lange tijd enige vrouw van MR research, tevens mijn kamergenootje op congres: ik herinner me dat je lang geleden zei dat ik er wel zou geraken en zie, je hebt gelijk gekregen. Het zijn vaak zulke kleine aanmoediging die veel betekenen. Bedankt voor de steun en het vertrouwen. De researchers van nucleaire (Ingeborg, Koen, Julie, ...) en radiofarmacie (Filip, Sara N, Domi, Lieselotte, Ken, Nick, ...): bedankt om zoveel interesse te tonen en voor de aangename momenten, vroeger & nu, op & na 't werk of op congres.

In de loop der jaren heb ik erg veel mensen ontmoet die elk op hun manier hun bijdrage hebben geleverd. Alle stille en minder stille supporters, familie en vrienden die me al dan niet expliciet aanmoedigden: bedankt! Een aantal mensen wil ik toch graag bij naam noemen. Sofie D, al lang niet meer mijn kleine zusje, je hebt me – misschien zonder het te beseffen – zoveel dingen geleerd die niet in een tekstboek staan. Eindelijk breekt er een periode aan om onze verloren tijd in te halen! Waar je ook terecht komt, weet dat ik je onvoorwaardelijk zal steunen! Dikke knuf! Sara DB, jij hebt me eind mei de ultieme boost gegeven om nog voor de zomer in te dienen! Ik was overtuigd dat dat nooit zou lukken, maar je liet me alsnog inzien dat het wél kon. Bedankt! Sofie DR, ik had het beloofd, je staat erin, en dan nog met een van je legendarische aanmoedigingen: “Ela ela, betrapt! Sms’jes lezen terwijl ge vlijtig en noest aan het werk moet zijn! Kkkkkjjssssttt!”. Bedankt dat ik je mocht leren kennen. Ook jij doet me beseffen dat het leven meer is dan werken. Ik bewonder je optimisme en veerkracht. Tine & Stefanie: bedankt voor de fijne UZ-lunchkes en dito babbels. Toen jullie aan een eerste paper bezig waren en ik nog nergens leek te staan, waren jullie een van de weinigen die me toch konden geruststellen dat alles wel goed zou komen. Bedankt! Heel wat andere ex-BMW’ers, waaronder Sofie VdAb en Josefien: blij dat we contact zijn blijven houden. Onze drukke bezigheden maken het niet makkelijk om mekaar regelmatig te zien, maar ik heb onze dates altijd erg fijn gevonden!

Alle crewtjes van het ballonteam (ondertussen te veel om allemaal op te noemen), en Bert & Jolien in het bijzonder: dankzij jullie kon ik de knop regelmatig eens écht omdraaien. Crewen was/is een van de weinige manieren om me mentaal helemaal te ontspannen en jullie zorg(d)en altijd voor een schitterende sfeer. Mats, met je guitige lach en je schitterende uitspraken & redeneringen: jou als onbezorgde kleuter zien groeien en bloeien doet me veel deugd! High five! Anaïs & Lisa, Annelies, Eva: jullie zijn fantastische vriendinnen. Ik veronderstel dat ik eindelijk wat makkelijker tijd voor jullie zal kunnen maken. Bedankt voor alle babbels, uitjes, enz! Mijn ouders en schoonouders: bedankt voor de vele hulp die jullie steeds geboden hebben. Nooit was het te veel gevraagd om bij te springen waar jullie konden. Ik heb het altijd enorm geapprecieerd, ook al zei ik het misschien niet altijd.

En ten slotte, Joris: we hebben ondertussen heel wat watertjes doorsparteld maar ik denk dat we gerust kunnen zeggen dat we er steeds sterker uitgekomen zijn. De verdediging van mijn thesis betekent het einde van een lastige periode, ook en niet in het minst voor jou. Ik besef dat ik vaak niet te genieten was en er al te vaak met mijn hoofd niet bij was (“Ik moet nog schrijven!”). Merci voor je geduld en uithoudingsvermogen! xXx

BEDANKT allemaal!

Bene(dicte)

Curriculum Vitae

Personalia

Name	Benedicte Descamps
Date and Place of Birth	17 June 1983, Bruges, Belgium
Civil status	Married to Joris De Flou
Phone	Mobile: +32 498 611 201 Work: +32 9 332 69 34
E-mail	benedicte_descamps@hotmail.com Benedicte.Descamps@UGent.be

Education

- 2001 – 2005 **Master of Science: Biomedical Sciences, option Neurosciences**
Magna Cum Laude
Ghent University
Master thesis: “Determining factors for pregnancy following cryotransfer”
- 1995 – 2001 **Sciences - Maths (8h)**
Royal Athenee, Maldegem, Belgium

Additional courses and workshops

- 2011 – 2012 **Laboratory Animal Science** (FELASA Cat. C)
Ghent University, Belgium
- 24 – 28 Jan 2011 **6th Small Animal Imaging Workshop**
Laboratory for Preclinical Imaging and Imaging Technology
of the Werner Siemens Foundation, Tübingen, Germany
- 13 – 15 Oct 2010 **Small Animal MR Imaging and Spectroscopy**
ESMRMB – Lectures on MR, Eindhoven, The Netherlands
- Feb – May 2008 **Advanced Academic English – Writing Skills**
UCT, Ghent University, Belgium
- 10 – 12 Oct 2007 **Quantitative Perfusion Imaging**
ESMRMB – Lectures on MR, Freiburg, Germany
- 2006 – 2007 **Statistics (modules 3-8)**
Institute for Continuing Education in Science, Ghent University, Belgium

Professional activities

1. 1 Jan 2006 – 31 Dec 2009 Ph D Student
Ghent University (Hospital), Dep. Neuroradiology, GE16
Grant: Institute for the Promotion of Innovation through Science and Technology in Flanders (IWT-Vlaanderen) n° 51437/53437.
Promoters: Eric Achten, M.D., Ph.D.
Koen Paemeleire, M.D., Ph.D.
Project: Functional changes in the stimulated visual cortex of migraine patients: a combined fMRI and fMRS study
2. 1 Sept 2005 – 31 Dec 2005;
1 Jan 2010 – 31 Mar 2011 Ph D Student
Ghent University (Hospital), Dep. Neuroradiology, GE16
Promoters: Eric Achten, M.D., Ph.D.
Koen Paemeleire, M.D., Ph.D.
Project: Functional changes in the visually stimulated cortex of patients with migraine without aura: an fMRI study
3. 1 April 2011 – to date Scientific staff
Infinity (Small animal imaging lab), Ghent University (TW06)
Focus on MRI and multimodality imaging

Supervision of Master Thesis Students

1. Sarah van Rijsbergen (Biomedical Imaging, UA), “Quantitative Proton MR Spectroscopy: Phantom Measurements and Calibration”, 2005 – 2006
2. Ann Van de Pol (Biomedical Imaging, UA), “Quantitative Phosphorus MR Spectroscopy: Phantom Measurements and Calibration”, 2005 – 2006
3. Pieter Vervaeke (Biomedical Sciences, UGent), “Measuring CBF in the visual cortex with Arterial Spin Labeling”, 2006 – 2007

Teaching

1. “fMRI application: fMRA”, 12th May 2009, Structural Aspects of the CNS, Prof. Dr. E. Achten, 1st Master Biomedical Sciences, UGent
2. “Migraine in beeld gebracht” (part fMRI), 1st March 2010, Studium Generale, Prof. Dr. A. Van der Linden, 1st Bachelor Biomedical Sciences, UA
3. “fMRI application: Migraine”, 27th April 2010, Structural Aspects of the CNS, Prof. Dr. E. Achten, 1st Master Biomedical Sciences, UGent

Organization Scientific Meeting

1. First Annual Meeting of the Benelux ISMRM Chapter, 10th December 2008, Antwerp, Belgium

Publication list

Meeting Abstracts and Presentations

1. **B. Descamps**, C. Roggeman, P. Vandemaele, E. Achten. Image acquisition order and input order of BOLD-fMRI data for slice time correction in fMRI data processing tools. Abstract presented at First Benelux In Vivo MR Methods Symposium [abstract n° 22], 12th December 2007, Nijmegen, The Netherlands
2. **B. Descamps**, P. Vandemaele, K. Paemeleire, L. Leybaert, E. Achten. Single-subject hemodynamic refractory effects in healthy volunteers. Abstract presented at 16th Scientific Meeting of the ISMRM [abstract n° 2353], May 2008, Toronto, Canada
3. **B. Descamps**, P. Vandemaele, H. Reyngoudt, K. Paemeleire, E. Achten. Detecting Hemodynamic Refractory Effects in Patients with Migraine without Aura. Abstract presented at 14th Congress of the International Headache Society [abstract n° LBPO02], September 2009, Philadelphia, USA
4. H. Reyngoudt, **B. Descamps**, K. Paemeleire, E. Achten. Absolute Quantification of Proton Magnetic Resonance Spectroscopy in Migraine Without Aura. Abstract presented at 14th Congress of the International Headache Society [abstract n° LBPO05], September 2009, Philadelphia, USA
5. H. Reyngoudt, **B. Descamps**, K. Paemeleire, E. Achten. Absolute Quantification of Phosphorous Magnetic Resonance Spectroscopy in Migraine Without Aura. Abstract presented at 14th Congress of the International Headache Society [abstract n° LBPO06], September 2009, Philadelphia, USA
6. **B. Descamps**, H. Reyngoudt, P. Vandemaele, K. Paemeleire, E. Achten. Hemodynamic refractory effects in patients with migraine without aura. Oral presentation at the 1st GfMI Symposium, 18th Sept 2009, Ghent, Belgium
7. H. Reyngoudt, **B. Descamps**, P. Vandemaele, Y. De Deene, K. Paemeleire, E. Achten. Absolute quantification of 1H and 31P MRS in migraine without aura. Oral presentation at the 1st GfMI Symposium, 18th Sept 2009, Ghent, Belgium
8. **B. Descamps**, P. Vandemaele, H. Reyngoudt, K. Paemeleire, E. Achten. Hemodynamic refractory effects in healthy volunteers and patients with migraine without aura. Oral presentation at 26th Annual Scientific Meeting of the ESMRMB [abstract n° 283], October 2009, Antalya, Turkey
9. H. Reyngoudt, **B. Descamps**, K. Paemeleire, E. Achten. Absolute quantification of metabolites in migraine patients: a ¹H MRS study. Oral presentation at 26th Annual Scientific Meeting of the ESMRMB [abstract n° 25], October 2009, Antalya, Turkey
10. **B. Descamps**, P. Vandemaele, H. Reyngoudt, K. Deblaere, L. Leybaert, K. Paemeleire, E. Achten. Fitting interictal hemodynamic response functions to characterize anomalous refractory effects in patients with migraine without aura. Abstract presented at the 2nd Annual Meeting of the Benelux ISMRM Chapter [abstract n° 11], 18th January 2010, Utrecht, The Netherlands
11. **B. Descamps**, P. Vandemaele, H. Reyngoudt, K. Deblaere, L. Leybaert, K. Paemeleire, E. Achten. Interictal anomalies in patients with migraine without aura: absence of hemodynamic refractory effects. Abstract presented at 18th Scientific Meeting of the ISMRM [abstract n° 2285], May 2010, Stockholm, Sweden
12. H. Reyngoudt, **B. Descamps**, Y. De Deene, K. Paemeleire, E. Achten. Decreased energy metabolism in patients with migraine without aura: a 31P MRS study. Abstract presented at 18th Scientific Meeting of the ISMRM [abstract n° 3347], May 2010, Stockholm, Sweden
13. **B. Descamps**, P. Vandemaele, H. Reyngoudt, K. Deblaere, L. Leybaert, K. Paemeleire, E. Achten. Neurovascular dishabituation in patients with migraine without aura. Abstract presented at 2nd EHMTIC [abstract n° 134], October 2010, Nice, France
14. H. Reyngoudt, K. Paemeleire, **B. Descamps**, Y. De Deene, E. Achten. Reduction of high-energy phosphates in the occipital lobe of migraine without aura patients: a ³¹P- and ¹H-MRS study. Abstract presented at 2nd EHMTIC [abstract n° 195], October 2010, Nice, France

15. L. Vlerick, K. Deblaere, **B. Descamps**, E. Achten. Presurgical evaluation using functional connectivity resting state fMRI. Abstract presented at 3rd Annual Meeting of the Benelux ISMRM Chapter [abstract n° 120], 19th January 2011, Roosendaal, The Netherlands
16. H. Reyngoudt, E. Achten, **B. Descamps**, A. Dierickx, Y. De Deene, K. Paemeleire. Brain energy metabolism in migraine without aura investigated by 31P- and 1H-MRS. Abstract presented at 25th International Symposium on Cerebral Blood Flow, Metabolism and Function [abstract n° 514], May 2011, Barcelona, Spain
17. D. De Wilde, B. Trachet, **B. Descamps**, C. Van der Donckt, S. Vandenberghe, C. Vanhove, G. De Meyer, P. Segers. Different Boundary Conditions to Simulate Carotid Hemodynamics in a Mouse Model. Abstract presented at 7th Annual International Conference on Biomechanics in Vascular Biology & Cardiovascular Disease [abstract n° 9], April 2012, Atlanta, USA
18. **B. Descamps**, S. Bruneel, V. Keereman, P. van Mierlo, I. Dauwe, S. Vandenberghe, R. Raedt, C. Vanhove. Continuous ¹⁸F-FDG Infusion for Dynamic PET Imaging of an Excitotoxic Insult in the Rat Brain. Oral presentation at 5th WMIC Meeting [abstract n° SS63], September 2012, Dublin, Ireland
19. Y. Kang, S. Symoens, F. Malfait, P. Coucke, M. Renard, B. Guillemin, J. De Backer, F. Branco-Madeira, W. Toussaint, L. Vanhoutte, S. Janssens, **B. Descamps**, C. Vanhove, P. Segers, B. Lambrecht, A. De Paepe. Development of a novel COL3A1 transgenic mouse model for vascular Ehlers-Danlos Syndrome. Abstract presented at 1st International Symposium on the Ehlers-Danlos Syndrome [abstract n° P.01], September 2012, Ghent, Belgium
20. P. van Mierlo, V. Keereman, **B. Descamps**, I. Dauwe, R. Van Hoven, S. Vandenberghe, R. Raedt, C. Vanhove. Multimodal imaging for the investigation of epileptogenesis in the intrahippocampal kainic acid model of epilepsy. Oral presentation at 29th Annual Scientific Meeting of the ESMRMB [abstract n° 402], October 2012, Lisbon, Portugal
21. **B. Descamps**, K. Deblaere, N. D'hondt, J.K.M. Aps, C. Vanhove. Image artifact comparison between ZTE MRI and Cone Beam CT for endodontic filling materials. Oral presentation at 29th Annual Scientific Meeting of the ESMRMB [abstract n° 412], October 2012, Lisbon, Portugal
22. R. Siugzdaitė, G.-R. Wu, P. van Mierlo, **B. Descamps**, R. Raedt, D. Marinazzo. How Lesions Change Resting State Functional Connectivity in Rat Brain. Abstract presented at Belgian Brain Congress 2012, doi: 10.3389/conf.fnhum.2012.210.00099, October 2012, Liège, Belgium

Peer-reviewed articles

1. H. Reyngoudt, Y. De Deene, **B. Descamps**, K. Paemeleire, E. Achten. ¹H-MRS of brain metabolites in migraine without aura: absolute quantification using the phantom replacement technique. *Magn Reson Mater Phy* 2010, 23(4), 227-41.
2. H. Reyngoudt, K. Paemeleire, A. Dierickx, **B. Descamps**, P. Vandemaele, Y. De Deene, E. Achten. Does visual cortex lactate increase following photic stimulation in migraine without aura patients? A functional (1)H-MRS study. *J Headache Pain* 2011, 12(3), 295-302.
3. **B. Descamps**, P. Vandemaele, H. Reyngoudt, K. Deblaere, L. Leybaert, K. Paemeleire, E. Achten. Absence of haemodynamic refractory effects in patients with migraine without aura – an interictal fMRI study. *Cephalalgia* 2011, 31(11), 1220-31.
4. H. Reyngoudt, K. Paemeleire, **B. Descamps**, Y. De Deene, E. Achten. ³¹P MRS demonstrates a reduction in absolute concentrations of high-energy phosphates in the occipital lobe of migraine without aura patients. *Cephalalgia* 2011, 31(12), 1243-53.
5. **B. Descamps**, P. Vandemaele, H. Reyngoudt, K. Deblaere, L. Leybaert, K. Paemeleire, E. Achten. Quantifying hemodynamic refractory BOLD-effects in normal subjects at single-subject level using an inverse logit fitting procedure. *J Magn Reson Imaging* 2012, 35(3), 723-30.

Award

1. **Educational Stipend Award** for the submitted work: "Interictal anomalies in patients with migraine without aura: absence of hemodynamic refractory effects" at the 18th Scientific Meeting of the ISMRM, 2010, Stockholm, Sweden